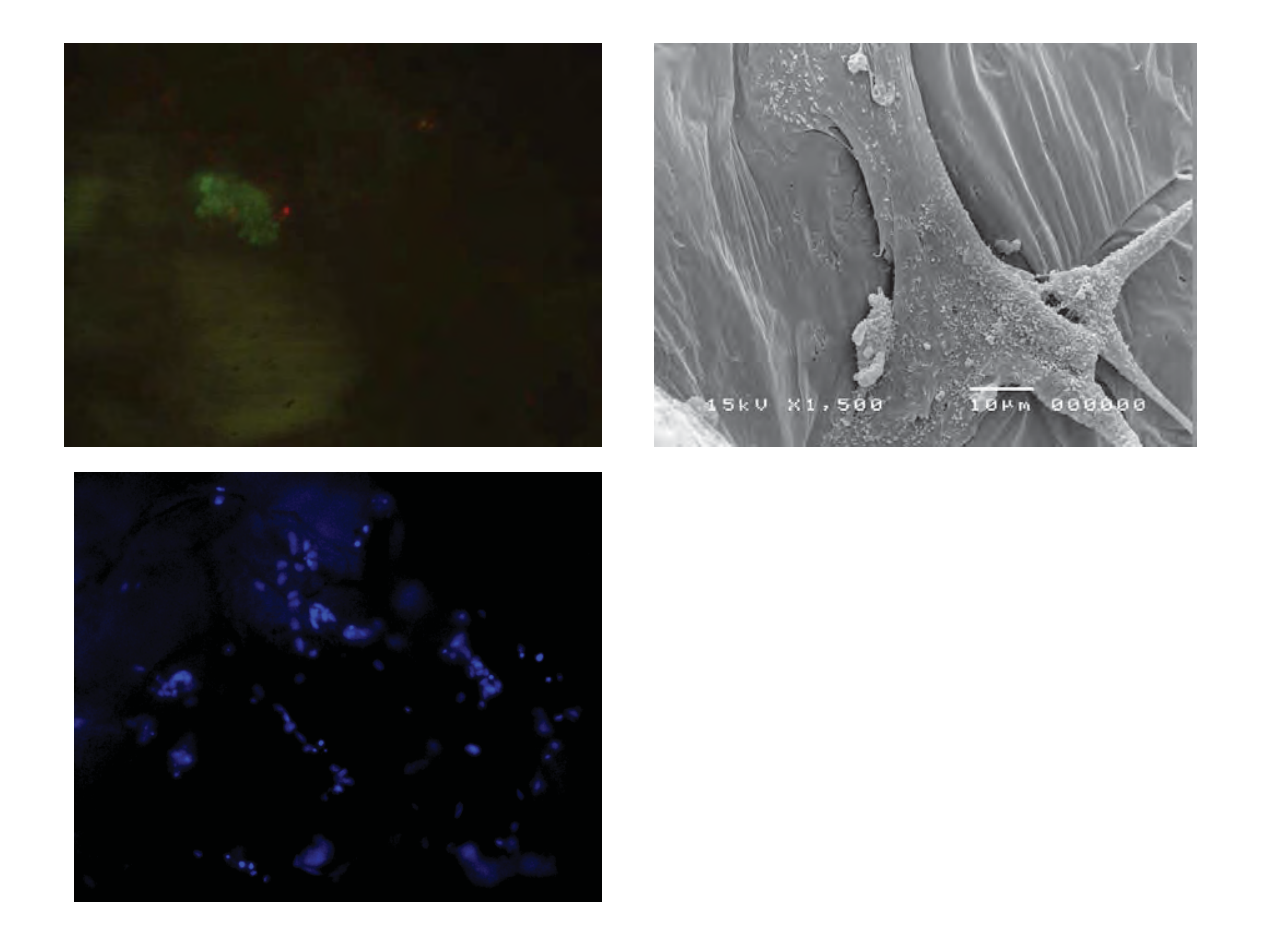


**Figure 2** Von Kossa Alizarin Red and Oil Red O staining were used to validate the differentiation capacity of canine MSC into the osteogenic lineage

In vitro studies of canine MSCs behavior on PCL/HA composite scaffold was evaluated in terms of MSC attachment, morphology, the ability to growth and proliferation within the scaffold. The combination of calcein AM and ethidium homodimer fluorescence staining was used to assess MSC viability. A green fluorescence from calcein AM represented the viable MSCs while a red fluorescence indicated the non-viable cells (Figure 8). On day 1 after seeding, a mixed population of viable and non-viable canine MSCs was observed. The majority of the cells exhibited green calcein fluorescence with a small number of cells was labeled with red fluorescence. In addition, MSCs were found throughout the sample represented a good cell distribution within the scaffold.



**Figure 3** Photomicrographs indicating viability of MSCs within the scaffold. A: viability of canine MSCs 12 hours after seeding and B: SEM image of canine MSCs attached and expanded the cellular process onto the scaffold (3 days after MSC seeding), c: fluorescent analysis of canine MSC proliferation using DAPI nuclear staining

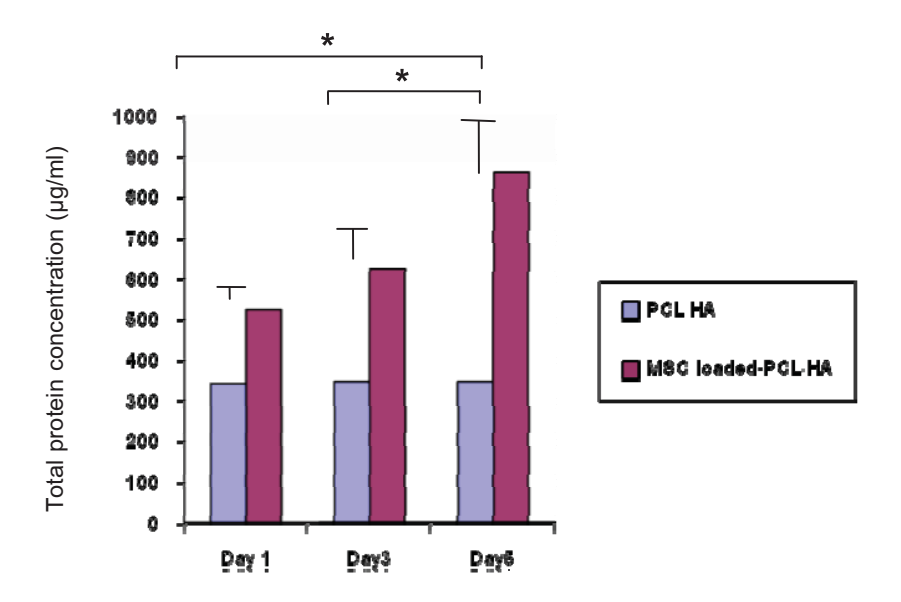
Canine MSC attachment and morphology was observed by SEM on day 1, 3 and 5 after seeding. On day 1 after seeding, MSCs appeared as flat cells spreading onto the surface of scaffold with finger-like projection of cell membrane (filopodia) adhered to the scaffold (Fig 9A). MSCs became

more spread and elongated with an enlargement of adhesive areas between cells and scaffold on day 3 of seeding. In addition, on day 3, more cells were observed and appeared to form small cell clusters with an intercellular connection (Fig 9B).

The proliferation of canine MSCs within PCL/HA scaffold was determined by qualitative comparison of serial DAPI fluorescent images on day1 (Figure 10A and B), 2 (Figure 10C and D) and 4 (Figure 10 E and F) after seeding. An increase MSC population was observed by an increase in DAPI-stained nuclei density over time. The quantitative analysis of the protein content was conducted to evaluate MSC growth and proliferation within PCL/HA scaffold using the BCA protein assay. The amount of protein (μg/ml) in each samples were calculated from the absorbance of the sample solution measured at a wavelength of 562 nm with reference to the standard protein (Table 6). The total protein concentration of MSC-loaded PCL/HA scaffold on day 1, 3 and 5 was 523±15.27, 626.67±71.12 and 861.67±127.16 μg/ml, respectively. A significant differences were found between protein content of PCL/HA alone and MSC-loaded PCL/HA scaffold at all time points. A significant increase in total protein concentration of MSC-loaded PCL/HA scaffold were observed between day 1 and day 5 and day 3 and day 5 (p<0.05). However, no significant difference was found between day 1 and 3 (Figure 11). Notably, the color of the sample solution was changed from green to purple in the proportion to the protein concentration in the scaffold (Figure 12).

To confirm an osteogenic differentiation potential of canine MSCs after seeding on PCL/HA scaffold, Alizarin Red staining was performed on day 14 of induction. Positive Alizarin Red staining was observed in both PCL/HA scaffolds alone and MSC-loaded PCL/HA scaffolds. After washed the samples several time with PBS, only PCL/HA scaffolds that combined with

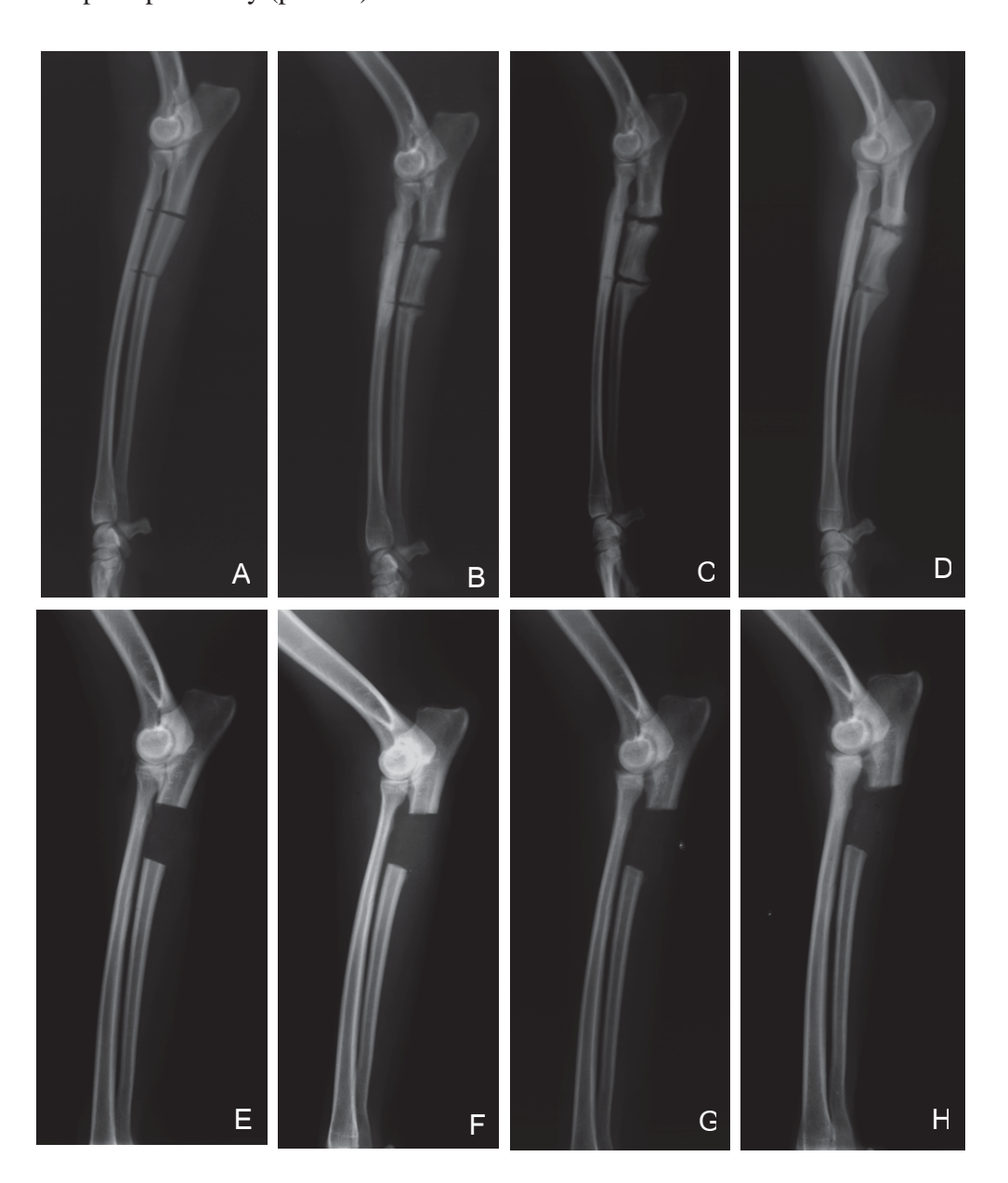
canine MSCs were still remained positive to Alizarin Red suggested the presence of calcium deposition within scaffolds.



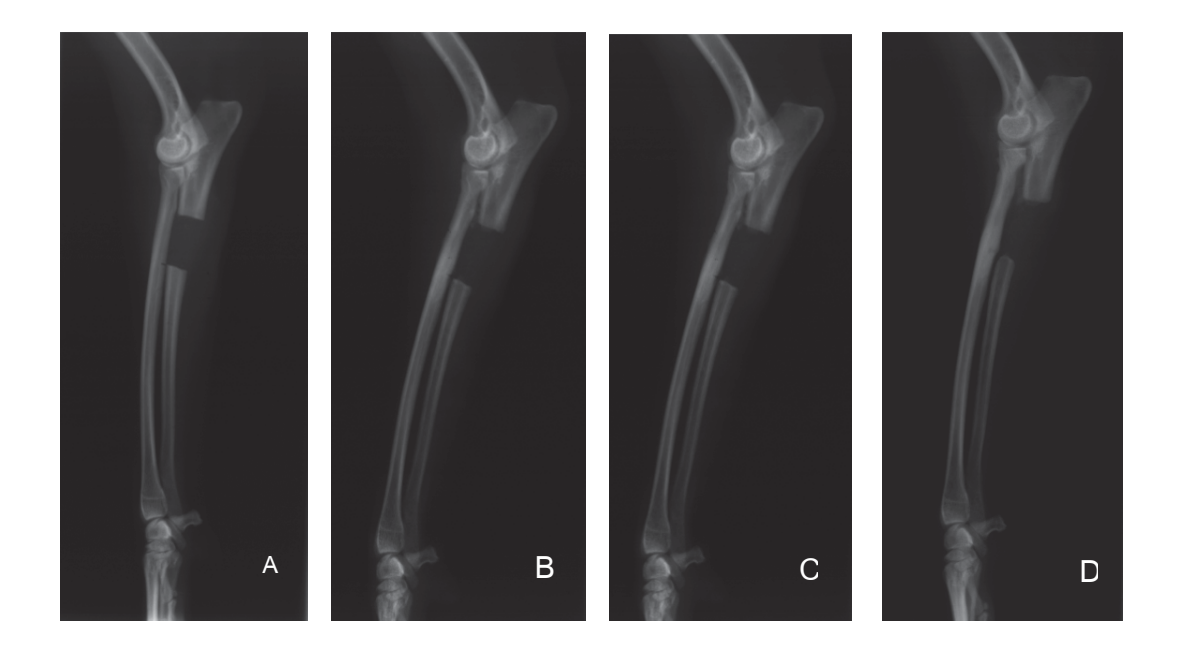
**Figure 4** Quantitative measurement of total protein concentrations of PCL/HA and MSC loaded-PCL/HA scaffolds on day 1, 3 and 5 of culture. \*Significant increase in protein concentration was observed (p<0.05).

The craniocaudal radiographs of the defects were taken immediately and at 2, 4, 6 and 8 week postoperatively (Fig. 13A, B, C and D) illustrated the progressive bone healing of the ulnar defect that treated with corticocancellous bone graft (group 1). Slightly new bone formation was visible during the first 4 weeks postoperatively. At 6week, the bone bridge formation between graft and host bone was evident at the distal part of the defect. By 8 weeks postoperatively, the bone bridging was clearly observed on both side of cortices. An increase in radiodensity of the graft-host bone interfaces with time demonstrated a progressive healing of the defect. Neither new bone nor callus formation was observed in the defect site treated with PCL/HA alone (group 2)

(Figure 14A, B, C and D) and MSC-loaded PCL/HA (group 3) (Figure 15A, B, C and D) at any time point. A slightly increase in radiodensity was observed within the implant site in both groups. There were statistically significant differences (p<0.05) in radiographic score between group 1, 2 and 3 at 6 weeks and between group 1 and 2 and group 1 and 3 at 8 weeks postoperatively. No significant differences in radiographic score were detected between treatment groups at 2 and 4 weeks postoperatively (p>0.05)



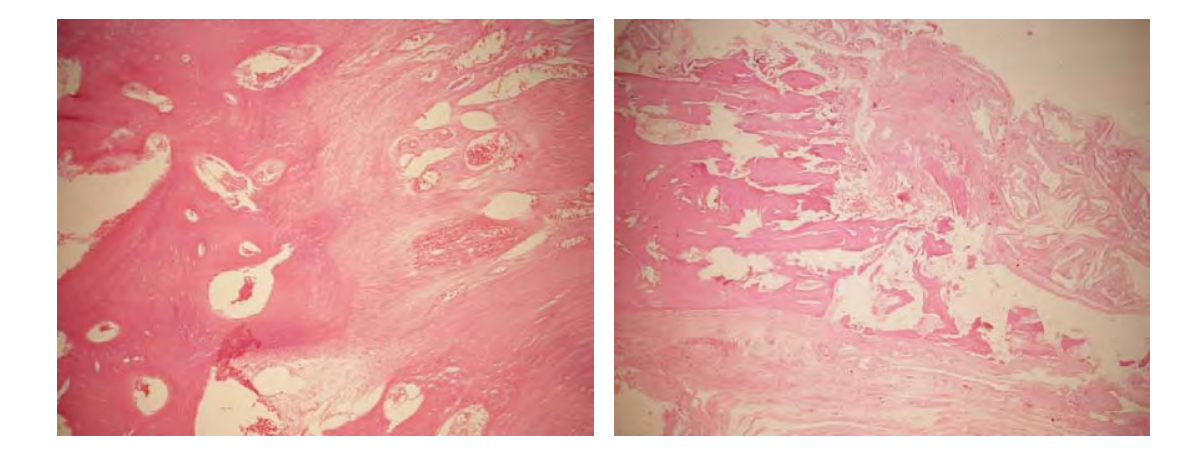
**Figure 5** Radiographs of canine ulnar segmental defects treated with the autogenous cancellous bone graft (A-D) and PCL/HA scaffold implant (E-H) at (A, E) 2 weeks; (B, F) 4 weeks; (C, G) 6 weeks and (D, H) 8 weeks postoperatively



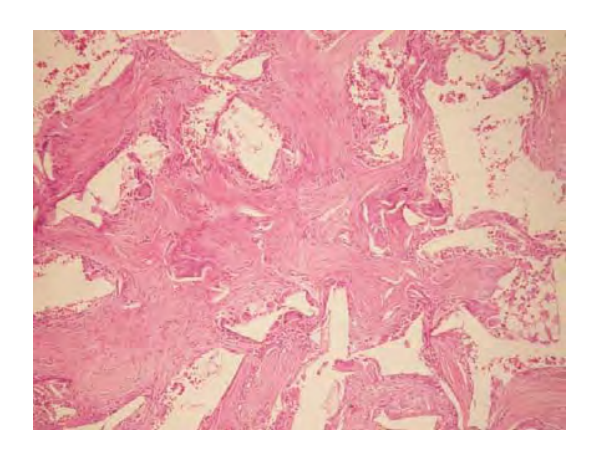
**Figure 6** Radiographs of canine ulnar segmental defects treated with MSC-loaded PCL/HA scaffold at (A) 2 weeks; (B) 4 weeks; (C) 6 weeks and (D) 8 weeks postoperatively

Histopathology of the defect implanted with autogenous cancellous bone graft (group 1) showed a good incorporation between the graft and host bone (Figure 16A) with the osteoid formation and new bone formation along the graft-host bone junction. The longitudinal section of

the graft revealed the re-establishment of vascular supply within the marrow cavity (Figure 16B). In group 2, the incorporation of the PCL/HA scaffold and host bone was mainly achieved by fibrocartilaginous tissue with minimal osteoid formation (Figure 17A). The defect site was filled with loose and unorganized connective tissue with new vascular ingrowth. There were still some remnants of the scaffold which sloughed off during the histological preparation (Figure 17B). Finally, in group 3, more fibrovascular tissue was observed in the defect, which implanted with MSC-loaded PCL/HA scaffold compared with PCL/HA group (Figure 18). The fibrous tissue is mainly comprised of spindle-shaped cells with extensive collagen deposition confirmed by Masson's Trichrome staining (Figure 19). It is notable that numerous of multinucleated giant cells were found adjacent to remnants of the scaffold indicating a chronic inflammation with foreign body giant cell response to the scaffold.



**Figure 7** Histological sections of an ulnar defect implanted with cancellous bone graft (A) and with PCL/HA scaffold (B) at 8 week postoperatively. The junction between host bone (HB) and the graft (CB) and scaffold (PCL/HA)



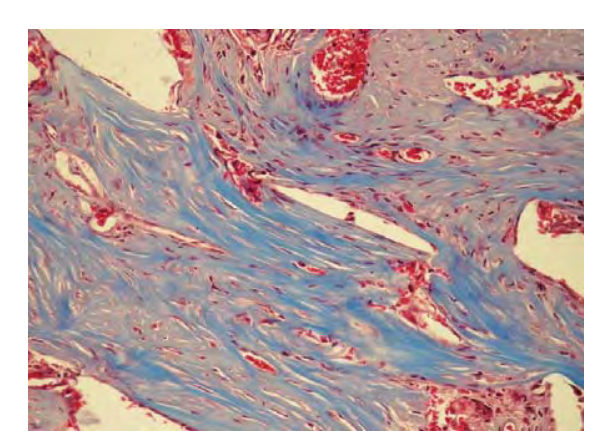


**Figure 8** Histological sections of an ulnar defect implanted with MSC-loaded PCL/HA scaffold at 8 week postoperatively. A: H&E staining and Masson's trichrome staining (B)

### **Discussion**

Implantation of biological bone substitutes is one of the promising bone tissue engineering strategies for treatment of extensive bone defects. Mesenchymal stem cell in combination with polymer/ceramic composite scaffold has been widely investigated as an alternative to autogenous cancellous bone graft. In this study, we successfully isolated canine MSCs from bone marrow and identified these cells according to the multipotent human MSCs characterization which recently proposed by International Society for Cellular Therapy (Dominici et al., 2006). Then, we investigated the interaction between canine MSCs and PCL/HA composite scaffold in terms of cell viability, proliferative capacity and ability to differentiate into osteoblast. Finally, we evaluated the

efficacy of canine MSCs combined with PCL/HA composite scaffold in comparison with PCL/HA alone and autogenous on the healing of ulnar critical sized defects in dog.

MSCs reside in various adult tissues such as bone marrow, adipose tissue, skin, periosteum and placenta (Tuan et al., 2002). These cells are responsible for regulating tissue homeostasis, repair and regeneration. Although MSCs originated from various tissue sources possess similar phenotypic expression, significant difference in cell proliferation and multilineage differentiation potentials are observed. In this study, bone marrow was chosen as a source of MSCs because it is easy to assess and can be aspirated in large volume. Moreover, MSCs derived from bone marrow and synovium are superior to periosteum-, adipogenic- and skeletal muscle- derived MSCs with regard to self renewal, expansion and differentiation potential (Sakaguchi et al., 2005). Canine MSCs were harvested from the bone marrow samples aspirated from the dorsal iliac crest of 4 dogs. Red blood cell lysing buffer was added to enrich the initial MSC population by eliminating the contaminated red blood cells before culture. Canine MSCs used in the present study were isolated by their ability to adhere to the polystyrene plastic plate and subsequently subcultured when cells reached 80-90% confluence. Owing to the absence of MSC specific antigen marker, at least three minimum criteria were required to characterize MSCs are as follows: the ability to adhere to plastic surface, the expression of cell surface antigen and the capacity to differentiate along the mesenchymal lineage (Dominici et al., 2006). The isolated cells exhibited classical spindle shaped morphology and expressed high levels of MSC markers inculding CD 44 and CD 90. The flow cytometric analysis of cell surface protein revealed more than 94% of the isolated cells were positive for both CD 44 and CD 90 which corresponding with previous study (Kern et al., 2006; Jung et al., 2008). No expression of CD34 was observed which indicated no contamination of hematopoietic stem cells was found in the culture. And finally, these isolated cells were capable of differentiation into a mesenchymal lineage when cultured in a proper condition.

Due to the major concern in the survival and proliferative capacity of cells within the large scaffold constructs, an in vitro study of canine MSCs behavior was performed on 3D PCL/HA scaffolds. Dual fluorescence viability assay using calcein AM and ethidium homodimer was performed to determine the MSC viability within PCL/HA scaffold. This assay allows the simultaneous visualization of viable and dead cells within the scaffold (Decherchi et al., 1997). Calcein AM is a hydrophobic compound which can diffuse through intact cell membrane of viable cells and subsequently hydrolyze intracellular esterase result in calcein, a green fluorescence, retained in the cytoplasm. In contrast to calcein AM, ethidium homodimer can penetrate only damaged cell membranes and bind to DNA of the dead cells result in emission of red fluorescence. From dual viability assay, an intense green fluorescence was mainly observed through the entire scaffold indicated the majority of canine MSCs remained viable on day 1 after seeding. A small number of dead cells were found in the outer part of the scaffold and became more prominent in the middle of the scaffold. This may be due to the diffuse limitation of oxygen and nutrient caused by the scaffold thickness. Moreover, all MSC loaded-scaffolds were cultured under a static condition may even hinder the fluid transportation result in an accumulation of waste products within the scaffold. To overcome these problems, dynamic culture conditions such as a spinner flask, orbital shaker or perfusion system has been used since the approach can improve cell viability, uniform distribution and subsequently increase in extracellular matrix deposition (Yeatts and Fisher, 2011). Nerurkar et al. (2011) suggested that the dynamic culture condition using orbital shaker enhanced MSC infiltration and collagen deposition on electrospun PCL nanofibrous scaffold. Additionally, transient shaking culture significantly improved MSC distribution, provided

favorable condition for chondrogenic differentiation and increased glycosaminoglycans accumulation within the scaffold. The results from SEM images showed that canine MCSs adhered favorably to PCL/HA scaffold. Cells exhibited flat morphology with filopodia projected from cell body and attached to the scaffold surface. Filopodia are protrusion of cell membrane which play an important role in the formation of adhesive connection between cell and the extracellular matrix (Yang et al., 2010). The attached cells became more elongated in shaped with an enlargement of focal adhesion suggested growth and maturation of canine MSCs in PCL/HA scaffold over time. MSC proliferative capacity on 3D PCL/HA scaffold was evidenced by comparison of serial DAPI fluorescence images. DAPI is a DNA-specific dye which has been commonly used for DNA detection and visualization. This dye binds specifically to A-T base pair in DNA sequence results in formation of the DAPI-DNA complex which exhibits a blue fluorescence emission under a fluorescence microscope. An increase in DAPI stained nuclei was observed over time reflected the proliferative capacity of the loaded MSCs. Notably, the background interference was observed during the fluorescent microscopical analysis of the loaded scaffold in both dual viability assay and DAPI fluorescent staining. It is thought that the autofluorescence emission of the polymers caused by an aromatic and aliphatic ester bond when excited with green or blue wavelength. Moreover, the fluorescent interference is even more exaggerated due to the light scattering caused by the thickness of the polymer and its porous nature. To avoid these interferences, a thin section of the sample can diminish light scattering and minimize over all autofluorescence from polymer or using other fluorescent probe that can be excited and emits in the different wavelength. Jaafar et al. (2011) applied the use of Sudan Black B (SB) as an autofluorescence quencher for 4 types of polymer, including polyglycerol sebacate, polyurethane, polylactice-co-caprolactone, and polylactic acid-co-glycolic acid. SB is a lysochrome diazo dye which has been commonly used as a neutral triglyceride and lipid staining. Reduction of an overall background interference was based on two mechanisms, the light absorption capacity of SB and the ability to modify the surface of the polymers. No interaction between SB and fluorescently labeled cells was observed.

Despite the promising result from the visual DAPI fluorescence image analysis, the uncertainty of the outcome may occur due to the subjective evaluation of these images. Therefore, the BCA protein assay was performed in order to quantify proliferative capacity of canine MSCs after seeded onto the scaffold (Sachana and Hargreaves, 2007). The assay is based on the ability of the peptide bonds in protein to reduce Cu<sup>+2</sup> into Cu<sup>+1</sup> and the chelation of Cu<sup>+1</sup> with BCA result in purple-colored products that can be measured with spectrophotometer. The total protein concentration are calculated from the optical density of each the samples at a wavelength of 562 nm with respect to the standard curve. Significant increases in the protein concentration were observed between day 1 and day 5 and day 3 and day 5 (p<0.05). An increase in the absorbance of the loaded PCL/HA is correlated with the greater amount of the protein concentration in the sample indicated the growth and proliferative capacity of canine MSCs resided in the scaffold. As expected, there was no significant difference in protein concentration was found between day 1 and day 3. These may result from the physical adaptation of cells to the change in environment. Moreover, the newly seeded cells may also require time to adjust and adhere onto the new surface condition and subsequently reformation of the intercellular connection which necessary for optimal cell proliferation. And finally, the present in vitro study demonstrated the ability of canine MSCs to differentiate into an osteogenic lineage after seeded onto 3D PCL/HA scaffold as evidenced by Alizarin staining on day 14 of induction.

As the combination of osteopotential cell and biolodegradable scaffold is one of the most successful strategies in bone tissue engineering and the use of PLC/HA composite scaffold fabricated by solvent casting and particular leaching techniques has been demonstrated as a promising approach for promoting new bone formation (Chuenjitkuntaworn et al., 2010). This study was performed as a further investigation using canine model in order to evaluate the efficacy of PCL/HA and MSC-loaded PCL/HA on the healing of ulnar critical size defects. Key (1934) has defined the ulnar critical sized defect as a segmental defect that larger than 1 to 1.5 times of the diameter of the shaft of the bone. All dogs were able to stand and ambulate on day 1 and 2 after surgery, respectively. Defects in PCL/HA group were healed with fibrous connective tissue consisted of long spindle-shaped fibroblastic cells and collagen fiber as an extracellular matrix. The presence of capillaries within the graft sites suggested that PCL/HA scaffolds can support the ingrowth of vascular tissue. Similar results were obtained in the group that treated with MSCloaded PCL/HA scaffold, however, Mason's trichrome staining suggested that more collagen deposition was found when compared to PCL/HA group. Although there was a good evidence of fibrovascular tissue infiltration with an extent matrix deposition throughout the entire PCL/HA scaffold, no osteogenic differentiation was observed. In contrast to the promising result in a calvarial defect of mouse (Chuenjitkuntaworn et al., 2010) neither new bone nor callus formation was observed in defects treated with PCL/HA alone or MSC-loaded PCL/HA scaffold. Several possible reasons could explain for this inconsistency. It is believed that larger animal possesses bone regenerative capacity to a lesser extent than small animal. Moreover, the physiological differences between dog and mouse with regard to the slower bone turnover rate lower basal metabolic rate and longer lifespan in dog may contribute to different bone healing result (Cook et. al., 1994). The variation in size, location and the mechanical environment of the defects may

impact on the biological response to the scaffold. PCL/HA scaffolds used in the present study were not only larger in size but also thicker in dimension than the previous study. This may cause a massive release of the degradation product, caproic acid, from the scaffold and subsequently creating an unfavorable environment for bone regeneration (Böstmann et al. 1990; Bergsma et al., 1995; Prokop et al., 2004). And finally, the major consideration was given to the different types of bone defect (flat bone versus long bone), the loading condition of the bone (non-loading calvarial versus loading ulnar bone). A calvarial defect is considered as a non-weight-bearing model which experiences lesser mechanical interference than a long bone model. Therefore, a calvarial bone defect may provide more favorable environment for new bone regeneration than an ulnar bone defect in a biomechanical aspects.

Canine ulna defect model has been extensively used as a study model to evaluate the efficacy of biomaterials in bone tissue engineering application because no fixation is required as the radius is the major load-bearing bone of the forearm and the interosseous ligament between the radius and the ulna was remained intact. Moreover, the ulnar ostectomy procedure can be done on both sides simultaneously, thus reducing the number of animal used in the study (Salkeld et al., 2001; Paskalev et al., 2006; Jones et al., 2008). Several successful results have been reported using a canine ulnar model without fixation (Heiple et al., 1963; Nillson et. al., 1986; Cook et al., 1994; Salkeld et al., 2001; Paskalev et al., 2006; Jones et al., 2008). However, there might be some mechanical interference between defect sites causing an unfavorable condition for mesenchymal stem cells to differentiate into osteoblastic cells. To overcome this problem, intramedullary pins or plates and screws may use to stabilize canine ulnar defect in order to optimize the new bone formation.

Last but not least, histological analysis demonstrated the presence of numerous multinucleated giant cells within defect sites that implanted with PCL/HA and MSC-loaded PCL/HA scaffold. These giant cells appeared adjacent to remnants of the scaffold which reflected chronic inflammation with foreign body response. For this reason, scaffold samples were sent to identify the contamination using scanning electron microscope with energy dispersive x-ray (SEM/EDX) analysis. The result of the SEM/EDX analysis showed that the scaffolds were contaminated with copper (Cu) from hydroxyapatite ceramic. Thus, chronic inflammation with foreign body giant cell response from copper contamination may result in an impaired new bone formation at defect site. Similar tissue reaction was reported by Linder and Lundskog (1975), Völker et al. (1997), Tindel et al. (2001) and Saitoh et al. (2010). Saitoh and his group investigated an in vivo tissue response to three different metal particles including copper, nickel and titanium by subcutaneous implantation in mouse. One week after implantation, subcutaneous tissue was excised for evaluation of tissue reaction using histological and transmission electron microscopic analysis. The result of this study showed that copper particles caused the highest degree of inflammation. Similar result was observed in the study of Linder and Lundskog that compared the reaction of bone to copper, stainless steel, titanium and vitallium.

### **Conclusions**

The present study was conducted in order to investigate the *in vitro* interaction between canine MSCs and PCL/HA composite scaffolds by seeding cells onto the scaffold and observed for cell behaviors with respect to cell viability, cell attachment and morphology, the proliferative capacity and the ability to differentiate into osteogenic lineage. The *in vitro* study demonstrated a good biocompatibility between canine MSCs and PCL/HA scaffolds. From dual fluorescence

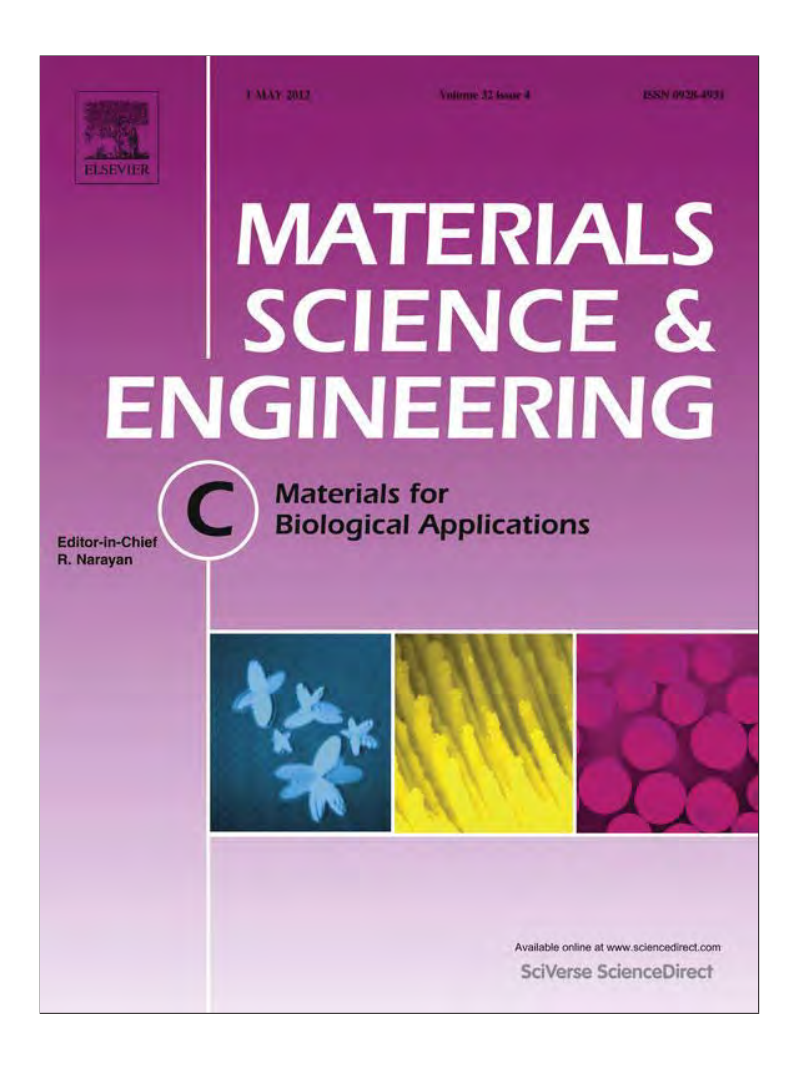
viability assay showed that the majority of seeded cells emitted green fluorescence indicating most of cells remained viable on day 1 after seeding. Similarly the result from SEM analysis revealed that canine MSCs adhered favorably onto PCL/HA scaffold. Cells already attached on the scaffold with flat morphology and filopodia projection within day 1 of seeding. More cell numbers were observed with formation of cell cluster in some area of scaffold suggested that canine MSCs were able to growth and maturation after seeding. To confirm the proliferative capacity of the seeded cell, serial DAPI florescent image analysis combined with BCA protein assay were performed. A progressive increase in DAPI-stained cells was observed under a fluorescent microscope on day 1, 2 and 4 after seeding which collated to an increase in total protein concentration on day 1 (523.33±15.27), day 3 (626.67±71.12) and day 5 (861.67±127.16) after seeding. Moreover, a significant increase (p<0.05) in protein concentration was observed between day 1 and 5 and day 3 and 5 of seeding. And finally, the ability of canine MSCs to differentiate into osteoblats were confirmed by Alizarin Red staining on day 14 of osteogenic induction. The present *in vitro* study concluded that there was a good interaction between canine MSCs and PCL/HA scaffold.

Despite a promising result from an *in vitro* study, neither bone nor callus formation was observed in canine ulnar defects that implanted with PCL/HA and PCL/HA scaffolds. Defects in these two groups were healed with fibrovascular tissue which infiltrated through the pore of the scaffold. Surprisingly, numerous of multinucleated giant cells were found indicating chronic inflammation with foreign body giant cell response due to the presence of remnants of PCL/HA scaffold.

4. ท่านได้พบอุปสรรคในการดำเนินงานหรือไม่	ถ้าพบกรุณาระบุว่ามีอะไรบ้าง และแก้ไขอย่างไรบ้าง
ไม่พบอุปสรรคในการดำเนินงาน	
5. ข้อคิดเห็นและข้อเสนออื่น ๆต่อสกว.	

ลงนาม	
	(ศาสตราจารย์พิชญ์ ศุภผล)
	(หัวหน้าโครงการวิจัยรับทุน)
วันที่	

Provided for non-commercial research and education use. Not for reproduction, distribution or commercial use.



This article appeared in a journal published by Elsevier. The attached copy is furnished to the author for internal non-commercial research and education use, including for instruction at the authors institution and sharing with colleagues.

Other uses, including reproduction and distribution, or selling or licensing copies, or posting to personal, institutional or third party websites are prohibited.

In most cases authors are permitted to post their version of the article (e.g. in Word or Tex form) to their personal website or institutional repository. Authors requiring further information regarding Elsevier's archiving and manuscript policies are encouraged to visit:

http://www.elsevier.com/copyright

# **Author's personal copy**

Materials Science and Engineering C 32 (2012) 758-762



Contents lists available at SciVerse ScienceDirect

# Materials Science and Engineering C

journal homepage: www.elsevier.com/locate/msec



# Hydroxyapatite/ovalbumin composite particles as model protein carriers for bone tissue engineering: I. Synthesis and characterization

Prae-ravee K-hasuwan a,b, Neeranut Kuanchertchoo c,\*, Nuanchawee Wetprasit d, Pitt Supaphol a,b,\*\*

- <sup>a</sup> The Petroleum and Petrochemical College, Chulalongkorn University, Bangkok 10330, Thailand
- <sup>b</sup> Center of Excellence on Petrochemical and Materials Technology, Chulalongkorn University, Bangkok 10330, Thailand
- <sup>c</sup> Department of Materials Technology, Faculty of Science, Ramkhamhaeng University, Bangkok 10240, Thailand
- <sup>d</sup> Department of Biotechnology, Faculty of Science, Ramkhamhaeng University, Bangkok 10240, Thailand

#### ARTICLE INFO

#### Article history: Received 6 April 2011 Received in revised form 20 November 2011 Accepted 19 January 2012 Available online 28 January 2012

Keywords: Hydroxyapatite Ovalbumin Composite particles

#### ABSTRACT

Hydroxyapatite (HAp) nanoparticles were synthesized from the co-precipitation reaction between calcium oxide from discarded egg shells and phosphoric acid in the absence and the presence of ovalbumin (OVA). 2-Amino-2-hydroxymethyl-propane-1,3-diol (tris-base) was used to control the pH during the co-precipitation (i.e., 7–9). The formation of HAp was confirmed by X-ray diffraction analysis, while both the Fourier-transform infrared spectroscopy and the thermogravimetric analysis confirmed the existence of OVA within the HAp–OVA particles. The crystallite sizes of the individual crystalline entities within the HAp and the HAp–OVA particles were approximated from the (002) reflection peaks by means of the Scherrer's equation. The average particle sizes of the HAp and the HAp–OVA particles were measured by particle size analysis. Transmission electron microscopy revealed that these particles were aggregates of rod-like HAp nanocrystals, whereas scanning electron microscopy revealed that these particles ultimately formed into larger aggregates. Lastly, the decrease in the pH during the precipitation process and the presence of OVA were responsible for the observed increase in the values of pore size, BET specific surface area, and pore volume of the resulting HAp particles.

© 2012 Elsevier B.V. All rights reserved.

#### 1. Introduction

Hydroxyapatite (HAp, Ca<sub>10</sub>(PO<sub>4</sub>)<sub>6</sub>(OH)<sub>2</sub>), the major inorganic composition of hard bone tissues, is usually fabricated or imparted into prosthetic devices for bone implantation/replacement. This is because of its biocompatibility and osteoconductivity [1–3]. Recently, porous HAp particles with pore sizes of 2–50 nm (mesoporous) or <2 nm (microporous) were deemed highly suitable for biomedical applications, especially for bone tissue engineering [4,5]. Mesoporous HAp particles having high surface areas and large pore volumes can be excellent carriers for delivery of functional biomolecules [6]. Such HAp particles can be prepared by many means, e.g., hydrothermal [3], emulsion [7], sol–gel [1,8], and precipitation [9,10]. They can also be synthesized from many types of chemical templates, such as cationic surfactants, e.g., cetyltrimethylammonium bromide (CTAB)

[6,10,11]; non-ionic surfactants, e.g., a triblock copolymer of pluronic F127 (EO99PO65EO99) [12]; and anionic surfactants, e.g., mono-*n*-dodecyl phosphate [13]. The chemical templating technique may pose some disadvantages, however. These are, for example, the deterioration of the mesopores [6] and the wide variation of the pore sizes [10] after calcination. Biosurfactants can also be used to prepare mesoporous apatitic materials, because of their non-toxicity, low production cost, and the possibility of imparting relatively large pore sizes (>5 nm) [14]. Among the various biosurfactants, ovalbumin is of high interest, because of its availability at low price and capability of forming into cross-linking structures that are highly hydrated and porous-like [14,15].

The present contribution reports an environmentally friendly strategy towards the synthesis of protein-incorporated hydroxyapatite (HAp) particles, using egg shells and egg ovalbumin (OVA) as raw materials. In addition to the use of OVA to enlarge the mesoporous structure of the obtained HAp particles, it was also used as the model, incorporating protein.

#### 2. Experimental procedures

#### 2.1. Materials and material synthesis

The chemical reagents, e.g., nitric acid (HNO<sub>3</sub>, A.R. grade), phosphoric acid (H<sub>3</sub>PO<sub>4</sub>, A.R. grade), 2-amino-2-hydroxymethyl-propane-1,3-

<sup>\*</sup> Correspondence to: N. Kuanchertchoo, Department of Materials Technology, Ramkhamhaeng University, Hua Mark, Bangkapi, Bangkok 10240, Thailand. Tel.:  $+66\,2\,310\,8408$ ; fax:  $+66\,2\,310\,8696$ .

<sup>\*\*</sup> Correspondence to: P. Supaphol, The Petroleum and Petrochemical College, Chulalongkorn University, Soi Chula 12, Phyathai Road, Pathumwan, Bangkok 10330, Thailand. Tel.: +66 2 218 4131; fax: +66 2 215 4459.

 $<sup>\</sup>label{lem:email} \textit{E-mail addresses: } neeranutk@gmail.com (N. Kuanchertchoo), pitt.s@chula.ac.th (P. Supaphol).$ 

diol (tris-base, A.R. grade), and chicken egg white ovalbumin (OVA, grade II), were purchased from Sigma-Aldrich (USA). These were used without further purification. In the synthesis process, calcium oxide (CaO) was first synthesized from discarded egg shells [16]. Briefly, the egg shells were cleaned with distilled water at 80 °C and dried in vacuo. They were then calcined at 1000 °C in a Lindberg LBF799C oven, in two heating stages (i. 25 to 700 °C for 2 h to eliminate organic substances and ii. 700 to 1000 °C for another 2 h to eliminate CO2 to finally obtain CaO powder). Then, 2.5 g of the CaO powder was dissolved in 25 mL of 1 M HNO<sub>3</sub> under gentle stirring at 70 °C for 3 h. Subsequently, 3.0 g of conc. H<sub>3</sub>PO<sub>4</sub> (85 wt.-%) was added dropwise into the solution to adjust the Ca/P ratio to 1.67. The pH of the mixed solution was maintained at 2.0 and the whole system was continuously stirred at room temperature. Precisely 2.0 g of OVA was then added into 500 mL of the obtained solution under vigorous stirring for 1 h. Precipitation was achieved after 200 mL of 1, 1.5, or 2 M tris-base had been added into the solution to impart the buffering effect to the solution at the pH of 7, 8, or 9, respectively. The mixture was vigorously stirred. The precipitates were filtered, washed several times with deionized water, and lyophilized for 48 h. The procedure was repeated to obtain the precipitates that did not contain OVA for comparative purposes.

#### 2.2. Characterization

A Rigaku D/MAX 2000 X-ray diffractometer (XRD) was used to investigate the crystalline nature of the obtained powdery precipitates, using Cu K $\alpha$  (1.54 Å) radiation over the  $2\theta$  range of 5–60° with 0.02° scanning step. The crystalline phase of the powder was identified with JCPDS standard (9-432). A Nicolet NEXUS 670 Fourier-transform infrared spectroscope (FT-IR), operating at a resolution of 4 cm<sup>-1</sup> over a wavenumber range of 4000 to 400 cm<sup>-1</sup>, was used to examine the chemical functionalities of the powdery products. A Perkin-Elmer TGA-7 thermogravimetric analyzer (TGA) was used to investigate the thermal degradation behavior of the powder at a heating rate of 10 °C·min<sup>-1</sup> in air. Some of the powdery products, after having been subjected to the thermal treatment in TGA, were reanalyzed by XRD. Microscopic morphology of the powder was observed by a JEOL JEM-2100 transmission electron microscope (TEM), operating at 200 kV. Surface morphology of the obtained products was investigated by a JEOL JSM-5410LV scanning electron microscope (SEM). Particle size distribution (PSD) of the powder was collected by a Mastersizer 2000 Malvern particle size analyzer (PSA). The powder was dispersed ultrasonically in water during the measurement. The pore characteristics and the Bruaauer-Emmett-Teller (BET) specific surface area of the obtained powdery products were determined based on the physisorption of N<sub>2</sub> at a temperature of 77 K using a Quantachrome AS-1 autosorb-1 instrument. Lastly, the  $\zeta$  potentials of the powdery products were measured by electrophoresis, using a Zeta-meter 3.0 + analytical system. Briefly, a suspension of 100 mg of the HAp or the HAp/OVA particles in 20 mL of deionized water was filled in an electrophoresis cell. Once energized, the powder was aroused to move towards one of the electrodes. The unit automatically converted the electrophoretic mobility of the particles into the  $\zeta$  values using the Smoluchowski equation.

## 3. Results and discussion

Because of the similarity of the results obtained for the HAp particles that had been obtained at pHs 7, 8, and 9, only those of the particles that had been obtained at pH 9 were extensively reported and discussed. As shown in Fig. 1, all of the crystalline peaks as observed in the XRD patterns of the precipitated powdery products that had been obtained, both in the absence and the presence of OVA, at pH 9 could be assigned to those of HAp [i.e., the hexagonal P63/m space group with the lattice constants of a = b = 0.9418 nm and c = 0.6884 nm (cf. JCPDS No. 09-0432)]. The average crystallite

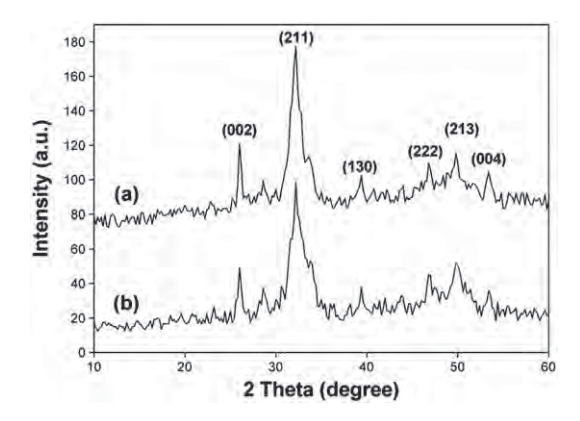
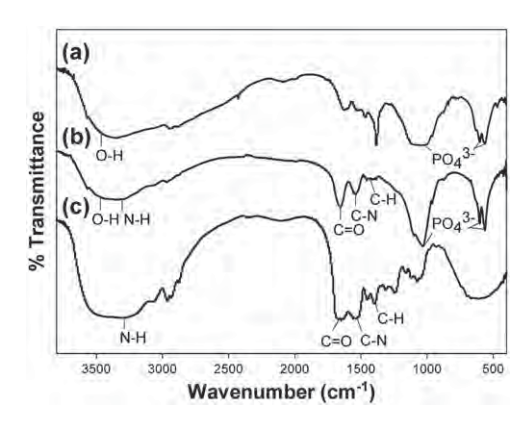


**Fig. 1.** XRD patterns of (a) pure HAp and (b) HAp–OVA particles that had been obtained at pH 9.

sizes, as estimated from the width of the (002) reflection peaks using the Scherrer's equation [17], were around 17.3–20.9 nm and 16.8–19.8 nm for the HAp and the HAp–OVA particles, respectively (see Table 1). In particular, the average value of the crystallite size decreased with an increase in the pH used during the precipitation process. As the pH increased, more tris-base molecules, in their free form, would be available to nucleate the HAp crystalline entities (cf. the p $K_a$  of tris-base = 8.06), hence the observed decrease in the crystallite size. At the same pH, the presence of OVA resulted in a slight reduction in the average value of the size of the obtained HAp crystals. The presence of OVA could retard the influx of  $Ca^{2+}$  and  $PO_4^{3-}$  into the growth face, as OVA would adsorb readily onto the HAp crystallites during the crystal growth.

The FT-IR spectra of the HAp and the HAp–OVA particles that had been obtained at pH 9 as well as that of the as-received OVA in its dry state are shown in Fig. 2. For the HAp particles, the adsorption bands centering at 3569 and  $1630~\rm cm^{-1}$  could be assigned to the OH stretching and the OH vibration of the apatitic group [18]. The bands centering at 1035, 601, and  $563~\rm cm^{-1}$  should correspond to  $PO_4^3$ —ions in the HAp structure. However, the band centering at  $1384~\rm cm^{-1}$  was thought to belong to the carbonate functionality, which might be a result of the contamination from the reaction with  $CO_2$  in the atmosphere [11]. As for the as-received OVA, the characteristic absorption peaks at 3299, 1652, 1539, and 1457 cm $^{-1}$  could be ascribed to the N–H stretching, the carbonyl, the C–N, and the C–H stretching vibrations, respectively [19]. For the HAp–OVA particles, the presence of the absorption bands centering at 1654 and 1539 cm $^{-1}$  confirmed the presence of OVA within the obtained HAp particles.

The HAp and the HAp–OVA particles that had been obtained at pH 9 were evaluated thermogravimetrically and the results are shown in Fig. 3a. For the HAp particles, three main stages in the loss of their mass were observed. The first stage, over the temperature range of



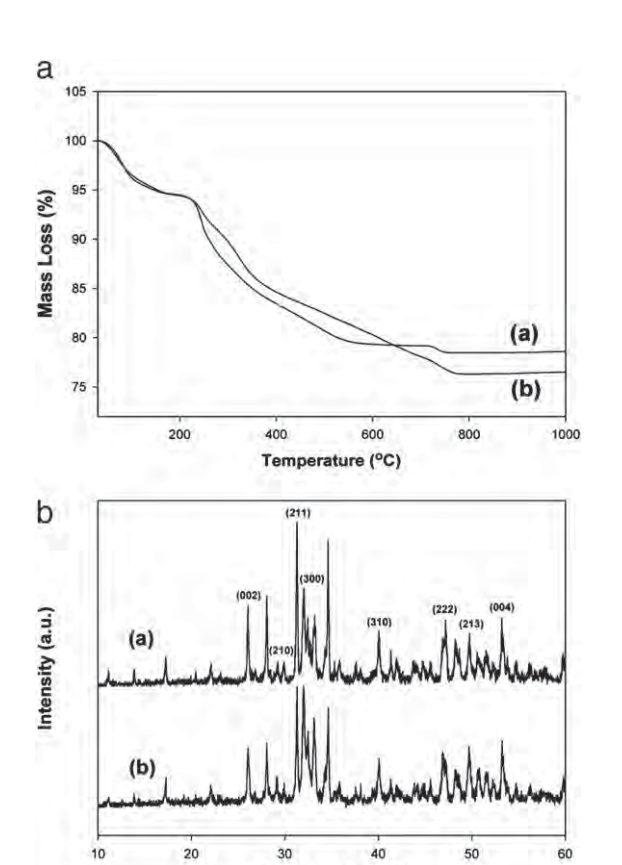
**Fig. 2.** FT-IR spectra of (a) pure HAp and (b) HAp–OVA particles that had been obtained at pH 9 as well as that of (c) as-received OVA in its dry state.

 Table 1

 Textural parameters of pure HAp and HAp-OVA particles that had been obtained at different pH conditions.

Type of HAp	Crystallite size (nm) (n=3)	Average size of primary particles (nm) (n=3)	Pore diameter (nm) (n=2)	BET Specific surface area $(m^2 g^{-1})$ (n=2)	Pore volume $(cm^3 \cdot g^{-1})$ $(n=2)$	$\zeta$ potential (mV) ( $n = 10$ )
HAp (pH 7)	$20.9 \pm 0.06$	$59.3 \pm 0.25$	$8.9 \pm 0.2$	$17.2 \pm 0.7$	$0.079 \pm 0.006$	$-31.6 \pm 2.4$
HAp (pH 8)	$19.2 \pm 0.08$	$57.7 \pm 0.43$	$8.3 \pm 0.1$	$16.1 \pm 0.5$	$0.053 \pm 0.003$	$-32.7 \pm 1.6$
HAp (pH 9)	$17.3 \pm 0.11$	$56.5 \pm 0.28$	$8.1 \pm 0.2$	$15.6 \pm 0.3$	$0.029 \pm 0.004$	$-36.9 \pm 2.5$
HAp-OVA (pH 7)	$19.8 \pm 0.09$	$50.4 \pm 0.27$	$15.5 \pm 0.4$	$21.3 \pm 0.3$	$0.089 \pm 0.002$	$-19.7 \pm 1.3$
HAp-OVA (pH 8)	$18.4 \pm 0.05$	$49.1 \pm 0.41$	$14.4 \pm 0.2$	$19.5 \pm 0.4$	$0.058 \pm 0.002$	$-20.2 \pm 0.7$
HAp-OVA (pH 9)	$16.8 \pm 0.06$	$46.2\pm0.36$	$14.1\pm0.3$	$16.6\pm0.7$	$0.036 \pm 0.003$	$-23.2 \pm 1.1$

60–160 °C, should correspond to the loss of adsorbed water. The second stage, with the onset temperature at about 240 °C, should relate to the loss of tris-base from the HAp structure. The last stage at the onset temperature of about 740 °C was thought to relate to the loss of the remaining organic residues within the HAp structure. As for the HAp-OVA particles, all of the three stages were evident. However, the presence of an additional step at the onset temperature of about 330 °C should correspond to the loss of the incorporated OVA. After the TGA analysis, these HAp and the HAp-OVA particles were reanalyzed by XRD (Fig. 3b). Apparently, the crystalline peaks associated with HAp became much sharper (cf. Fig. 1), indicating further crystallization of HAp during the thermal treatment. Additionally, crystalline peaks that belong to other calcium-based chemical species such as CaO and carbonate apatite became much more evident (cf. Fig. 1). This suggests that parts of the imperfectly-formed HAp entities may undergo thermal decomposition or solid state chemical reaction at high temperatures. Notwithstanding, both the FT-IR and the TGA



**Fig. 3.** (a) TGA curves of (a) pure HAp and (b) HAp–OVA particles that had been obtained at pH 9 and (b) XRD patterns of these particles after having been subjected to the TGA analysis.

2 Theta (degree)

results confirmed the presence of OVA within the structure of the obtained HAp–OVA particles.

The particle size distribution (PSD) curves of the HAp and the HAp-OVA particles that had been obtained at pH 9 are shown in Fig. 4. Based on the PSD results, the HAp and the HAp-OVA primary particles had the average sizes of around 56-59 nm and 46-50 nm, respectively. The average sizes of the HAp and the HAp-OVA primary particles that had been obtained at all pH levels investigated were measured and summarized in Table 1. Apparently, the presence of OVA resulted in significant reduction in the sizes of the obtained HAp primary particles. On the contrary, the average value of the primary particle size decreased slightly with an increase in the pH used during the precipitation process. Both of these should be a result of the increase in the number of nucleation sites, i.e., owing to the presence of OVA in the former and the more availability of the free tris-base molecules in the latter [20]. As for the effect of tris-base, the greater the amount of tris-base used, the greater the number of nuclei, hence the observed reduction in the sizes of the HAp primary particles.

The nano-crystalline structure of the HAp and the HAp-OVA particles that had been obtained at pH 9 was investigated by TEM (see Fig. 5). The rod-like morphology of the obtained HAp crystals, both in the absence and in the presence of OVA, was evident. The TEM results were consistent with the results obtained from the particle size analyzer (i.e., the PSD results), which revealed that the primary particles were in the nanometer range and the presence of OVA led to the reduction in the size of the primary particles. Despite the nano-crystalline nature of the individual primary particles, representative SEM images of the precipitated HAp and HAp-OVA powder that had been obtained at pH 9 (see Fig. 6) revealed the existence of large agglomerates and the extent of the agglomeration was accented by the presence of OVA. In addition, the HAp particles obtained at higher pH values existed as larger aggregates, owing possibly to the increase in the overall crystallization rate (viz. due to the increase in the nucleation rate, earlier mentioned) [21]. Notwithstanding, the existence of such agglomerates could easily be a result of lyophilization during the drying of the powdery products.

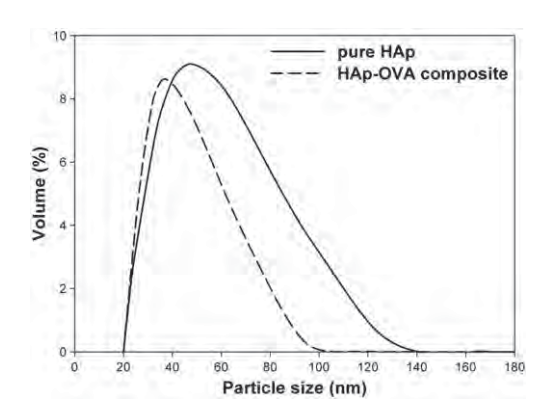
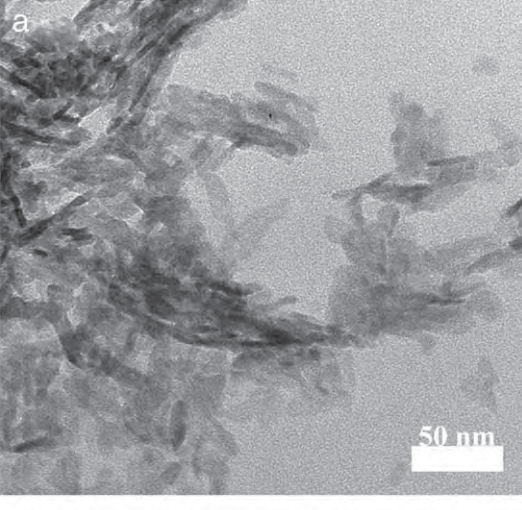


Fig. 4. PSD curves of pure HAp and HAp–OVA particles that had been obtained at pH 9.



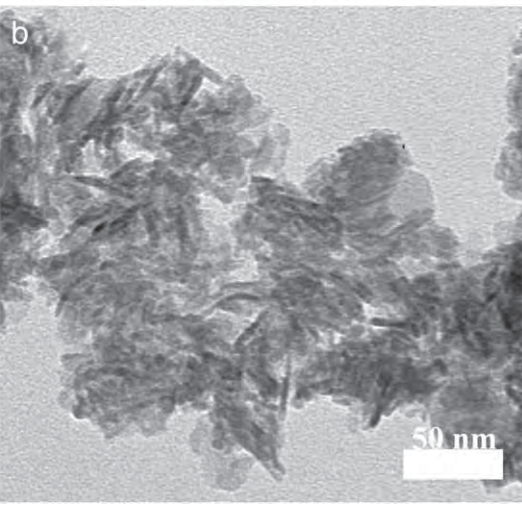
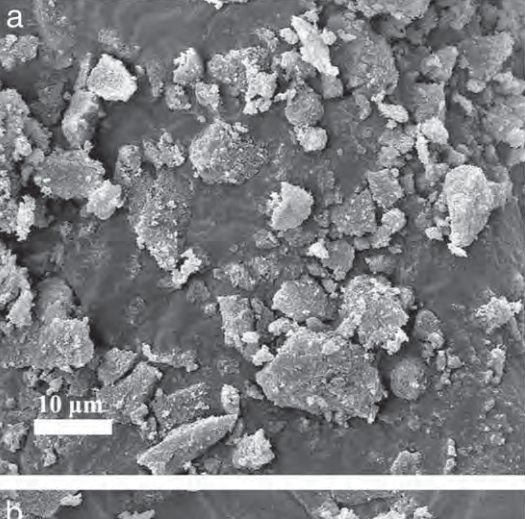
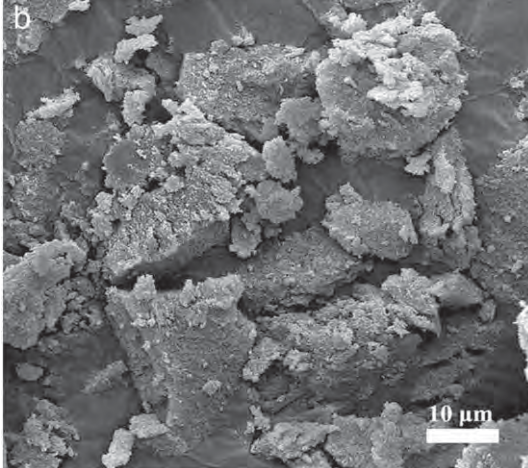


Fig. 5. TEM micrographs of (a) pure HAp and (b) HAp–OVA particles that had been obtained at pH 9.

The N<sub>2</sub> adsorption-desorption isotherms and the pore size distribution as calculated from the adsorption branch of the isotherms based on the Bopp-Jancsó-Heinzinger (BJH) model for the HAp and the HAp-OVA particles that had been synthesized at pH 9 are shown in Fig. 7 and in the inset of the figure, respectively. The isotherms can be categorized as type IV, which can be further categorized into H1-hysteresis loops of mesoporous materials [22]. The average pore sizes of the HAp and the HAp-OVA particles were determined to be about 8.1 nm and 14.1 nm, respectively. The isotherms and the pore size distribution of these two cases were slightly different. For the HAp-OVA particles, the isotherm exhibited a slightly steeper slope with a greater pore volume and the pore size distribution was narrower, owing to the more uniform pore sizes. This indicates that the aggregation of OVA within the HAp structure affected slightly the basic pore structure of the obtained mesoporous HAp particles. The pore diameter and the BET specific average surface area for each of the obtained products are summarized in Table 1. In the absence of OVA within the HAp structure, the pore sizes were 8.1-8.9 nm. Larger pore sizes were observed for the OVA-incorporated HAp particles (i.e., 14.1-15.5 nm). These correspond to the BET specific average surface area values of 15.6-17.2 and 16.6–21.3  $\text{m}^2 \cdot \text{g}^{-1}$ , respectively, and the pore volume values of 0.029–0.079 and 0.036–0.089 cm $^{3} \cdot g^{-1}$ , respectively. These pores were thought to be generated upon the sublimation of the ice crystals formed during the lyophilization step [23,24]. The presence of OVA

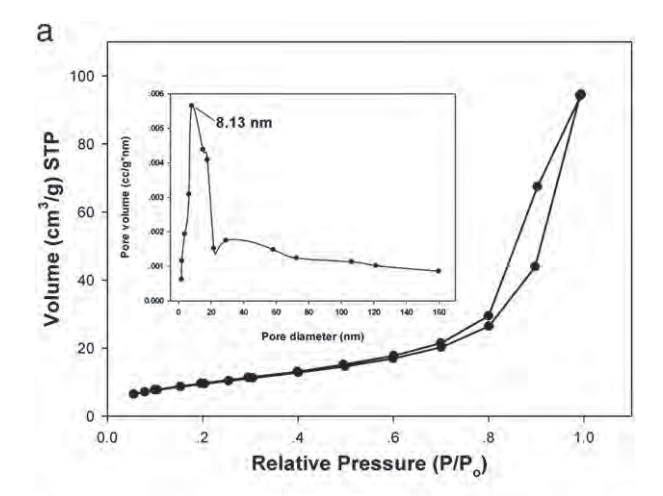




 $\mbox{\bf Fig. 6.} \mbox{ SEM images of (a) pure HAp and (b) HAp-OVA particles that had been obtained at pH 9. } \\$ 

resulted in hypothetical increases in the values of all of the pore parameters of the resulting HAp particles, while the increase in the pH during the precipitation process led to opposing trends. Furthermore, since the characteristic FT-IR bands associated with both HAp and OVA components were not shifted, it is expected that the mesopores may be present as the voids located at the grain boundaries of the aggregates of the rod-like HAp particles.

The  $\zeta$  potentials of the HAp and the HAp–OVA particles were finally measured based on the electrophoretic mobilities of these particles in deionized water. The average values for the HAp particles were in the range of -31.6 to -36.9 mV, while those for the HAp-OVA particles were in the range of -19.7 to -23.2 mV. Evidently, an increase in the pH during the precipitation process caused the  $\zeta$ potentials of the HAp and the HAp-OVA particles to become more negative. It was reported that the  $\zeta$  potentials of commercial HAp particles depended strongly on the pH of the suspending medium [25], in which the values varied from -5 to -37 mV as the pH increased from 5.0 to 8.0. Over the pH levels of 7.0-8.0 however, the  $\zeta$  potentials varied within a small range of -35 to -37 mV. Such a value for commercial HAp particles in phosphate buffer solution (pH = 7.4) was determined to be -36 mV [26]. Clearly, the values of the  $\zeta$  potentials for the HAp particles, as obtained here, agreed particularly well with those reported in the literature. Upon the addition of OVA, which is an acidic protein (cf. isoelectric point = 4.7 [26]) during the precipitation process to obtain the HAp-OVA particles, the  $\zeta$  potentials decreased by about 12 mV on average. This reduction is a clear indication of the adsorption of P. K-hasuwan et al. / Materials Science and Engineering C 32 (2012) 758-762



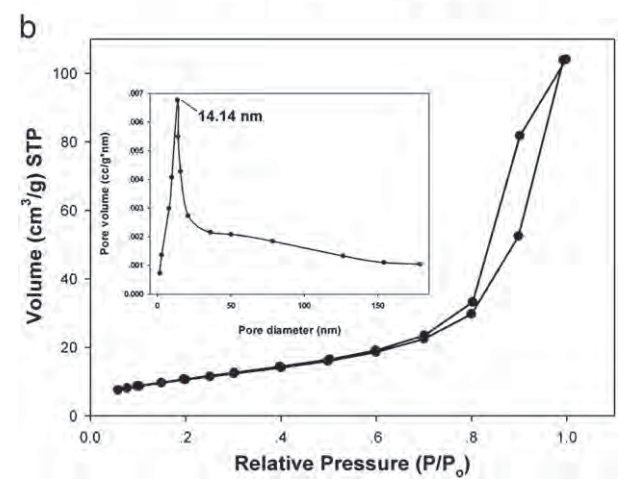


Fig. 7. Adsorption-desorption isotherms of N<sub>2</sub> within the pore structures of (a) pure HAp and (b) HAp-OVA particles that had been obtained at pH 9. The size distribution of the pores as determined based on the Bopp-Jancsó-Heinzinger (BJH) model is shown as the inset.

the protein on the surface of the HAp crystallites. Marginal reduction in the values of the  $\zeta$  potentials of the HAp particles was observed when their surfaces were covered with acidic and neutral proteins, while more significant reduction was observed when their surface was covered with basic proteins [25,26].

#### 4. Conclusions

An economical and simple synthetic route for HAp-OVA particles from discarded egg shells and OVA, as the model incorporating protein, by co-precipitation method was proposed. Both XRD and FT-IR results confirmed the formation of HAp, while PSD and TEM results indicated the formation of discrete HAp nanocrystals, which were rod-like in nature. Both the crystallite sizes (as calculated from breadth of the (002) reflection peak) and the sizes of the individual nanocrystalline particles decreased in the presence of OVA. Electrophoretic analysis indicated that OVA adsorbed readily on the surfaces of the HAp nano-crystallites and this was responsible for their agglomeration into larger particles, as revealed by SEM analysis. The knowledge obtained from the preparation of these HAp-OVA materials could be used as a promising archetype for synthesizing composite particles of HAp and another functional protein for biomedical applications or bone tissue engineering purposes in particular.

#### Acknowledgements

The authors acknowledge the partial support received from 1) The Thailand Research Fund (TRF, grant no.: DBG5280015), 2) The Institute for the Promotion of Teaching Science and Technology (IPST, for the doctoral scholarship of PK), 3) The Petroleum and Petrochemical College (PPC), Chulalongkorn University, and 4) Center of Excellence on Petrochemical and Materials Technology, Chulalongkorn University.

#### References

- [1] T.A. Kuriakose, S.N. Kalkura, M. Palanichamy, D. Arivuoli, K. Dierks, G. Bocelli, C. Betzel, J. Cryst. Growth 263 (2004) 517-523.
- M.S. Djošic, V.B. Miškovic-Stankovic, S. Minlojic, Z.M. Kacarevic, N. Bibic, J. Stojanovic, Mater. Chem. Phys. 111 (2008) 137-142
- K. Ioku, M. Kamitakahara, Phosphorus Res. Bull. 23 (2009) 25-30.
- P.M.S.L. Shanthi, R.V. Mangalaraia, A.P. Uthirakumar, S. Velmathi, T. Balasubramanian, M. Ashok, J. Colloid Interface Sci. 350 (2010) 39-43.
- [5] E.M. Fischer, P. Layrolle, C.A. Van Blitterswijk, J.D. De Bruijn, Tissue Eng. 6 (2003)
- Y.B. Li, W. Tjandra, K.C. Tam, Mater. Res. Bull. 43 (2008) 2318-2326.
- S. Bose, S.K. Saha, Chem. Mater. 15 (2003) 4464-4469.
- S. Bose, S.K. Saha, J. Am. Ceram. Soc. 86 (2003) 1055-1057.
- B. Viswanath, N. Ravishankar, Biomaterials 29 (2008) 4855–4863. [10] H. Wang, L. Zhai, Y. Li, T. Shi, Mater. Res. Bull. 43 (2008) 1607-1614.
- [11] Y.J. Wang, J.D. Chen, K. Wei, S.H. Zhang, X.D. Wang, Mater. Lett. 60 (2006)
- [12] Y.F. Zhau, J. Ma, Microporous Mesoporous Mater. 87 (2005) 110-117.
- Y. Wu, S. Bose, Langmuir 21 (2005) 3232-3234.
- [14] H.S. Zhao, W. He, Y.J. Wang, Y.Z. Yue, X.G. Guo, Z.M. Li, S.P. Yan, W.J. Zhou, X.D. Zhang, Mater. Chem. Phys. 111 (2008) 265–270.
- [15] H.S. Zhao, W. He, Y.J. Wang, X.D. Zhang, Z.M. Li, S.P. Yan, W.J. Zhou, G.C. Wang, Mater. Lett. 62 (2008) 3603-3605.
- E.M. Rivera, M. Araiza, W. Brostow, V.M. Castaño, J.R. Díaz-Estrada, R. Hernández,
- J.R. Rodríguez, Mater. Lett. 41 (1999) 128–134. [17] A.L. Patterson, Phys. Rev. 56 (1939) 978–982.
- Y. Suwa, H. Banno, M. Mizuno, H. Saito, J. Ceram. Soc. Jpn. 101 (1993) 642–647.
- H.S. Zhao, W. He, Y.J. Wang, X.Z. Zhang, Z.M. Li, S.P. Yan, W.J. Zhou, J. Chem. Eng. Data 53 (2008) 2735-2738
- M.C. Chang, C.C. Ko, W.H. Douglas, Biomaterials 24 (2003) 2853-2862.
- W.P. Inskeep, J.C. Silvertooth, Geochim. Cosmochim. Acta 52 (1998) 1883–1893.
- S.J. Gregg, K.S.W. Sing, Adsorption, Surface area and Porosity, Academic Press, London, 1982, pp. 233–238.
- [23] Y. Zhang, K.H. Zuo, Y.P. Zeng, Ceram. Int. 35 (2009) 2151-2154.
- [24] S. Yunoki, T. Ikoma, A. Monkawa, M. Kikuchi, S. Sotome, K. Shinomiya, J. Tanaka, Mater. Lett. 60 (2006) 999-1002.
- M. Matsumoto, T. Miyake, H. Noshi, M. Kambara, K. Konishi, Colloids Surf. 40 (1989) 77-84.
- [26] K. Kawasaki, M. Kambara, H. Matsumura, W. Norde, Colloids Surf. B Biointerfaces 32 (2003) 321-334

# Comparative Study of Protein Carriers Based on Hydroxyapatite Particles for Bone Tissue Engineering

Prae-ravee K-hasuwan<sup>a,b</sup>, Neeranut Kuanchertchoo<sup>c</sup>, Prasit Pravasant<sup>d</sup>, Pitt Supaphol<sup>a,b,\*</sup>

<sup>a</sup> The Petroleum and Petrochemical College, Chulalongkorn University, Bangkok, 10330,

### Thailand

<sup>b</sup> The Center for Petroleum, Petrochemicals and Advanced Materials, Chulalongkorn
University, Bangkok 10330, Thailand

<sup>c</sup> Department of Materials Technology, Faculty of Science, Ramkhamhaeng University,

Bangkok, 10240, Thailand

<sup>d</sup> Department of Anatomy, Faculty of Dentistry, Chulalongkorn University, Bangkok, 10330,

Thailand

### **ABSTRACT**

Different starting materials (natural and chemical substances) were employed for synthesizing hydroxyapatite (HAp) particles as a protein carrier. Egg albumin (OVA), the main constituent of egg white with high functionality including modifying HAp properties, was used as a model protein. HAp particles were prepared via a co-precipitation method with various amounts of OVA (1g, 2g, and 3g/500 ml distilled water) and pH conditions (pH 7 and pH 9); also, the chemical properties of the obtained HAp particles were investigated. The incorporated and released amounts of OVA from the HAp particles were examined. Both incorporated and released OVA contents slightly increase with increasing the initial amount of OVA, but significantly increase with lowering pH value. Besides, a larger number was observed in the obtained carriers synthesized from the chemical starting material compared to the natural one. The release profiles demonstrated a slowly releasing behavior within 21 days,

2

followed by a plateau release without the initial bursting, suggesting that the OVA release

was clearly prolonged by the incorporation. This release characteristic could be promising for

bone tissue engineering applications.

Keywords: Protein carriers; Hydroxyapatite; Egg albumin; Bone tissue engineering

\* Corresponding author. Postal Address: The Petroleum and Petrochemical College

Chulalongkorn University, Soi Chula 12, Phyathai Road, Pathumwan, Bangkok 10330,

Thailand. Tel.: +66-2-218-4131; fax: +66-2-215-4459.

E-mail address: pitt.s@chula.ac.th (P. Supaphol)

#### 1. Introduction

To be bone substitutes as orthopedic or dental prostheses, artificial materials with the chemical and morphological similarity to the natural bone are required [1,2]. A large number of biomaterials have been widely investigated as the synthetic bone substitutes [3]. Owing to its mineral phase resemblance to human bone, Hydroxyapatite (HAp), one of calcium phosphate (CaP) based ceramic materials, has been applied in various medical applications such as dental implants, drug delivery systems, and so forth. More importantly, this bioactive ceramic is the best for inducing osteogenesis and new bone formation in soft tissues [4,5].

Considering the several utilizations of HAp in clinical fields, many preparation methods of HAp particles, including electrochemical synthesis [6], reflux procedure [7], capillary microfluidic technique [8], hydrothermal treatment [9], microemulsion route [10], precipitation [11,12], and sol-gel approach [13] have been reported. Besides, numerous biosurfactants have also been presented to be efficient templates for particle size, shape, and morphology. For instance, yeast cells, sucrose, and even proteins were employed as template materials to improve the surface area and the formation of the HAp particles [13-15]. Among them, the proteins have been documented to have better biocompatibility and more sufficient hemostatic properties [16]. Thus, extensive studies in combining of proteins on apatite forms have been indicated to analyze the release characteristics for enhancing osteoinduction [17]. Egg albumin (OVA), a stable and inexpensive protein readily extracted from egg white, can lead to either controlled HAp growths or modified HAp properties. With its functional groups, this phosphoglycoprotein has strong negative dipoles to chelate the free Ca<sup>2+</sup> cations in calcium phosphate solution [18]. Hence, it is of interest to incorporate OVA during HAp formation to generate protein carriers for the release applications.

Herein, we performed two kinds of starting materials with various OVA contents and pH values through a simple co-precipitation method for OVA-incorporated HAp (HAp-OVA) synthesis. Firstly, we purpose egg shells (CaO) as a calcium source and H<sub>3</sub>PO<sub>4</sub> as a phosphorous source. Secondly, Calcium carbonate (CaCO<sub>3</sub>) and Calcium hydrogen phosphate dihydrate (CaHPO<sub>4</sub>.2H<sub>2</sub>O) were used as calcium and phosphorous sources, respectively. The comparative studies of these two cases OVA carriers were evaluated. Also, the incorporation capacities and release kinetics of OVA were examined.

# 2. Experimental procedure

# 2.1. Materials

All chemical reagents including Calcium hydrogen phosphate dihydrate (CaHPO<sub>4</sub>.2H<sub>2</sub>O, A.R. grade, Fluka), Calcium carbonate (CaCO<sub>3</sub>, A.R. grade, Carlo Erba), Nitric acid (HNO<sub>3</sub>, A.R. grade, Labscan), Phosphoric acid (H<sub>3</sub>PO<sub>4</sub>, A.R. grade, Labscan), Tris (hydroxymethyl)-aminomethane (tris-base, A.R. grade, Sigma), and Egg albumin (OVA, grade II, Sigma) were used without further purification. CaO from egg shells was prepared following the previous report of Rivera *et al.* [19].

# 2.2. Synthesis of hydroxyapatite

HAp was prepared by co-precipitation method. In the typical procedure, 2.00 g of CaHPO<sub>4</sub>.2H<sub>2</sub>O (as a phosphorous source) and 0.79 g of CaCO<sub>3</sub> (as a calcium source) were dissolved in 1 M HNO<sub>3</sub> 25 ml under gentle stirring at 70 °C for 2 h and the pH of the solution was kept to 2. OVA, subsequently, was added in the amount of 0, 1, 2, and 3 g/ 500 ml of the

mixed solution at room temperature. 200 ml of 1 M and 2 M tris-base solution were then poured into the mixture generating the precipitation at pH 7 and pH 9, respectively. The precursor solution was stirred vigorously to yield a homogeneous product. The product was then filtered off and washed several times with deionized water. After centrifugation, the resulting material was freeze-dried for 48 h to obtain the fine powder products. The similar process with the use of 1.25 g of CaO and 1.50 g of H<sub>3</sub>PO<sub>4</sub> as calcium and phosphorous sources respectively was performed for comparison. With many synthetic conditions above, the sample names were specified as shown in Table 1.

# 2.3. Release kinetics of OVA from HAp particles

About 20 mg of HAp-OVA particles were immersed in 10 ml phosphate buffer solution at pH 7.4, in which matches the normal body and blood system of a human being. The controlled release systems were shaken in the water bath with a stirring rate of 70 rpm at 37 °C. The amount of released OVA in the supernatant was measured at various times by UV-VIS spectrophotometer (UV-1800) at the wavelength of 280 nm through the use of a predetermined standard calibration curve. Furthermore, the gravimetric analysis was used to confirm the amounts of OVA loss again after 21 days.

#### 2.4. Characterization

The crystallographic phases of the HAp-OVA particles were analyzed by X-ray diffractometer (WDXRD, D/MAX 2000 series Rigaku) with an incident X-ray wavelength of 1.54 Å (Cu K $\alpha$  line) at the scanning rate of 0.02° per minute over a range of 2 $\theta$  from 5° to 60° with JCPDS database (9-432). Fourier transform infrared (FT-IR) spectrograph carried

out on a Nicolet Nexus spectrometer (NEXUS 670, Nicolet) was performed using the KBr pellet technique, working in the wavelength from 4000 to 400 cm<sup>-1</sup>. The structural morphology images were recorded on a transmission electron microscope (TEM, JEM-2100, JEOL) with an acceleration voltage of 200 kV. Energy dispersive X-ray (EDX) element analysis of the samples was also investigated with scanning electron microscope (SEM, JSM-5410LV, JEOL) operated at 15 kV. The average pore diameters of the obtained particles were taken on autosorb-1 instrument (AS-1, Quantachrome) using physisorption of nitrogen at temperature of 77 K. Thermogravimetric analysis (TGA, TGA7, Perkin Elmer) was carried out on the dried samples (5 mg) to examine the relative amount of OVA associated with HAp particles with a heating rate of 10 °C /min under a flowing air atmosphere.

# 2.5. Statistical Analysis

All quantitative examinations were collected in triplicate and the results were presented as means and standard deviations. Significance between the mean values was determined by ANOVA one-way analysis using Tukey's test for variances at a 95% confidence level.

#### 3. Results and discussion

# 3.1. Material characterization

The formation of HAp particles was ascertained by X-ray diffraction (XRD) analysis. The XRD patterns of the HAp-OVA particles with particular peaks ascribed to the lattice constant of HAp according to the JCPDS database (9-432) were given in the comparative

chart of Fig. 1. From these results, the presence of the OVA during the synthesis does not have an influence on the structural development of HAp. Besides, no difference in HAp-OVA characteristic diffraction peaks was perceived for all synthetic cases given above. These XRD data also show poorly-crystallized traces of the powders due to water sublimation in the freeze-drying process [20], resulting in estimated crystallite sizes. Calculations of the crystallite size using the Scherrer equation were performed for the (002) reflection peak corresponding to  $2\theta = 26^{\circ}$  because of well resolved characteristics [21]. The mean sizes of crystallites are within the range of 16-20 nm.

Fig. 2 exhibits the FT-IR spectra of the HAp-OVA particles. The IR spectra of pure OVA and HAp are also shown for comparison. The OVA spectrum displayed the typical bands at 3299 cm<sup>-1</sup>, 1652 cm<sup>-1</sup>, 1539 cm<sup>-1</sup>, and 1457 cm<sup>-1</sup> represented to the nitrogen-hydrogen stretch (N-H), the carbonyl vibration (C=O), the carbon-nitrogen vibration (C-N), and the stretching vibration of carbon-hydrogen (C-H), respectively [15]. The spectrum of pure HA demonstrates the adsorption bands at 3569 cm<sup>-1</sup> assigned to OH stretching, 1630 cm<sup>-1</sup> assigned to OH vibration of the apatitic group, 1035 cm<sup>-1</sup> assigned to PO<sub>4</sub><sup>3-</sup> stretching vibration, as well as 601 cm<sup>-1</sup> and 563 cm<sup>-1</sup> assigned to PO<sub>4</sub><sup>3-</sup> deformation vibration [22,23]. The bands at 1654 cm<sup>-1</sup> and 1539 cm<sup>-1</sup> of HAp-OVA spectra, therefore, ascertained that OVA was incorporated in HAp particles.

EDX analysis was performed to give further confirmation of a molar Ca/P ratio of the samples. The EDX characteristic peaks indicated the existence of calcium (Ca), phosphorous (P), and oxygen (O) with proportional counts (Fig. 3). The molar Ca/P ratio of all samples revealed that the obtained samples synthesized by using the chemical starting material have the Ca/P ratio of 1.67-1.68 very close to the ideal one of 1.67 for HAp in human bone, while the Ca/P ratio measured for the obtained samples synthesized from the natural starting

material are within the range 1.62-1.65. On the other hand, there were not statistically significant differences for the Ca/P ratio of both starting materials (p > 0.05).

The HAp-OVA particles were also examined by transmission electron microscopy (TEM). The TEM micrographs of the samples synthesized from both natural and chemical substances at pH 7 and pH 9 with 1 g OVA show little difference in morphology (Fig. 4). In all obtained specimens, the primary particles have a rod-like shape with dimensions of 3-10 nm in diameter and 15-30 nm in length. However, it was noticed that the sizes of primary particle slightly increase with a higher OVA content and a lower pH condition.

# 3.2. Incorporation of OVA into HAp particles

The physi-sorption of nitrogen was performed to collect the average pore diameters of the pure HAp and HAp-OVA particles (see Table 2). The average pore sizes of HAp particles with the presence of OVA are larger than those of the absence ones, suggesting the incorporation of OVA within HAp particles by bond formation. The mechanism was that the carbonyl group and the phosphorous group of OVA have negative dipoles which could chelate the free Ca<sup>2+</sup> ions; subsequently, the PO<sub>4</sub><sup>3-</sup> ions may bond with OVA-associated calcium to generate HAp-OVA aggregates [18]. OVA, furthermore, could be adsorbed on the HAp surfaces by the crystal surface area available for growth [24]. When considering HAp-OVA particles, their average pore diameters at lower pH are bigger than those at higher pH. At the same pH, the chemical starting material shows the higher values of the average pore diameter compared with the natural one. The average pore diameters, nevertheless, are quite similar in cases of varying initial OVA contents. Therefore, it could be assumed that difference in these initial amounts of added OVA has a little influence on the average pore size.

For thermal behavior, TGA profiles of the obtained HAp and HAp-OVA powders prepared in several conditions are presented in Fig. 5. The mass loss could be differentiated into four regions in the investigated temperature range of (1) 60-200°C, (2) 200-400 °C, (3) 400-780 °C, and (4) 780-1200 °C. The mass loss below 200 °C was attributed to the loss of adsorbed water. From 200-400 °C, an obvious mass loss was detected due to the loss of trisbase (endothermic peak around 240°C), OVA (endothermic peak around 330°C), and other absorbed species. The mass loss between 400 and 780°C corresponded to the decomposition of remained organic residues was rather small for all particulate HAp samples. Above 780 °C, a very small transition was mainly attributed to the weight loss of carbonate. The amounts of incorporated OVA within HAp particles based on the total amount of 5 mg of the dried samples shown in Table 2 could be determined from these TGA results by subtracting pure HAp content. For all obtained specimens, the mass loss slightly increased when increasing the initial amounts of OVA, which meant that the amounts of incorporated OVA did not significantly increase with the increase of the initial OVA contents (p > 0.05). However, a larger quantity of incorporated OVA was noticed in the HAp particles synthesized from the chemical starting material compared to those prepared from the natural one. The startingmaterial type, therefore, caused honestly significant differences in the incorporated OVA content (p < 0.05). A lower pH in the synthesis procedure resulted in a significantly greater amount of incorporated OVA for both starting materials (p < 0.05) because there is the electrostatic repulsion force between OVA and HAp, which predominates in a higher pH solution (pH 9) compared to a lower pH solution (pH 7). As a result, increasing pH solution brought about a decreased amount of incorporated OVA [25].

# 3.2. Controlled release of OVA

The OVA release experiments carried out in PBS (pH 7.4) to simulate the local pH of the homeostatic body fluid were performed for all particulate HAp and HAp-OVA. The OVA release profiles and its release amounts based on the incorporated OVA amounts all the obtained particles are shown in Fig. 6 and Table 2, respectively. It was found that the obtained particles prepared from both starting materials demonstrated a slow release behavior increased time dependently within 21 days; a plateau release was then followed and the burst release was not observed. The OVA release profiles, suggesting a single-stage release mechanism, were assigned to the OVA molecules incorporated into HAp particles (OVA-HAp complex) [25]. The complex was formed by the adsorption of OVA on the Ca-site of HAp by ionic interaction between carboxyl acid groups on OVA and the positively charged Ca-sites. Phosphate ions from PBS can be also adsorbed onto the Ca-sites, so the competition between acidic protein molecules and phosphate ions occurs, resulting in the desorption of OVA from the HAp particles [26,27]. The sustained release profiles of OVA, moreover, can be possibly attributed to the formation of porous structure of HAp particles. About 50-54% and 38-41% of loaded OVA was released from the HA particles synthesized by using the natural starting material after 35 days in pH 7 and 9, respectively. A more sustained OVA release was fulfilled for the HAp particles prepared from the chemical starting material. Around 57-62% and 42-44% of loaded OVA was release out after the same period for pH 7 and 9, respectively. Hence, the OVA releases from the chemical starting material were significantly greater than those from the natural one (p < 0.05). The higher OVA releases were also noticed in pH 7 significantly than those in pH 9 (p < 0.05) because of a smaller adding amount of tris-base leading to a looser and weaker bond formation. Thereby, the quantity of OVA release considerably relies on the pH condition and the type of the starting material. All of the release patterns also reveal the OVA incomplete release owing to OVA instability problems such as non-specific adsorption and aggregation [28]. The HAp particles

with the presence of higher initial OVA amount manifest a little higher OVA-release percentage, depending on the incorportaed OVA content, so the OVA release amount was not significantly dependent on the initial amount of added OVA (p > 0.05).

### 4. Conclusions

Protein carriers based on HAp were designed as potential devices for the controlled release system. HAp-OVA particles were obtained by the co-precipitation method with varying the starting material, pH value, and initial amount of OVA. The incorporated and released OVA amounts highly increased with lowering pH value to be neutral and slightly increased with increasing initial OVA content. A greater OVA incorporation and release were also observed in the HAp-OVA particles synthesized from the chemical starting material compared to those prepared from the natural one. All of the release kinetics exhibited a slow release in a sustained manner without initial OVA burst, resulting in prolonged release behavior. Consequently, it may be practicable to use these HAp particles with other protein drugs and growth factors as effective carries to achieve specific targets for bone tissue engineering applications.

# Acknowledgements

The authors acknowledge the partial support received from 1) the Thailand Research Fund (TRF), 2) Development and Promotion of Science and Technology talents project (DPST), and 3) The Petroleum and Petrochemical College (PPC), Chulalongkorn University.

#### References

- [1] I. Sopyan, M. Mel, S. Ramesh, K.A. Khalid, Porous hydroxyapatite for artificial bone applications, Sci. Technol. Adv. Mater. 8 (2007) 116-123.
- [2] G. Carutenuto, G. Spagnuolo, L. Ambrosio, L. Nicolais, Mesoporous hydroxyapatite as alloplastic material for dental applications, J. Mater. Sci.: Mater. Med. 10 (10/11) (1999) 671-676.
- [3] T. Kokubo, H.M. Kim, M. Kawashita, Novel bioactive materials with different mechanical properties, Biomaterials 24 (2003) 2161-2175.
- [4] H.N. Wang, Y.B. Li, Y. Zuo, J.H. Li, S.S. Ma, L. Cheng, Biocompatibility and osteogenesis of biomimetic nano-hydroxyapatite/polyamide composite scaffolds for bone tissue engineering, Biomaterials 28 (2007) 3338-3348.
- [5] A. Krisanapiboon, B. Buranapanitkit, K. Oungbho, Biocompatibility of hydroxyapatite composite as a local drug delivery system, J. Orthop. Surg. 14 (3) (2006) 315-318.
- [6] M.S. Djosic, V.B. Miskovic-Stankovic, S. Milonjic, Z.M. Kacarevic-Popovic, N. Bibic, J. Stojanovic, Electrochemical synthesis and characterization of hydroxyapatite powders, Mater. Chem. Phys. 111 (2008) 137-142.
- [7] F. Ye, H.F. Guo, H.J. Zhang, Biomimetic synthesis of oriented hydroxyapatite mediated by nonionic surfactants, Nanotechnology 19 (2008) 245605.
- [8] H.C. Shum, A. Bandyopadhyay, S. Bose, D.A. Weitz, Double emulsion droplets as microreactors for synthesis of mesoporous hydroxyapatite, Chem. Mater. 21 (22) (2009) 5548-5555.
- [9] Y.J. Wang, J.D. Chen, K. Wei, S.H. Zhang, X.D. Wang, Surfactant-assisted synthesis of hydroxyapatite particles, Mater. Lett. 60 (2006) 3227-3231.

- [10] G.C. Koumoulidis, A.P. Katsoulidis, A.K. Ladavos, P.J. Pomonis, C.C. Trapalis, A.T. Sdoukos, T.C. Vaimakis, Preparation of hydroxyapatite via microemulsion route, J. Colloid Interface Sci. 259 (2003) 254-260.
- [11] C. Santos, R.P. Franke, M.M. Almeida, M.E.V. Costa, Nanoscale characterization of hydroxyapatite particles by electron microscopy, Microsci. Microanal. 14 (2008) 67-70.
- [12] B. Viswanath, N. Ravishankar, Controlled synthesis of plated-shape hydroxyapatite and implications for the morphology of the apatite phase in bone, Biomaterials 29 (2008) 4855-4863.
- [13] S. Bose, S.K. Saha, Synthesis of hydroxyapatite nanopowders via sucrose-templated solgel method, J. Am. Ceram. Soc. 86 (6) (2003) 1055-1057.
- [14] W. He, Z.M. Li, Y.J. Wang, X.F. Chen, X.D. Zhang, H.S. Zhao, S.P. Yan, W.J. Zhou, Synthesis of mesoporous structured hydroxyapatite particles using yeast cells as the template, J. Mater. Sci.: Mater. Med. 21 (1) (2010) 155-159.
- [15] H.S. Zhao, W. He, Y.J. Wang, X.D. Zhang, Z.M. Li, S.P. Yan, W.J. Zhao, Biomimetic synthesis and characterization of hydroxyapatite crystal with low phase transformation temperature, J. Chem. Eng. Data 53 (2008) 2735-2738.
- [16] M. Sivakumar, K.P. Rao, Preparation, characterization and in vitro release of gentamicin from coralline hydroxyapatite-gelatin composite microsphere, Biomaterials 23 (2002) 3175-3181.
- [17] Y. Liu, P. Layrolle, J. de Bruijn, C.V. Blitterswijk, K. de Groot, Biomimetic coprecipitation of calcium phosphate and bovine serum albumin on titanium alloy, J. Biomed. Mater. Res. 57 (3) (2001) 327-335.
- [18] H.S. Zhao, W. He, Y.J. Wang, X.D. Zhang, Z.M. Li, S.P. Yan, W.J. Zhou, G.C. Wang, Biomineralization of large hydroxyapatite particles using ovalbumin as biosurfactant, Mater. Lett. 62 (2008) 3603-3605.

- [19] E.M. Rivera, M. Araiza, W. Brostow, V.M. Castano, J.R. Diaz Estra, R. Hernandez, J.R. Rodriguez, Synthesis of hydroxyapatite from egg shells, Mater. Lett. 41 (1999) 128-134.
- [20] S. Jalota, S.B. Bhaduri, A.C. Tas, A new rhenanite (β-NaCaPO<sub>4</sub>) and hydroxyapatite biphasic biomaterial for skeletal repair, J. Biomed. Mater. Res. Part B.: Appl. Biomater. 80 (2007) 304-316.
- [21] V.M. Suru, C.H. Ng, M. Wilke, B. Tiersch, P. Fratzl, M.G. Peter, Size-controlled hydroxyapatite nanoparticles as self-organized organic-inorganic composite materials, Biomaterials 26 (2005) 5414-5426.
- [22] Y. Suwa, H. Banno, M. Mizuno, H. Saito. Synthesis of compositionally regulated hydroxyapatite from Ca(OH)<sub>2</sub> and H<sub>3</sub>PO<sub>4</sub>, J. Ceram. Soc. Japan, Int. Edition 101 (1993) 642-647.
- [23] Q.G. Xu, Y. Tanaka, J.T. Czernuszka, Encapsulation and release of a hydrophobic drug from hydroxyapatite coated liposomes, Biomaterials 28 (2007) 2687-2694.
- [24] K. IJntema, W.J.M. Heuvelsland. C.A.M.C. Dirix, A.P. Sam, Hydroxyapatite microcarriers for biocontrolled release of protein drugs, Inter. J. Pharmaceutics 112 (1994) 215-224.
- [25] T.Y. Liu, S.Y. Chen, D.M. Liu, S.C. Liou, On the study of BSA-loaded calcium-deficient hydroxyapatite nano-carriers for controlled drug delivery, J. Control. Release 107 (2005) 112-121.
- [26] T. Kawasaki, M. Niikura, Y. Kobayashi, Fundamental study of hydroxyapatite high-performance liquid chromatography: II. Experimental analysis on the basis of the general theory of gradient chromatography, J. Chromatogr. 515 (1990) 91-123.
- [27] T. Akasawa, M. Kobayashi, Surface characteristics of hydroxyapatite controlling albumin adsorption behavior, J. Mater. Sci. Lett. 15 (1996) 1319-1320.

[28] H.K. Kim, T.G. Park, Comparative study on sustained release of human growth hormone from semi-crystalline poly(L-lactic acid) and amorphous poly(D,L-lactic-co-glycolic acid) microsphere: morphological effect on protein release, J. Control. Release 98 (2004) 115-125.

**Table 1**Experimental conditions of HAp and HAp-OVA particles

Starting materials	Initial amounts of OVA (g)	pH conditions	Sample names
CaCO <sub>3</sub>	-	7	0D-7
+	1	7	1D-7
CaHPO <sub>4</sub> .2H <sub>2</sub> O	2	7	2D-7
	3	7	3D-7
	-	9	0D-9
	1	9	1D-9
	2	9	2D-9
	3	9	3D-9
CaO (Egg shells)	-	7	0E-7
+	1	7	1E-7
$H_3PO_4$	2	7	2E-7
	3	7	3E-7
	-	9	0E-9
	1	9	1E-9
	2	9	2E-9
	3	9	3E-9

Table 2

Physico-chemical characteristics of HAp and HAp-OVA particles

Samples	Average pore	-	ated OVA		ased OVA
	diameter (nm)	amounts		amounts	
		(%)*	(mg)*	(%)#	(mg)#
0D-7	$9.43 \pm 0.02$	-	-	-	-
1D-7	$16.4 \pm 0.15$	$8.01 \pm 0.92$	$0.40 \pm 0.08$	$57.5 \pm 3.71$	$0.92 \pm 0.04$
2D-7	$16.8 \pm 0.11$	$9.32 \pm 0.37$	$0.47 \pm 0.03$	$60.0 \pm 4.10$	$1.12 \pm 0.07$
3D-7	$16.9 \pm 0.07$	$9.94 \pm 0.96$	$0.49 \pm 0.08$	$62.0 \pm 3.82$	$1.23 \pm 0.06$
0D-9	$8.69 \pm 0.14$	-	-	-	-
1D-9	$13.7 \pm 0.18$	$7.54 \pm 0.83$	$0.38 \pm 0.07$	$42.1 \pm 2.73$	$0.63 \pm 0.04$
2D-9	$14.2 \pm 0.06$	$7.99 \pm 0.68$	$0.40 \pm 0.06$	$43.7 \pm 2.90$	$0.70 \pm 0.05$
3D-9	$14.8 \pm 0.03$	$8.21 \pm 0.74$	$0.41 \pm 0.07$	$44.0 \pm 1.95$	$0.72 \pm 0.03$
0E-7	$8.91 \pm 0.19$	-	-	-	-
1E-7	$15.0 \pm 0.14$	$6.17 \pm 0.45$	$0.31 \pm 0.04$	$50.1 \pm 3.06$	$0.62 \pm 0.05$
2E-7	$15.3 \pm 0.27$	$7.61 \pm 0.33$	$0.38 \pm 0.03$	$52.6 \pm 2.81$	$0.80 \pm 0.04$
3E-7	$15.6 \pm 0.29$	$8.89 \pm 0.87$	$0.44 \pm 0.07$	$54.2 \pm 3.66$	$0.96 \pm 0.06$
0E-9	$8.18 \pm 0.03$	-	-	-	-
1E-9	$13.5 \pm 0.22$	$5.24 \pm 0.72$	$0.26 \pm 0.06$	$38.8 \pm 1.13$	$0.41 \pm 0.02$
2E-9	$13.9 \pm 0.26$	$6.01 \pm 0.79$	$0.30 \pm 0.08$	$40.3 \pm 2.09$	$0.48 \pm 0.03$
3E-9	$14.3 \pm 0.15$	$6.93 \pm 0.44$	$0.35 \pm 0.04$	$40.8 \pm 1.84$	$0.56 \pm 0.03$

<sup>\*</sup> based on around 5 mg of total weight of the particle analyzed from TGA

<sup>#</sup> based on the incorporated OVA amounts into 20 mg of total weight of the particle

# **Captions of Figures**

- **Fig. 1.** XRD patterns of HAp-OVA particles prepared under various conditions: (a) 1D-7, (b) 1D-9, (c) 1E-7, (d) 1E-9.
- **Fig. 2.** FT-IR spectra of pure HAp: (a) 0D-7, HAp-OVA particles synthesized under different starting materials and pH conditions: (b) 1D-7, (c) 1D-9, (d) 1E-7, (e) 1E-9, and as-received OVA in its dry state (f).
- Fig. 3. EDX analysis of HAp-OVA particles: (a) 1D-7, (b) 1D-9, (c) 1E-7, (d) 1D-9.
- **Fig. 4.** TEM micrographs of HAp-OVA particles synthesized under different conditions: (a) 1E-7, (b) 1E-9, (c) 1D-7, (d) 1D-9.
- **Fig. 5.** TGA profiles of the obtained HAp and HAp-OVA particles synthesized at various conditions.
- **Fig. 6.** OVA release profiles of the obtained HAp and HAp-OVA particles synthesized under different conditions.

# Polycaprolactone Fibrous Membranes Modified with Gelatin, Bovine Serum Albumin or Crude Bone Protein Extract and Their Potential for Use as Bone Scaffolds.

Sutthilak Chaichamnarn, Prasit Pavasant, and Pitt Supaphol 1,\*

#### 1. ABSTRACT

Immobilization of biomolecules; i.e. gelatin type-A, gelatin type-B, bovine serum albumin (BSA) and crude bone protein (CBP), making polycaprolactone (PCL) fibrous scaffolds that have been fabricated by electrospinning more suitable for bone tissue engineering. PCL scaffolds were first covalently introduced with amino groups on their surfaces through the aminolysis reaction using 1,6-hexamethylenediamine (HMD) and later immobilized with the above mentioned biomolecules using disuccinimidyl carbonate (DSC) as the coupling agent. Various techniques; ATR-FTIR, XPS, SEM, and water contact angle measurement were used to monitor the scaffold surfaces after each modification step. The potential use of the modified materials as bone scaffolds was evaluated with a murine preosteoblastic cell line (MC3T3-E1). MC3T3-E1 proliferation was improved remarkably on the modified surface, especially the BSA-immobilized PCL fibrous scaffolds which showed the greatest proliferation after cell culture as well as the highest ALP activity. In mineralization, the deposited minerals was highest on the CBP-immobilized PCL scaffolds. All the obtained results suggested that immobilization of BSA and CBP is an attractive method for fabricating of fibrous scaffolds for bone tissue engineering.

Keywords: Polycaprolactone / Immobilization/ Bovine serum albumin/

Crude bone proteins / X-ray Photospectroscopy / Contact

angle

#### 2. INTRODUCTION

Tissue engineering is the new approach field of science that applies the principles of engineering and the life sciences towards the development of biological substitutes that restore, maintain, or improve tissue function. In contrast to classic biomaterial approach, Tissue engineering is based on the

<sup>&</sup>lt;sup>1</sup> The Petroleum and Petrochemical College and The Center for Petroleum, Petrochemicals and Advanced Materials (C-PPAM), Chulalongkorn University, Bangkok 10330, Thailand

<sup>&</sup>lt;sup>2</sup> Department of Anatomy, Faculty of Dentistry, Chulalongkorn University, Bangkok 10330, THAILAND

<sup>\*</sup> Authors to whom correspondence should be addressed: pitt.s@chula.ac.th (P. Supaphol)

understanding of tissue formation and regeneration, and aims to regenerate new functional tissues, rather than just to implant new spare parts (Salgado *et al.*, 2004). Therefore, harvested cells, signalling molecules (e.g. protein, and growth factor) and biocompatible scaffolds are the main components of tissue engineering. For the restoration of large tissue defects, scientific efforts have demonstated the utility of implanting tissue scaffolds, to which allow cell attachment, growth and proliferation. In bone tissue engineering need to develop a suitable bone scaffold with sufficient mechanical strength and porosity to allow the ingrowth of new tissue, enhancing growth and proliferation results in good integration with surrounding tissue. Accordingly, the following discussion examines novel, degradable, polymeric scaffolds developed to act as a temporary matrix for cell growth and extracellular matrix deposition, with consequent bone in-growth until the new bony tissue is totally restored or regenerated (Hutmacher D. W., 2000).

Thermoplastic aliphatic polyesters such as polylactide, polyglycolide, polycaprolactone and especially the copolymers of lactide and glycolide such as poly(lactide-co-glycolide) have generated interest for bone regeneration because of their excellent biocompatibility, biodegradability, and mechanical strength. PCL was chosen as a model polymer due to its lack of toxicity, low cost and slow degradation.(Yoshimoto *et al.*, 2003) The challenge in tissue engineering is the design of scaffolds that can mimic the structure and biological functions of the natural extracellular matrix (ECM). Electrospinning has drawn a lot of attention recently as a suitable method to fabricate scaffolds, owing to its simple process, its increased surface areas, ability to mimic the extracellular matrix (Venugopal *et al.*, 2008), its versatility to create fibrous scaffolds from a wide range of starting materials, and as a carrier to deliver clinically relevant proteins like growth factors.

It has been known that certain surface characteristics of polymer can influence the interactions between cells and material. The hydrophobic surface of PCL was not adequate for cell attachment and growth. Therefore, it is important to develop different physical and/or chemical methods to modify the scaffold surface for cytocompatibility improvement for cell

attachment and proliferation. It has been reported that several methods (such as plasma treatment, ozone or photoinduced grafting and surface oxidation) have been employed to introduce hydrophilic compounds onto polymeric scaffold surfaces. Moreover, biomaterials can be coated with extracellular matrix (ECM) proteins (such as collagen, fibronectin, laminin), which usually have promoted cell adhesion and proliferation (Zhu *et al*, 2002).

In this study, PCL scaffolds were prepared by electrospinning techniques followed by immobilization of gelatin, bovine serum albumin (BSA), and crude bone protein extracted from pork bone via chemical surface modification method to promote cell behavior including their adhesion, growth, differentiation. The potential use of these electrospun fibrous scaffolds was further evaluated *in vitro* with MC3T3-E1 in terms of cytotoxicity, attachment, proliferation, alkaline phosphatase activity (ALP), and mineralization of the cells that were cultured directly on the scaffolds, in comparison to those of the cells on a tissue-culture polystyrene plate (TCPS).

#### 3. EXPERIMENTAL SECTION

#### a. Materials

# Materials used in the Fibrous Scaffolds Preparation and Surface Modification

- Poly( $\epsilon$ -caprolactone) (PCL) (M<sub>n</sub> = 80,000 g/mol; Aldrich, USA)
- Dichloromethane (DCM; Lab-Scan (Asia), Thailand)
- *N,N'*-dimethylformamide (DMF; Lab-Scan (Asia), Thailand)
- 1,6-hexamethylenediamine (HMD; Aldrich, USA)
- *N,N'*-disuccinimidyl carbonate (DSC; Aldrich, USA)
- Ninhydrin (Aldrich, USA)
- Bovine serum albumin (BSA; Sigma, USA)
- Gelatin from porcine skin ,type A (Sigma, USA)
- Gelatin type-B (Sigma, USA)

- Triethylamine (TEA; Sigma, USA)
- Ethanol (J. T. Beaker, USA)
- Isopropanol (IPA; Fisher Sciencific (Asia), Thailand)
- 1,4-dioxane (Fisher Sciencific (Asia), Thailand)
- Dimethylsulfoxide (DMSO; Lab-Scan (Asia), Thailand)
- Phosphate buffer saline (PBS)

# Materials used for cell culture

#### Model Cells

Model cells in this study were mouse calvaria-derived preosteoblastic cells (MC3T3-E1).

#### Medium for MC3T3-E1 cells

Minimum Essential Medium (with Earle's Balanced Salts) (MEM; Hyclone, USA), supplemented by 10% fetal bovine serum (FBS; Sorali, Campo Grande, Brazil), 1% L-glutamine (Invitrogen Corp., USA) and 1% antibiotic and antimycotic formulation [containing penicillin G sodium, streptomycin sulfate, and amphotericin B (Invitrogen Corp., USA)] was used as culture media for MC3T3-E1.

#### Material for Cell Culture Study

- 3-(4,5-dimethyl-thiazol-2-yl)-2,5-diphenyltetrazolium bromide (MTT; USB Corporation., USA)
- Trypsin-EDTA (GibThai Co.,Ltd.)
- Fetal Bovine Serum (Sorali, Campo Grande, Brazil)
- DMEM without phenol red (GibThai Co.,Ltd.)
- L-Glutamine (GibThai Co.,Ltd.)
- 50% Glutaraldehyde solution (Sigma, USA)
- Hexamethyl disilazane HMDS; Sigma, USA)
- p-nitrophenylphosphate (PNPP; Zymed Laboratories, USA)
- Bicinchoninic acid protein assay (BCA; Pierce Biotechnology, USA)
- L-ascorbic acid (Sigma, USA)

- β-glycerophosphate (Sigma, USA)
- Cetylpyridinium chloride (Sigma, USA)

# b. Equipment

#### Equipment for Electrospinning Process

- High voltage power supply from Gamma High Voltage Research Inc. (Ormond Beach, Florida), model D-ES30PN/M692 DC
- Syringe with volume size of 25 ml
- Stainless steel needle with gauge number 20 (or the inner diameter of 0.91 mm)
- The rotating drum which covered with aluminum sheet has the width and OD about 14 and 15 cm, respectively.

# **Equipment for Characterization of Materials**

- UV-Vis spectrophotometer (UV-1800; Shimadzu, Kyoto, Japan)
- quartz tube
- Fourier-transformed infrared spectrometer (FT-IR);
   attenuated total reflection (ATR-FTIR; Thermo Nicolet
   Nexus 670; resolution of 4 cm-1 and 128 scans)
- Contact angle goniometer (KRUSS Gmbh Germany; Model: DSA10-Mk2 T1C)
- Scanning electron microscope (SEM; A JEOL JSM 5200)
- X-ray Photoelectron Spectrometer (XPS; Thermo Fisher Scientific Thetaprobe; Monochromatic Al Kα X-ray, the analysis area was approximately 400 μm, while the maximum analysis depth lay in the range of ~4 to 8 nm.)

#### Equipment for Study of Cell Culture

- A Thermo Spectronic Genesis10 UV-vis spectrophotometer
- Laminar flow hood

#### c. Experimental Procedures

#### Preparation of Polycaprolactone Scaffolds

Preparation and Characterization of Fibrous Scaffolds

Electrospun Polycaprolactone fibrous scaffolds were prepared by electrospinning from a neat 12 % w/v PCL solution in 50:50 v/v DCM/DMF. The as-prepared PCL solution was contained in a glass syringe, the open end of which was connected to a blunt gauge-20 stainless steel hypodermic needle (o.d.0.91 mm) used as the nozzle. An Al sheet wrapped around a rotating cylinder (width and o.d. of the cylinder: 15 cm; rotational speed: 50 rpm) was used as the collector. The distance from the tip of the needle to the surface of the Al sheet defining the collection distance was fixed at 10 cm. A gamma high-voltage research D-ES30PN/M692 power supply was used to generate a high dc potential (i.e., 21 kV). The spinning time was carried out continuously for 10 hours.

Morphological appearance and size of the individual fibers of the scaffolds were examined by a JEOL JSM-5200 scanning electron microscope (SEM). Fibrous scaffolds were dried in vacuum at 30 °C overnight to remove solvent. Each sample was plated in the stub and coated with a thin layer of gold by using a JEOL JFC-1100E ion sputtering device prior to SEM observation. The average diameters of as-spun fibers were determined by measuring the diameters. At least 100 readings of the fiber diameters from at least five SEM images are statistically analyzed using SemAphore 4.0 software, from which the arithmetic mean values of the individual fibers in the PCL fibrous scaffolds were determined to be 0.93 and 1.26 μm, respectively.

Preparation of Crude Bone Protein.

Crude bone protein (CBP) was extracted from the pork bone. In particular, bone was initially washed and cleaned thoroughly in tap water and then sectioned into small pieces with a high speed motor machine. Pieces of sectioned bones were further crushed into powder in liquid nitrogen. Then, the as-prepared powder was immersed in 0.6 N HCl at 4°C and shaken continuously on an orbital shaker. After three days, the bony solution was centrifuged and the supernatant was collected, dialyzed for 48 h and lyophilized. The dry CBP was kept in desiccators until use.

Surface Modification of PCL Scaffold via Aminolysis and Immobilization of Proteins

The scaffold was cut into disc shape with diameter 1.4 cm and immersed in ethanol/water (1:1, v/v) solution for 2 to 3 hours to clean oily dirt and then washed with a large amount of deionized water. The scaffold was subsequently immersed in various concentrations of 1,6-hexamethylene diamine (HMD) /isopropanol (IPA) solution (0.04, 0.06, 0.08, 0.10, 0.20 ,and 0.40 g/ml) for 2 hours at 30 °C. The resulting aminolyzed PCL scaffold was rinsed with deionized water for 24 hours at room temperature to remove free 1,6-hexamethylenediamine and dried under vacuum at 30 °C to constant weight. To determine the optimum concentration of HMD used for aminolysis using ninhydrin method, degreadation experiment, water retention experiment and SEM observation.

Aminolyzed PCL scaffold obtained using the optimum condition was immersed in 0.1 M *N,N'*-disuccinimidyl carbonate (DSC)/dimethylsulfoxide (DMSO) solution in the presence of 0.1 M triethylamine (TEA) for 1 hour at ambient temperature followed by rinsing with large amount of deionized water. The scaffold was then directly transferred to 3 mg/ml of gelatin type-A, gelatin type-B, bovine serum albumin (BSA) or crude bone protein (CBP) in phosphate buffer saline (PBS) solution at ambient temperature for 24 hours. PCL scaffolds immobilized with proteins were rinsed by soaking in deionized water for 24 hours. The samples were dried under vacuum before surface characterization.

Characterization of Fibrous Scaffolds

# Density, Porosity and Pore Volume

The density of the scaffolds  $(\rho_{\text{scaffolds}})$  can be calculated using the following equation

Apparent density (
$$\rho_{\text{scaffold}}$$
, g/cm<sup>3</sup>)=  $\frac{m}{txA}$ -----(3.1)

where m is the mass of the scaffold (g), t is the thickness of the scaffold (cm) and A is the area of the scaffold (cm<sup>2</sup>)

The porosity and pore volume of the scaffolds can be calculated using the following equation (Hou *et al.* 2003).

Porosity (%) = 
$$\left(1 - \frac{\rho_{scaffold}}{\rho_{polymer}}\right) x 100$$
 ......

Pore volume = 
$$\left(\frac{1}{\rho_{scaffold}} - \frac{1}{\rho_{polymer}}\right)$$
 ......(3.3)

where  $\rho_{\text{scaffold}}$  is the apparent density of the fibrous scaffolds(g/cm<sup>3</sup>) and  $\rho_{\text{polymer}}$  is the density of the non-fibrous polymer ( $\rho_{\text{polymer}}$  of PCL is 1.145 g/cm<sup>3</sup>).

# Water Retention Capacity

The dry scaffolds were weighed and then immersed in 5 mL of 0.1 M PBS solution at 37 °C within 48 hours. At the predetermined time point, scaffold were removed from the solution and carefully placed on glass for 5 seconds to remove the excessive water and weighed immediately.

The water retention was calculated by using the following equation (Kothapalli *et al.*, 2005).

Water Retention (%) = 
$$\left(\frac{M_{wet} - M_{dry}}{M_{dry}}\right) x 100$$
 -----(3.4)

where  $M_{dry}$  and  $M_{wet}$  are the weight of the scaffold before and after immersion in 0.1 M PBS solution respectively. Five measurements were performed for the calculation of an average water retention value.

#### Degradation Study of Fibrous Scaffolds

In degradation study, the disc shape of the fibrous scaffolds with diameter 1.4 cm had been immersed in the 0.1 M PBS pH 7.4 at 37 °C within 48 hours. The fibrous scaffolds were then dried in the vacuum to constant weight.

The rate of degradation can be calculated using the following equation.

Weight loss (%) = 
$$\left(\frac{Mf - Mi}{Mi}\right) x 100 - \dots$$
 (3.5)

where  $M_i$  is the initial weight of the scaffolds and  $M_f$  and is the weight of the scaffold at the given degradation time point, immersed in 0.1 M PBS solution. Five measurements were performed for the calculation of an average water degradation rate value.

# <u>Determination of the Amino Groups on PCL Surface after</u> <u>Aminolysis and Protein Immobilization</u>

The ninhydrin analysis method was carried out to quantitatively determine the amount of NH<sub>2</sub> groups on the aminolysed PCL and biomolecule-immobilized PCL scaffolds. The scaffold was immersed in 1 M ninhydrin/ethanol solution for 15 minutes. After the adsorbed ethanol had

evaporated, 1,4-dioxane was added to dissolve the scaffold. When the scaffold surface turned blue, isopropanol (IPA) was then added to stabilize the blue compound. This mixture was transfered to quartz tube and measured the absorbance at the wavelength of 538 nm using a UV-vis spectrophotometer. A calibration curve was obtained with known concentration of 1,6-hexamethylenediamine in 1,4-dioxane/IPA (1:1, v/v) solution.

#### Surface Characterization

Water Contact Angle Measurements

Contact angle goniometer (KRUSS Gmbh Germany; Model: DSA10-Mk2 T1C) were used for the determination of water contact angles. The measurements were carried out by the sessile drop method in air at room temperature. The reported angle was an average of 5 measurements on different area of each sample.

# **UV-Vis Spectrophotometer**

UV-vis spectrophotometer Model Shimadzu, UV-1800 was used for determination of the amount of amino group using ninhydrin method on the modified PCL surface. Ninhydrin will react with a free alphamino group, NH<sub>2</sub>-C- which is contained in all amino acids, peptides, or proteins, producing Ruhemann's purple colored complex of ninhydrin absorbs the visible light at the wavelength of 538 nm.

Attenuated Total Reflectance-Fourier Transform
Infrared Spectrometer (ATR-FTIR)

All spectra are collected at resolution of 4 cm<sup>-1</sup> and 128 scans using Nicolet Magna 750 FT-IR spectrometer equipped with a liquid-nitrogen-cooled mercury-cadmium-telluride (MCT) detector. A single attenuated total reflection accessory with 45° germanium (Ge) IRE (spectra Tech, USA) and a varible angle reflection accessory (Seagull<sup>TM</sup>, Harrick Scientific, USA) with a hemispherial Ge IRE are employed for all ATR spectral acquisitions. Chemical functional groups that were present on the surfaces of both the neat and the surface-modified fibrous scaffolds were analyzed by ATR-FTIR spectrometer.

# X-ray Photoelectron Spectrometer (XPS)

XPS was used to estimate the elemental composition and chemical state of the elements on the surface. The analysis of the samples was carried out using a Thermo Fisher Scientific Thetaprobe XPS. Monochromatic Al  $K_{\alpha}$  X-ray was employed for analysis of one spot on each sample with photoelectron take-off angle of 50° (with respect to surface plane). The analysis area was approximately 400  $\mu$ m, while the maximum analysis depth lay in the range of ~4 to 8 nm. A special designed electron flood gun with a few eV Ar<sup>+</sup> ion was used for the charge compensation. Electron beam and ion beam were focused and steered towards the analysis position. Further correction was made based on adventitious C 1s at 285.0 eV using the manufacturer's standard software. Survey spectra were acquired for surface composition analysis with Scofield sensitivity factors.

#### Scanning Electron Microscope

The morphology of cells on the materials was examined by using a JEOL JSM 5200 scanning electron microscope (SEM). Each sample was coated with a thin layer of gold using JEOL JFC 1100E ion sputtering device prior to SEM observation.

#### Cell Culture Studies

Osteoblast (MC3T3-E1) cell lines are used. MC3T3-E1 cells are cultured in  $\alpha$ -MEM medium supplemented with 10 % FBS, 1 % L-glutamine and 1 % antibiotic and antimycotic formulation (containing penicillin G sodium, streptomycin sulfate, and amphotericin B). The medium was replaced every 2 days and the cultured cells were maintained at 37 °C in a humidified atmosphere containing 5% CO<sub>2</sub>.

# Cytotoxicity Evaluation Direct Cytotoxicity

This test was used to evaluate the potential for use of protein directly to the cell.  $4\times10^4$  MC3T3-E1 cells/well were cultured in 24-well plate to allow cell attachment on the plate. After incubation

under 5 % CO<sub>2</sub> at 37 °C at least 4 hours, the cells were starved with a 2 % culture media (2 % MEM; containing MEM, 2 % FBS, 1 % L-glutamine, 1 % lactabumin, and 1 % antibiotic and antimycotic formulation.) for 24 hours. After starvation, the culture medium was removed and replaced with the asprepared extraction media (2 % culture media with appropriate amount of proteins; gelatin type-A, gelatin type-B, bovine serum albumin, and crude bone protein) and later incubated for 1, 2, and 3 days. The number of living cells was finally quantified with MTT assay.

# Indirect Cytotoxicity

The indirect cytotoxicity evaluation was conducted on modified and unmodified PCL scaffolds in adaptation from the ISO10993-5 standard test method . The samples are pre-washed with 70 % ethanol in water for 30 minutes, washed twice with PBS solution and deionized water and immerged in a 2% MEM culture medium (2 % MEM; containing MEM, 2 % FBS, 1 % L-glutamine, 1 % lactabumin, and 1 % antibiotic and antimycotic formulation.) under 5 % CO<sub>2</sub> at 37 °C in 24-well plate for 24 hours to prepare the extraction media. 4×10<sup>4</sup> MC3T3-E1 cells/well were separately cultured in other 24-well plate to allow cell attachment on the plate at least 4 hours. The cells were further starved with a 2 % MEM and replaced in 2 hours for 3 times. After incubation under 5 % CO<sub>2</sub> at 37 °C, the culture medium was removed and replaced with the asprepared extraction media and later incubated for another 1, 2 and 3 days. The number of living cells was finally quantified with MTT assay.

#### Cell Adhesion and Proliferation

Both modified and unmodified PCL scaffolds (diameter 1.4 cm) are sterilized by soaking in 70 % ethanol in water for 30 minutes, washed twice with PBS solution and deionized water and immerged in a 10 % MEM culture medium under 5 % CO<sub>2</sub> at 37 °C in 24-well plate for 24 hours. After removing of culture media, approximately 4×10<sup>4</sup> MC3T3-E1 cells and 0.5 mL culture medium were pipetted into each well containing asprepared scaffolds as well as into the bottom of tissue culture polystyrene

plates (TCPS) as a control and then incubated under 5 % CO<sub>2</sub> at 37 °C. Cell adhesion was studied on 2, 4, 6 hours culture period while cell proliferation was investigated on 1, 2 and 3 days culture period. The number of living cells was finally quantified with MTT assay.

# MTT Assay

The MTT assay is based on the reduction of the yellow tetrazolium salt to purple formazan crystals by dehydrogenase enzymes secreted from the mitochondria of metabolically active cells. The amount of the purple formazan crystal formed is proportional to the number of viable cells. After desirable culture period, the culture medium was removed to discard the unattached cell and incubated at 37 °C for 30 minutes with 300 µl/well of MTT solution at 0.5 mg/ml culture medium without phenol red. After incubation, MTT solution was removed. A buffer solution containing dimethylsulfoxide (DMSO : 900 µl/well) and glycine buffer (pH =  $10:125~\mu l/well$ ) was added into the wells to dissolve the formazan crystals. After 10 minutes of rotary agitation, the solutions were then transferred into a cuvette and placed in a spectrophotometer (Thermospectronic Genesis10 UV-visible spectrophotometer) to measure the number of viable cells at absorbance 540 nm .

#### Morphological Observation of Cultured Cells

After removal of the culture medium, the cell-cultured scaffold samples were rinsed with PBS twice and the cells were then fixed with 3% glutaraldehyde solution (diluted from 50 % glutaraldehyde solution with PBS), at 500 µl/well. After 30 minutes, they were rinsed again with PBS. After cell fixation, the samples were dehydrated in an ethanol solution of varying concentration (i.e. 30, 50, 70, 90, and 100 %, respectively) for about 2 minutes at each concentration. The samples were then dried in 100 % hexamethyldisilazane (HMDS) for 5 minutes and later let dry in air after removal of HMDS. After completely dried, the samples were mounted on an SEM stub, coated with gold, and observed by a JEOL JSM 5200 scanning electron microscope (SEM).

# Production of Alkaline Phosphatase of Cultured Cells

ALP is considered as a relatively early marker of osteoblast differentiation. Cells were cultured on scaffold samples for 3, and 7 days to observe the production of alkaline phosphatase (ALP). The samples were rinsed with PBS after removal of culture medium. Alkaline lysis buffer (10 mM Tris-HCl, 2 mM MgCl<sub>2</sub>, 0.1 % Triton-X 100, pH 10) (100 µl/well) was added and the samples were scrapped and then frozen at -20°C for at least 30 minutes prior to the next step. An aqueous solution of 2 mg/ml p-nitrophenyl phosphate mixed with 0.1 M amino propanol (10 µl/well) in 2 mM MgCl<sub>2</sub> (100 µl/well) having a pH of 10.5 was prepared and added into the samples. The samples were incubated at 37 °C for 15 minutes. The reaction was stopped by adding 0.9 ml/well of 50 mM NaOH and the extracted solution was transferred to a cuvette and placed in the UV-visible spectrophotometer, from which the absorbance at 410 nm was measured. The amount of ALP was then calculated against a standard curve. In order to calculate for the ALP activity, the amount of ALP had to be normalized by the amount of total protein synthesized. In the protein assay, the samples were treated in the same manner as the ALP assay up to the point was the samples were frozen. After freezing, bicinchoninic acid (BCA; Pierce Biotechnology, USA) solution was added into the samples. The samples were incubated at 37 °C for 15 minutes. The absorbance of the medium solution was then measured at 562 nm by the UV-vis spectrophotometer and the amount of the total protein was calculated against a standard curve.

#### Mineralization

Mineralization refers to cell-mediated deposition of extracellular calcium and phosphorus salts where anionic matrix molecules take up the Ca<sup>2+</sup>, phosphate ions and serve as nucleation and growth sites leading to calcification. Mineralization was quantified by Alizarin Red-S which is a dye that binds selectively calcium salts and is widely used for mineral staining (the staining product i.e., an Alizarin Red S-calcium chelating product). MC3T3-E1 cells (4×10<sup>4</sup> cells/well in 24-well plate) were cultured on

scaffold samples for 16 days to observe the production of mineralization. The isolated cells were plated in 24-well plate and cultured in the cultured medium. The cultured cells were changed after a 24 hours attachment period with culture medium in the presence of 5 mM  $\beta$ -glycerophosphate and 50 μg/ml ascorbic acid. The media was replaced every 2 days thereafter. After 16, 21 and 30 days, respectively, the cells were washed twice with PBS, fixed with cold methanol for 10 minutes, and stained with 1 % Alizarin red solution (prepared in distillated water and adjusted the pH about 4.1 to 4.3 using 10 % ammonium hydroxide) for 5 minutes. After removing the alizarin red-S solution, the cells were rinsed with deionized water and dried at room temperature. The images of each culture were captured and the strain was extracted with 10 % cetylpyridinium chloride in 10 mM sodium phosphate for 1 hour and the absorbance of collected dye was read at wavelength 570 nm spectrophotometer (A Thermo Spectronic Genesis10 UV-visible spectrophotometer). In comparison, tissue culture plate without cell was treated with the procedure as previously described.

# Statistical analysis

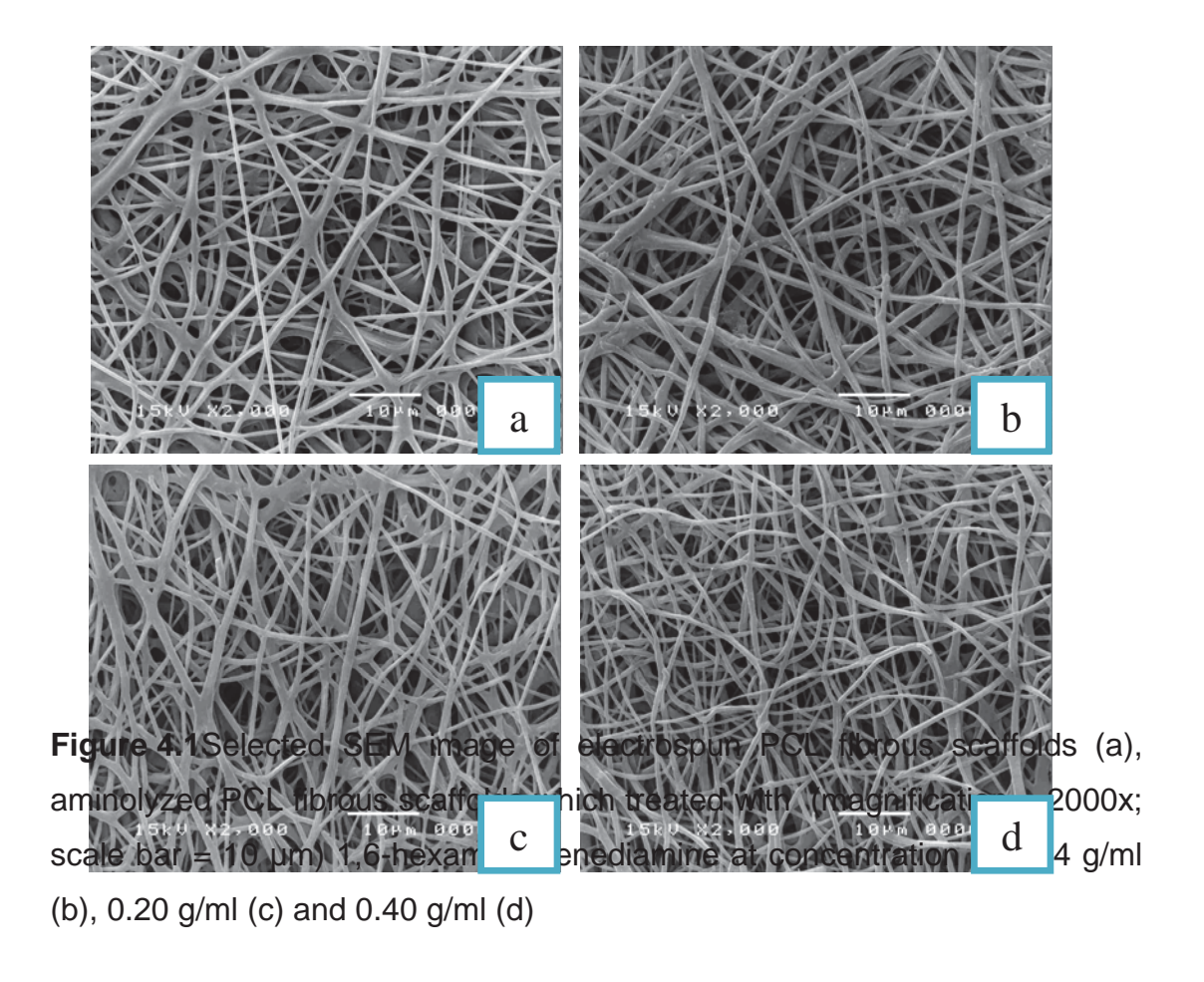
Values are expressed as the mean  $\pm$  SD. Experiments are performed at least five times and results of representative experiments are presented except where otherwise indicated. Statistical analysis was performed using One-Way Analysis of Variance (ANOVA) with the Least Square Difference (LSD) test multiple comparisons posttest using SPSS version 17 software. p < 0.05 or p < 0.01 is considered statistically significant.

#### 4. RESULTS AND DISCUSSION

# 4.1 Preparation of Poly(*e*-caprolactone) Electrospun Fibrous Scaffold

Poly( $\varepsilon$ -caprolactone) (PCL;  $M_n = 80,000$  g/mol) electrospun fibrous scaffold was prepared via electrospinning process under fixed conditions as

mentioned in the previous chapter. Translucent electrospun PCL fibrous scaffolds with a thickness of (130 ± 5) µm were obtained. Morphological appearance and size of the individual fibers of the scaffolds were examined by JEOL JSM 5200 scanning electron microscopy (SEM) as shown in Figure 4.1(a). At least 100 readings of the fiber diameters from various SEM images were statistically analyzed using SemAphore 4.0 software, from which the arithmetic mean value of the individual fibers within the PCL fibrous scaffolds was determined to be (0.93 ± 0.30) µm. After surface modification of PCL electrospun fibrous scaffold via aminolysis with various hexamethylenediamine (HMD) concentration treatments, the morphology of the surface-modified scaffolds was also observed [Figure 4.1 (b,c and d)].



#### 4.2 Characterization of Fibrous Scaffolds

# 4.2.1 Density, Porosity, and Pore Volume

The density, porosity and pore volume of the unmodified PCL scaffolds and modified PCL scaffolds are shown in Table 4.1. The porosity and pore volume of these scaffolds were in the range of (96 to 97) % and (22 to 29) cm<sup>3</sup>/g, respectively. Moreover, the density, porosity percentage and pore volume of all type of the surface-modified scaffolds were not significantly different from the unmodified PCL scaffolds.

Material	density (x10 <sup>-2</sup> g/cm <sup>3</sup> )	porosity (%)	pore volume (cm³/g)
PCL pure	4.69 0.44	95.91 0.38	20.62 2.07
aminolyzed PCL	4.25 0.97	96.29 0.85	23.63 5.28
activated PCL	4.14 0.57	96.39 0.50	23.64 3.07
gelatin A immobilized PCL	3.75 0.59	96.72 0.51	26.33 4.52
gelatin B immobilized PCL	3.59 0.88	96.86 0.77	28.15 6.17
BSA immobilized PCL	3.85 0.74	96.64 0.65	25.88 4.97
CBP immobilized PCL	4.58 0.93	96.00 0.81	21.64 4.35

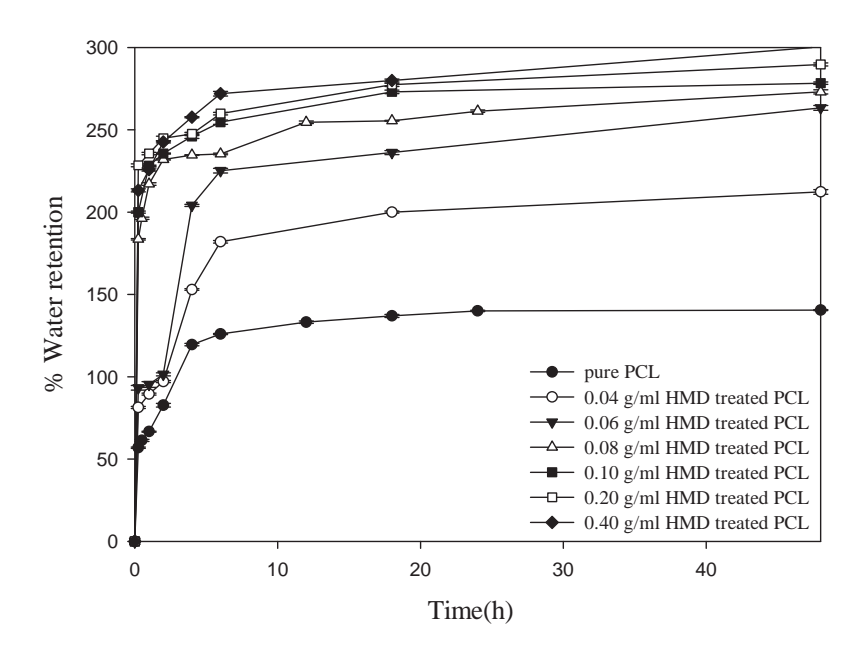
#### 4.2.2 Water Retention Capability

Figure 4.2 demonstrates the water retention capability of these unmodified and modified PCL scaffolds via aminolysis process with different 1,6-hexamethylenediamine (HMD) concentration at 37 °C within 48 hours. In the figure shows the water retention rate increased with increasing HMD concentration treatment.

# 4.2.3 <u>Degradation Study of PCL Fibrous Scaffolds</u>

In degradation study, the disc shape of the PCL fibrous scaffolds with diameter  $\sim$  (100 to 150)  $\mu m$  had been immersed in the 0.1 M phosphate buffer saline (PBS), pH 7.4 at 37 °C within 48 hours. Figure 4.3 shows the degradation rate of the PCL scaffolds at different HMD

concentration treatments. The weight loss increased with time and rapidly increased in the early 2 hours and steady stable after 18 hours. Furthermore, the weight loss values increased with increasing HMD concentration treatment.



**Figure 4.2**Water retention capability of these unmodified and modified PCL scaffolds via aminolysis process with different 1,6-hexamethylenediamine(HMD) concentration at 37 °C within 48 hours.

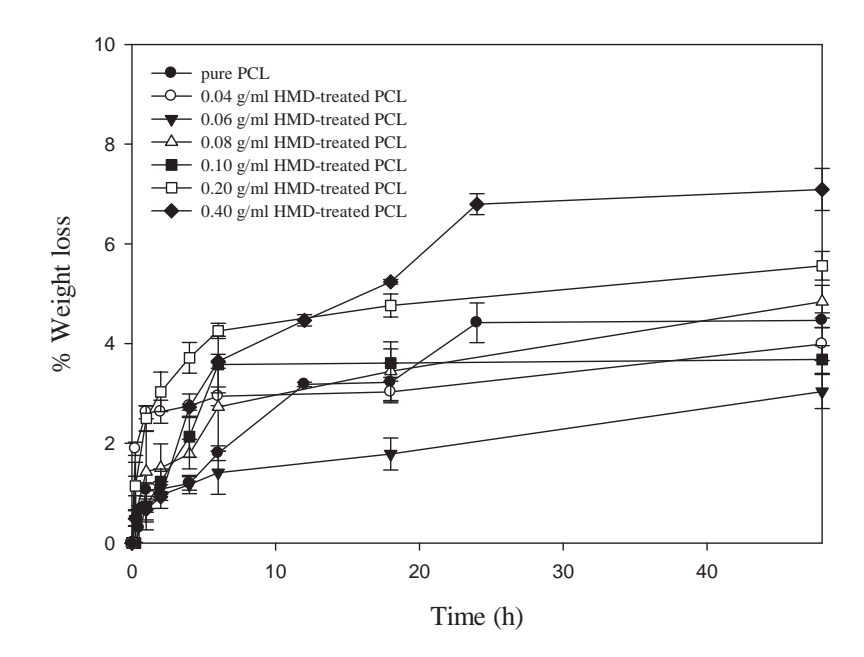


**Figure 4.3**The degradation rate of the PCL scaffolds at different HMD concentration treatments.

## 4.3 Surface Characterization

# 4.3.1 Quantification of Amino Groups

Amino groups can be covalently introduced onto the surface of the electrospun **PCL** fibrous scaffolds reaction with 1,6by hexamethylenediamine (HMD), One amino group (NH<sub>2</sub>) of HMD reacts with an ester group (—COO—) of PCL to form the amide linkage (—CONH—), while another amino group which is unreacted and free can be used as active sites through which biomolecules (i.e;proteins) can be bonded to the surface using N, N'-disuccinimidyl carbonate (DSC) as a coupling agent. However, two-step procedure was carried out to avoid aggregation,. The attached amino groups had been first activated with DSC which N-hydroxysuccinimide was lost from the reaction and the as-formed succinimidyl esters were later reacted with respective biomolecules, N-hydroxysuccinimide again being cleaved from the reaction. The chemical pathway for the immobilization of biomolecule on the surface of electrospun PCL fibrous scaffolds is summerized in the Figure 4.4.

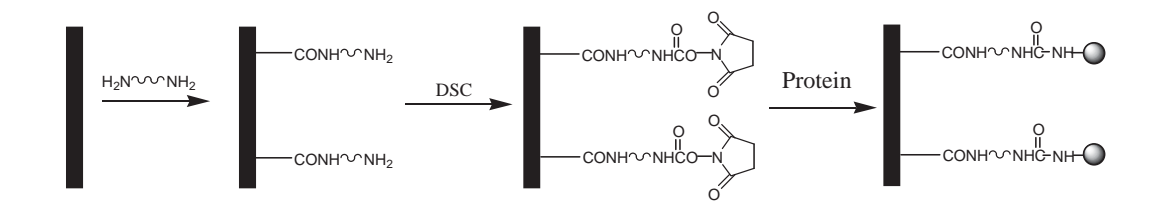


**Figure 4.4**The chemical pathway for the immobilization of proteins.

The existence of free amino groups (NH<sub>2</sub>) on PCL surface is essential for protein bonding in this modification method. It is important to confirm the existence of amino groups before protein is further introduced. Therefore, ninhydrin is used to confirm and quantify the -NH<sub>2</sub> density on the aminolyzed PCL surface. The NH<sub>2</sub> density on electrospun PCL fibrous scaffold surfaces is relative to the concentration of 1,6hexamethylenediamine, aminolyzing time, temperature, and so on. Figure 4.5 shows that NH<sub>2</sub> density increased with increasing 1,6-hexamethylenediamine concentration. However. when the concentration of 1,6hexamethylenediamine is greater than 0.20 g/ml, the structural morphology of the electrospun PCL fiber scaffolds became worse (as shown in Figure 4.1 d). To maintain structural morphology of the electrospun PCL fiber scaffolds for practical applications, PCL electrospun fibrous scaffolds were aminolyzed in a 0.20 g/ml 1,6-hexamethylenediamine/isopropanol solution at evaluated temperature for 2 hours. According to the calibration curve obtained with 1,4dioxane-isopropanol (1:1, v/v) solution containing 1,6-hexamethylenediamine of known concentration, the NH<sub>2</sub> density on PCL electrospun fibrous scaffolds aminolyzed under these conditions was  $1.37 \times 10^{-7} \text{ mol/cm}^2$ .

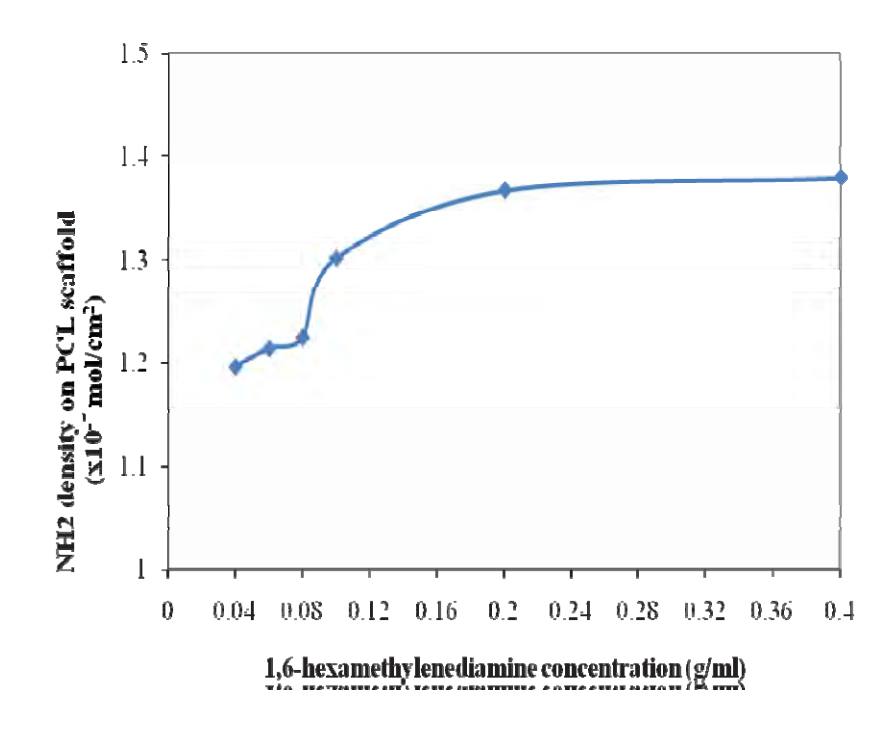


**Figure 4.5**NH<sub>2</sub> density on PCL electrospun fibrous scaffolds as a function of concentration of 1,6-hexamethylenediamine/isopropanol solution. The PCL scaffold was aminolyzed for 2 hours.

#### 4.3.2 Surface Wettability

To further evaluate the effect of aminolysis, surface wettability of the modified PCL fibrous scaffolds was measured. Therefore, water contact angle measurement was used to evaluate the surface wettability of the surface modified PCL fibrous scaffolds. Table 4.2 shows the water contact angle measured by the sessile drop method decreased gradually from 123.8° to 118.0° after the scaffolds were aminolyzed with 0.04 g/mL of HMD/IPA solution for 2 hours and slightly decreased with increasing HMD concentration. That is, the introduction of the amino groups on the surface of the PCL fibrous scaffolds improved the hydrophilicity of the surface. Figure 4.6 and 4.7 show that the surface became more hydrophilic after aminolysis and protein immobilization. After the aminolyzed PCL fibrous scaffolds have been activated with DSC, their surface became more hydrophobic than the neat PCL scaffold and water contact angle also decreased after the proteins

were bonded. The water drop appearance on the surface of neat PCL, gelatin type-A immobilized PCL, BSA immobilized PCL and CBP immobilized PCL are shown in Figure 4.7. CBP immobilized PCL scaffold has largest decrease of contact angle as compared with the neat PCL scaffold (control). This means that immobilization of gelatin crude bone protein can most improve the hydrophilicity of the surface.

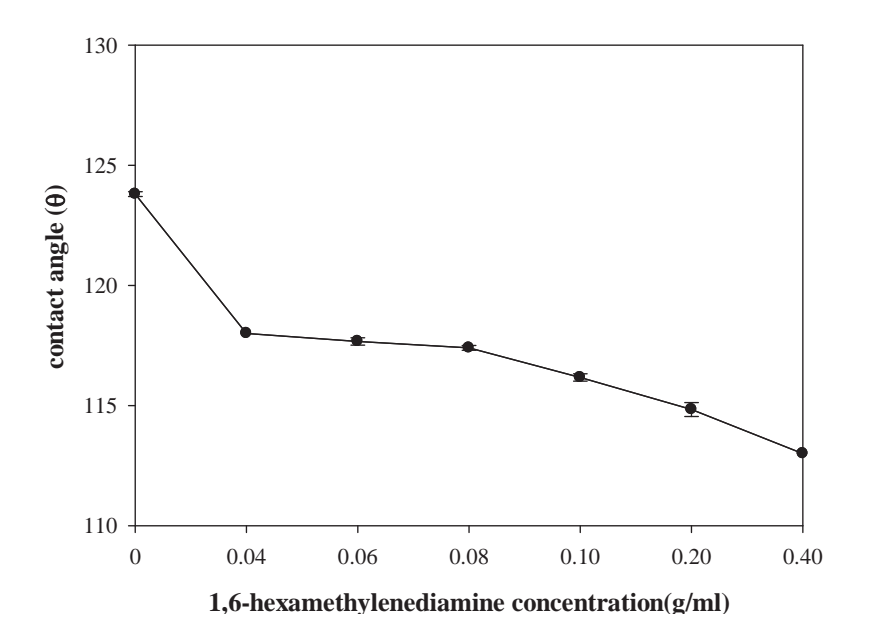


**Figure 4.6**Water contact angles of the control and aminolyzed PCL scaffolds at different HMD concentration treatments measured by the sessile drop method.

**Table 4.1** The water contact angle of the control and all modified PCL fibrous scaffolds measured by the sessile drop method

	Contact
Material	angle( $\theta$ )
Neat PCL (control)	123.7 ± 0.1
Aminolyzed PCL <sup>a</sup>	115.3 ± 0.2
Activated PCL <sup>b</sup>	118.7 ± 0.3

Gelatin type-A immobilized PCL <sup>c1</sup>	95.5 ± 1.1
Gelatin type-Bimmobilized PCL	
c2	94.4 ± 2.1
BSA immobilized PCL c3	97.5 ± 2.0
CBP immobilized PCL c4	48.5 ± 1.8

<sup>a</sup>The PCL electrospun fibrous scaffolds was immersed in 0.20 g/ml 1,6-hexamethylenediamine solution at 30 °C for 2 hours.

<sup>b</sup>The aminolyzed PCL scaffolds were immersed in 0.1 M DSC solution in the presence of TEA for 1 hour.

<sup>c1,c2,c3,c4</sup> The activated PCL scaffolds were immersed in 3.0 mg/mL gelatin type-A, gelatin type-B, BSA, and CBP solutions, respectively, for 24 h followed by the rinsing process.

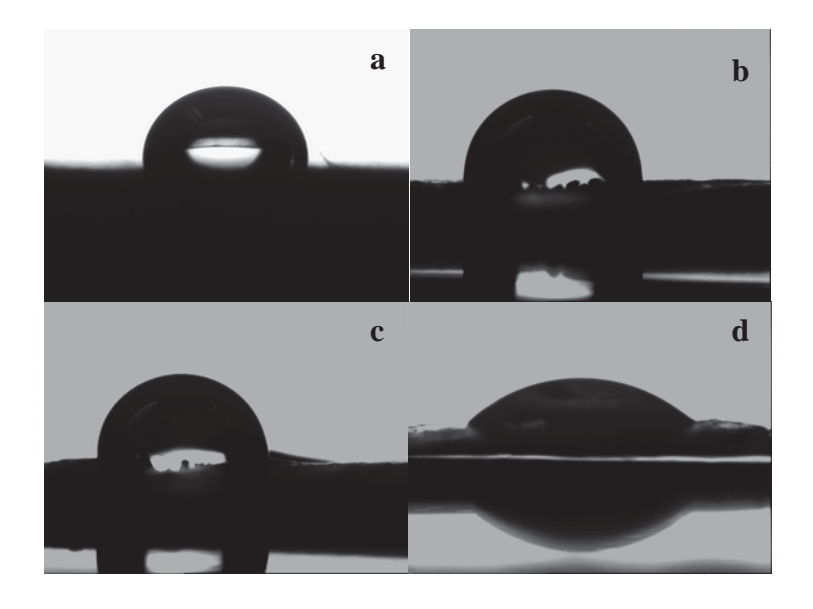


**Figure 4.7**Water dropped on the surface of neat PCL fibrous scaffold (a), and PCL fibrous scaffold immobilized with 3.0 mg/ml gelatin type-A (b), 3.0 mg/ml bovine serum albumin (c) and 3.0 mg/ml crude bone protein (d).

# 4.3.3 Chemical Analysis of Surface

ATR-FTIR spectra of PCL and modified PCL fibrous scaffolds are shown in Figure 4.8 and 4.9 There was a major absorption peak assigned to the ester carbonyl of neat PCL appeared at 1755 cm<sup>-1</sup>.

The low broad signals from N–H stretching of NH $_2$  at  $\sim$  (3300 to 3500) cm $^{-1}$  or carbonyl stretching of amide group at 1650 cm $^{-1}$  were observed on those surface modified PCL. After biomolecule immobilization, C=O stretching peak occurs at 1650 cm $^{-1}$  (amide I) and N–H bending peak at 1550 cm $^{-1}$  (amide II) and 1350 cm $^{-1}$  (amide III) evidently appeared in the spectra of all biomolecule-immobilized PCL scaffolds. Moreover, the higher broad peak in the range of 3000 to 3600 cm $^{-1}$  corresponding to N–H stretching of NH $_2$  in gelatin type-A, gelatin type-B, BSA and CBP was observed indicating that gelatin type-A, gelatin type-B, BSA and CBP have been successfully immobilized on the amino-containing PCL scaffolds. However, the signal of FTIR spectrum were low, resulting from the extremely low concentration of NH $_2$  present within the sampling depth of ATR-FTIR (1 to 2 µm).

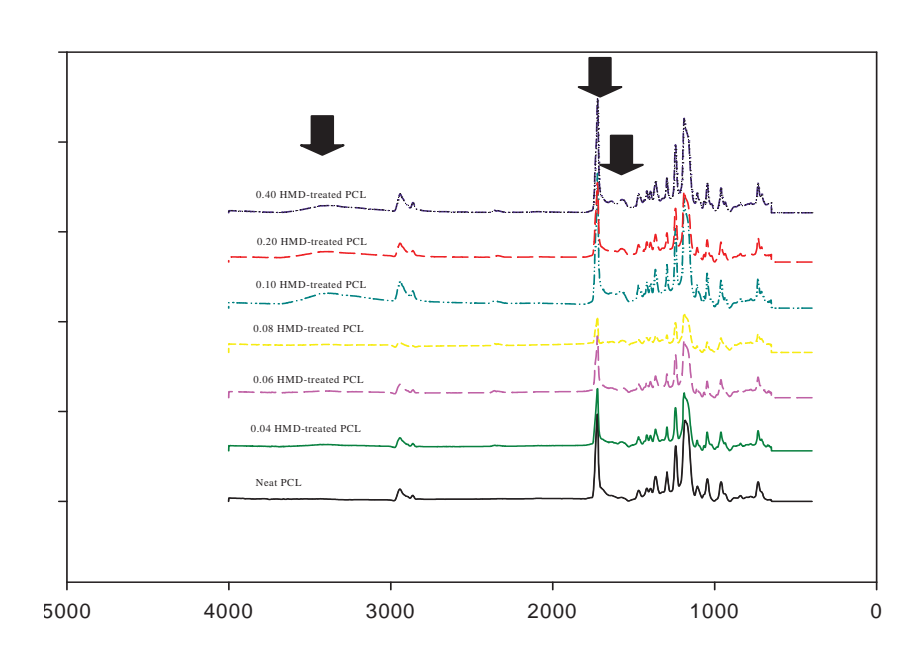


**Figure 4.8**ATR-FTIR spectra of neat and aminolyzed PCL fibrous scaffolds with different HMD concentration treatments.

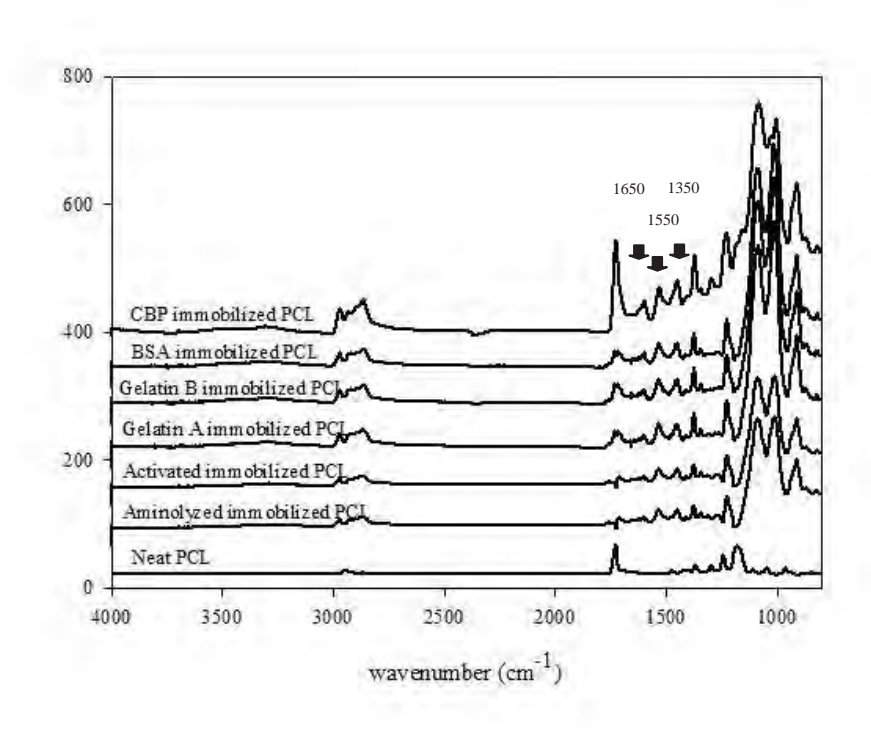


Figure 4.9ATR-FTIR spectra of neat and modified PCL fibrous scaffolds.

# 4.3.4 Elemental Composition of the Surface

The surface of modified PCL fibrous scaffolds were further determined the elemental composition by using X-ray Photoelectron Spectrometer (XPS). To study the effect of the aminolysis condition on the surface,  $N_{1s}/C_{1s}$  ratios as a function of HMD concentration treatment were evaluated. Table 4.4 shows that the more diamine concentration treated, the more  $N_{1s}/C_{1s}$  ratio observed due to the increasing in  $NH_2$  groups. After aminolysis, the  $N_{1s}/C_{1s}$  ratio was increased from 0 to 0.0168 because  $NH_2$  groups were introduced on the PCL surface. Figure 4.10 demonstrated that  $N_{1s}$  peak appeared after immobilization with proteins (gelatin type-A , gelatin type-B , bovine serum albumin, and crude bone protein) due to the large amount of nitrogen atom in proteins structure was introduced.

**Table 4.2**  $N_{1s}/C_{1s}$  ratios as a function of 1,6-hexanediamine concentration

1,6-hexamethylenediamine concentration (g/ml)	N <sub>1s</sub> /C <sub>1s</sub> ratio
0.04	0.0063
0.06	0.0079
0.08	0.0163
0.10	0.0169
0.20	0.0170
0.40	0.0170

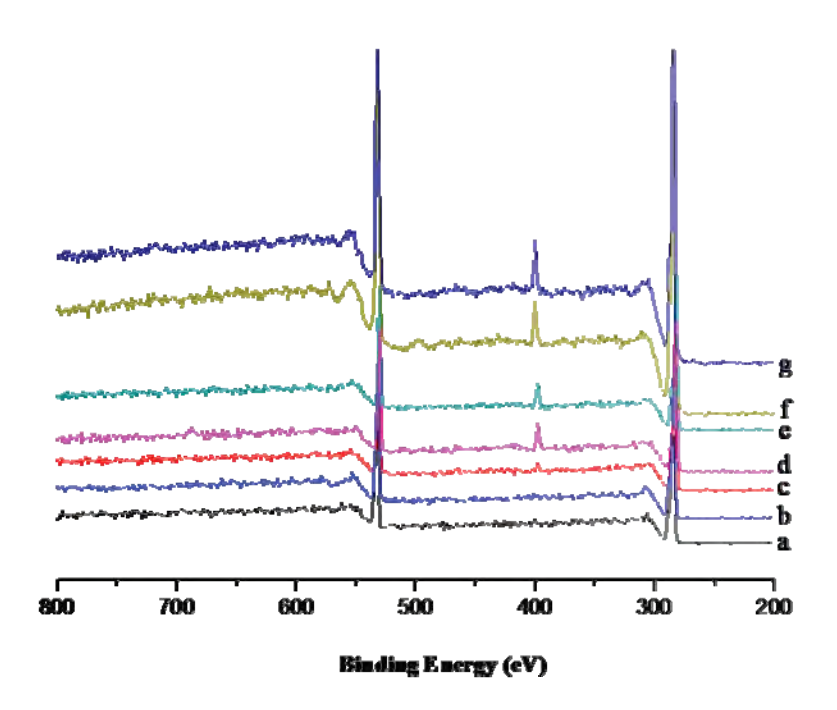


**Figure 4.10** The survey XPS spectra of (a) neat PCL, (b) aminolyzed PCL with 0.20 g/ml HMD treatment, (c) activated PCL, (d) PCL immobilized with 3 mg/ml gelatin type-A solution, (e) 3 mg/ml gelatin type-B solution, (f) 3 mg/ml bovine serum albumin solution, and (g) 3 mg/ml crude bone protein solution.

# 4.4 Biological Characterizations

# 4.4.1 Cytotoxicity

## 4.4.1.1 Direct Cytotoxicity

Direct cytotoxicity test is a method to evaluate the toxic effect of proteins directly to cells. The effect was investigated with mouse calvaria-derived pre-osteoblastic cells (MC3T3-E1), based on the initial 40,000 cells/well seeded. MC3T3-E1 were cultured in 24-well culture plate to allow cell growth. The test was conducted by adding gelatin type-A, gelatin type-B, BSA protein and crude bone protein extracts in 2% serum-containing MEM diluted with 7-day extraction medium in seeded cells as mentioned above and cultured for 1, 2, and 3 d. Figure 4.11 shows that the viability of MC3T3-E1, cultured with 2% serum-containing MEM extraction media adding with all types of proteins for 1, 2 and 3 days, was increased with increasing the culturing time in the respective media. The viability of cells (relative with control TCP) of all material is more than 80 %. All of the obtained results clearly suggested that all types of proteins, released no substances at levels that were harmful to cells.

#### 4.4.1.2 Indirect Cytotoxicity

The potential use of these fibrous scaffolds as bone scaffolds was first evaluated by an indirect cytotoxicity test with mouse calvaria-derived pre-osteoblastic cells (MC3T3-E1), based on the initial 40,000 cells/well seeded. The test was carried out on TCP (control), the neat PCL, aminolyzed PCL, activated PCL, gelatin type-A, gelatin type-B, BSA and CBP immobilized PCL fibrous scaffolds. MC3T3-E1 were cultured in a 24-well culture plate in 2 % serum-containing MEM extraction medium from all type of fibrous scaffolds for 1, 2, and 3 days. Figure 4.12 shows that the viability of MC3T3-E1, cultured with 2 % serum-containing MEM diluted with 1-day extraction media prepared by all types of modified scaffolds, was increased with increasing the culturing time in the respective media and the viability of cells on all types of material measured by MTT assay was more

than 80 %. All of the obtained results clearly suggested that all types of the PCL fibrous scaffolds, released no substances at levels that were harmful to cells.

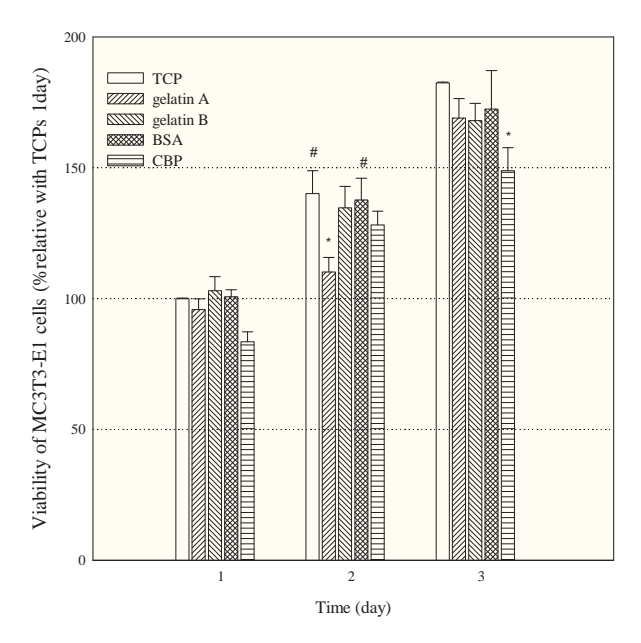


**Figure 4.11**The viability of MC3T3-E1, cultured with 2% serum-containing MEM extraction media adding with all types of proteins for 1, 2 and 3 days. Statistical significance: p < 0.05 compared with control and p < 0.05 compared to the neat PCL fibrous scaffolds at any given time point.

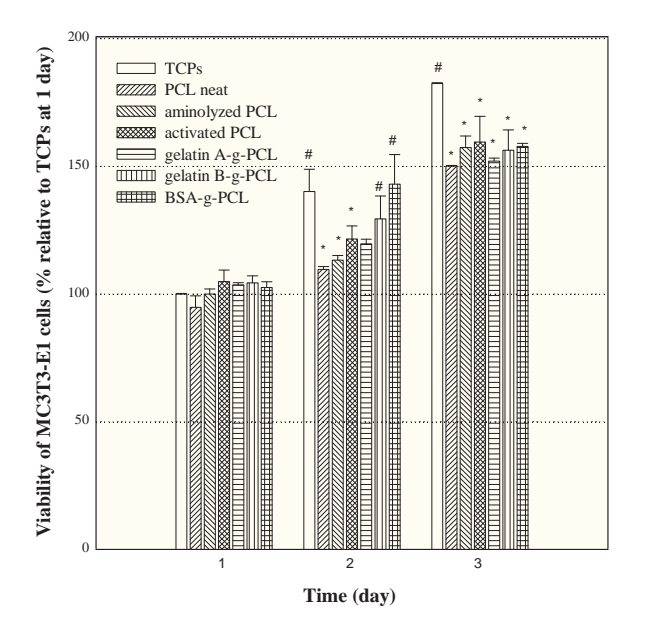


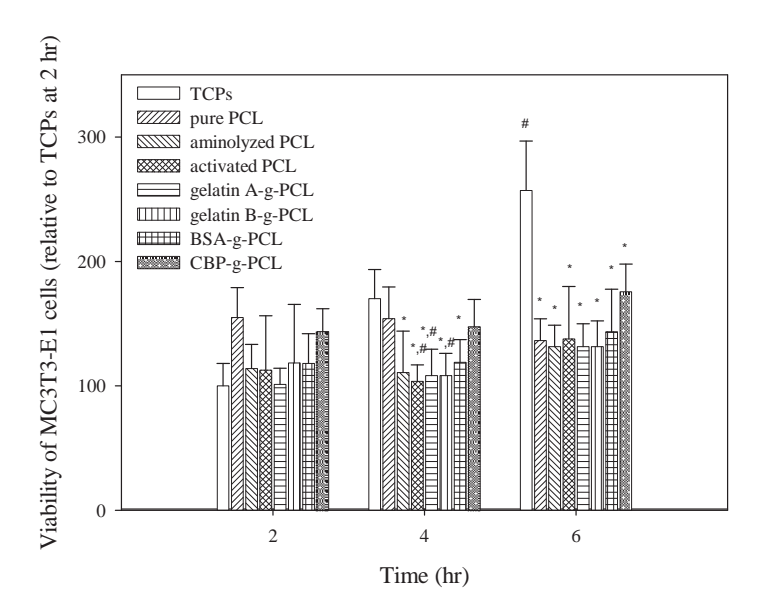
**Figure 4.12** The viability of MC3T3-E1, cultured with 2% serum-containing MEM extraction media from all type of PCL fibrous scaffolds for 1, 2, and 3 days relative to TCPS at 1 day Statistical significance: \*p < 0.05 compared with control and \*p < 0.05 compared to the neat PCL fibrous scaffolds at any given time point.

# 4.4.2 Cell Attachment and Proliferation

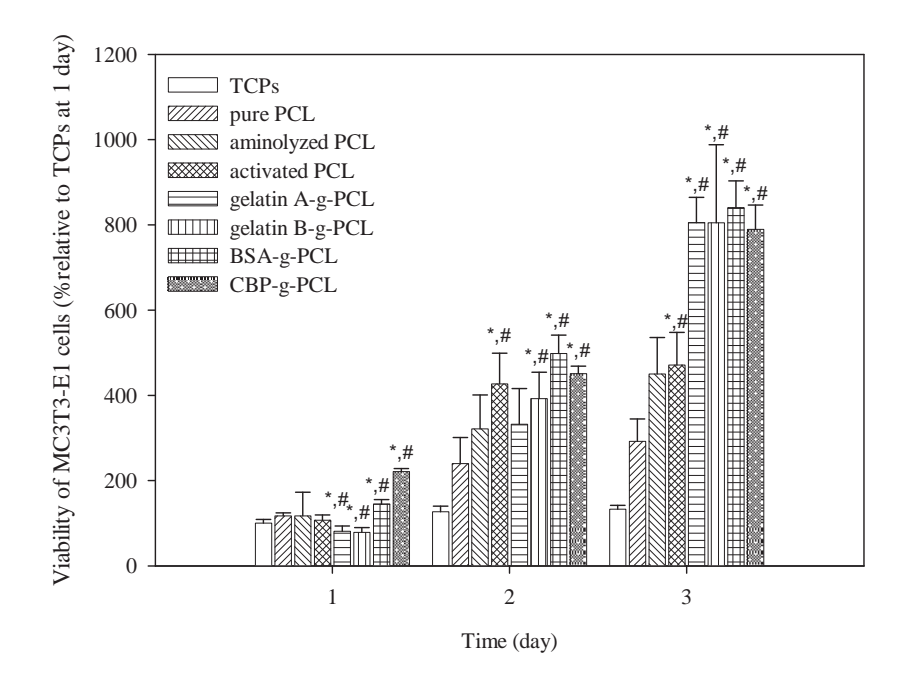
The potential for use of the neat and the modified PCL fibrous scaffolds was further evaluated by determination their ability to support both the adhesion and the proliferation of MC3T3-E1. The viability of the cells that had been cultured on the surface of TCPS for 2 h was taken as the basis to arrive at the relative viability shown in a Figure. Figure 4.13 shows the attachment of MC3T3-E1 on the surfaces of TCPS, neat PCL, aminolyzed PCL, activated PCL, and protein-immobilized PCL at 2, 4, and 6 h after cell seeding in terms of viability. On TCPS, the number of the attached cells increased rapidly from ~100% at 2 h after cell seeding to ~257% at 6 h after cell seeding, based on the initial number of cells seeded (40,000 cells/well). While, the number of cells attached on these fibrous scaffolds was lower in comparison with that on TCPS at any given time point. There was the most viability of cells on crude bone protein-immobilized PCL fibrous scaffold among various types of the modified fibrous scaffolds. This obtained result suggested that the cells prefer to adhere on CBP-immobilized PCL fibrous scaffold rather than other modified scaffolds. However, The lesser viability of cells in the attachment period on various types of the fibrous scaffolds in comparison with that on TCPS could be due to the lesser number of cells that were able to attach on the rough surface of the fibrous scaffolds in comparison with the smoother and hydrophilic surface of TCPS.

Figure 4.14 shows the proliferation of MC3T3-E1 on the surfaces of TCPS, neat PCL, aminolyzed PCL, activated PCL and protein-immobilized PCL on day 1, 2, and 3 after cell culture in terms of viability (%relative to TCPS at day1). On TCPS, the number of cells increased from ~100% at 1 day after cell culture to ~133 % at 3 days after cell culture, based

on the initial 40,000 cells/well seeded. In comparison with that on TCPS, the viability of the cells cultured on various types of PCL fibrous scaffolds were significantly higher at any given time point. The viability of cells proliferated on these fibrous scaffolds, at day 3, was higher than TCPS of about (3 to 4) fold for neat PCL, aminolyzed PCL, and activated PCL and about 8 fold for all type of protein-immobilized PCL. The improvement was achieved with the protein-immobilized PCL fibrous scaffolds on day 3 after cell culture. The greater number of cells in the proliferation period on all types of fibrous scaffolds could be because of high surface area to volume and high porosity of the electrospun fibrous scaffolds through which the cells were able to penetrate into the scaffolds. Among the various modified PCL fibrous scaffolds, the BSA-immobilized PCL fibrous scaffolds provided the most significant improvement in the ability to support the proliferation of the cells which could be due to the protein-containing and more hydrophilic surface of the substrate.



**Figure 4.13**Attachment of MC3T3-E1 that had been seeded or cultured on the surfaces of TCPS and the neat and the modified PCL fibrous scaffolds for 2, 4, and 6 h. Statistical significance:  $^*p$  < 0.05 compared with control and  $^#p$  < 0.05 compared to the neat PCL fibrous scaffolds at any given time point.



**Figure 4.14**Proliferation of MC3T3-E1 that had been seeded or cultured on the surfaces of TCPS and the neat and the modified PCL fibrous scaffolds for 1, 2, and 3 days. Statistical significance: \*p < 0.05 compared with control and \*p < 0.05 compared to the neat PCL fibrous scaffolds at any given time point.

#### 4.4.3 Cell Morphology

Table 4.6 and 4.7 show selected SEM image (magnification = 2000X; scale bar = 10 μm) of MC3T3-E1 that were cultured on the surfaces of neat PCL, activated PCL and gelatin type-A, gelatin type-B, bovine serum albumin, and crude bone-immobilized PCL at different time points. These images provided snap shots in time that revealed the morphology of the cells and interaction between the cells and the tested surfaces. At 2 hours after cell seeding, based on the initial 40,000 cells/well seeded, the morphology of cells on almost all types of the modified PCL scaffolds became round. Exceptionally, the morphology of cells on BSA-immobilized and CBP-immobilized started to extend their cytoplasm and became ellipse. At 4 h after cell seeding, the majority of the cells on all types of modified PCL scaffolds extended their cytoplasm, an evidence of the ability of the cells to

attach on the modified surface. At 6 h after cell seeding, expansion of the cytoplasm of the majority of the cells was evident. The majority of MC3T3-E1 that had been seeded on the surfaces of unmodified PCL fibrous scaffolds for 4 h was remained round, but a closer examination around the edge of the cells revealed an evidence of filopodia. The majority of the cells were evidently expanded after 6 h of cell seeding. On the other hand, the majority of the cells seeded on the surfaces of various types of modified PCL fibrous scaffolds showed an evidence of the extension of their cytoplasm on the fibrous surface even at 4 h after cell seeding. These results suggested that the cells prefer the fibrous surfaces of modified PCL over that of the unmodified. At 1,2, and 3 days after cell seeding, the majority of the cells seeded on the surfaces of all types of modified PCL fibrous scaffolds expanded over the area of the scaffolds which was the most expansion on the surface of BSA-immobilized and CBP-immobilized PCL fibrous scaffolds. From the attachment, proliferation and cell morphology results, we can suggest that the cell prefer to grow and expand on BSA-immobilized and CBP-immobilized PCL fibrous scaffolds over other materials.

**Table 4.3** Selected SEM images of cultured specimens, i.e., glass (i.e., control), neat PCL, aminolyzed PCL, activated PCL, and protein-immobilized PCL fibrous scaffolds at various time points after MC3T3-E1 were seeded on their surfaces (magnification = 2,000X; scale bar =  $10 \mu m$ )

Material	2 h	4 h	6 h
Glass (control)	<u> </u>		1510 32.000 1070 000000
Neat PCL			
Aminolyzed PCL			
Activated PCL			
Gelatin A immobilized PCL			
Gelatin B immobilized PCL			
BSA immobilized PCL			
CBP immobilized PCL			

**Table 4.4** Selected SEM images of cultured specimens, i.e., glass (i.e., control), neat PCL, aminolyzed PCL, activated PCL, and protein-immobilized PCL fibrous scaffolds at various time points after MC3T3-E1 were seeded on their surfaces (magnification = 2,000X; scale bar =  $10 \mu m$ )

Material	1 day	2 day	3 day
iviaterial	2000x	2000x	2000x
Glass(control)	1510 N.2. 008 100-000000	1510 12,000 100-00000	1310 1200
Neat PCL			
Aminolyzed PCL			
Activated PCL			
Gelatin A immobilized PCL			
Gelatin B immobilized PCL			
BSA immobilized PCL			
CBP immobilized PCL			

#### 4.4.4 Alkaline Phosphatase Activity (ALP)

The ability for these PCL fibrous scaffolds to support differentiation, in addition to attachment and proliferation, of cultured cells is another important purpose suggesting potential for use of the scaffold. Alkaline phosphatase is used as an osteoblastic differentiation marker, as it is produced only by cells showing mineralized ECM. The ALP activity of MC3T3-E1 on TCPS (i.e. controls), neat PCL, aminolyzed PCL, activated PCL, and protein-immobilized PCL were evaluated at 3 and 7 days in culture. Figure 4.15 apparently shows the amount of ALP synthesized by the cells that were cultured on TCPS and all of the fibrous scaffolds increased with the initial increase in time in culture. In comparison with other substrates, BSA immobilized PCL fibrous scaffolds exhibited the highest ALP activity of MC3T3-E1 which is close to that of the activated PCL and TCPS at day 7 of cell culturing time. From the obtained results, it was suggested that BSAimmobilized PCL fibrous scaffold was the best among the fibrous scaffolds that promoted both proliferation and differentiation of MC3T3-E1. However, additional long term experiments in order to clarify the effect of scaffolds on the differentiation of osteoblasts are currently determined.

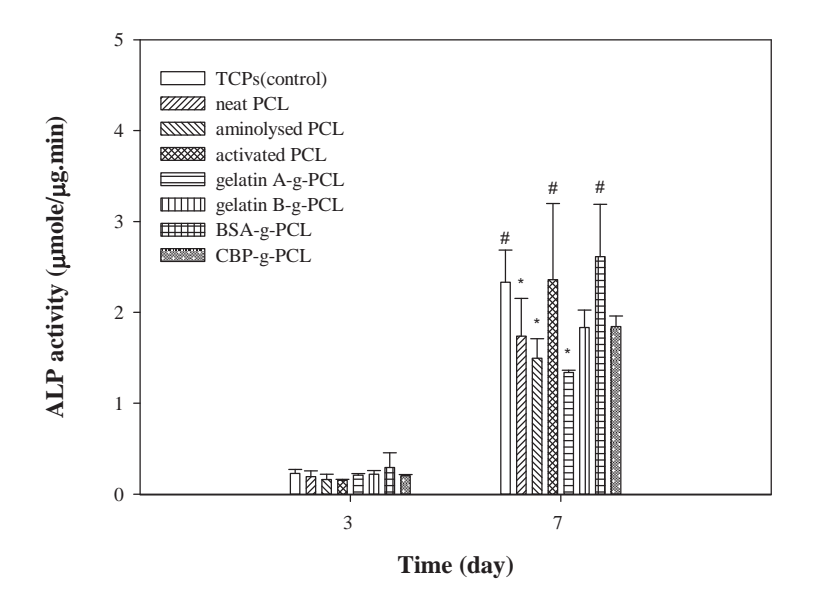


**Figure 4.15**Alkaline phosphatase activity (ALP) of MC3T3-E1 that were cultured on the surfaces of TCPS and the neat and the modified PCL fibrous scaffolds for 3 and 7 d. Statistical significance: \*p < 0.05 compared with control and \*p < 0.05 compared to the neat PCL fibrous scaffolds at any given time point

## 4.4.5 Mineralization

Mineralization was quantified by Alizarin Red-S which is a dye that binds selectively calcium salts. The strain was extracted with 10 % cetylpyridinium chloride in 10 mM sodium phosphate for 1 hour and the absorbance of collected dye was read at wavelength 570 nm in spectrophotometer (A Thermo Spectronic Genesis10 spectrophotometer). The absorbance is relative to the quantity of deposited minerals on the materials as shown in Figure 4.16. The images of scaffolds seeded with MC3T3-E1 for 21 days and stained with Alizarin Red-S illustrated in Figure 4.17 confirmed that the above data where high intensity of stained minerals were observed on all type of immobilized PCL scaffolds. and. The CBP-immobilized PCL scaffolds showed the highest mineral deposition compared with control, neat PCL, and other modified materials. This result can be used to support that the crude bone protein immobilization is an attractive method to be used for fabrication of further developed fibrous scaffolds for bone tissue engineering.

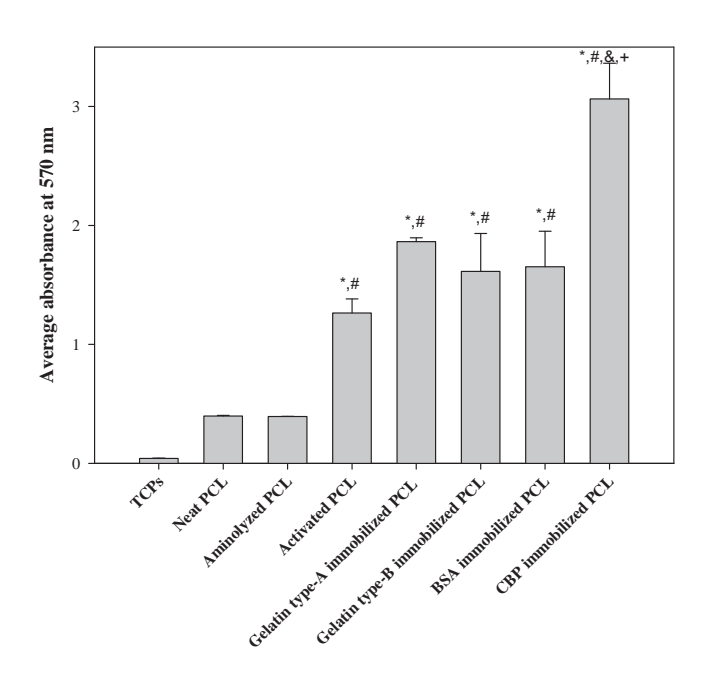


**Figure 4.16**Quantification of mineral deposition in MC3T3-E1 at 21 d by the method of Alizarin Red-S staining measured the absorbance by UV-vis spectrometer at 570 nm. Statistical significance:  $^*p$  < 0.01 compared with control,  $^*p$  < 0.01 compared to the neat PCL,  $^8p$  < 0.01 compared with gelatin type-A immobilized PCL, and  $^*p$  < 0.01 compared with gelatin type-B immobilized PCL fibrous scaffolds at any given time point.

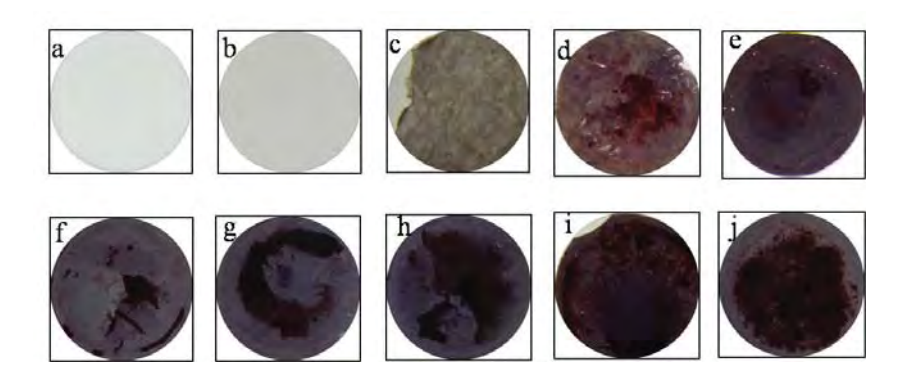


**Figure 4.17** Image of Alizarin Red-S staining for the mineralization in MC3T3-E1 cells for 21 d: TCPS without (a) and with (b) cells, neat PCL without (c) and with (d) cells, aminolyzed (e) and activated PCL (f), and gelatin type-A

(g), gelatin type-B (h), bovine serum albumin (i) and crude bone protein (j) immobilized PCL fibrous scaffold

#### 5. Conclusions

Polycaprolactone fibrous scaffolds were prepared by electrospinning process from a neat 12 % w/v PCL solution in 50:50 v/v DCM/DMF. The PCL electrospun fibrous scaffolds with a thickness of  $(130 \pm 5) \mu m$  were obtained. The scaffold was subsequently immersed in various concentrations of 1,6hexamethylene diamine (HMD) / isopropanol (IPA) solution (0.04, 0.06, 0.08, 0.10, 0.20, and 0.40 g/ml) for 2 hours at 30 °C. To determine the optimum concentration of HMD used in the step of aminolysis, ninhydrin method, degradation experiment, water retention experiment and SEM observation were used. The results show that the optimum condition for aminolysis are 0.20 g/ml HMD treatment for 2 hours at 30 °C. Density, porosity, and pore volume were evaluated to characterize the electrospun scaffolds. The NH<sub>2</sub> density on the aminolyzed PCL surface was confirmed and quantified using ninhydrin method. The NH<sub>2</sub> density increased with increasing 1,6hexamethylenediamine concentration. However, when the concentration of 1,6-hexamethylenediamine is greater than 0.20 g/ml, the structural morphology of the electrospun PCL fiber scaffolds became worse. In the other word, water contact angle slightly decreased with increasing HMD concentration. This means that aminolysis can improve the hydrophilicity of the surface. Macromolecules i.e. gelatin type-A, gelatin type-B, bovine serum albumin, and crude bone protein were further immobilized using N,N'disuccinimidyl carbonate (DSC) as a coupling agent. Various techniques; Attenuated Total Reflectance-Fourier Transform Infrared Spectrometer (ATR-FTIR), X-ray Photospectroscopy (XPS), Scaning Electron Microscopy (SEM), and water contact angle measurement were used to monitor the scaffold surfaces after each modification step. In XPS experiment, The  $N_{1s}/C_{1s}$  ratio was increased after immobilization with proteins (gelatin type-A, gelatin type-B, bovine serum albumin and crude bone protein) due to the large amount of nitrogen atom in protein structure was introduced. The potential use of the surface-modified PCL scaffolds as bone scaffolds was evaluated with a murine pre-osteoblastic cell line (MC3T3-E1). The cytotoxicity test showed all types of proteins and PCL fibrous scaffolds released no substances at levels that were harmful to cells. The number of cells attached on these fibrous scaffolds was lower in comparison with that on TCPS at any given time point. There was the most viability of cells on crude bone protein-immobilized PCL fibrous scaffold among various types of the modified fibrous scaffolds. MC3T3-E1 proliferation was improved remarkably on the modified surface, with the cells growing on the bovine serum albumin-immobilized PCL fibrous scaffolds showing the greatest proliferation after cell culture as well as the highest ALP activity. In long term experiments, the image of scaffolds seeded with MC3T3-E1 for 21 days and stained with Alizarin Red-S and quantification of deposited minerals measured by UV-vis spectrometer confirmed that high intensity of stained minerals were observed on all type of immobilized PCL scaffolds. The CBP-immobilized PCL scaffold showed the highest mineral deposition compared with control, neat PCL, and other modified materials. This result supported that the crude bone protein immobilization was able to induce the cell differentiation to bone the most. All the obtained results suggested that bovine serum albumin and crude bone protein immobilization are an attractive method to fabricate of further developed fibrous scaffolds for bone tissue engineering.

#### **6.REFERENCES**

- Ayhan, H. and Ayhan, F. (2002) In Vitro Evaluation of 3T3 and MDBK Cells
  Attachment and Proliferation on Collagen and Fibronectin
  Immobilized NonwovenPolylactide Matrices. <u>Journal of Bioactive and Compatible Polymers.</u>, 17, 463-476.
- Boelgen, N., Menceloglu, Y.Z., Acatay, K., Vargel, I., and Piskin, E. (2005) In vitro
  - and in vivo degradation of non-woven materials made of poly( $\epsilon$ -caprolactone) nanofibers prepared by electrospinning under different

- conditions. <u>Journal of Biomaterials Science</u>. <u>Polymer Edition</u>,16(12), 1537-1555.
- Burg, K.J.L., Porter, S.,and Kellam, J.F. (2000) Biomaterial developments for bone tissue engineering. <u>Biomaterials</u>, 21, 2347-2359.
- Calvert, J.W., Marra, K.G., Cook, L., Kumta, P.N., DiMilla, P.A., and Weiss, L.E. (2000) Characterization of osteoblast-like behavior of cultured bone marrow stromal cells on various polymer surfaces. <u>Journal of Biomedical Materials Research</u>, 52(2), 279-284.
- Carter, D. C. and Ho, J. X. (1994) Structure of Serum Albumin. <u>Advance in Protein Chemistry</u>., 45, 153-203.
- Cheng, Z., and Teoh, S.-H. (2004) Surface modification of ultra thin poly(ε-caprolactone) films using acrylic acid and collagen. <u>Biomaterials</u>, 25(11), 1991-2001.
- Edlund, U., Dånmark, S., and Albertsson, A.-C. (2008) A Strategy for the Covalent Functionalization of Resorbable Polymers with Heparin and Osteoinductive
- Growth Factor. <u>Biomacromolecules</u>, 9(3), 901-905.
- Figge, J., Rossing, T. H. and Fencl, V. (1991) The Role of serum-proteins in Acid-Base Equilibria. <u>The Journal of Laboratory and Clinical</u> Medicine., 117, 453 467.
- Gao, C., Guan, J., Zhu, Y., and Shen, J. (2003) Surface Immobilization of Bioactive Molecules on Polyurethane for Promotion of Cytocompatibility to Human Endothelial Cells. Macromolecular Bioscience, 3(3-4), 157-162.
- Guan, J., Gao, C., Feng L., and Shen, J. (2001) Surface modification of polyurethane for promotion of cell adhesion and growth 1: Surface photo-grafting with N,N-dimethylaminoethyl methacrylate and cytocompatibility of the modified surface. <u>Journal of Materials Science: Materials in Medicine.</u>, 12 (5), 447-452
- Habraken, W.J.E.M., Wolke, J.G.C., and Jansen, J.A. (2007) Ceramic composites

- as matrices as matrices and scaffolds for drug delivery in Tissue engineering.
- Adanced drug delivery review, 59, 234-248.
- Hou, Q., Grijpma, D. W., Feijen, J. (2003) Porous polymeric structures for tissue engineering prepared by a coagulation, compression moulding and salt leaching technique. <u>Biomaterials</u> 24(11), 1937-1947.
- Huang,W., Carlsen,B., Wulur,I., Rudkin,G., Ishida,K., Wu,B., Yamaguchi,D.T., Miller,T.A. (2004) BMP-2 exerts differential effects on differentiation of rabbit bone marrow stromal cells grown in two-dimensional and three-dimensional systems and is required for in vitro bone formation in a PLGA scaffold. Experimental Cell Research, 299, 325–334
- Hutmacher, D. W. (2000) Scaffolds in tissue engineering bone and cartilage. Biomaterials, 21, 2259.
- Jeon,O., Songa,S.J., Kanga,S-W., Putnam,A.J., and Kim,B-S. (2007) Enhancement of ectopic bone formation by bone morphogenetic protein-2 released from a heparin-conjugated poly(L-lactic-co-glycolic acid) scaffold Biomaterials; 28: 2763–2771
- Lee, S-H., and Shin, H. (2007) Matrices and scaffolds for delivery of bioactive molecules in bone and cartilage tissue engineering. <u>Advanced drug delivery reviews</u>,59, 339-359.
- LeGero, R.Z. (2002) Properties of osteoconductive biomaterials: calcium phosphates. <u>Clin Orthop Relat Res</u>, 395, 81-98.
- Ma, Z., Gao, C., Yuan, J., Ji, J., Gong ,Y., and Shen,J. (2002) Surface modification of poly-L-lactide by photografting of hydrophilic polymers towards improving its hydrophilicity. <u>Journal of Applied Polymer</u> <u>Science</u>, <u>85 (10)</u>, 2163 – 2171
- Mattanavee, W., Suwantong, O., Puthong, S., Bunaprasert, T., Hoven, V.P., and Supaphol, P. (2009) Immobilization of Biomolecules on the

- Surface of Electrospun Polycaprolactone Fibrous Scaffolds for Tissue Engineering. <u>ACS Applied Materials & Interfaces</u>.
- Meinel, L., Zoidis, E. Zapf, J. Hassa, P. Hottiger, M.O., Auer, J.A., Schneider, R., Gander, B., Luginbuehl, V., Wolfisberger, R.B., Illi, O.E., Merkle, H.P., and Rechenberg B.von. (2003) Localized insulin-like growth factor I delivery to enhance new bone formation. Bone; 33: 660–672
- Mikos, A.G., Bao, Y., Cima, L.G., Ingber, D.E., Vacanti, J.P., Langer, R. (1993) Preparation of poly (glycolic acid) bonded fibres structures for cell attachment and transplantation. <u>Journal of biomedical materials</u> research, 27, 183-189.
- Mikos, A.G., Sarakinos, G., Vacanti, J.P., Langer, R., and Cima, L.G. (1996)

  Biocompatible polymer membranes and methods of preparation of three dimensional membrane structures. <u>United States Patent</u> 5514378
- Mikos, A.G., Thorsen, A.J., Czerwonka, L.A., Bao, Y., Langer, R.(1994)

  Preparation and characterisation of poly(L-lactic acid) foams.

  Polymer, 35, 1068-1077.
- Park,K., Jung, H.J., Kim, J-J., Ahn, K-D. and Han, D.K. (2006) Acrylic Acid-Grafted Hydrophilic Electrospun Nanofibrous Poly(L-lactic acid) Scaffold. Macromolecular Research, 14 (5), 552-558
- Prasansuklarb, A. (2008) Osteoblastic cell growth and enzymatic degradation of different aliphatic polyester scaffolds. Master thesis. The Petroleum and Petrochemical College, Chulalongkorn University.
- Saito,N., Okada,T., Horiuchi,H., Ota,H., Takahashi,J., Murakami,N., Nawata,M., Kojima,S., Nozaki,K., and Takaoka,K. (2003) Local bone formation by injection of recombinant human bone morphogenetic protein-2 contained in polymer carriers. <u>Bone</u>, 32, 381–386
- Salgado, A.J., Coutinho, O.P., and Reis, R.L. (2004) Bone Tissue Engineering: State of the Art and Future Trends. Macromolecular Bioscience; 4:743–765
- Santiago, L.Y., Nowak, R.W., Rubin, J.P., and Marra, K.G. (2006) Peptidesurface modification of poly(caprolactone) with laminin-derived

- sequences for adipose-derived stem cell applications. <u>Biomaterials</u>, 27(15), 2962-2969.
- Savarino, L., Baldini, N., Greco, M., Capitani, O., Pinna, S., Valentini, S., Lombardo, B., Esposito, M.T., Pastore, L., Ambrosio, L., Battista, S., Causa, F., Zeppetelli, S., Guarino, V., and Netti, P.A. (2007) The performance of poly-ε-caprolactone scaffolds in a rabbit femur model with and without autologous stromal cells and BMP4. <u>Biomaterials</u>, 28(20), 3101-3109.
- Shen, H., Hu, X., Yang, F., Bei, J., and Wang, S. (2009) The bioactivity of rhBMP-2 immobilized poly(lactide-co-glycolide) scaffolds.

  <u>Biomaterials</u>, 30(18), 3150-3157.
- Sumner , D.R., Turner , T.M., Urban , R.M., Leven, R.M., Hawkins ,M., Nichols, E.H., McPherson, J.M., and Galante, J.O. (2001) Locally delivered rhTGF-β<sub>2</sub> enhances bone ingrowth and bone regeneration at local and remote sites of skeletal injury. <u>Journal of Orthopaedic Research</u>, 19, 85-94.
- Venugopal, J.R., Low, S., Choon, A.T., Kumar, A.B., and Ramakrishna, S. (2008) Nanobioengineered Electrospun Composite Nanofibers and Osteoblasts for Bone Regeneration. <u>Artificial Organs</u>, 32(5), 388–397.
- Wang,X., Wenk,E., Zhang,X., Meinel,L., Vunjak-Novakovic,G., and Kaplan,D.L. (2009) Growth factor gradients via microsphere delivery in biopolymer scaffolds for osteochondral tissue engineering. Journal of Controlled Release, 134, 81–90
- Ward, A.G.; Courts, A. (1977) The Science and Technology of Gelatin. New York: Academic Press
- Wei,G., Jin,O., Giannobile,W.V., and Ma.P.X. (2007) The enhancement of osteogenesis by nano-fibrous scaffolds incorporating rhBMP-7 nanospheres. <u>Biomaterials</u>, 28, 2087–2096
- Wenk, E., Meinel, A.J., Wildy, S., Merkle, H.P., and Meinel, L. (2009) Microporous silk fibroin scaffolds embedding PLGA microparticles for

- controlled growth factor delivery in tissue engineering. <u>Biomaterials</u>, 30, 2571–2581
- Whang, K., Thomas, C. H., Healy, K. E. and Nuber, G. (1995) A novel method to fabricate bioabsorbable scaffolds. Polymer, 36, 837-842
- Yoneda, M., Teraia, H., Imaia, Y., Okada, T., Nozaki, K., Hikarulno, Miyamoto, S., and
- Takaoka,K. (2005) Repair of an intercalated long bone defect with a Synthetic biodegradable bone-inducing implant. <u>Biomaterials</u>, 26, 5145–5152
- Yoshimoto, H., Shin, Y.M., Terai, H., and Vacanti, J.P. (2003) A biodegradable nanofiber scaffold by electrospinning and its potential for bone tissue engineering. <u>Biomaterials</u>, 24(12), 2077-2082.
- Zhu, Y., Chian, K.S., Chan-Park, M.B., Mhaisalkar, P.S., and Ratner, B.D. (2006) Protein bonding on biodegradable poly(I-lactide-co-caprolactone) membrane for esophageal tissue engineering. <u>Biomaterials</u>, 27(1), 68-78.
- Zhu, Y., Cao, Liu, Y., and Shen, J. (2004) Endothelial cell functions in vitro cultured on poly(L-lactic acid) membranes modified with different methods. <u>Journal of Biomedical Materials Research Part A</u>, 69A(3), 436-443.
- Zhu, Y., Gao, C., Liu, X., and Shen, J. (2002a) Surface Modification of Polycaprolactone Membrane via Aminolysis and Biomacromolecule Immobilization for Promoting Cytocompatibility of Human Endothelial Cells. <u>Biomacromolecules</u>, 3(6), 1312-1319.
- Zhu, Y., Gao, C., and Shen, J. (2002 b) Surface modification of polycaprolactone with poly(methacrylic acid) and gelatin covalent

immobilization for promoting its cytocompatibility. <u>Biomaterials</u>, 23(24), 4889-4895.

# DEVELOPMENT OF POROUS HYDROXYAPATITE PARTICLES AS CARRIERS OF PROTEINS FOR BONE TISSUE ENGINEERING

Sujittra Chaisuntharanon, 1 Prasit Pavasant, 2 and Pitt Supaphol 1,\*

<sup>1</sup>The Petroleum and Petrochemical College and The Center for Petroleum, Petrochemicals and Advanced Materials (C-PPAM), Chulalongkorn University, Bangkok 10330, Thailand

#### 4.1 Abstract

Incorporation of proteins by physical absorption within porous Hydroxyapatite (HAp)-based implants has been frequently reported for orthopaedic uses whereas sequential release is hardly properly controlled. This work aims at developing HAp particles as a controlled release carrier of proteins. HAp carriers were synthesized by coprecipitation technique from dicalcium phosphate dihydrate (CaHPO<sub>4</sub>·2H<sub>2</sub>O, DCPD) and calcium carbonate (CaCO<sub>3</sub>). Incorporation of proteins was accomplished during the coprecipitation of the two reactants. Desorption behavior of proteins from HAp particles will be investigated by UV-Visible spectrophotometry.

(**Key-words**: Hydroxyapatite, protein carrier)

#### 4.2 Introduction

Hydroxyapatite (HAp), having a chemical formula  $Ca_{10}(PO_4)_6(OH)_2$  is a naturally occurring inorganic constitutent of tooth enamel, dentine, bone and other hard tissues of vertebrates. It has been widely used as bone filler, spacer, and bone graft. HAp has been well-recognized as it is an excellent affinity to biological substances such as collagen, proteins, enzymes, cells, and viruses, biocompatible, osteoconductive and bioactive material (Liu, T-Y. et al., 2005). With the osteoconductive properties, HAp ceramic has been

Authors to whom correspondence should be addressed: pitt.s@chula.ac.th (P. Supaphol)

<sup>&</sup>lt;sup>2</sup> Department of Anatomy, Faculty of Dentistry, Chulalongkorn University, Bangkok 10330, THAILAND

also investigated as scaffolds for cell delivery and tissue engineering. In addition, porous hydroxyapatie ceramics have a considerable potential as carriers for controlled drug release (Ijntema, K. *et al.*, 1994), protein delivery agent, catalyst, and absorbent (Li, Y. *et al.*, 2008). The apatite crystal often used to carry drugs or proteins has regularly a stoichiometric composition, i.e., Ca/P=1.67 (Liu, T-Y. *et al.*, 2005). The adsorption of protein onto HAp is important to accelerate tissue healing when placed in vivo (Yang, Q. *et al.*, 2006) in a variety of oral or osseous biological events. HAp has also adsorptive capabilities with respect to proteins and biologically active molecules, such as osteogenic agents and growth factors. Up to now, many methods such as sol-gel, precipitation, hydrothermal, mechno-chemical, spray pyrolysis, freeze-drying and electrochemical deposition have been developed to prepared HAp powders. In these methods, wet chemical process was usually used to prepare HAp powders because it is easy to operate and need not any expensive equipments (Cao, Li-yun, *et al.*, 2005).

The interaction of proteins with hydroxyapatite appeared to depend on the overall protein charge, the number of acidic and basic groups, and the specific protein structure (ljntema, K. *et al.*, 1994).

The purpose of this study is to fabricate proteins-HAp powder to control the release rate behavior of different proteins.

### 4.3 Experimental section

#### 4.3.1 Materials

- Dicalcium phosphate dihydrate (DCPD; Fluka, Germany)
- Calcium carbonate (CaCO<sub>3</sub>; Carlo Erba, Italy)
- Tris-base (Tris[hydroxymethyl]amino methane) (Sigma-Aldrich, USA)
- Nitric acid (ACS reagent 69%; J.T.Baker, USA)
- Ovalbumin (OVA; Sigma-Aldrich, USA)
- Gelatin type B (Sigma-Aldrich, USA)

- Bovine serum albumin (BSA; Sigma-Aldrich, USA)
- Sodium phosphate monobasic (NaH<sub>2</sub>PO<sub>4</sub>) and sodium phosphate dibasic (Na<sub>2</sub>HPO<sub>4</sub>; Ajex Finechem, Australia)

#### 4.3.2 <u>Preparation of Protein-Loaded Hydroxyapatite</u>

Calcium hydrogen phosphate dihydrate (CaHPO<sub>4</sub>.H<sub>2</sub>O, DCPD) and calcium carbonate (CaCO<sub>3</sub>) were used as precursors of Ca and P to prepare protein-loaded hydroxyapatite. The molar ratios of Ca to P were fixed at 1.67 which mixed with nitric acid 1 mol/l at 75 °C for 1 h under stirring. Then, pour distilled water at room temperature following protein. Ovalbumin (Sigma-Aldrich A-5253), Gelatin type B, Bovine serum albumin (BSA, Aldrich A-3912) and Crude bone protein from pork bone were selected as candidate proteins in this study. The proteins aqueous solution were prepared by dissolving proteins powder or pellet into distilled water for each synthesis. Regulated pH at a constant value, tris(hydroxymethyl) aminomethane. The aggregates were rinsed with the distilled water until pH=7 (DI water was boiled and decarbonated before use) and further centrifuged at 4500 rpm for 10 mins, freezed at -45 °C and lyophilized at -50 °C. The samples were kept in dessicator until used.

#### 4.3.3 <u>Crude Bone Protein preparation</u>

CBP was extracted from the pork bone. In particular, bone was initially washed and cleaned thoroughly in tap water and then sectioned into small pieces with a high speed motor machine. Pieces of bones were further crushed into powder in liquid nitrogen. Then, the as-prepared powder was immersed in 0.6 N HCl at 4 °C. After three days, the bony solution was centrifuged and the supernatant was collected, dialyzed for 48 h and lyophilized. The dry CBP was kept in desiccators until use (Hariraksapitak, *et al.*, 2009).

#### 4.3.4 Characterization

#### 4.3.4.1 Thermogravimetric Analysis (TGA)

The relative amount of the proteins associated with the HAp was determined using thermogravimetric analysis, TG-DTA (Perkin Elmer) instrument under  $N_2$  flow of 5 ml/min. The heating process was conducted from 30-950 °C at a rate of 10 °C/min.

4.3.4.2 Fourier-transformed infrared spectrophotometer (FT-IR)

A Thermo Nicolet Nexus<sup>®</sup> 670 Fourier-transformed infrared spectrophotometer (FT-IR) was used to investigate chemical functionalities of hydroxyapatite powder by the KBr disk method. Hydroxyapatite powders were randomly selected from each group of samples and detected for the FT-IR spectra with a resolution of 4 cm<sup>-1</sup> in the range of 4000-400 cm<sup>-1</sup> and were averaged from 32 scans.

#### 4.3.4.3 Autosorb-1

The BET method uses gas with a known adsorption area per 1 g to measure the surface area of samples based on gas quantites adsorbed to the sample surface. Fifty mg of the sample was preheated at 200 °C for 10 min to remove water and gas completely. Surface areas of HAp particles were analyzed by nitrogen adsorption in a Autosorb-1.

# 4.3.4.4 Scanning Electron Microscope (SEM)

For the morphological study, hydroxyapatite were mounted on brass stubs, coated with gold using a JEOL JFC-1100 sputtering device, and observed for their microscopic morphology using JEOL JSM-5200 scanning electron microscopy (SEM). For the morphology of the surface, pore size, distribution and also the interconnectivity.

## 4.3.4.5 Transmission Electron Microscope (TEM)

The microstructural and morphological features of HAp powders were analysed in JEM-2100 operating voltage of 200 kV. Sample for TEM were prepared by air-drying a drop of a sonicated ethanol suspension of particles onto a carbon-coated copper grid and air-dried.

# 4.3.4.6 Energy Dispersive Spectrophotometer (EDS)

The Ca/P ratio of the hydroxyapatite was studied by the X-ray microanalysis, using the method of Energy dispersive X-ray spectroscopy (EDS). EDS is an analytical technique used for the elemental compositions of the HAp.

## 4.3.4.7 X-ray Diffraction (XRD)

The phase compositions, crystal shape and size of HAp powders were characterized by X-ray diffraction (XRD) with copper target. Data were collected over the scanning range (20) from 5  $^{\circ}$  to 60  $^{\circ}$  at a scan speed 2  $^{\circ}$  /min.

The average crystallite size of the prepared hydroxyapatite samples was determined using the scherrer equation.

## D= $K \cdot \lambda / \beta \cdot Cos\theta$

In which D is the average crystallite size (Å), K denotes the shape factor (K=0.9),  $\lambda$  is the X-ray wavelength (for CuK $\alpha$   $\lambda$ =1.5418 Å),  $\beta$  represents the peak at half width (in rad), and  $\theta$  is the Bragg angle of the peak (002 reflection of hydroxyapatite at  $2\theta$ =26 °).

#### 4.3.4.8 UV-Visible Spectrophotometer

Determination of protein by UV/Vis spectrophotometry at 215 nm for Gelatin type B, 280 nm for OVA and BSA and 275 nm for CBP.

## 4.3.4.9 Zeta potential (ZP)

Zeta potentials (or electrophoretic mobility) of the hydroxyapatite were determined using Zeta-Meter 3.0+ (Zeta-Meter, Inc., USA). Briefly, the suspension of 100 mg hydroxyapatite in 20 ml of deionized water was filled in an electrophoresis cell. Two electrodes were inserted into the cell and connected to the Zeat-Meter 3.0+ unit. Once the electrodes were energized, microspheres were aroused to move toward one electrode. Particles were observed under a microscope for its movement along a specific distance which was indicated by a built in grid. The zeta potential value was detected at a right time point when the microsphere moved to the end. Measurement was repeated 10 times for each preparative condition and the average values were calculated.

#### 4.3.4.10 Particle size distribution

The Malvern Particle size of hydroxyapatite was measured by Mastersizer 2000 a solution of the particles was sonicated in an ultra-sonic bath for 7 min immediately before measurement to ensure separation of particles. A sample of this mixture was injected into the sample cell of the Malvern Mastersizer. The obscuration was between 10 and 30 %, as required by the instrument. The Mastersizer calculates automatically the particle size and distribution from small angle light scattering using Mie theory and Fraunhofer diffraction theory. The measurements were taken with the stirrer in the Mastersizer to ensure even distribution of particles and prevent sedimentation in the sample cell. Shear forces were not a problem in this case as the goal was to measure the primary particle size. A least 10 measurements were recorded and the average value recorded.

#### 4.3.4.11 In vitro protein-HAp release test

Proteins-loaded Hydroxyapatite (20 mg) were dispersed in 10 ml 0.1M phosphate buffer saline (PBS) solution at pH 7.4. All samples were incubated in a shaking water bath (70 rpm) at 37 °C. The releasing medium was withdrawn 1 ml and an equal amount of fresh medium was added to maintain a constant volume of the medium. The amount of protein in the sample solution was determined by UV-visible spectroscopy. Absorbance peaks at 280 nm to determine the ovalbumin and BSA concentration, 215 nm to determine the gelatin type B, and 275 nm to determine the crude bone protein. Concentration through the use of a predetermined standard concentration—intensity calibration curve. An average value was calculated at each time point. The protein content of the encapsulated particles can be described by two quantities in terms of Encapsulating efficiency of protein-loaded hydroxyapatite (EE) and Loading capacity of hydroxyapatite particle (LC), which were determined according to the following equation (Freiberg and Zhu, 2004).

Encapsulating efficiency (%) = total mg proteins-encapsulated x

100

initial mg proteins-loaded

Loading capacity (%) = total mg proteins-encapsulated x 100 total mg particles

## 4.4 Results and Discussion

## 4.4.1 <u>Thermogravimetric Analysis (TGA)</u>

The samples were analyzed by TGA using a Perkin Elmer (TG-DTA) instrument under  $N_2$  flow of 5 ml/min. The heating process was conducted from 30-950 °C at a rate of 10°C/min. To investigate amount of proteins-loaded hydroxyapatite.

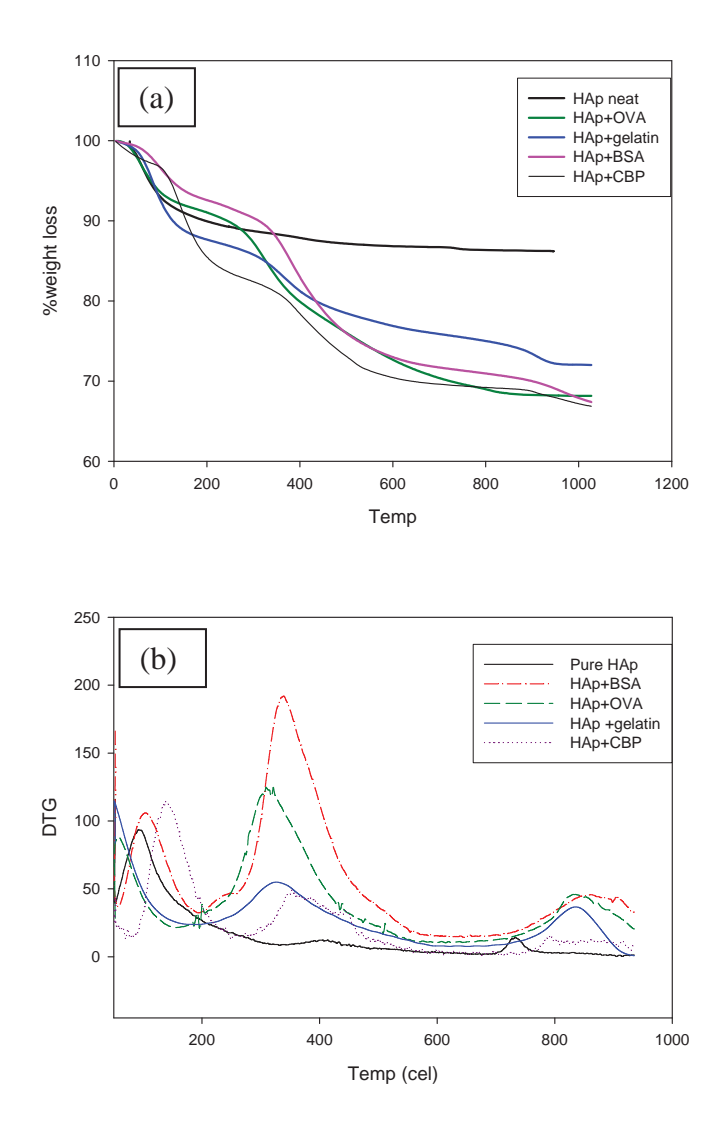


**Figure 4.1** TGA-DTG curves (a) TGA, (b) DTG of proteins-loaded hydroxyapatite.

The features of TGA and DTA profiles of proteins-loaded hydroxyapatite were presented in Figure 4.1. The weight loss could be differentiated into three regions in the investigated temperature range such as (i) 25-210 °C, (ii) 210-570 °C, and (iii) 750-950 °C. In the first region of 25-210 °C, the weight loss for all precursors could be attributed to the removal of physically absorbed water. The second region of 210-570 °C is a major weight loss, probably due to the combustion of proteins residuals (organic matter) and with the maximum rate at 350 °C, and decomposition of calcium

hydroxide and carbonate to water and carbon dioxide. The third region of 750-950 °C, the weight loss can be assigned to the decomposition of carbonate compounds.

The TGA curves of the samples (Figure 4.1) show differences in the amount of protein weight loss. Weight loss of ovalbumin was 16.8 %, Gelatin type B was 10.22 %, BSA was 20.61 % and CBP from pork bone was 22 %.

#### 4.4.2 <u>UV-Visible Spectrophotometer</u>

Take water after finish synthesis reaction measured by UV-Visible to determine the remaining protein after reaction. OVA and BSA were measured the wavelength with 280 nm, Gelatin type B with 215 nm and CBP from pork bone with 275 nm.

To investigate amount of proteins-loaded hydroxyapatite. Remaining OVA in the DI water is 6.12 %, Gelatin type B is 14.30 %, and BSA is 2.38 %. So, OVA, Gelatin type B, and BSA are entrapped in hydroxyapatite 20.26 %, 12.08 %, and 24% respectively. It is possible that protein may be lost during the washing HAp with DI water about 5-6 times to become neutral.

#### 4.4.3 X-ray Diffraction

In the X-ray diffraction analysis, all synthesized precipitates showed a HAp-like pattern (Figure 4.2). The crystallinity of each precipitate was evaluated from the data of the inverse of half value breadth of the (002) peak of HAp (Figure 4.2). The crystallinity of HAp depends on its synthesized temperature in such a way that HAp synthesized at low temperature has low crystallinity. The solubility of HAp also depended on its synthesized temperature and HAp synthesized at low temperature showed high solubility (Matsumoto, T. et al., 2004).

For HAp powders, the crystallite size in a direction perpendicular to the crystallographic plane is always estimated according to Scherrer's formula as followed:

# $d = (0.9\lambda) / FWHM*Cos\theta$

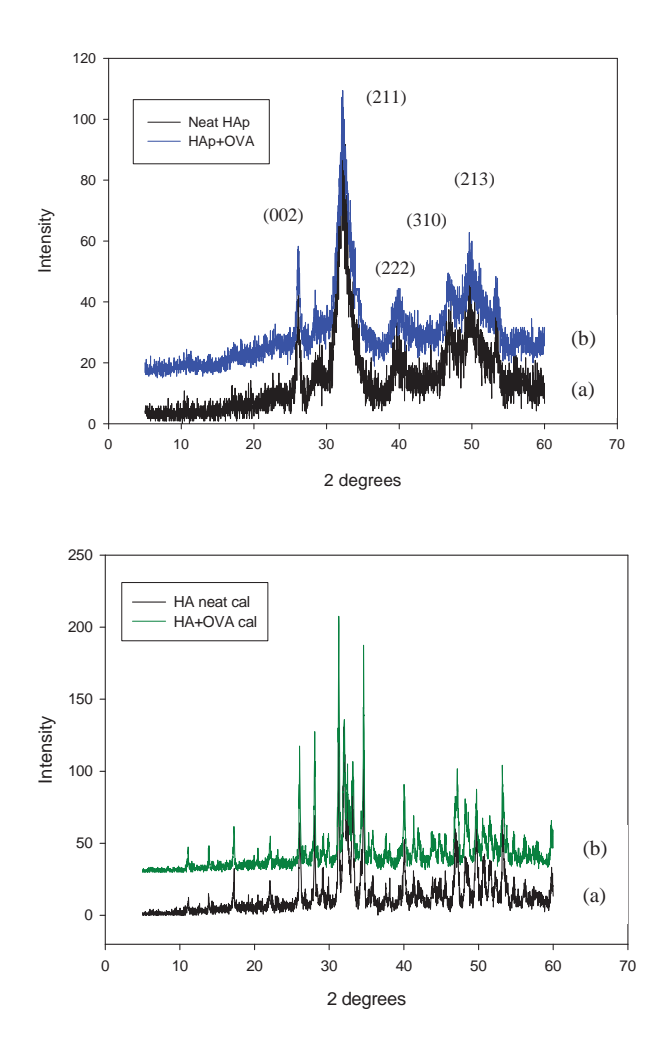


**Figure 4.2** XRD pattern of HAp powders : (a) Neat HAp; (b) OVA-loaded HAp.

where d is the crystallite size (nm);  $\lambda$ =0.15406 nm for Cu Kα radiation of X-ray beam; FWHM the full width at half maximum for the diffraction peak (rad); and  $\theta$  is the Bragg angle of the (002) diffraction angle (°). Two major characteristic diffraction peaks could be obtained for all the powdered samples: one closed at 2 $\theta$  of ~26° and the other broad one at ~32°. According to PDF no.01-1008, The uncalcined HAp is shown the broad

patterns around at (002) and (211). It indicates that the crystallites were very tiny in nature. The (002) peak (2θ~26 °) from XRD patterns was chosen for calculating the crystallite size as shown in Table 4.1 since it contains the least overlap of the broadened peaks. It could be found that the crystallite size depends on the size of the particle that observed from SEM. Crystallite size of calcined HAp powders was larger than uncalcined powder. Figure 4.2 indicated that uncalcined HAp powders were amorphous and did not form CaP crystals, because HAp crystallization is mediated by protein and shown in Figure 4.3.

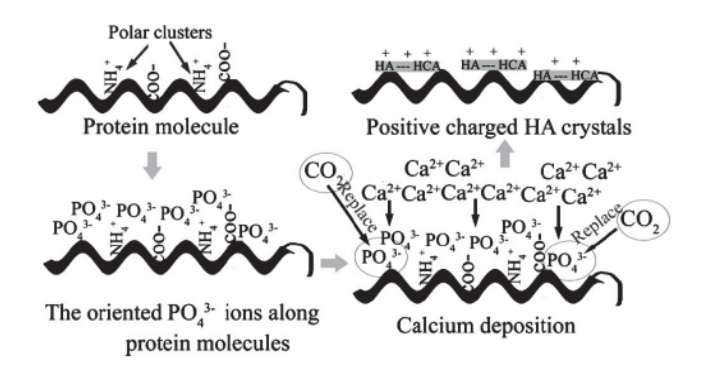


**Figure 4.3** Schematic illustration of the protein-medicated crystallization of HAp crystals with positive charges (Zhao, H. *et al.*, 2008).

**Table 4.1** The different crystallite size of (a) calcined HAp at 800 °C; (b) uncalcined HAp powder (a)

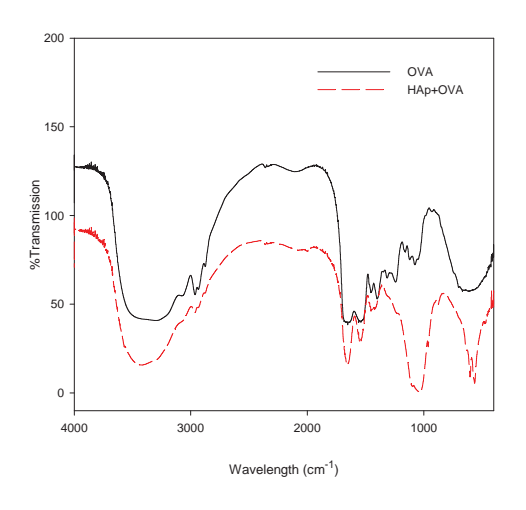
Crystal plane (002)	2θ	FWHM	Crystallite size
			(nm)
Neat HAp calcine	26.07	0.22	40.01
OVA-HAp calcine	26.05	0.15	58.16
Gealtin-HAp calcine	26.00	0.23	38.37
BSA-HAp calcine	25.82	0.23	37.03

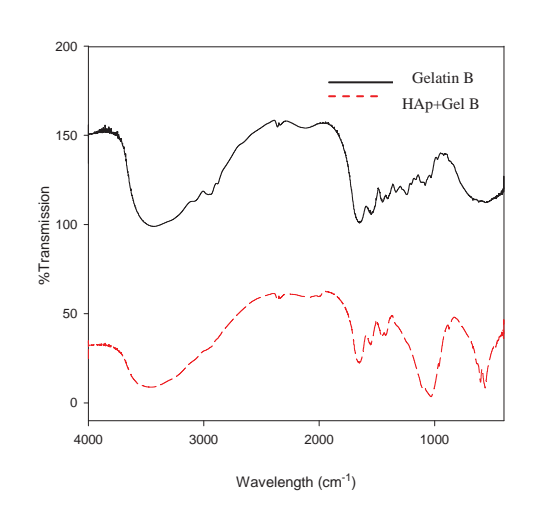
(b)

Omiotal plana (000)	2θ	FWHM	Crystallite size
Crystal plane (002)			(nm)
Neat HAp uncalcine	26.11	0.44	20.45
OVA-HAp uncalcine	26.12	0.51	17.69
Gelatin-HAp uncalcine	25.80	0.51	19.37
BSA-HAp uncalcine	25.91	0.51	16.88

4.4.4 Fourier-Transformed Infrared Spectrophotometer

Adsorption of protein on HAp particles was detected by FTIR analysis (Figure 4.4). The spectra show the characteristic peaks of absorbed water, hydroxyl, phosphate and carbonate species. The broad peak around 3250 cm<sup>-1</sup> to 3500 cm<sup>-1</sup> corresponds to the adsorbed water. The spectrum clearly indicates a peak at 1640 cm<sup>-1</sup> which is attributed to the presence of water associated with HAp. The absorption bands at 1460 cm<sup>-1</sup> and 875 cm<sup>-1</sup> suggest the presence of CO<sub>3</sub><sup>2-</sup>. The absorption bands at 1040, 1093, 962 and 571 cm<sup>-1</sup> detected in the spectra are attributed to the PO<sub>4</sub><sup>3-</sup> ion. The absorption bands at 1210 cm<sup>-1</sup> together with one at 1130 cm<sup>-1</sup> and clear absorption band at 879 cm<sup>-1</sup> are attributed to the HPO<sub>4</sub><sup>2-</sup>. The spectrum of protein exhibited an appearent absorption band at 1654 cm<sup>-1</sup> assigned to amide I, C=O stretching mode. The absorption band at 1540 cm<sup>-1</sup> assigned to amide II, N-H bending mode and 1384 cm<sup>-1</sup> assigned to amide III, C-N stretching mode and N-H bending mode.





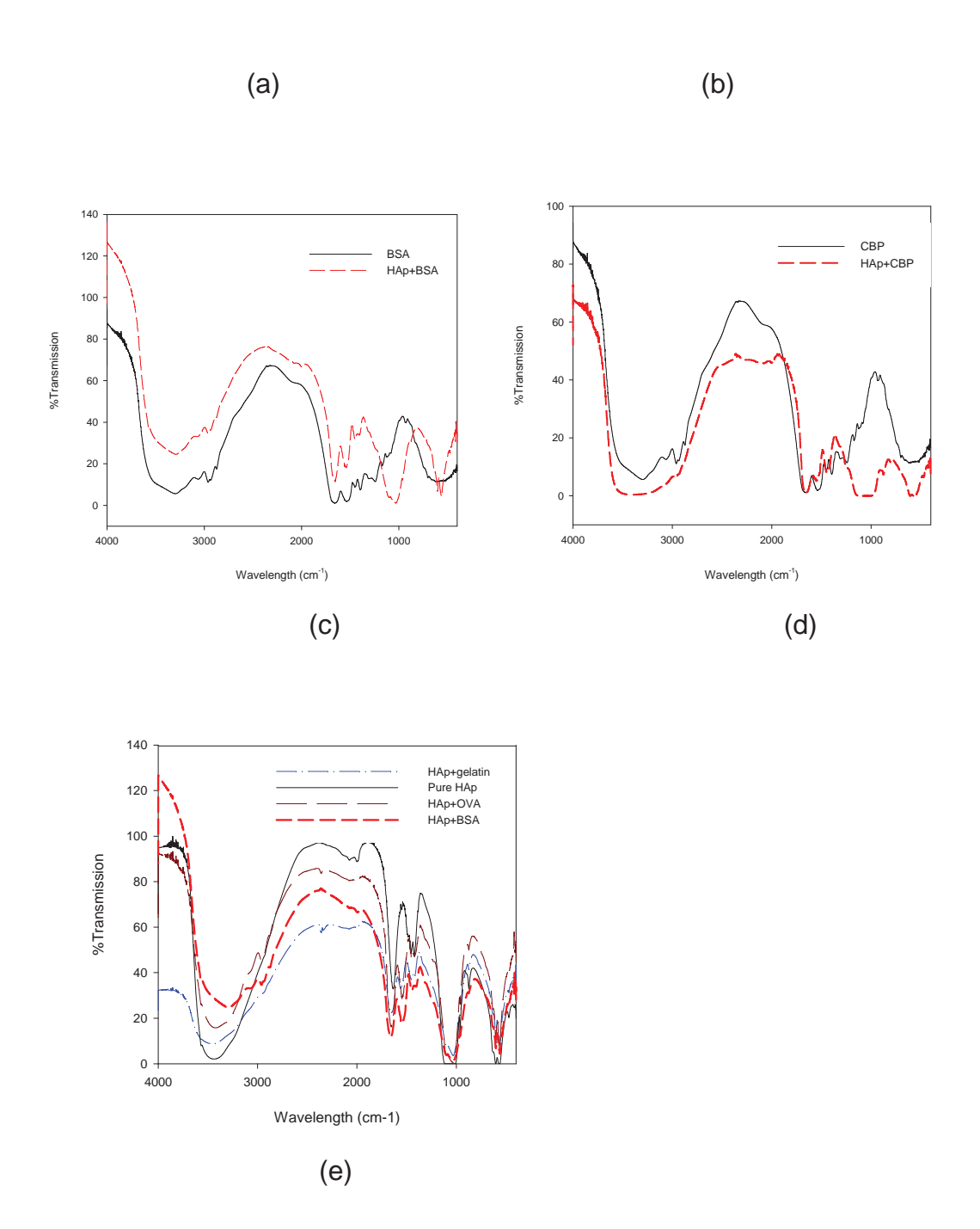


**Figure 4.4** The FTIR spectra of HAp powders of : (a) OVA-loaded HAp; (b) Gelatin-loaded HAp; (c) BSA-loaded HAp; (d) CBP-loaded HAp; (e) including protein/HAp.

The possible mechanisms can be adapted to explain the interaction between the HAp and proteins molecules. The mechanism can be operated through the electrostatic interaction between the positive Ca<sup>2+</sup> and COO<sup>-</sup> (protein): this has been also reported by Liu who suggested that there is an intermediate complex between COO- and HAp. This complex can be formed via the electrostatic interaction between the negative COO<sup>-</sup> on protein molecules and positive Ca<sup>2+</sup> on the C-sites of HAp surface. Kazuhiko K. indicated that the C-sites were located on the crystal planes that are perpendicular to a-axis and b-axis of apatite crystal.

## 4.4.5 <u>Scanning Electron Microscope (SEM)</u>

To investigate the morphology of HAp powder by using SEM (JEOL, model JEM-5200). It is found that HAps have an arbitrary shape. Some gelatin grafting on the surface of HAp shown in Table 4.2.

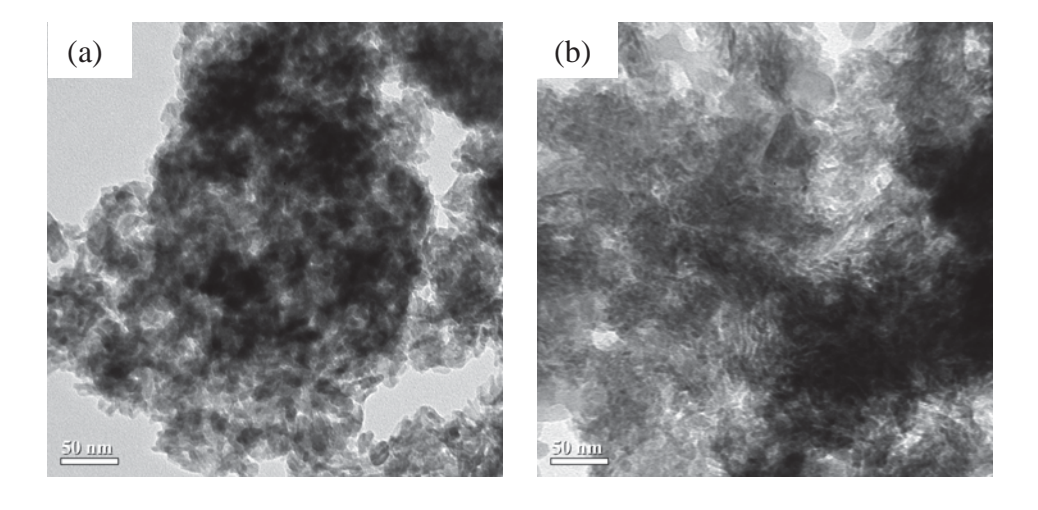
**Table 4.2** SEM of proteins-loaded HAp powder

	X200	X2000
Neat HAp	1510 1500 SOOM 969990	13(1) 1, 200 - 1000 001010
HAp+OVA	1350 MSO 3904 00000	15: 0-42: 000 - Tora Daosdo S.
HAp+gelatin	15kU 50 500m a00000	1514 22.000 Tabe 00000

	X200	X2000
HAp+BSA	13kU 850 1360un 100003	13. 4 22. 00% (10- woste)
HAp+CBP	100m 00000	1024 (2.000 100 to 100 to

# 4.4.6 <u>Transmission Electron Microscope (TEM)</u>

Figure 4.5 shows the TEM photographs of HAp powders obtained neat HAp and proteins-loaded HAp. The HAp powders contain agglomerated particles consisting of rod-like shaped particle. Neat HAp powders are the short-rod crystal than proteins-loaded HAp. It is found that there are not much differences in morphology and size from the photographs of proteins-load HAp samples.



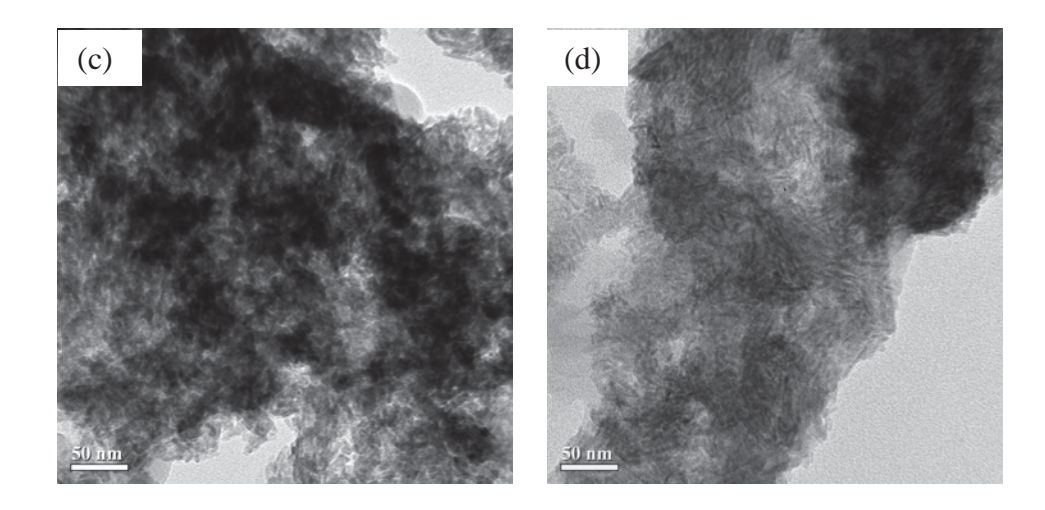


**Figure 4.5** TEM micrographs of proteins-loaded HAp powder: (a) Neat HAp; (b) OVA-loaded HAp; (c) Gelatin-loaded HAp; (d) BSA-loaded HAp.

# 4.4.7 Zeta Potential (ZP).

Twenty mililiter of the suspension was placed in an electrophoresis cup, and the movable images of the particles were recorded by the electrophoresis apparatus. The value would also be beneficial in the study of protein-loaded HAp and releasing through HAp particles. The zeta potentials were measured by appling the electric field in the dispersion and particles in the dispersion will be migrated to electrode of opposite charge. Protein-loaded HAps were dispersed in the DI water pH about 6-7 if protein can releases from HAp, it will be showed negative charge, so zeta potential is the positive. The zeta potentials of all the samples are negative, indicating that the particles themselves have superfluous positive electrical charges. It was indicated that protein entrapped in the HAp particle

The electrical conductivities values were so close as ~ -18, -16, and -20 mV for neat HAp, OVA-loaded HAp, and Gelatin B loaded HAp particle, respectively. Zeta potential is an indicator of charge density (Brown *et al.*, 1998). Particle size of Gelatin B-loaded HAp is the largest, so it has the highest charge density.

#### 4.4.8 Energy Dispersive Spectrophotometer

The EDS spectrum from HAp particles (Figure 4.6) shows the characteristic peaks of calcium (Ca), phosphorus (P), and oxygen (O). EDS is composed mainly of HAp and exhibits a molar Ca/P ratio of 1.67.

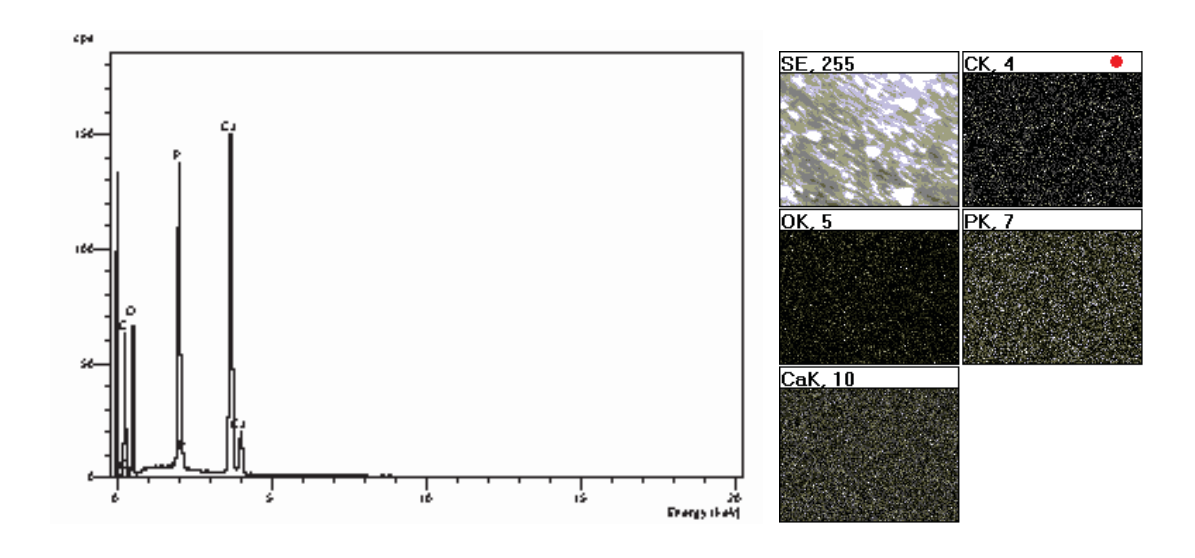


Figure 4.6 EDS spectrum of the biomimetic apatite layer deposited.

## 4.4.9 The Brunauer—Emmett—Teller (BET)

Surface areas and pore size of the powders were analyzed by nitrogen adsorption in Autosorb-1. The BET surface areas of the calcined samples at 800 °C are summarized in Table 4.3. We found that they are a few differences in surface area and pore size of neat and proteins-loaded HAp. Pore size of proteins-loaded HAp are a few larger than neat HAp due to the existence of pores after the removal of organic materials (proteins) so, surface area of proteins-loaded HAp are a few lower than neat HAp.

 Surface area (m²/g)
 Pore size (nm)

 Neat HAp
 22.64
 8.75

 OVA-loaded HAp
 19.65
 9.35

 Gelatin-loaded HAp
 20.06
 11.42

 BSA-loaded HAp
 20.99
 12.14

Table 4.3 BET surface area and pore size of the calcined samples at 800 °C

## 4.4.10 Particle size distribution of Hydroxyapatite

We were ground and sieved through a mesh size of 400 micron of protein-loaded HAp particles. About twenty miligrams of HAp were dispersed in water. The size distributions of HAp were measured by light scattering using particle sizer (Malvern, UK). The average particle size distributions of neat HAp and proteins-loaded HAp were about 316 µm.

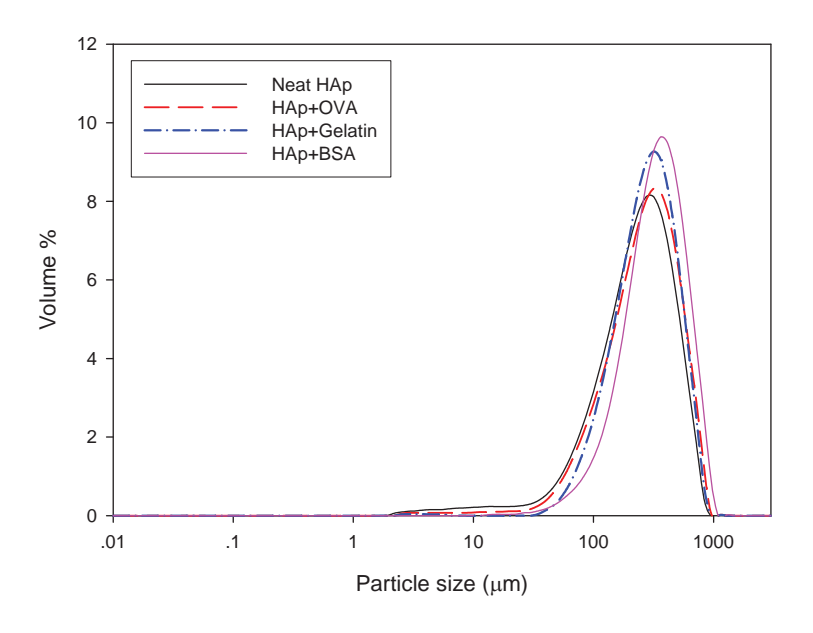


**Figure 4.7** Average particle size distribution of Hydroxyapatite.

## 4.4.11 Controlled Release of Proteins from HAp particles

The protein content of the encapsulated particles can be described by two quantities in terms of encapsulating efficiency of proteinloaded hydroxyapatite (EE) and loading capacity of hydroxyapatite particle (LC). For encapsulating efficiency of protein-loaded hydroxyapatite (EE), the proteins release from hydroxyapatite in phosphate buffer saline solution pH 7.4 was shown in Figure 4.8. The release profile of OVA, BSA and CBP were shown long-term proteins release at least 3 week. The maximum accumulative releases were about 50 % - 60 %. For the release profile of gelatin type B, it was shown the bursting release. The accumulative release was about 12 %. For loading capacity of proteins-loaded hydroxyapatite (LC), the proteins release from hydroxyapatite in phosphate buffer saline pH 7.4 was shown in Figure 4.9. The LC of OVA, BSA, and CBP from HAp particles were shown maximum accumulative releases were about 8-12 %. For the LC of Gelatin type B from HAp particle was shown maximum accumulative releases was about 1 %. Encapsulation of proteins into hydroxyapatite particles in this study was on the basis of polyion complexation. It was expected that a degree of molecular interaction was able to take place between proteins and hydroxyapatite particles of opposite charges (Young et al., 2005); as a consequence, a higher yield of the ionic complexes should result in higher encapsulation efficiency and loading capacity (Tabata and Ikada, 1998; Hoffman, 2002; Young et al., 2005).

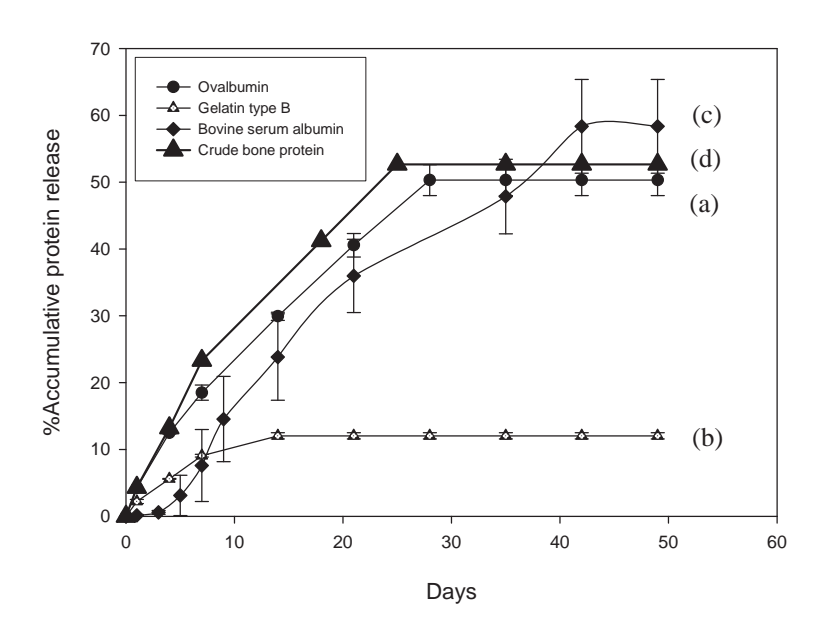


**Figure 4.8** Encapsulating efficiency of protein-loaded hydroxyapatite (EE): (a) Ovalbumin (OVA); (b) Gelatin type B; (c) Bovine serum albumin (BSA) and (d) Crude bone protein (CBP) release from HAp in phosphate buffer saline solution.

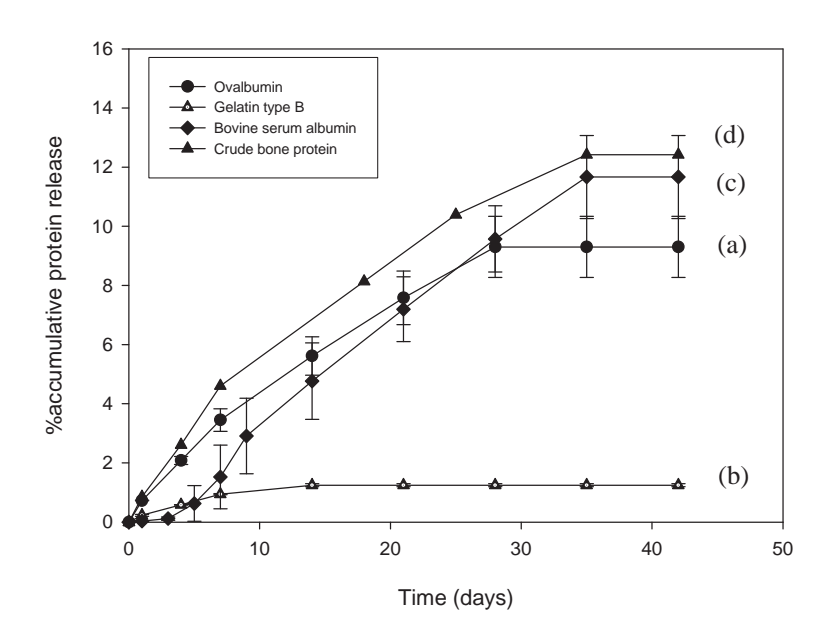


**Figure 4.9** Loading capacity of protein-loaded HAp (LC): (a) Ovalbumin (OVA); (b) Gelatin type B; (c) Bovine serum albumin (BSA) and (d) Crude bone protein (CBP) release from HAp in phosphate buffer saline solution.

### 4.5 Conclusion

The porous hydroxyapatite particle as a controlled release carrier of proteins were successfully synthesized by co-precipitation technique. The precursors were obtained DCPD and CaCO<sub>3</sub>. Incorporation of proteins was accomplished during the co-precipitation of the two reactants. Characteristics of the HAp particles were determined by XRD, EDS, FT-IR, TGA, ZP, SEM, TEM, and Autosorb-1. Proteins-loaded HAps were dissolution tested in prolonged PBS solution. Proteins release could be regulated using HAp particles resulting in prolonged release of proteins except gelatin type B. Mechanism of proteins-loaded HAp release was believed to be the combination of diffusion or degradation of the carrier. Many factors play roles and synergistically control on the release of proteins from the hydroxyapatite which were electrostatic interaction between protein and hydroxyapatite.

# 4.6 Acknowledgements

The author would like to thank Prof. Pitt Supaphol, Assoc. Prof. Prasit Pavasant, Assoc. Prof. Nuanchawee wetprasit, Asst. Prof. Hathaikarn Manuspiya and Dr. Neeranut Kuanchertchoo for their sincere assistances. They have provided the very useful guidance and the great encouragement throughout this research.

The author also thanks to all of colleagues, staff and teachers in the Petroleum and Petrochemical college, Chulalongkorn University who helps greatly during studies.

The author is grateful for funding of the thesis work provided by petroleum and petrochemical college; and Center for petroleum, Petrochemicals, and Advanced Materials.

The author wishes to give thanks to all of friends in Pitt Supaphol group's student for helps and suggestions.

Finally, the author would like to express appreciation for supporting scholarship and caring a great love of family especially mother, father, brother, and grandmother.

# 4.7 References

- Cao, Li-Yun., Zhang, Chuan-bo., and Huang, Jian-feng (2005). Synthesis of hydroxyapatite nanoparticles in ultrasonic precipitation. <u>Ceramics International</u>, 31, 1041-1044.
- Li, Yanbao., Tjandra, Wiliana., and Tam, Kam C (2008). Synthesis and characterization of nanoporous hydroxyapatite using cationic surfactants as templates. <a href="Materials Research Bulletin">Materials Research Bulletin</a>, 43, 2318–2326.
- Liu, Tse-Ying., Chen, San-Yuan., Liu, Dean-Mo., and Liou, Sz-chian (2005).

  On the study of BSA-loaded calcium-deficient hydroxyapatite nano-carriers for controlled drug delivery. Controlled Release, 107, 112-121.
- Freiberg, S., Zhu, X.X. (2004). Polymer microspheres for controlled drug release. International Journal of Pharmaceutics, 282, 1-18.
- Hariraksapitak, P. (2009). Development of protein delivery scaffold with a separate drug carrier system for bone tissue regeneration. Doctor dissertation. The Petroleum and Petrochemical College, Chulalongkorn University.
- Hoffman, A.S. (2002). Hydrogels for biomedical applications. Advanced <u>Drug</u> <u>Delivery Reviews</u>, 54(1), 3-12.
- Matsumoto, T., Okazaki, M., Inoue, M., Yamaguchi, S., Kusunose, T., Toyonaga, T., Hamada, Y., and Takahashi (2004). Hydroxyapatite particles as a controlled release carrier of protein. <u>Biomaterials</u>, 25, 3807-3812.
- Kandori, Kazuhiko., Shohei, Oda., Masao, Fukusumi., Yoshiaki Morisada. (2009). Synthesis of positively charged calcium hydroxyapatite nano-

- crystals and their adsorption behavior of proteins. <u>Biointerfaces</u>, 73, 140-145.
- IJntema, K., Heuvelsland, W.J.M., Dirix, C.A.M.C., and Sam, A.P (1994).
  Hydroxyapatite microcarriers for biocontrolled release of protein drugs. <u>International Journal of Pharmaceutics</u>, 112, 215-224.
- Tabata, Y. and Ikada, Y. (1998) Protein release from gelatin matrices.

  <u>Advanced Drug Delivery Reviews</u>, 31(3), 287-301.
- Yang, Qing., Chen, Lin., Shen, Xinyuan., and Tan Zhiqing (2006).

  Preparation of Polycaprolactone Tissue Engineering Scaffolds by Improved Solvent Casting/Particulate Leaching Method.

  Macromolecular, 45, 1171-1181.
- Young, S., Wong, M., Tabata, Y., and Mikos, A.G. (2005) Gelatin as a delivery vehicle for the controlled release of bioactive molecules.

  <u>Journal of Controlled Release</u>, 109(1-3), 256-274.
- Zhao, Hongshi, He, Wen., Wang, Yingjun., Zhang Xudong., Li, Zhengmao., Yan, Shunpu., Zhou, Weija. Biomimetic (2008). Synthesis and Characterization of Hydroxyapatite Crystal with Low Phase Transformation Temperature. <u>Journal of chemical & engineering data</u>, 53 (12), 2735-2738.

# DEVELOPMENT OF POROUS HYDROXYAPATITE PARTICLES AS CARRIERS OF PROTEINS IN A POLYCAPROLACTONE SCAFFOLD FOR BONE TISSUE ENGINEERING

Sujittra Chaisuntharanon, Prasit Pavasant, and Pitt Supaphol 1,\*

<sup>1</sup>The Petroleum and Petrochemical College and The Center for Petroleum, Petrochemicals and Advanced Materials (C-PPAM), Chulalongkorn University, Bangkok 10330, Thailand

### 5.1 Abstract

This study aimed to develop the porous hydroxyapatite (HAp) particles as a controlled release carrier of proteins were embedded in polycaprolactone (PCL) to fabricate porous HAp-PCL scaffolds. Proteins (Ovalbumin, Gelatin type B, Bovine Serum Albumin and Crude bone protein) had been entrapped within the HAp particles. The porous HAp-PCL scaffolds were prepared by solvent casting/particulate leaching method. Desorption behavior of HAp-PCL scaffolds was investigated by **UV-Visible** spectrophotometry. The potential for use of HAp-PCL as bone scaffolds was assessed by mouse calvaria derived pre-osteoblastic cells, MC3T3-E1, in terms of indirect cytotoxicity, cell attachment, cell proliferation, alkaline phosphatate (ALP) activity, and mineralization.

(**Key-words**: bone scaffolds; particulate leaching; polycaprolactone; hydroxyapatite)

#### 5.2 Introduction

Modern tissue engineering combines materials science with biotechnology and biology to repair and replace damaged. It has been shown

\_

<sup>&</sup>lt;sup>2</sup> Department of Anatomy, Faculty of Dentistry, Chulalongkorn University, Bangkok 10330, THAILAND

Authors to whom correspondence should be addressed: pitt.s@chula.ac.th (P. Supaphol)

that new tissues can be engineered from living cells and three-dimensional scaffolds. The success of these approaches is largely dependent on the scaffold properties. The ideal scaffold should have the following characteristics: (1) Appropriate porosity, pore size and pore structure to ensure the nutrition of cells, cell attachment and cell proliferation within the scaffold (2) Mechanically strong enough to maintain structural integrity during culture, which is particularly important in load-bearing bone tissues. The material should be strong enough to withstand physiological stresses, and to transfer loads after implantation. (3) Adequate degradation properties in which the rate of scaffold degradation supports the maintenance of structure support for cellular proliferation and extracellular matrix (ECM). (4) Biocompatible so that the material used to manufacture the scaffold does not evoke an extreme adverse inflammatory or immune response once implanted. Instead, the material should be able to integrate with the host tissue and support cell infiltration, cell attachment for bone formation (5) Appropriate manufacturing process, the manufacturing processes should not affect the material's biocompatibility as a result of residual chemicals involved in these processes (Choong C. et al., 2004).

In this research, three-dimensions HAp-PCL porous scaffolds were prepared by solvent casting/particle leaching method with sodium chloride as a porogen. The inclusion of calcium phosphates (CaPs) in biodegradable polymers enhances the osteoconductive of bone scaffold. Specifically, the inclusion of CaPs in polymer scaffolds enhances its mineral deposition rate, mechanical properties, and protein adsorption, thus improving the overall potential of bone scaffold (Porter, Joshua R *et al.*, 2009).

# 5.3 Experimental

# 5.3.1 Materials

- Polycaprolactone (PCL;80,000 g mol<sup>-1</sup>; Sigma-Aldrich, USA)
- Sodium chloride (Ajax Finechem, Australia)

- Chloroform (Labscan; Asia, Thailand)
- Modified Eagle's medium (MEM; Thermo Scientific, USA)
- Fetal bovine serum (FBS;Sorali, Campo Grande Brazil)
- 1% L-glutamine (Invitrogen Corp., USA)
- 1% Lactabumin (Invitrogen Corp., USA)
- 1% antibiotic (Invitrogen Corp., USA)
- Bicinchoninic acid (BCA; Thermo Scientific, USA)

# 5.3.2 <u>Preparation of Polycaprolactone (PCL)-Hydroxyapatite (HAp)</u> Scaffold

A solvent casting and salt particulate leaching was used to prepare the scaffold. Firstly, PCL granules were put into a glass bottle with chloroform to make up a PCL solution in the concentration of 14 percentages of polymer weight by volume of the solution (w/v), then the solution was stirred at room temperature for 2 h. Secondly, protein-loaded HAp were added into the glass bottle and they were stirred together. Thirthly, NaCl salt particles with size of 400 µm (PCL/NaCl = 1/30) (w/w) were added into the glass bottle and they were mixed together. And finally, the mixture was packed into the petri-dish with the dimension of 10x10 cm. The mold was then left in the hood for 24 h and immersed in the distill water 1 day for taking the mold out. The materials that come out were immersed in DI water for 2 days, during with time the water was changed approximately every 8 h under the room temperature for the leaching out the salt particles. Then the materials were air-dried for 24 h and freeze-dried overnight to obtain porous scaffolds (Prasansuklap *et al.*, 2008).

# 5.4 Characterization of porous Scaffolds

# 5.4.1 Porosity, Pore Volume and Pore Size

The density of the scaffolds ( $\rho$  scaffold) is determined by using a Sartorius YDK01, Germany density measurement kit (Buoyancy method) which can be calculated using the following equation.

$$\rho_{\text{ scaffold}} = \frac{W_a \times \rho_{fl}}{W_a \times W_{fl}}$$

Where  $W_a$  is the weight of the scaffold in air,  $W_{fl}$  is the weight of the scaffold in water and  $\rho_{scaffold}$  is the density of the water (at 25°C,  $\rho_{ft} \approx 1 \text{ g/cm}^3$ ).

The porosity and pore volume of the scaffolds were calculated using the following equation (Hou, Qingpu *et al.*, 2003)

Porosity (%) = 
$$\left(1 - \rho_{\text{scaffold}} \right) \times 100$$

Pore volume = 
$$\frac{1}{\rho_{\text{ scaffold}}}$$
 -  $\frac{1}{\rho_{\text{ polymer}}}$ 

where  $\rho$  scaffold is the apparent density of the porous scaffolds and  $\rho$  polymer is the density of the non-porous polymer, compression moulded in the same manner.

Pore size of the scaffold was measured on the SEM micrograph with the UTHSCSA Image Tool version 3.0 software. The average values were calculated from the total 25 pores and accept as the mean pore sizes.

# 5.4.2 Water Absorption Capability

The dry scaffold scaffolds were weighted and then were immersed in 5 ml of phosphate buffer silane solution (PBS pH 7.4) solution at room temperature for 3 days. Scaffolds were removed from the solution and carefully placed on the glass for 5 seconds to remove the excessive water and weight immediately. The water absorption was calculated using the following equation.

Water absorption (%) 
$$= (M_{\text{wet}} - M_{\text{dry}}) \times 100$$

Where M <sub>dry</sub> and M <sub>wet</sub> are the weight of the scaffold before and after immersion in water respectively. Five measurements were performed for the calculation of an average water absorption value.

# 5.4.3 Morphology of Porous Scaffolds

The morphology of the pores size of the porous scaffold were observed by a JEOL JSM-5200 scanning electron microscopy (SEM). The scaffolds were cut with razor blade at the middle of the scaffolds and mounted on stubs. Cross sections of the scaffolds were coated with thin film of gold using JEOL JFC-1100E sputtering devices for 120 second.

# 5.4.4 In Vitro Release of Proteins from Scaffold

The proteins/HAp-PCL were immersed in 1 ml of the minimum essential medium (MEM; Hyclone, Thermoscientific, USA) in 24 well plate. All samples were incubated in a shaking water bath (70 rpm) at 37°C. The amount of proteins releasing from scaffold to the supernatant was measured by BCA protein assay at various times. After the releasing medium (sample solution) was withdrawn 20 µl to mixed with BCA solution, an equal amount of fresh medium was added to maintain a constant volume of the medium. The amount of protein in the sample solution was determined by UV-visible spectroscopy at 562 nm. The MEM used in this study contained plenty of much high molarity inorganic salts comparing with those in PBS such as NaCl 117.24 M, KCl 5.33 M, CaCl<sub>2</sub> 1.8 M, NaH<sub>2</sub>PO<sub>4</sub>-H<sub>2</sub>O 1.01 M (Invitrogen, 2009).

### 5.5 Cell culture

Mouse calvaria-derived, pre-osteoblastic cells (MC3T3-E1) were cultured as monolayers in minimum essential medium with Earle's Balanced

Salts (MEM; Hyclone, Thermoscientific, USA), supplemented with 10% FBS, 1% L-glutamine and 1% antibiotic and antimycotic formulation (containing penicillin G sodium, streptomycin sulfate, and amphopericin B (Invitrogen Corp, USA). Cells were cultivated in 5% CO<sub>2</sub> at 37 °C in a humidified atmosphere.

# 5.5.1 Indirect Cytotoxic Study.

An indirect cytotoxic test was conducted on the proteins-loaded hydroxyapatite and PCL-HAp scaffold by use MC3T3-E1. First, extraction medias were prepared by immersing powder of each protein-loaded hydroxyapatite and circular shape of each PCL-HAp scaffold specimens about (15 mm in diameter) in wells of a 24-well culture plate in a 2% MEM (containing MEM, 2% FBS, 1% L-glutamine, 1% antibiotic and antimycotic formulation) for 24 h. Each of these extraction media was used to evaluate the cytotoxicity of the HAp powder and scaffold. MC3T3-E1 was separately cultured in wells of a 24-well culture plate in serum-containing MEM for 16 h to allow cell attachment on the plate. The cells were then starved with 2% MEM for 24 h, after which time the medium was replaced with an extraction medium. After 24, 48, and 72 h of cell culturing in the extraction medium, a 3-(4,5-dimethylthiazol-2-yl)-2,5-diphenyl-tetrazolium bromide (MTT) assay was carried out to quantify the amount of via cells.

The MTT assay is based on the reduction of the yellow tetrazolium salt to purple formazan crystals by dehydrogenase enzymes secreted from the mitochondria of metabolically active cells. The amount of purple formazan crystals formed is proportional to the number of viable cells. First, each of culture medium was aspirated and replaced with 400 µl per well of MTT solution at 0.5 mg/ml for a 24-well culture plate. Secondly, the plate was incubated for 30 mins at 37°C. The solution was then aspired and 900 µl per well of dimethylsulfoxide (DMSO) containing 125 µl per well of glycine buffer (pH=10) is added to dissolve the formazan crystals. Finally, after 10 min of rotary agitation, the absorbance of the DMSO solution at 570 nm was

measured using a Thermospectronic Genesis 10 UV-Visible spectrophotometer.

# 5.5.2 Cell Attachment and Cell Proliferation Study

Mouse calvaria-derived, pre-osteoblastic cells (MC3T3-E1) were allowed to attach on the porous scaffold specimens and empty wells for 2, 4, and 6 h. For the proliferation study, the cells were allowed to attach on the porous scaffold specimens and empty wells for 1, 3, and 5 d. At each time point, a number of the attached and proliferated cells were quantified by MTT assay. Each specimen was rinsed with phosphate buffered saline to remove unattached cells prior to the MTT assay. The morphology of the cells during the attachment and proliferation periods was observed by SEM. At each time point, the culture medium was removed and then the cell-cultured scaffold specimens were rinsed with PBS twice, the cells were then fixed with 3% glutaraldehyde solution, which was dilute from 50% glutaraldehyde solution with PBS 500 µl/well. After 30 min, they were rinsed again with PBS. After cell fixation, the specimens were dehydrated in an ethanol solution of varying concentration (30%, 50%, 70% and 90%, respectively). The specimens were the dried in air. After completely dried, the specimens were mounted on an SEM blass stubs, coated with gold and observed by SEM.

# 5.5.3 Alkali Phosphate Analysis (ALP)

Mouse calvaria-derived, pre-osteoblastic cells (MC3T3-E1) were cultured on porous scaffolds for 5 and 7 d and in different proteins for 5 and 7 d to observe ALP activity. Each porous specimen was rinsed with PBS after removal of the culture medium. Alkaline lysis buffer (10 mM tris-HCl, 2mM MgCl<sub>2</sub>, 0.1% Triton-X100), pH 10) (1000 μl/well) was added, and the specimen was scrapped and then frozen at -20°C for at least 30 min prior to the next step. An aqueous solution of 2 mg ml<sup>-1</sup> p-nitrophenyl phosphate (PNPP; Zymed Laboratories) mixed with 0.1 M aminopropanol (10μl/well) in 2 mM MgCl<sub>2</sub> (100μl/well) having a pH of 10.5 was prepared and added into the specimen. It was then incubated at 37°C for 2 min. The reaction was stopped by the addition of 0.9 ml/well of 50 mM NaOH, and the extracted solution was

transferred to cuvette and placed in the UV-Vis spectrophotometer, from which the absorbance at 410 nm was measured. The amount of ALP was then calculated against a BSA standard curve. To determine the ALP activity, the amount of ALP had to be normalized by the amount of total proteins synthesized. In the protein assay, each specimen was treated in the same manner as in the ALP assay up to the point where it was frozen. After freezing, a bicinchoninic acid (BCA; Thermoscientific, USA) solution was into the specimen. It was subsequently incubated at 37°C for 5 min. The absorbance of the medium solution was then measured at 562 nm by the UV-Vis spectrophotometer, and the amount of the total proteins was calculated against a BSA standard curve.

# 5.5.4 Mineralization Analysis

Calcium deposition was quantified by Alizarin Red S staining. MC3T3-E1 were cultured on the porous scaffolds in 24-well plate for 21 days. The cultures in 24-well plate were rinsed with PBS after that the cells were fixed with cold methanol for 10 min and washed with deionized water prior to immersion for 3 min in 370 µl of 1% Alizarin Red S solution dissolved in 1:100 (v/v) ammonium hydroxide/water mixture for 3 min (pH=3.3). Each stained specimen was washed several times with DI water and air-dried at room temperature. Calcium forms an Alizarin Red S-calcium complex in a chelating process. The stained specimen was photographed and eluted dye with 10% cetylpyridinium chloride for 20 min. The Alizarin Red concentration was determined by measuring the absorbance at 562 nm.

# 5.6 Results and discussion

# 5.6.1 Microstructure observation

Figure 5.1 demonstrated the SEM images microstructure of the as-prepared scaffolds when being viewed on the surface and cross sections. For PCL and HAp/PCL scaffold with NaCl: PCL, 30:1 weight ratio. The SEM images of (a) and (c) showed many square units occurring from the shape of

NaCl porogens used in the fabricating process. They showed clearly square units due to neat PCL scaffold whereas (b) and (d) exhibited the lost square because HAps embedded in the PCL scaffold.

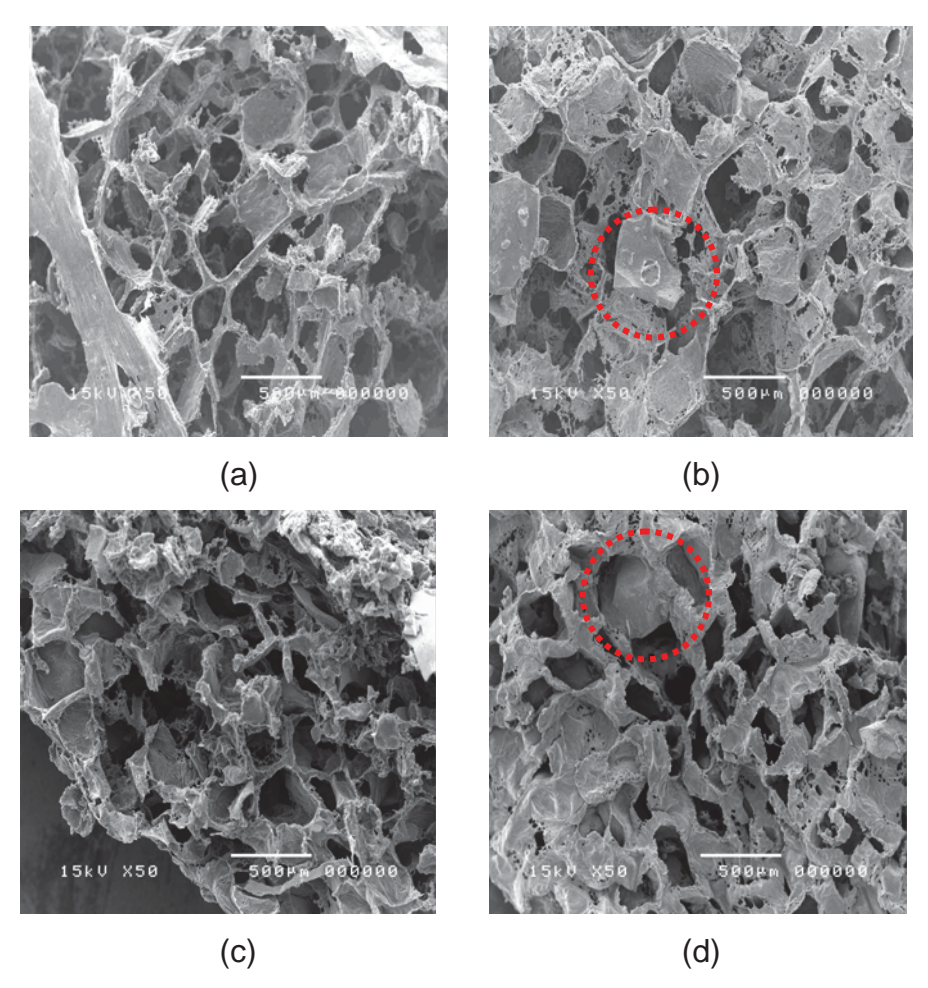


**Figure 5.1** SEM images illustrate microstructure of the scaffolds on the surface: (a) PCL, (b) HAp-PCL and on the cross-sections: (c) PCL, (d) HAp-PCL.

# 5.6.2 Density, Porosity, Pore volume and Pore size

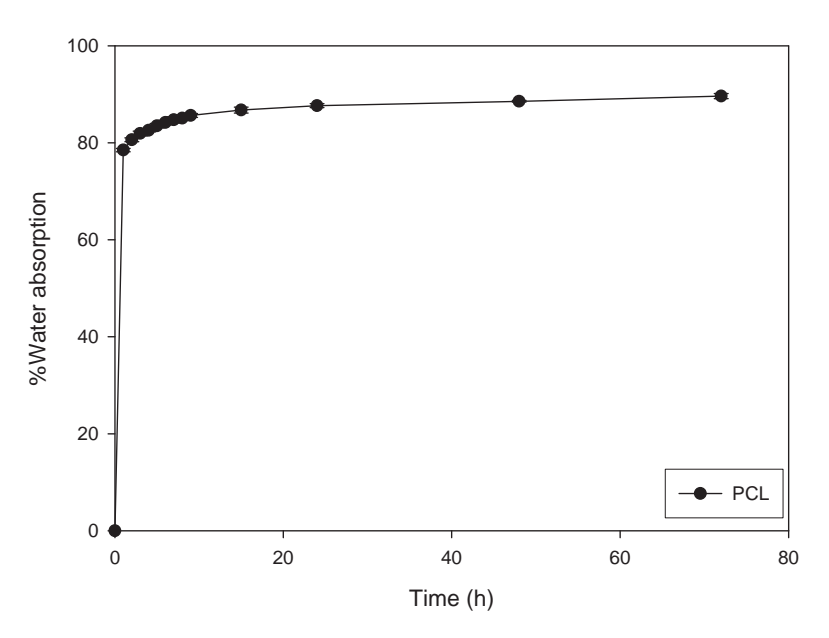
The density, porosity, pore volume and pore size of the scaffold was shown in Table 5.1.

Table 5.1 Density, porosity, pore volume and pore size of PCL scaffold

Scaffolds	Density	Dorocity (0/)	Pore volume	Pore size
	(g/cm <sup>3</sup> )	Porosity (%)	(cm <sup>3</sup> /g)	(µm)
PCL	0.1139	90.05	7.91	347.07 ±
PCL				42.19

# 5.6.3 Water absorption capability and in vitro degradability

Figure 5.2 illustrates the water absorption capabilities of the PCL scaffolds in 0.1 M PBS at room temperature within 3 days (72 h). The water absorption rate was rapidly increased in the early 24 hours and maintained stable.



**Figure 5.2** Water absorption capability of the PCL scaffolds in 0.1 M PBS at room temperature within 3 days.

# 5.6.4 *In vitro* OVA, Gelatin type B, BSA, and CBP Release

The release of proteins from HAp-PCL scaffolds were investigated by immersing HAp-PCL scaffolds into *in vitro* culturing environment, 10% MEM (containing MEM, 10% FBS, 1% L-glutamine, 1%

antibiotic). All samples were incubated in a shaking water bath (70 rpm) at 37°C for 21 days. The result shows gelatin and CBP started to before day 7 whereas OVA and BSA release after day 7. The amount of released proteins gradually increased time dependently. This result correspond to the work done by proteins releasing from HAp particles, however, protein release from scaffold spends a longer time due to different media. It is different in ionic strength, in MEM shows higher ionic strength. High ionic strength should promote aggregation of protein and retard release.

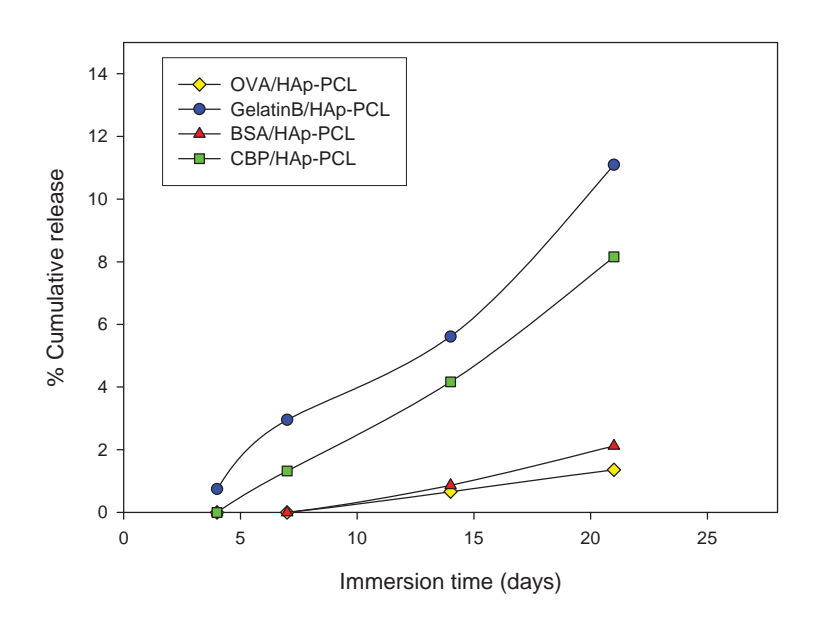


Figure 5.3 Release profile from protein-loaded HAp-PCL scaffold in MEM.

### 5.7 Cell Culture

# 5.7.1 Cytotoxicity

Indirect cytotoxicity in this studied can be classified into 3 process are indirect cytotoxicity for protein, HAp, and HAp-PCL scaffold. Firstly, an direct cytotoxicity test of proteins were performed in 4 types which are Ovalbumin (OVA), Gelatin type B, Bovine serum albumin (BSA), and

Crude bone protein. MC3T3-E1, pre-osteoblast cell lines, in culture of 40,000 cell/well seeded with 10  $\mu$ g/ml concentration in 2% MEM for 24, 48, and 72 h. The results are shown in Figure 5.4 with %viability of MC3T3-E1 relative to tissue culture polystyrene (TCPS) in all types of proteins show that increasing with cuturing time. The %viability of MC3T3-E1 is more than 80%, so all types of proteins were no toxicity to cells. Secondly and Thirdly are indirect cytotoxicity test of proteins-loaded HAp and HAp-PCL scaffold. MC3T3-E1 were cultured in 2% MEM extraction media from proteins-loaded HAp (Figure 5.5) and HAp-PCL scaffold (Figure 5.6) for 24, 48, and 72 h. The %viability of MC3T3-E1 in extraction media of each time are more than 80%, so proteins-loaded HAp and HAp-PCL scaffold were no toxicity to cell.

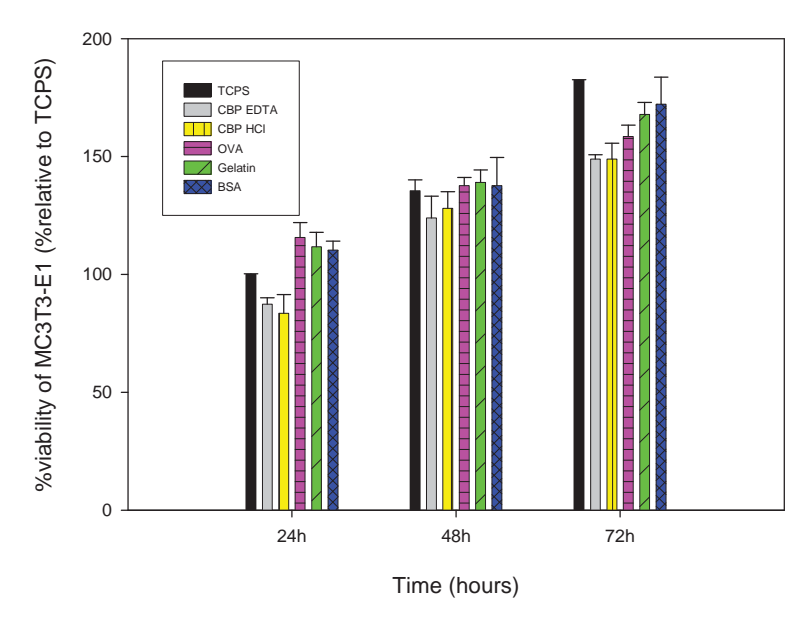


**Figure 5.4** Direct cytotoxicity evaluation of proteins based on the viability of MC3T3-E1.

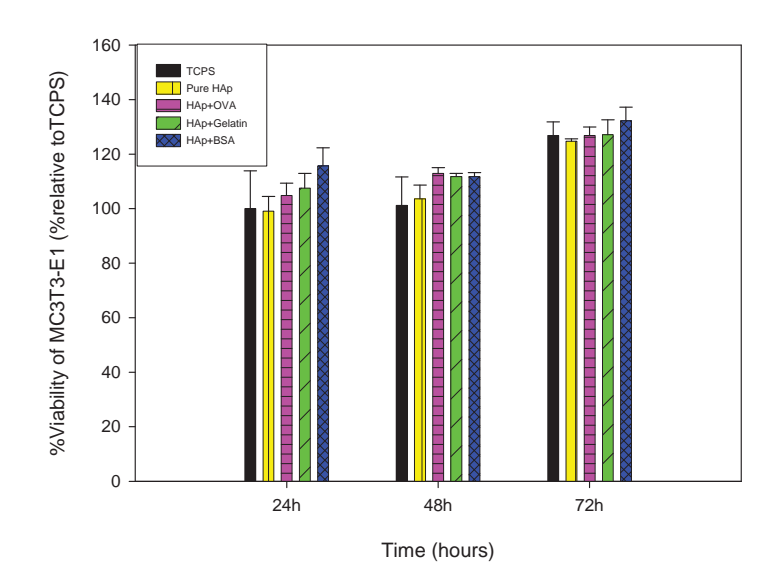


**Figure 5.5** Indirect cytotoxicity evaluation of protein-loaded HAp based on the viability of MC3T3-E1.

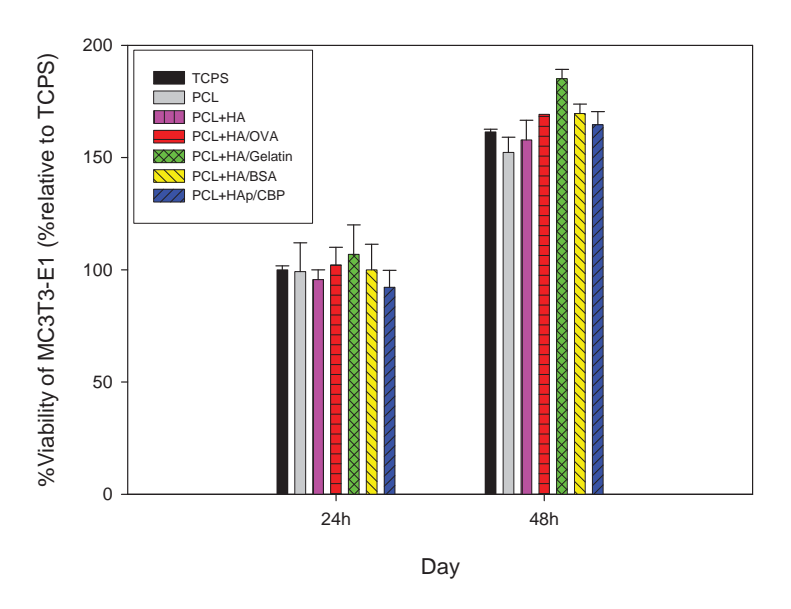


**Figure 5.6** Indirect cytotoxicity evaluation of HAp-PCL scaffold based on the viability of MC3T3-E1.

# 5.7.2 Cell Attachment and Proliferation

Attachment of mouse calvaria-derived, pre-osteoblastic cells (MC3T3-E1) on scaffolding substrate could be quantified by the UV

absorbance from MTT assay. Figure 5.7 shows attachment of MC3T3-E1 on the surface of TCPS, PCL, HAp-PCL, OVA/HAp-PCL, Gelatin type B/HAp-PCL, BSA/HAp-PCL, CBP/HAp-PCL at 2, 4, and 6 h after cell seeding. The number of cell attachment on all of the surfaces increase with culturing time. The number of cell attachment on TCPS was the greatest than all of HAp-PCL and proteins-loaded HAp scaffolds at any given time point, in culture of 40,000 cell/well. On TCPS, the number of cell attachment rapidly increased from 100% at 2 h after cell seeding to ~200% at 4 h after cell seeding. Whereas the number of cell attachment on PCL, HAp-PCL and proteins-loaded HAp were lower than TCPS could be because MC3T3-E1 like to attach the smoother surface of TCPS than rough surface of PCL, HAp-PCL and proteins-loaded HAp-PCL scaffold. However, Table 5.2 shows that almost of the formazan crystal still adhere within the scaffolds after using DMSO as eluting agent.

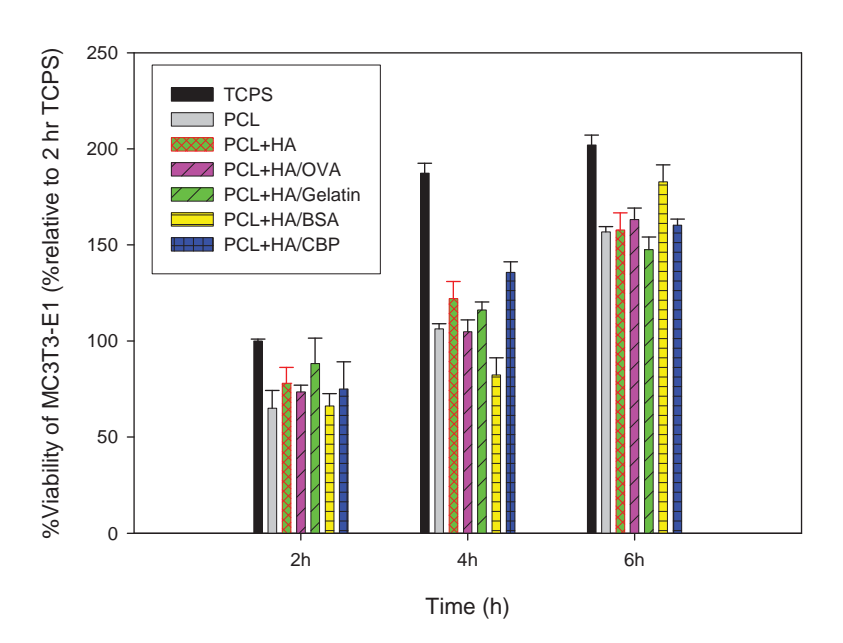
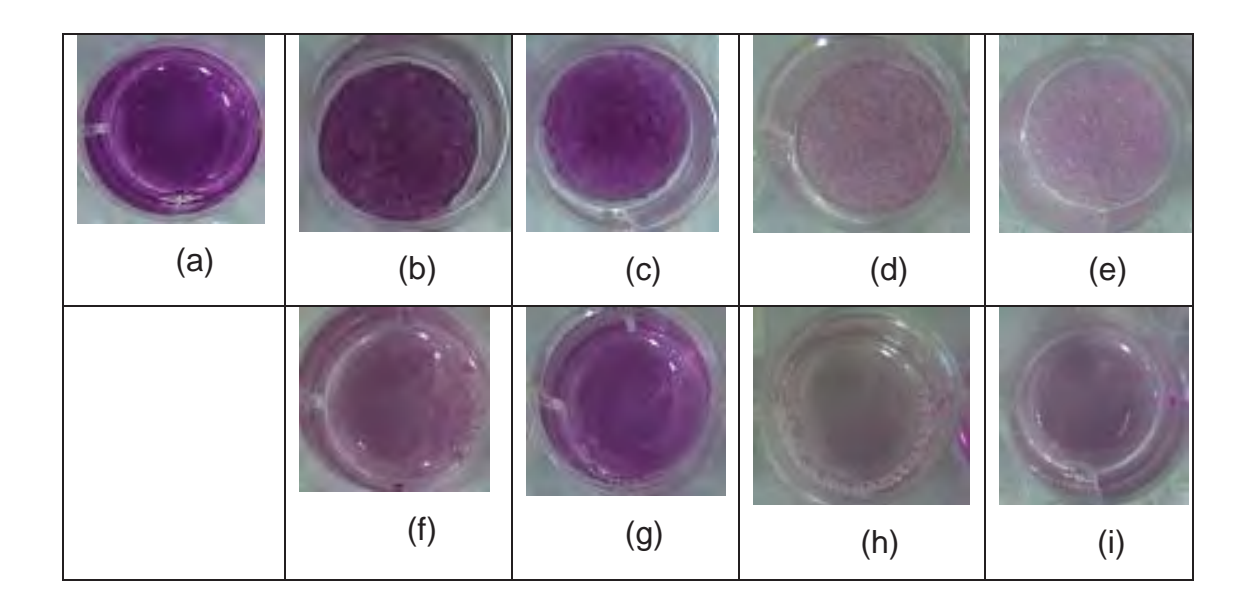


**Figure 5.7** Attachment of MC3T3-E1 on control TCPS, PCL, HAp/OVA-PCL, HAp/gelatin B-PCL, and HAp/BSA-PCL

**Table 5.2** Formazan crystal within TCPS, PCL, HAp-PCL scaffold were eluted with DMSO after cell seeding 6 h. (a) Eluted formazan from TCPS. (b), (c) Formazan still adhere in scaffold. (f), (g) Eluted formazan from scaffold. (d), (e) scaffold without cells inside. (h), (i) Eluted scaffolds without cells



Proliferation of mouse calvaria-derived, pre-osteoblastic cells (MC3T3-E1) on scaffolding substrate could be quantified by the UV absorbance from MTT assay. Figure 5.8 shows proliferation of MC3T3-E1 on the surface of TCPS, PCL, HAp-PCL, OVA/HAp-PCL, Gelatin type B/HAp-PCL, BSA/HAp-PCL, CBP/HAp-PCL at 1, 2, and 3 d after cell seeding in culture of 40,000 cell/well. The number of cell prolieration on all of the surfaces at any given time point were constant. The number of cell proliferation on TCPS was greater than all of PCL, HAp-PCL, and proteins-loaded HAp-PCL scaffolds at any given time point. On PCL, HAp-PCL and proteins-loaded HAp-PCL scaffold, the number of cell proliferation was only 60%. Whereas the number of cell attachment on HAp-PCL and proteins-loaded HAp were lower than TCPS could be because MC3T3-E1 like to proliferate the smoother surface of TCPS than rough surface of PCL, HAp-

PCL and proteins-loaded HAp-PCL scaffold. The difference between the number of cell proliferation to PCL, HAp-PCL, and protein-loaded HAp-PCL scaffold are not clear because of no effect of proteins release from HAp. However, Table 5.3 shows that almost of the formazan crystal still adhere within the scaffolds after using DMSO as eluting agent.

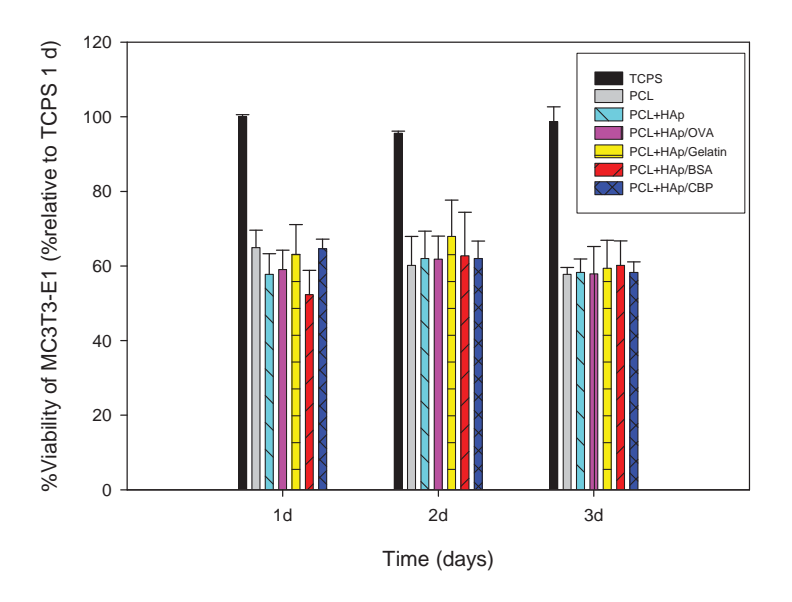
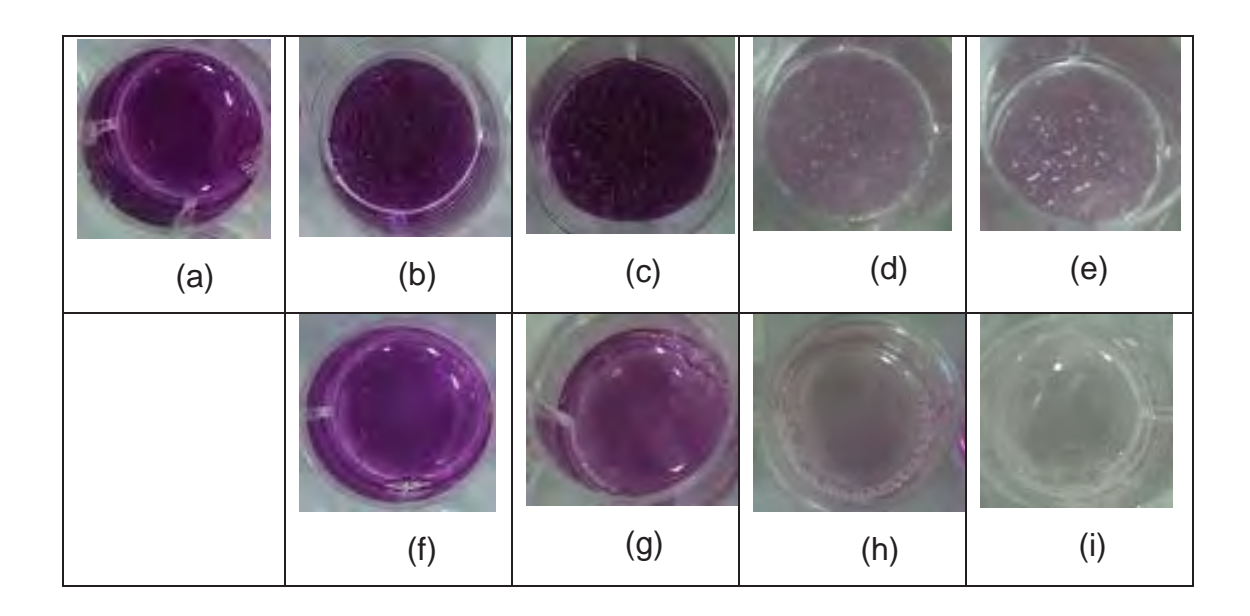


**Figure 5.8** Proliferation of MC3T3-E1 that had been seeded or cultured on the surfaces of TCPS, PCL, HAp-PCL and proteins-loaded HAp-PCL scaffolds at 2 and 3 d.

**Table 5.3** Formazan crystals within scaffolds after using eluting dye (DMSO) after cell seeding 1 d. (a) Eluted formazan with DMSO from TCPS. (b), (c) Formazan crystal still adhere in scaffolds. (f), (g) eluted formazan crystal with DMSO from scaffolds. (d), (e) scaffold without cells inside. (h), (i) eluted DMSO from scaffolds without cells.



# 5.7.3 Cell Morphological

Table 5.4 shows selected the attachment SEM images of MCT3T-E1 (magnification = 2000X; scale bar = 10  $\mu$ m) at 2, 4, and 6 h. Based on the initial 40,000 cells/well of cells seeded, the majority of the cells on the glass surface and porous scaffolds were still in the round shape at 2 h and started to extend their cytoplasm at 4 h. After cell seeding, expansion of the cytoplasm of the majority of the cells was evident at 6 h. Table 5.5 shows that the selected proliferation SEM images of MC3T3-E1 (magnification = 2000X; scale bar = 10  $\mu$ m) were cultured on the surfaces of glass, PCL, HAp-PCL, and proteins-loaded HAp scaffolds. The use of glass as the control instead of TCPS was due to the ease of taking the samples to SEM observation. These images provided snap shots in time that revealed the morphology of the cells and interaction between the cells and the tested surfaces. The expansion of the cells was evident with depend on the increasing time at 1, 2, and 3 days. All proteins within the HAp show the same results due to at that time the proteins were no affect to the cells.

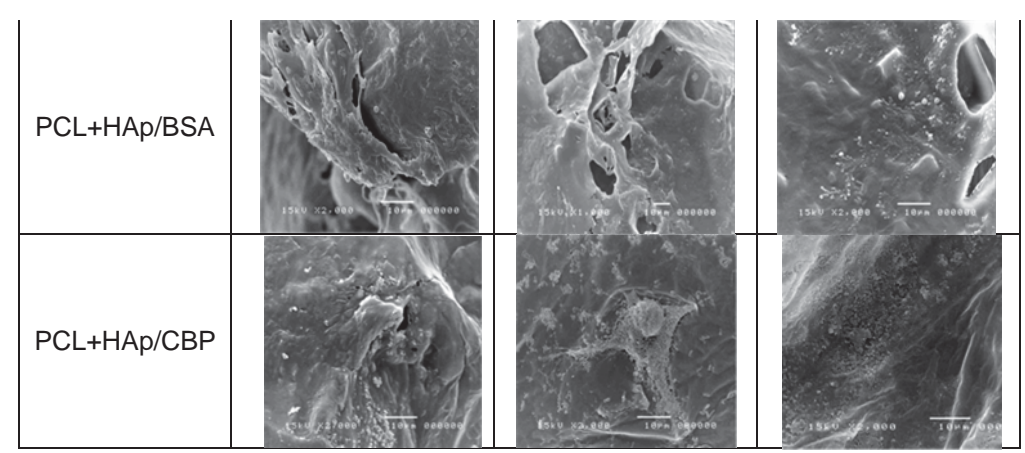
**Table 5.4** Selected SEM images of MC3T3-E1 after seeding on TCPS, PCL, OVA/HAp-PCL, Gelatin type B/HAp-PCL, BSA/HAp-PCL, and CBP/HAp-PCL scaffolds at 2, 4, and 6 h (magnification = 2,000X; scale bar =  $10 \mu m$ )

	2 h	4 h	6 h
Glass	1510 X2.000 127× 000000	1540 X1.000 1074 00000	154 22.00 32.000
PCL			
PCL + HAp			
PCL+HAp/OVA		3510 CT. NO. 1374 00000	
PCL+HAp/Gel B	23 121 122 11000 120000 12000		
PCL+HAp/BSA			100 1700 100 100
	0		



**Table 5.5** Selected SEM images of MC3T3-E1 after seeding on TCPS, PCL, HAp-PCL, OVA/HAp-PCL, Gelatin type B/HAp-PCL, and BSA/HAp-PCL scaffolds at 1, 2, and 3 days

X 2000	1 d	2 d	3 d
Glass	1510 X2 800 T8/m 800088	151U X2.000 Torn 000000	1510 XX 500 1074 000000
PCL			13.14 de passe - 10.000 person
PCL + HAp	1510 25.400 = 1000		
PCL+HAp/OVA	15:10 25:489 14:00E		1370 rayor Marketina
PCL+HAp/Gel B			1550 ET. 000 102-00000



5.7.4 Alkaline phosphatase (ALP) activity

Alkaline phosphatase is an indicator of osteoblast phenotype activity. It was determined after culturing the cells seeded onto the scaffold. The ALP activity of MC3T3-E1 on TCPS, PCL, HAp-PCL, OVA/HAp-PCL, Gelatin type B/HAp-PCL, BSA/HAp-PCL and CBP/HAp-PCL were monitored at 3 and 7 days in culture. In Figure 5.9 at 3 days shows the maximum level of ALP activity and at 7 days, ALP activity was decreased. In actually, ALP activity of PCL, HAp-PCL, OVA/HAp-PCL, Gelatin type B/HAp-PCL, BSA/HAp-PCL and CBP/HAp-PCL scaffold should be the same result of cell proliferation due to at that time the proteins were no effect to the cell, however, they were slightly fluctuated because PCL, HAp-PCL, OVA/HAp-PCL, Gelatin type B/HAp-PCL, BSA/HAp-PCL and CBP/HAp-PCL scaffolds were porous materials, so the cells could go through their scaffolds and could not extract the cells completely. In Figure 5.9, The ALP activity of MC3T3-E1 in OVA, Gelatin type B, BSA, and CBP with 100 µg/ml concentrations in 2%MEM was monitored at 5 and 7 days in culture. At 5 days shows the maximum level of ALP activity and at 7 days, ALP activity was decreased due to cellular process switching to mineralization. This result correspond to the work done by ALP activity of MC3T3-E1 on substrates.

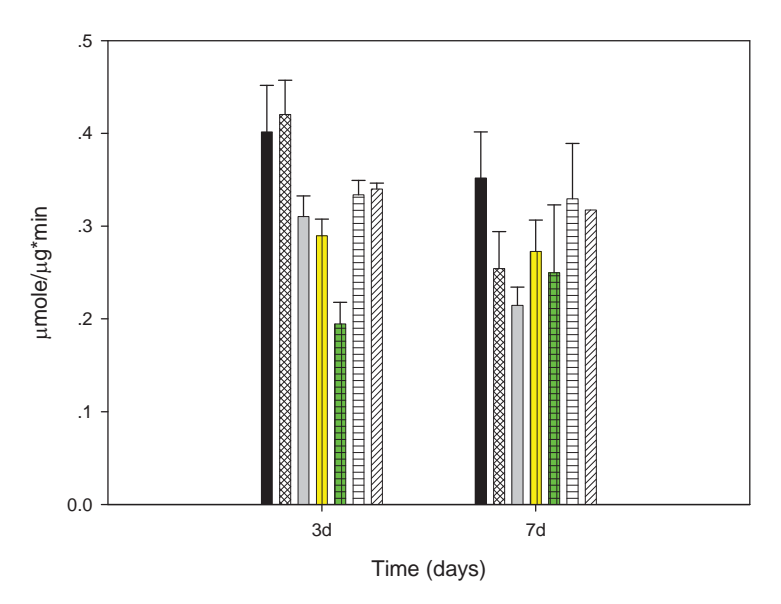


**Figure 5.9** ALP activity of MC3T3-E1 cultured on TCP, PCL, HAp-PCL, OVA/HAp-PCL, Gelatin B/HAp-PCL, BSA/HAp-PCL and CBP/HAp-PCL porous scaffolds after 3 and 7days in culture.

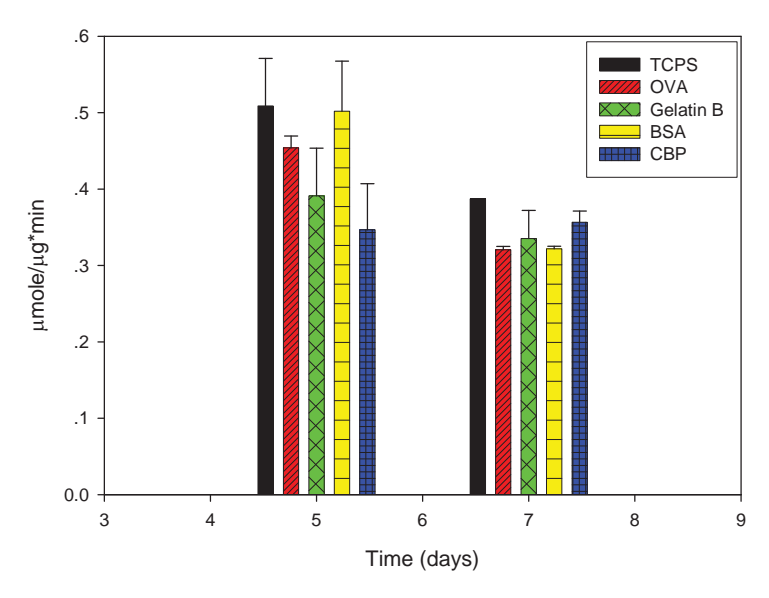


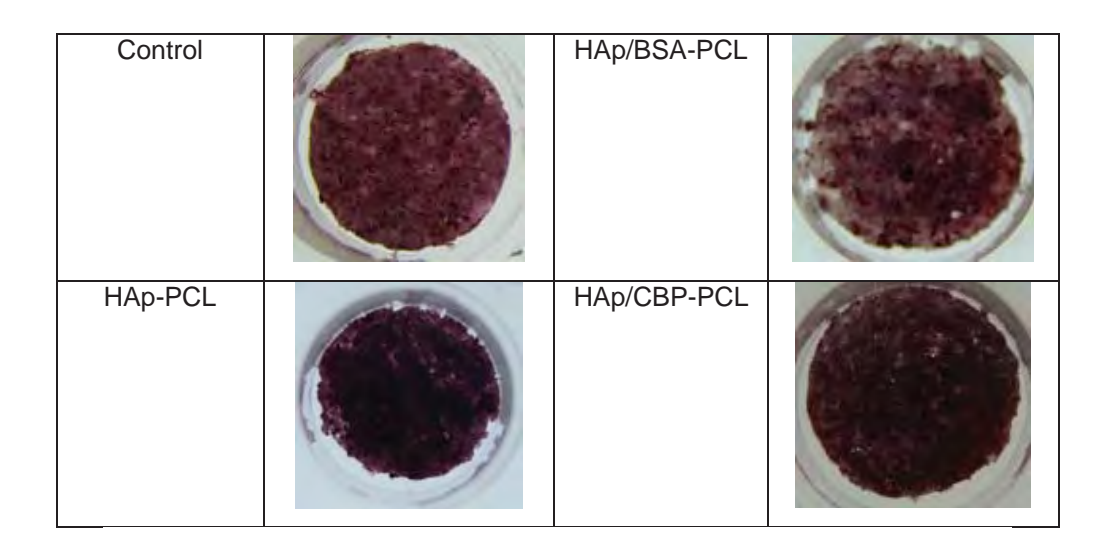
**Figure 5.10** ALP activity of MC3T3-E1 cultured with 100  $\mu$ g/ml in 2%MEM, OVA, Gelatin type B, BSA and CBP after 5 and 7 days in culture.

# 5.7.5 Mineralization

Mineralization refers to the process where an organic substrance is converted to an inorganic substrance. Alizalin Red S staining was used to characterize the bone formation of MC3T3-E1. Table 5.6, and Figure 5.11 show photographic images of Alizarin Red S staining of cells cultured on the different surfaces on 21 days. In the presence of calcium, the staining product such as an Alizarin red S-calcium chelating product appeared red. The results showed that PCL, HAp-PCL, and proteins-loaded-HAp scaffold were significantly higher than that on TCPS. Calcium content from MC3T3-E1 culture on CBP/HAp-PCL scaffold was the most positive staining.

**Table 5.6** Alizarin Red S staining for mineralization assessment of MC3T3-E1 on 21 days after being cultured on the surfaces of neat PCL, HAp-PCL, HAp/OVA-PCL, HAp/Gelatin-PCL, HAp/BSA-PCL, and HAp/CBP-PCL

Substrate	21 d.		21 d.
TCPS		HAp/OVA-PCL	
Neat PCL		HAp/GelB-PCL	



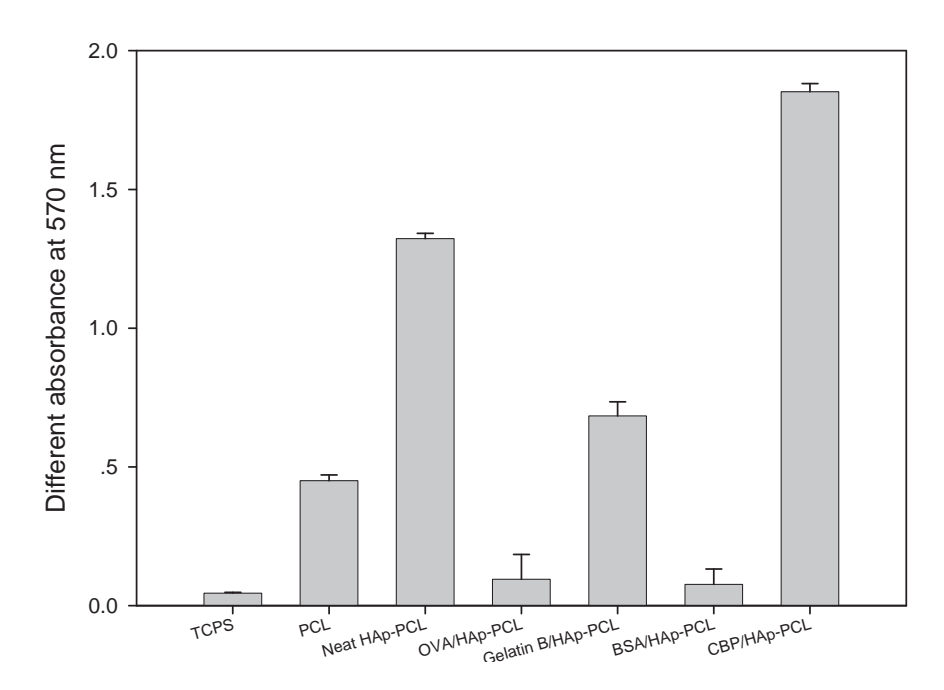


**Figure 5.11** Different absorbance of alizalin red S from MC3T3-E1 on TCPS, PCL, HAp-PCL, proteins-loaded HAp-PCL at 21 days.

# 5.7 Conclusions

The amount of HAp in the PCL scaffold was 40% (w/w, based on the amount of PCL). The direct and indirect cytotoxicity evaluation of the proteins, HAp and protein-loaded HAp-PCL scaffold with MC3T3-E1 indicated that non-toxic. Potential for using of proteins-loaded HAp-PCL

scaffolds was assessed in terms of cell attachment, cell proliferation, and ALP activity were no effect of proteins release from HAp. Alkaline phosphatate (ALP) activity at 7 days showed decreasing of the ALP activity due to cellular process switching to mineralization. According to mineralization or calcium deposition of cell for 21 days, the CBP/HAp-PCL scaffold was better than HAp/PCL, PCL, Gelatin/HAp-PCL, OVA/HAp-PCL, BSA/HAp-PCL, TCPS respectively.

# 5.8 Acknowledgements

The author would like to thank Prof. Pitt Supaphol, Assoc. Prof. Prasit Pavasant, Assoc. Prof. Nuanchavee wedprasit, Asst. Prof. Hathaikarn Manuspiya and Dr. Neeranut Kuanchertchoo for their sincere assistances. They have provided the very useful guidance and the great encouragement throughout this research.

The author also thanks to all of colleagues, staff and teachers in the Petroleum and Petrochemical college, Chulalongkorn University who helps greatly during studies.

The author is grateful for funding of the thesis work provided by petroleum and petrochemical college; and Center for petroleum, Petrochemicals, and Advanced Materials.

The author wishes to give thanks to all of friends in Pitt Supaphol group's student for helps and suggestions.

Finally, the author would like to express appreciation for supporting scholarship and caring a great love of family especially mother, father, brother, and grantmother.

#### 5.10 References

- Choong, C., Triffitt, J.T., and Cui, Z.F. (2004). Polycaprolactone scaffolds for bone tissue engineering: effects of a calcium phosphate coating layer on osteogenic cells. <u>Food and bioproducts processing</u>, 82(C2), 117-125.
- Porter, Joshua R., Henson, Andrew., and Popat, Ketul C. (2009). Biodegradable poly (ε-caprolactone) nanowires for bone tissue engineering applications. <u>Biomaterials</u>, 30, 780-788.
- Prasansuklarb, A. (2008) Osteoblastic cell growth and enzymatic degradation of different aliphatic polyester scaffolds. Master thesis. The Petroleum and Petrochemical College, Chulalongkorn University.
- Hou, Qingpu., Grijpma, Dirk W., and Feijen, Jan (2003). Porous polymeric structures for tissue engineering prepared by a coagulation, compression moulding and salt leaching technique. <u>Biomaterials</u>, 24, 1937-1947.

# SURFACE MODIFICATION OF POLY(LACTIC ACID) FIBERS VIA AMINOLYSIS AND COLLAGEN IMMOBILIZATION FOR BONE TISSUE ENGINEERING

Palita U-prasitwong, 1 Prasit Pavasant, 2 Voravee P. Hoven, 3 and Pitt Supaphol 1,\*

<sup>1</sup> The Petroleum and Petrochemical College and The Center for Petroleum, Petrochemicals and Advanced Materials (C-PPAM), Chulalongkorn University, Bangkok 10330, Thailand
 <sup>2</sup> Department of Anatomy, Faculty of Dentistry, Chulalongkorn University, Bangkok 10330, THAILAND
 <sup>3</sup> Organic Synthesis Research Unit, Department of Chemistry, Faculty of Science, Chulalongkorn University, Bangkok 10330, Thailand

New biomaterial effective for bone regeneration consisting of electro-spun (e-spun) fiber mats of poly(lactic acid) (PLA) with type-I collagen peptide bonded covalently was developed. Surface modification techniques have been instrumental in the development of scaffolds that promote cellsurface interactions. Surface modification of PLA in the form of e-spun fibers, was achieved by introducing the amino groups (NH<sub>2</sub>) on the scaffold surface via aminolysis with 1,6hexamethylenediamine (HMD) as precursors. The reactive groups were subsequently used to graft extracellular matrix molecule, type-I collagen, by using N,N'-disuccinimidylcarbonate (DSC) as coupling agent. The existence of NH<sub>2</sub> groups was verified quantitatively by ninhydrin analysis method. XPS analysis confirmed the presence of collagen as indicated by the increase in the nitrogen/carbon ratio on the surface of the polymer. Water contact angle results showed that the hydrophilicity of the surface has improved obviously after aminolysis and collagen immobilization. The potential for use of the neat and the modified PLA fibrous scaffolds as bone scaffolds was evaluated in vitro with mouse calvaria-derived, pre-osteoblastic cells (MC3T3-E1). Indirect cytotoxicity evaluation revealed that both the neat and the modified PLA fibrous scaffolds released no substances at levels that were harmful to cells. The attachment on various types of PLA fibrous scaffolds was lower compared with that on TCPS. While, the proliferation, ALP activity, and mineralization were improved on the modified surface, with the cells grown on the collagen-immobilized PLA fibrous scaffolds showed the greatest.

**Key-words:** Electrospinning; Poly(lactic acid); Immobilization; Collagen

-

<sup>\*</sup> Authors to whom correspondence should be addressed: pitt.s@chula.ac.th (P. Supaphol)

#### 1. Introduction

Bone injury and bone pathologies, as well as continued bone loss associated with aging, has resulted in increased research efforts focused on understanding cell-matrix interactions required for promoting bio-mineralization. Bone tissue engineering strategies, which combine materials engineering, cellular biology, and genetic engineering, are targeted at developing living bone replacements. One promising approach is to culture cells in three-dimensional (3D) scaffolds and to develop tissues of practical size scale and predetermined shapes. The scaffolds must support and maintain the normal state of differentiation within the cellular compartment. Ideally, a functional scaffolds should mimic the structure and biological function of native extracellular matrix (ECM) proteins, which provide mechanical support and regulate cellular activities. Due to the high surface area to volume or mass ratio and the vast possibilities for surface functionalities, fibers as obtained by the process known as electro-spinning (e-spinning) have recently become the most studied form of tissue engineered scaffolds. <sup>2,3</sup>

Biodegradable polyesters such as poly(lactide-*co*-glycotide) (PLGA), polycaprolactone (PCL), poly(lactic acid) (PLA), and poly(3-hydroxybutyrate-co-3-hydroxyvalerate) (PHBV) are paid more attentions in tissue engineering because they not only provide the necessary substance on which cells can adhere, but also guide and regulate the proliferation and activities of the supported cells. <sup>4-7</sup> Poly(lactic acid) (PLA) is a thermoplastic polyester synthesized from ring opening polymerization of lactides which is widely used because of its robust mechanical properties and the ability to be processed into scaffolds of different shapes. PLA has a crystallinity around 37%, the glass transition temperature, T<sub>g</sub> around 60–70°C is followed by melting behavior between 150 and170°C. The presence of ester linkages in the polymer backbone allows gradual hydrolytic degradation of the polymer with carbon dioxide and water as the degradation products which are endogenous compounds and as such are non-toxic. PLA has therefore gained the approval of US Food and Drug Administration (FDA) for a variety of human clinical applications. However, their hydrophobicity leads to the inefficiency of the scaffolds in constructing a friendly interface with living cells.

Because the initial response of cells to the biomaterials mostly depends on the surface properties, surface modification of polyesters to improve their cytocompatibility is necessary. Hydrophilic and protein-containing surfaces are known to promote cellular growth, therefore, many researches have been focusing on immobilizing biomolecules, such as, gelatin, <sup>10,11</sup> lamanin, <sup>12-14</sup> chitosan, <sup>15,16</sup> Arg-Gly-Asp (RGD)-containing peptide, <sup>17-19</sup> collagen <sup>20-23</sup> etc., on the surface of polymeric scaffolds. Four major protein immobilization techniques are currently used. These are: (i) covalent binding, in which attachment of the active component to the substrate surface uses a chemical reaction or linkage to activated surface groups; <sup>15,22</sup> (ii) entrapment, which is a physical trapping of the active components into a film, a gel or coating; <sup>9</sup> (iii) crosslinking, which combines features of both covalent binding and entrapment in which crosslinking agents are used both to polymerize a base layer or film and to anchor the entrapped protein molecules by forming intermolecular linkages between the substrate and the protein molecules; <sup>24</sup> and (iv) adsorption, which applies a protein solution to a substrate or film and allows the molecule to adsorb to the substrate over a specified time

period.<sup>25</sup> Among all the methods, covalent binding of biomolecules by coupling-agent bridging after aminolysis is one of the most acceptable method for the convenience and applicability to scaffolds. In addition it is suitable for both plane membrane and scaffolds with irregular shape and inner structure.<sup>26</sup> Due to the lack of chemical functionalities, it is usually difficult for polyesters to favor polymer-protein interaction, the covalent binding. The method of aminolysis between diamine and polyester matrix introduces functional amino groups, through which proteins such as collagen, chitosan etc., can be further introduced on the surface of polymeric scaffolds. <sup>27,28</sup> Mattanavee *et al.* <sup>28</sup> revealed that among the various biomolecule-immobilized PCL fibrous scaffolds, the one that had been immobilized with type-I collagen showed the greatest ability in supporting both the attachment and the proliferation of mouse fibroblasts (L929), human epidermal keratinocytes (HEK001), and mouse calvaria-derived, preosteoblastic cells (MC3T3-E1). In this work, the surface hydrophobicity of e-spun PLA fiber mats was improved by aminolysis with 1,6-hexamethylenediamine (HMD) to introduce free amino groups onto a ester-containing polymer surface. Type-I collagen, which is the major collagen-based protein synthesized by osteoblasts, 29-30 was subsequently immobilized with N,N'-disuccinimidyl carbonate (DSC) as a coupling agent. Indirect cytotoxicity evaluation of the neat and modified PLA e-spun fiber mats based on mouse fibroblasts (L929) and pre-osteoblasts (MC3T3-E1) was investigated. The potential for use of these e-spun fiber mats as bone scaffold was further evaluated in vitro with MC3T3-E1 in terms of attachment, proliferation, alkaline phosphatase (ALP) activity, and mineralization of the cells that were cultured directly on the scaffolds, in comparison to those of the cells on a tissue-culture polystyrene plate (TCPS).

# 2. Experimental Section

- **2.1. Materials.** Materials used in the fabrication of the fibrous scaffolds were poly(lactic acid) (PLA;  $M_n = 80,000 \text{ g mol}^{-1}$ ; Aldrich, USA), dichloromethane (DCM; Carlo Erba, Italy), and N,N' dimethylformamide [DMF; Lab-Scan (Asia), Thailand]. Materials used in the surface modification of the PLA fibrous scaffolds were type-I collagen (from calf skin; Sigma, USA), 1,6-hexamethylene-diamine (HMD; Aldrich, USA), and N,N'-disuccinimidylcarbonate (DSC; Aldrich, USA). All other chemicals were of analytical reagent grade and used without further purification.
- **2.2. Preparation and characterization of e-spun PLA fibrous scaffolds.** Electro-spun fiber mats of poly(lactic acid) were prepared by e-spinning from 10% w/v PLA solution in 7:3 v/v dichloromethane/ N,N-dimethylformamide (DCM/DMF). The as-prepared PLA solutions were continuously stirred until clear solutions were obtained. The solution was fed into a glass syringe fitted with a blunt 20-gauge stainless steel hypodermic needle (OD = 0.91 mm), which used as the nozzle. An aluminum sheet wrapped around a home-made rotating cylinder (width and diameter  $\approx$ 15 cm; rotational speed  $\approx$  50 rpm) was used as the collector. The distance from the tip of the needle to the surface of the Al sheet (measured at right angle to the surface) defining the collection distance was fixed at 18 cm. A Gamma High-Voltage Research Inc. (Ormond Beach, Florida), DC power supply was used to generate a high dc potential which was fixed at 20 kV. The emitting electrode of positive polarity was connected to the needle, while the grounding one was to the collector. E-spinning of the

as-prepared PLA solution was done continuously for 12 h. The obtained translucent electro-spun PLA fibrous scaffolds were dried in *vacuo* at room temperature prior to further modification. The thickness of the obtained PLA fiber mats was ~136  $\pm$  5  $\mu$ m. Morphological appearance and size of the individual fibers of the scaffolds were examined by JEOL JSM 5410LV scanning electron microscopy (SEM) (see Supporting Information). At least 100 readings of the fiber diameters from various SEM images were statistically analyzed using SemAphore 4.0 software, from which the arithmetic mean value of the individual fibers within the PLA fiber mats was determined to be 0.63  $\pm$  0.1  $\mu$ m.

2.3. Surface modification of PLA fibrous scaffolds. The PLA fibrous membranes were first immersed in an ethanolic aqueous solution (1:1 v/v) for 2 to 3 h to cleanse the fiber surface and then washed with a large amount of deionized water. The scaffolds were subjected to aminolysis through an immersion in a 1,6-hexamethylene-diamine/isopropanol (HMD/IPA) solution of varying concentration (i.e., 0.02, 0.04, 0.06, 0.08, and 0.1 gml<sup>-1</sup>) and varying reaction time (i.e., 2, 5, 8, 15, 20, 30 min) at 50°c. The aminolyzed PLA fibrous scaffolds were then rinsed with deionized water for 24 h at room temperature to remove unreacted HMD and dried in vacuo at room temperature to reach a constant weight. Immobilization of type-I collagen on the surface of the PLA fibrous scaffolds was carried out by first activating the aminolyzed PLA fibrous scaffolds in 0.1 M N,N'-disuccinimidyl carbonate/dimethylsulfoxide (DSC/DMSO) solution in the presence of 0.1 M triethylamine (TEA) for 3 h at room temperature, followed by rinsing the fiber mats with a large quantity of deionized water. The activated PLA fibrous scaffolds were then immersed in 0.5 or 3 mg·ml<sup>-1</sup> of collagen/phosphate buffer saline (PBS) solution at ambient temperature for 24 h. The collagen-immobilized PLA fibrous scaffolds were rinsed by soaking in a large quantity of deionized water for 24 h and finally dried in vacuo at room temperature. The chemical pathway for the immobilization of type-I collagen on the surface of espun PLA fibrous scaffolds is summarized in the Figure 1.

#### 2.4. Characterization of neat and modified PLA fibrous scaffolds.

**Quantification of free amino groups on the surface.** UV-Vis spectroscopy was used for determination the amount of amino (NH<sub>2</sub>) groups on the surface of the aminolyzed and the collagen-immobilized PLA fibrous scaffolds using ninhydrin method. First, the fibrous scaffolds were immersed in 1 M ninhydrin/ethanol solution for 1 min in a glass tube, followed by heating at 80°C for 15 min to accelerate the reaction between ninhydrin and the NH<sub>2</sub> groups that might be present on the surface of the scaffolds. As an evidence for the actual presence of the NH<sub>2</sub> groups, the surface of the scaffolds would turn blue. After complete evaporation of absorbed ethanol, 1,4-dioxane was added in the tube to dissolve the scaffolds. IPA was then added to stabilize the blue compound. Absorbance of the obtained compound in the UV-visible range was measured in a spectrophotometer (UV-2550, Shimadzu, Kyoto, Japan) at 538 nm against a predetermined calibration curve that was obtained from HMD solutions in 1,4-dioxane/IPA (1:1 v/v) (see Supporting Information).

**Surface Wettability.** Water contact angles of the neat and modified PLA fibrous scaffolds were measured at room temperature and, using sessile drop method on a telescopic goniometer (KRUSS Gmbh, DSA10-Mk2 T1C, Germany) equipped with a Gilmont syringe and a 24-gauge flat-tipped needle. The measurements were carried out in pentuplicate on different areas of each sample and the resulting values were averaged.

Elemental composition of the surface. X-ray Photoelectron Spectrometer (XPS; AMICUS, KRATOS, Japan), also known as Electron Spectroscopy for Chemical Analysis (ESCA), was used to investigate the elemental composition and chemical state of the elements on the surface. The XPS  $N_{1s}/C_{1s}$  peak-area rations was used as a marker for the analysis of the relative amount of free amino groups and collagen immobilized on the surface.

#### 2.5. Biological characterization of neat and modified PLA fibrous scaffolds.

Cell culture and cell seeding. Mouse fibroblasts (L929) and mouse calvaria-derived, preosteoblastic cells (MC3T3-E1) were used as reference cell lines. L929 were cultured as monolayer in Dulbecco's modified Eagle's medium (DMEM; Sigma-Aldrich, USA), supplemented with 10% fetal bovine serum (FBS; BIOCHROM AG), 1% L-glutamine (Invitrogen Corp.), and a 1% antibiotic and antimycotic formulation [containing penicillin G sodium, streptomycin sulfate, and amphotericin B (Invitrogen Corp., USA)]. MC3T3-E1 were cultured in Minimum Essential Medium (with Earle's Balanced Salts) (MEM; Hyclone, USA), supplemented by 10% fetal bovine serum (FBS; BIOCHROM AG, Germany), 1% L-glutamine (Invitrogen Corp., USA) and 1% antibiotic and antimycotic formulation [containing penicillin G sodium, streptomycin sulfate, and amphotericin B (Invitrogen Corp., USA)]. The medium was replaced every 2 days and the cultures were maintained at 37°C in a humidified atmosphere containing 5% CO<sub>2</sub>.

Each scaffold was cut into circular discs (about 15 mm in diameter) and the disc specimens were placed in wells of a 24-well tissue-culture polystyrene plate (TCPS; Biokom Systems, Poland), and were later sterilized in 70% ethanol for 30 min. The specimens were then washed with autoclaved de-ionized water, PBS and subsequently immersed in MEM overnight. To ensure a complete contact between the specimens and the wells, the specimens were pressed with a metal ring (about 12 mm in diameter). MC3T3-E1 from the culture was trypsinized [0.25% trypsin containing 1 mM EDTA (Invitrogen Crop., USA)] and counted by a hemacytometer (Hausser Scientific, USA). MC3T3-E1 were seeded at a density of about 60,000 cells/well for attachment study and 30,000 cells/well for proliferation study, on the scaffold specimens and empty wells of TCPS that were used as control. For indirect cytotoxicity, alkaline phosphatase activity, mineralization evaluations, MC3T3-E1 were seeded at a density of about 40,000 cells/well on the scaffold specimens and empty wells of TCPS. The culture was maintained in an incubator at 37°C in a humidified atmosphere containing 5% CO<sub>2</sub>.

Cytotoxicity evaluation. Two types of cells were used: 1) mouse calvaria-derived, preosteoblastic cells (MC3T3-E1) and 2) mouse fibroblasts (L929). Indirect cytotoxicity test was conducted on TCPS, neat PLA, aminolyzed PLA, activated PLA, collagen-immobilized PLA, and polycaprolactone/hydroxyapatite (PCL/HA) which used as positive control. First, extraction media were prepared by immersing samples (about 15 mm in diameter) in a serum-free medium (SFM; containing DMEM, 1% L-glutamine, 1 % lactabumin, and 1% antibiotic and antimycotic formulation for L929 and containing MEM, 1% L-glutamine, 1 % lactabumin, and 1% antibiotic and antimycotic formulation for MC3T3-E1) for 1, 3, and 7 days. Each of these extraction media was used to evaluate the cytotoxicity of the scaffolds. L929 or MC3T3-E1 were separately cultured in wells of a 24-well culture plate in 10%serum-containing DMEM and MEM, respectively, for 16 h to allow cell attachment on the plate. Then, the cells were starved with SFM for 24 h, after which time the medium was replaced with an

extraction medium. After 24 h of cell culturing in the extraction medium, 3-(4,5-dimethylthiazol-2-yl)-2,5-diphenyl-tetrazolium bromide (MTT) assay was carried out to quantify the amount of viable cells (see Supporting Information). The experiments were carried out in triplicate.

Another experiment was conducted to confirm the cytocompatibility of the materials on MC3T3-E1. Extraction media were prepared by immersing samples (about 15 mm in diameter) in a serum-free medium (SFM; MEM, 1% L-glutamine, 1 % lactabumin, and 1% antibiotic and antimycotic formulation for MC3T3-E1) for 7 d. The sample was treated in the same manner as the previous experiment up to the point was the cells were starved. After that the SFM was replaced with 2%serum-containing MEM diluted with as-prepared 7-day extraction medium for 1, 2, and 3 d to allow cell growth on the plate. After which time the viability of cell was again quantified by MTT assay in triplicate.

Cell attachment and cell proliferation. Cell behavior such as adhesion and proliferation represent the initial phase of cell–scaffold communication that subsequently effect differentiation and mineralization. For attachment study, MC3T3-E1 was allowed to attach to TCPS, aminolyzed PLA, activated PLA, collagen-immobilized PLA for 2, 4 and 16 h, respectively. At each specified seeding time, the number of the attached cells was quantified by MTT assay. Each sample was rinsed with PBS to remove unattached cells prior to MTT assay. Morphological appearance of the cells during attachment period was observed by SEM. For proliferation study, the viability of cells on the specimens was determined after 1, 2, and 3 day of cell culturing by MTT assay. The experiments were carried out in triplicate.

Morphological observation of cultured cells. After removal of the culture medium, the cell-cultured scaffold specimens were rinsed with PBS twice and the cells were then fixed with 3% glutaraldehyde solution, which was diluted from 50% glutaraldehyde solution (Sigma, USA) with PBS, at 500 μl/well. After 30 min, they were rinsed again with PBS. After cell fixation, the specimens were dehydrated in an ethanol solution of varying concentration (i.e. 30, 50, 70, 90, and 100%, respectively) for about 2 min at each concentration. The specimens were then dried in 100% hexamethyldisilazane (HMDS; Sigma, USA) for 5 min and later let dry in air after removal of HMDS. After completely dried, the specimens were mounted on an SEM stub, coated with gold, and observed by a JEOL JSM-5200 scanning electron microscope (SEM).

Production of Alkaline Phosphatase of Cultured Cells. ALP activity of MC3T3-E1 was measured using Alkaline Phosphate Yellow Liquid. In this reaction, ALP catalyzes the hydrolysis of colorless organic phosphate ester substrate, *p*-nitrophenyl phosphate (pNPP) to a yellow product, p-nitrophenol, and phosphate. MC3T3-E1 was cultured on scaffold specimens for 3, 5, and 7 day to observe the production of alkaline phosphatase (ALP). The specimens were rinsed with PBS 2 times after removal of culture medium. Alkaline lysis buffer (10 mM Tris-HCl, 2 mM MgCl<sub>2</sub>, 0.1% Triton-X100, pH 10) (100 μl/well) was added and the samples were scrapped and then frozen at -20°C for at least 30 min prior to the next step. An aqueous solution of 2 mg/ml *p*-nitrophenyl phosphate (pNPP; Zymed Laboratories, USA) mixed with 0.1 M amino propanol (10 μl/well) in 2 mM MgCl<sub>2</sub> (100 μl/well) having a pH of 10.5 was prepared and added into the specimens (110 μl/well). The specimens were incubated at 37°C for 15 min. The reaction was stopped by adding 900 μl /well of 50 mM NaOH and the extracted solution was transferred to a cuvette and placed in the UV-visible spectrophotometer,

from which the absorbance at 410 nm was measured. The amount of ALP was then calculated against a standard curve. In order to calculate for the ALP activity, the amount of ALP had to be normalized by the amount of total protein synthesized. In the protein assay, the samples were treated in the same manner as the ALP assay up to the point was the specimens were frozen. After freezing, bicinchoninic acid (BCA; Pierce Biotechnology, USA) solution was added into the specimens. The specimens were incubated at 37°C for 15 min. The absorbance of the medium solution was then measured at 562 nm by the UV-visible spectrophotometer and the amount of the total protein was calculated against a standard curve.

Mineralization analysis. Alizarin Red-S is a dye that binds selectively calcium salts and is widely used for mineral staining (the staining product i.e., an Alizarin Red S-calcium chelating product). The isolated osteoblastic cells were plated in 24-well plates at 40,000 cells/well and cultured in the culture medium. After 24 h, the cultures were treated with culture medium, with the supplement of 50 μg/ml ascorbic acid (Sigma, USA), 5 mM β-glycerophosphate (Sigma, USA), and 0.2 μg/ml dexamethasone (Sigma, USA), the medium was replaced every 2 days. After 16 days treatment, cells were washed with PBS and fixed with ice-cold absolute methanol for 10 min. Fixed cells were stained with 1% Alizarin Red in deionized water (Sigma, USA) (pH 4.2) for 2-3 min. After removing alizarin red-S solution, the cells were rinsed with deionized water and dried at room temperature. The images of each culture were captured and the stain was extracted with the use of 10% cetylpyridinium chloride (Sigma, USA) in 10 mM sodium phosphate for 1 h and absorbance of the collected dye was read at 570 nm in spectrophotometer (Thermo Spectronics Genesis10 UV-visible spectrophotometer).

**2.6. Statistical analysis.** Values expressed as the mean  $\pm$  standard deviation. Statistical analysis of different data groups was performed using One-Way Analysis of Variance (ANOVA) with the least-significant difference (LSD) test using SPSS software version 11.5. The values of p lower 0.05 were considered statistically significant.

#### 3. Results and Discussion

By reaction with diamine, 1,6-hexanediamine (HMD), amino groups can be covalently introduced onto the surface of the electro-spun PLA fibrous membranes to obtain the aminolyzed PLA fibrous membranes. One amino group (NH<sub>2</sub>) of HMD reacts with an ester group (—COO—) of PLA to form the amide linkage (—CONH—), while another amino group is unreacted and free for the further reaction. These free NH<sub>2</sub> groups can be used as active sites through which proteins like collagen can be bonded to the surface using *N*,*N'*-disuccinimidyl carbonate (DSC) as a coupling agent. However, to avoid aggregation, two-step procedure was employed. The attached amino groups had been first activated with DSC with *N*-hydroxysuccinimide being lost from the reaction and the as-formed succinimidyl esters were later reacted with respective collagen, with *N*-hydroxysuccinimide again being cleaved from the reaction.

#### 3.1. Characterization of neat and modified PLA fibrous scaffolds.

**Quantification of free amino groups on the surface.** The existence of free amino groups (NH<sub>2</sub>) on PLA surface is a prerequisite for protein bonding in this modification method. It is important to

confirm the existence of amino groups before protein is further introduced. Herein, ninhydrin is used as an indicator to confirm and quantify the -NH2 moiety on the aminolyzed PLA surface. The NH2 density on e-spun PLA fibrous scaffold surface was influenced by the concentration of HMD, aminolyzing time, temperature, and so on. Because the glass transition temperature (T<sub>0</sub>) of the present PLA is ~60-70°C, the aminolyzing temperature should be lower than this value to maintain the shape of the material. Hence, 50°C was chosen to perform the following reactions. Table 1 shows that NH<sub>2</sub> density increased with increasing HMD concentration. However, when the concentration of HMD is equal to or greater than 0.1 g/ml, the mechanical integrity of the e-spun PLA fiber mats was affected. Table 2 shows that the surface-bound NH<sub>2</sub> increased with increasing aminolyzing time to reach a maximum value at about 15 min, and then decreased slightly. The decrease at the longer reaction time may be caused by a further reaction of the free amino group on the terminal chain with other ester groups, or by the degradation of the superficial layer<sup>27</sup>. Both of these situations will reduce the density of the surface amino groups and thus intensity of purple colored complex. To maintain enough mechanical integrity for practical applications, PLA e-spun fiber mats were aminolyzed in a 0.04 g/ml HMD/IPA solution at 50°C for 15 min. According to the calibration curve obtained with 1,4dioxane/isopropanol (1:1, v/v) solution containing HMD of known concentration, the NH2 density on PLA e-spun fiber mat aminolyzed under these conditions was  $(3.7 \pm 0.02) \times 10^{-7} \text{ mol/cm}^2$  (see Table 3). It also shows that after immobilization with 0.5 mg/ml and 3.0 mg/ml type-I collagen, the average areal density of the amino groups on the surface of the PLA fibrous scaffolds were  $(4.52 \pm 0.08) \times 10^{-9}$ and  $(3.21 \pm 0.2) \times 10^{-8}$ , respectively.

Surface Wettability. To further evaluate the effect of aminolysis and collagen immobilization, surface wettability of the modified PLA fibrous scaffolds with respect to that of the neat PLA fibrous scaffolds was measured. Table 4 shows the surface wettability of neat PLA, aminolyzed PLA, activated PLA, collagen-immobilized PLA (without coupling agent; collagen = 0.5 mg/ml), collagenimmobilized PLA (collagen = 0.5 mg/ml), and collagen-immobilized PLA (collagen = 3 mg/ml) fibrous scaffolds. The water contact angle measured by the sessile drop method decreased slightly from 106.8° to 99.5° after the scaffold was aminolyzed with 0.04 g/ml of HMD/IPA solution for 15 min. That is, the introduction of the amino groups on the surface of the PLA fibrous scaffolds improved the hydrophilicity of the surface. After the aminolyzed PLA fibrous scaffolds has activated with DSC, their surface became more hydrophobic as evidenced by the water contact angle of 112.5°. Water contact angle decreased substantially after the collagen was bonded. Figure 2 shows that the surface became much more hydrophilic after collagen immobilization. Water contact angle was 79.4° for collagen 0.5 mg/ml immersion and was 73.0° for collagen 3 mg/ml immersion. These results show that the more collagen concentration used, the more collagen can be bonded to the PLA surface. It has been known that physisorption processes are virtually always involved in a coating procedure. In our case, we had tried physical coating of collagen on unactivated PLA fibrous scaffolds. Water contact angle measurements showed that water contact angle of physisorbed collagen-coated PLA surfaces was slightly lower than the aminolyzed PLA surface. On the other hand, for collagen-covalently bonded surface, they exhibited much lower water contact angle. That means activation step is an important step in protein grafting process.

**Elemental composition of the surface.** The surface alteration after the PLA fibrous scaffolds were modified was studied by X-ray Photoelectron Spectrometer (XPS). To study the effect of the aminolysis condition on the surface alteration,  $N_{1s}/C_{1s}$  ratios as a function of HMD concentration and aminolyzing time were evaluated. Table 5 shows that the more diamine concentration used, the more  $N_{1s}/C_{1s}$  ratio observed which could be due to increasing in introduced  $NH_2$  group concentration. Table 6 shows that the  $N_{1s}/C_{1s}$  ratio increased with increasing aminolyzing time to reach a maximum value at about 15 min, and then decreased slightly, which, in addition to the results on ninhydrin analysis method. Figure 3 shows that  $N_{1s}$  peaks obviously appeared after immobilization of collagen, which confirmed protein grafting. Table 7 shows  $N_{1s}/C_{1s}$  ratio of the neat and the modified PLA fibrous scaffolds. After aminolysis of PLA fibrous scaffold, the  $N_{1s}/C_{1s}$  ratio was increased from 0 to 0.0290 because of  $NH_2$  groups introduced on the surface. The  $N_{1s}/C_{1s}$  ratio was further increased to 0.0381 by reaction with DSC. It shows that the nitrogen concentration increased when succinimidyl esters was formed. Finally, it was obviously increasing in  $N_{1s}/C_{1s}$  ratio after collagen immobilization due to the large amount of nitrogen atom in collagen structure was additionally introduced.

# 3.2. Biological evaluation of neat and modified PLA fibrous scaffolds.

Indirect cytotoxicity evaluation. The biocompatibity of these PLA e-spun fiber mats as bone scaffolds was assessed by an indirect cytotoxicity evaluation with mouse fibroblastic cells (L929) and mouse calvaria-derived pre-osteoblastic cells (MC3T3-E1), based on the initial 40,000 cells/well of cells seeded. Indirect cytotoxicity test was conducted on neat, aminolyzed, activated, collagenimmobilized PLA fibrous scaffolds. In this experiment, the PCL/HA that was prepared from particulate leaching technique, was chosen to be the positive control. Even though we were interested in using the obtained modified fiber mats as potential bone scaffolds, it was mandatory to test the materials with L929 just to comply with the ISO10993-5 standard test method. Figure 4a shows %viability obtained from MTT assay of L929 which were cultured with the 1, 3, 7 day- extraction media in comparison with those cultured with SFM (i.e. control). The viability of the cells that had been cultured with SFM at any given time point was taken as the basis to arrive at the relative viability shown in the figure. Evidently, the viability of L929 for all types of modified PLA fibrous scaffolds exhibited slightly lower, in comparison with that of the control (100%). While the neat PLA fiber and PCL/HA scaffold which used as positive control exhibited comparable viability. In a similar manner was found for MC3T3-E1 (see Figure 4b). However, the viability of cells that were cultured with 7-day extraction media prepared from modified scaffolds were significantly lower, in comparison with that were cultured with 7-day extraction media prepared from the neat PLA scaffold and PCL/HA. Thus, we had to set other experiment to confirm the cytocompatibility of the modified PLA fibrous scaffolds.

MC3T3-E1 was cultured in wells of a 24-well culture plate in 2%serum-containing MEM diluted with 7-day extraction medium for 1, 2, and 3 d to allow cell growth on the plate. Figure 5 shows that the viability of MC3T3-E1, cultured with 2%serum-containing MEM diluted with 7-day extraction media prepared by all types of modified scaffolds, were increased with increasing the culturing time in the respective media. All of the obtained results clearly suggested that all types of the PLA fibrous scaffolds, released no substances at levels that were harmful to both types of cells.

Cell attachment and cell proliferation. The potential for use of the neat and the modified PLA fibrous scaffolds was further evaluated by observing their ability to support both the adhesion and the proliferation of MC3T3-E1. The viability of the cells that had been cultured on the surface of TCPS for 2 h was taken as the basis to arrive at the relative viability shown in a figure. Figure 6 shows the attachment of MC3T3-E1 on the surfaces of TCPS, neat PLA, aminolyzed PLA, activated PLA and collagen-immobilized PLA at 2, 4, and 16 h after cell seeding in terms of viability. On TCPS, the number of the attached cells increased from ~100% at 2 h after cell seeding to ~111% at 16 h after cell seeding, based on the initial number of cells seeded (60,000 cells/well). With regards to MC3T3-E1, the surfaces of all of the PLA fibrous scaffolds were inferior in supporting the attachment of the cells to that of TCPS. Specifically, the number of cells attached on these fibrous scaffolds was only ~50% in comparison with that on TCPS at any given time point. There was not significantly different in the viability among all types of the fibrous scaffolds. Figure 7 shows the proliferation of MC3T3-E1 on the surfaces of TCPS, neat PLA, aminolyzed PLA, activated PLA and collagen-immobilized PLA on day 1, 2, and 3 after cell culture in terms of viability (%relative to TCPS at day1). On TCPS, the number of cells increased from ~100% on day1 after cell culture to ~187% (i.e., an increase of about 2 fold from the initial number of cells seeded) on day 3 after cell culture, based on the initial 30,000 cells/well of cells seeded. In comparison with that on TCPS, the viability of the cells cultured on the modified PLA fibrous scaffolds were significantly higher at any given time point. The viability of cells proliferated on these fibrous scaffolds, at day 3, was higher than TCPS of about 2 fold for neat PLA, aminolyzed PLA, and activated PLA and about 3.5 fold for collagen-immobilized PLA. Marked improvement was achieved with the collagen-immobilized PLA fibrous scaffolds on day 3 after cell culture.

The lesser viability of cells in the attachment period on various types of the fibrous scaffolds in comparison with that on TCPS could be due to the lesser number of cells that were able to attach on the rougher and more hydrophobic surface of the fibrous scaffolds in comparison with the smoother and hydrophilic surface of TCPS. On the contrary, the greater number of cells in the proliferation period on all types of PLA fibrous scaffolds could be because of high surface area to mass or volume and high porosity of the e-spun fiber mats though which the cells were able to penetrate into the scaffolds. Among the various modified PLA fibrous scaffolds, the collagen-immobilized PLA fibrous scaffolds provided the most significant improvement in the ability to support the proliferation of the cells which could be due to the protein-containing and hydrophilic surface of the substrate.

Cell Morphology. Table 8 shows selected SEM image (magnification = 2000X; scale bar = 10 μm) of MC3T3-E1 that were cultured on the surface of glass, neat PLA, aminolyzed PLA, activated PLA and collagen-immobilized PLA at two different time points, while the SEM images at magnification = 500X are available as Supporting Information. The use of glass as the control instead of TCPS was due to the ease of taking the samples to SEM observation. These images provided snap shots in time that revealed the morphology of the cells and interaction between the cells and the tested surfaces. At 4 h after cell seeding, based on the initial 60,000 cells/well of cells seeded, the majority of the cells on the glass surface started to extend their cytoplasm, an evidence of the ability of the cells to attach on the surface. At 16 h after cell seeding, expansion of the cytoplasm of the majority of the cells was

evident. While the majority of MC3T3-E1 that had been seeded on the surfaces of unmodified PLA fibrous scaffolds for 4 h was remained round, but a closer examination around the edge of the cells revealed an evidence of filopodia (i.e., slender cytoplasmic projections extending from the leading edge of the migrating cells that help the cells during their migration over the surface of a scaffolds). The majority of the cells were evidently expanded after 16 h of cell seeding. On the other hand, the majority of the cells seeded on the surfaces of various types of modified PLA fibrous scaffolds showed an evidence of the extension of their cytoplasm on the fibrous surface even at 4 h after cell seeding, with collagen-immobilized PLA surface did so to a greater extent. These results suggested that the cells prefer the fibrous surfaces of modified PLA over that of the unmodified. Specifically, the cells were seemed to prefer the collagen-containing than others.

Alkaline Phosphatase (ALP) Activity. The ability for these PLA fibrous scaffolds to support differentiation, in addition to attachment and proliferation, of cultured cells is another important aspect suggesting actual applicability of the scaffold. Alkaline phosphatase is a membrane bound enzyme and its activity is used as an osteoblastic differentiation marker, as it is produced only by cells showing mineralized ECM. The ALP activity of MC3T3-E1 on TCPS (i.e. controls), neat PLA, aminolyzed PLA, activated PLA, and collagen-immobilized PLA were monitored at 3, 5 and 7 days in culture (see Figure 8). Apparently, the amount of ALP synthesized by the cells that were cultured on TCPS and all of the fibrous scaffolds increased with the initial increase in time in culture between day 3 and 5, reached a maximum level on day 5, and decreased with a further increase in culture after day 3. In comparison with other substrates, TCPS exhibited the highest ALP activity of MC3T3-E1. According to Figure 8, activated PLA and collagen-immobilized PLA fibrous scaffolds showed the highest ALP activity among the various fibrous scaffolds investigated at day 3 of cell culturing time. And at day 5 and day 7 collagen-immobilized PLA fibrous scaffolds exhibited the highest ALP activity.

The decrease in the ALP activity, after day 5 for the cells grown on both TCPS and PLA fibrous scaffolds, with a further increase in the culturing time can be due to cellular process switching onto further step (i.e. mineralization). Since ALP is not an exclusive protein synthesized by osteoblasts as it is also found in tissues of such organs as kidneys, small intestines, and placenta, the presence of ALP of MC3T3-E1 that were cultured on these substrates could not be used as the sole marker to confirm the osteoblastic phenotype of the cells. From the obtained results, it was suggested that collagen-immobilized PLA fibrous scaffold was the best among the PLA fibrous scaffolds that promoted both proliferation and differentiation of MC3T3-E1.

*Mineralization.* Mineralization refers to cell-mediated deposition of extracellular calcium and phosphorus salts where anionic matrix molecules take up the Ca<sup>2+</sup>, phosphate ions and serve as nucleation and growth sites leading to calcification. Mineralization was quantified by Alizarin Red-S studies (see Figure 9), showing degree of mineralization as indicated by extracted stain absorbance obtained on day 16 of cell culture was in the order of collagen-immobilized PLA > aminolyzed PLA > neat PLA > activated PLA > TCPS > glass. The collagen-immobilized PLA scaffold showed 16% higher mineralization than neat PLA scaffold with significant level of p < 0.05 confirming the effectiveness of collagen immobilization of PLA e-spun fibers in mineral formation by MC3T3-E1. The photographic images (see Figure 10) of scaffolds stained with Alizarin Red-S for 16 days supported

the above data where high intensity of staining minerals was observed on various type of PLA fibrous scaffolds displaying an overall enhancing effect in mineralization of MC3T3-E1 cells and proving collagen immobilization as an indispensable method for the fabrication of superior fibrous scaffolds for bone tissue engineering.

### 4. Conclusion

In the present study, type-I collagen was used to modify PLA in the form of electro-spun fibrous membranes for the purpose of improving cytocompatibility. The XPS confirmed that collagen was immobilized on the surface of PLA fiber mats by the reaction of aminolyzed PLA and type-I collagen employing DSC as a coupling agent. The existence of NH<sub>2</sub> groups on aminolyzed PLA surfaces has been characterized by ninhydrin analysis method, which revealed that the NH<sub>2</sub> density was influenced by the HMD concentration and aminolyzing time. The data of contact angle against water revealed that it had improved the surface hydrophilicity by the aminolysis and the further immobilization of collagen. The cultured MC3T3-E1 *in vitro* proved that the cell proliferation, alkaline phosphatase (ALP) activity and mineralization of modified PLA e-spun fibers were improved compared with the neat PLA fiber. Among the various modified PLA scaffolds, collagen-immobilized PLA showed the greatest ability to support cell proliferation, alkaline ALP activity, and mineralization. Therefore, collagen-immobilized PLA fibrous scaffold is promising material to accelerate bone regeneration.

Acknowledgments. This research work was partial supported in by 1) the Petroleum and Petrochemical College (PPC), Chulalongkorn University, 2) the National Center of Excellence for Petroleum, Petrochemicals, and Advanced Materials, Thailand, and 3) Department of Anatomy, Faculty of Dentistry, Chulalongkorn University. Associate Professor Varong Pavarajarn, department of Chemical Engineering, Faculty of Engineering, Chulalongkorn University, is acknowledged for the access to the XPS research facility.

# **References and Notes**

(1) Rho, K. S.; Jeong, L.; Lee, G.; Seo, B. M.; Park, Y. J.; Hong, S. D.; Roh, S.; Cho, J. J.; Park, W. H.; Min, B. M. *Biomaterials* **2006**, *27*, 1452-1461.

- (2) Fujihara, K.; Kotakib, M.; Ramakrishna, S. *Biomaterials* **2005**, 26, 4139–4147.
- (3) Suwantong, O.; Waleetorncheepsawat, S.; Sanchavanakit, N.; Pavasant, P.; Cheepsunthorn, P.; Bunaprasert, T.; Supaphol, P. *International Journal of Biological Macromolecules*. **2007**, 40, 217–223.
- (4) Hsu, S.H.; Chu, W.P.; Lin, Y.S.; Chiang, Y.L. Journal of Biotechnology 2004, 111, 143–154.
- (5) Wutticharoenmongkol, P.; Sanchavanakit, N.; Pavasant, P.; Supaphol, P. *Macromolecular Bioscience* **2006**, 6, 70-77.
- (6) Chen, F.; Lee, C.N.; Teoh S.H. Materials Science and Engineering 2007, 27, 325–332.
- (7) Sombatmankhong, K.; Sanchavanakit, N.; Pavasant, P.; Supaphol, P. *Polymer* **2007**, 48, 1419-1427.
- (8) Gupta, B.; Revagade, N.; Hilborn, J. Progress in Polymer Science 2007, 32, 455–482.
- (9) Cui, Y.L.; Qi, A.D.; Liu, W.G.; Wang, X.H.; Wang, H.; Ma, D.M.; Yao, K.D. *Biomaterial* **2003**, 24, 3859–3868.
- (10) Zhu, Y.; Gao, C.; Shen, J. *Biomaterials* **2002**, 23, 4889–4895.
- (11) Zhu, Y.; Gao, C.; He, T.; Shen, J. Tissue Engineering 2004, 10, 1/2.
- (12) Matsuda, A.; Kobayashi, H.; Itoh, S.; Kataoka, K.; Tanaka, J. *Biomaterials* **2005**, 26, 2273–2279.
- (13) Santiago, L.Y.; Nowak, R.W.; Rubin, J.P.; Marra, K.G. Biomaterials 2006, 27, 2962–2969.
- (14) Koh, H.S.; Yong, T.; Chan, C.K.; Ramakrishna, S. *Biomaterials* **2008**, 29, 3574–3582.
- (15) Wang, X.H.; Li, D.P.; Wang, W.J.; Feng, Q.L.; Cui, F.Z.; Xub, Y.X.; Song, X.H. *International Journal of Biological Macromolecules* **2003**, 33, 95–100.
- (16) Ding, Z.; Chen, J.; Gao, S.; Chang, J.; Zhang, J.; Kang, E.T. *Biomaterials* **2004**, 25, 1059–1067.
- (17) Hersel, U.; Dahmen, C.; Kessler, H. *Biomaterials* **2003**, 24, 4385–4415.
- (18) Hsu, S.H.; Chu, W.P.; Lin, Y.S.; Chiang, Y.L. Journal of Biotechnology 2004, 111, 143–154.
- (19) Sun, H.; Wirse A.; Albertsson, A.C. Biomacromolecules 2004, 5, 2275-2280.
- (20) Ma, Z.; Gao, C.; Ji, J.; Shen, J. European Polymer Journal 2002, 38, 2279-2284.
- (21) Zhu, Y.; Gao, C.; Liu, X.; Shen, J. Biomacromolecules 2002, 3, 1312-1319.
- (22) Yang, Y.; Porté, M.C.; Marmey, P.; Haj, A.J.E.; Amédéé, J.; Baquey, C. *Nuclear Instruments and Methods in Physics Research B* **2003**, 207, 165–174.
- (23) Cheng, Z.; Teoh, S. H. Biomaterials 2004, 25, 1991-2001.
- (24) Karakeçili, A.G.; Satriano, C.; Gümüşderelioğlu; Marletta, G. *Acta Biomaterialia* **2008**, 4, 989–996.
- (25) Woo, K.M.; Jun, J.H.; Chen, V.J.; Seo, J.; Baek, J.H.; Ryoo, H.M.; Kim, G.S.; Somerman, M.J.; Ma, P.X. *Biomaterials* **2007**, 28, 335–343.
- (26) Zhu, Y.; Gao, C.; Liu, Y.; Shen J. Wiley InterScience 2004 http://www.interscience.wiley.com

(27) Zhu, Y.; Chian, K.S.; Chan-Park, M.B.; Mhaisalkar, P.S.; Ratner, B.D. *Biomaterials* **2006**, 27, 68–78.

- (28) Mattanavee, W.; Suwantong, O.; Puthong, S.; Bunaprasert, T.; Hoven, V.P.; Supaphol, P., Under submission.
- (29) Hernández-Gil, I. F.-T.; Gracia, M. A. A.; Pingarrón, M. D. C.; Jerez, L. B. *Medicina Oral, Patología Oral y Cirugía Bucal* **2006**, *11*,47-51.
- (30) Mano, J. F.; Silva, G. A.; Azevedo, H. S.; Malafaya, P. B.; Sousa, R. A.; Silva, S. S.; Boesel, L. F.; Oliveira, J. M.; Santos, T. C.; Marques, A. P.; Neves, N. M.; Reis, R. L. Journal of the Royal Society: Interface 2007, 4, 999
- (31) Choi, J. Y.; Lee, B. H.; Song, K. B.; Park, R. W.; Kim, I. S.; Sohn, K. Y.; Jo, J. S.; Ryoo, H. M. *Journal of Cellular Biochemistry* **1996**, 61(4), 609-618.
- (32) Yu, H.S.; Hong, S.J.; Kim, H.W. *Materials Chemistry and Physics* **2009**, 113, 873–877.
- (33) Tsukamoto, Y.; Fukutani, S.; Mori, M. *Journal of Materials Science Materials in Medicine* **1992**, 3, 180-183.

# **CAPTION OF FIGURES**

- Figure 1. The chemical pathway for the immobilization of collagen.
- Figure 2. Water dropped on the surface of neat PLA fibrous scaffold(a), and PLA fibrous scaffold immobilized with 3.0 mg/ml collagen.
- Figure 3. The survey XPS spectra of (a) neat PLA, (b) PLA aminolyzed at a concentration of 0.04 g/ml 1,6-hexanediamine for 15 min at 50 °C, (c) activatedPLA, (d) PLA immobilized with collagen (0.5 mg/ml), and (c) PLA immobilized with collagen (3 mg/ml).
- Figure 4. Indirect cytotoxic evaluation of neat PLA fibers, modified PLA fibers, and PCL/HA based on viability of mouse fibroblasts (L929) that had been cultured with the extraction media from each of these materials against the viability of the cells that had been cultured with the respective culture media for 1 day as a function of the incubation time of the extraction and the culture media of 1, 3, or 7 d. Statistical significance: \*p < 0.05 compared with control and \*p < 0.05 compared to the neat PLA fibrous scaffolds at any given time point.
- Figure 5. Indirect cytotoxic evaluation of neat PLA fibers, modified PLA fibers, and PCL/HA based on viability of pre-osteoblast (MC3T3-E1) that had been cultured with the extraction media from each of these materials against the viability of the cells that had been cultured with the respective culture media for 1 day as a function of the incubation time of the extraction and the culture media of 1, 3, or 7 d. Statistical significance: \*p < 0.05 compared with control and \*p < 0.05 compared to the neat PLA fibrous scaffolds at any given time point.
- Figure 6. Indirect cytotoxic evaluation of neat PLA fibers, modified PLA fibers, and PCL/HA based on viability of pre-osteoblast (MC3T3-E1) that had been cultured with the 7-day extraction media from each of these materials with 2% serum-containing MEM against the viability of the cells that had been cultured with the respective culture media for 1, 2, and 3 day. Statistical significance: \*p < 0.05 compared with control and \*p < 0.05 compared to the neat PLA fibrous scaffolds at any given time point.
- Figure 7. Attachment of MC3T3-E1 that had been seeded or cultured on the surfaces of TCPS, the neat and the modified PLA fibrous scaffolds for 2, 4, or 16 h. Statistical significance: p < 0.05 compared with control and p < 0.05 compared to the neat PLA fibrous scaffolds at any given time point.
- Figure 8. Proliferation of MC3T3-E1 that had been seeded or cultured on the surfaces of TCPS, the neat and the modified PLA fibrous scaffolds for 1, 2, or 3d. Statistical significance: \*p < 0.05 compared with control and \*p < 0.05 compared to the neat PLA fibrous scaffolds at any given time point.
- Figure 9. Alkaline phosphatase (ALP) activity of MC3T3-E1 that were cultured on the surfaces of TCPS, the neat and the modified PLA fibrous scaffolds for 3, 5, or 7 d.

Figure 10. Quantification of mineral deposition in MC3T3-E1 by the method of Alizarin Red-S staining. Statistical significance: \*p < 0.05 compared with control and \*p < 0.05 compared to the neat PLA fibrous scaffolds at any given time point.

Figure 11. Images of Alizarin Red-S staining for the mineralization in MC3T3-E1 for day 16 (a) glass (b) TCPS (c) neat PLA (d) aminolyzed PLA (e) activated PLA (f) collagen-immobilized PLA fibrous scaffold.

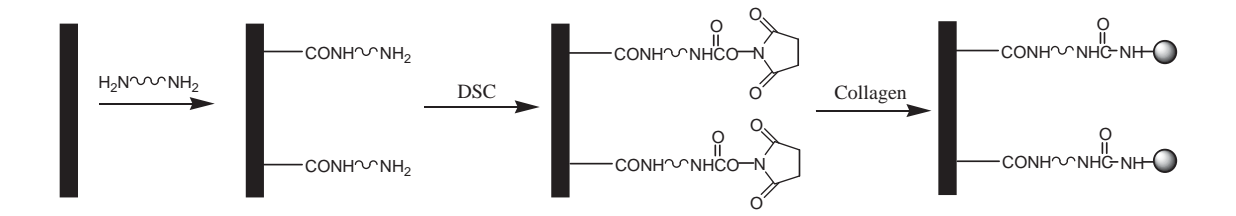


**Figure 1.** The chemical pathway for the immobilization of collagen.

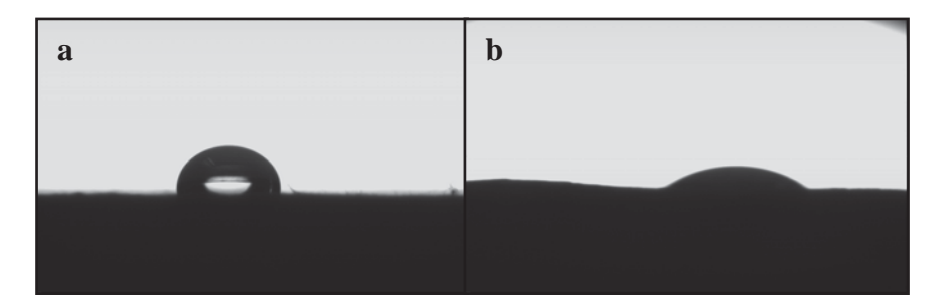
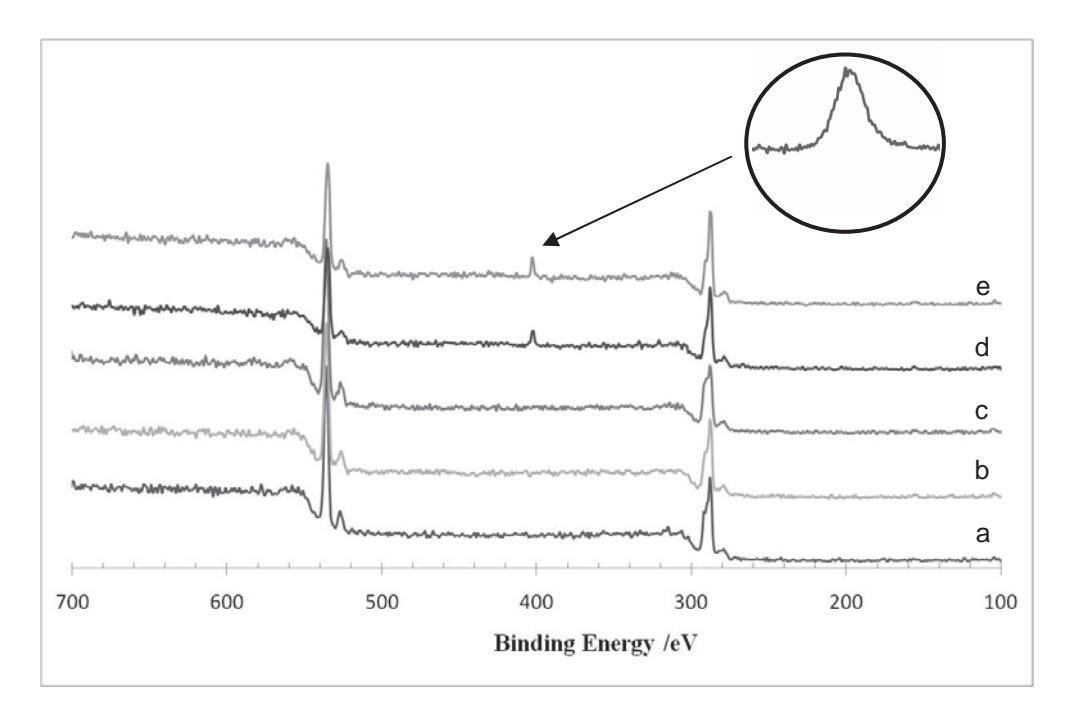
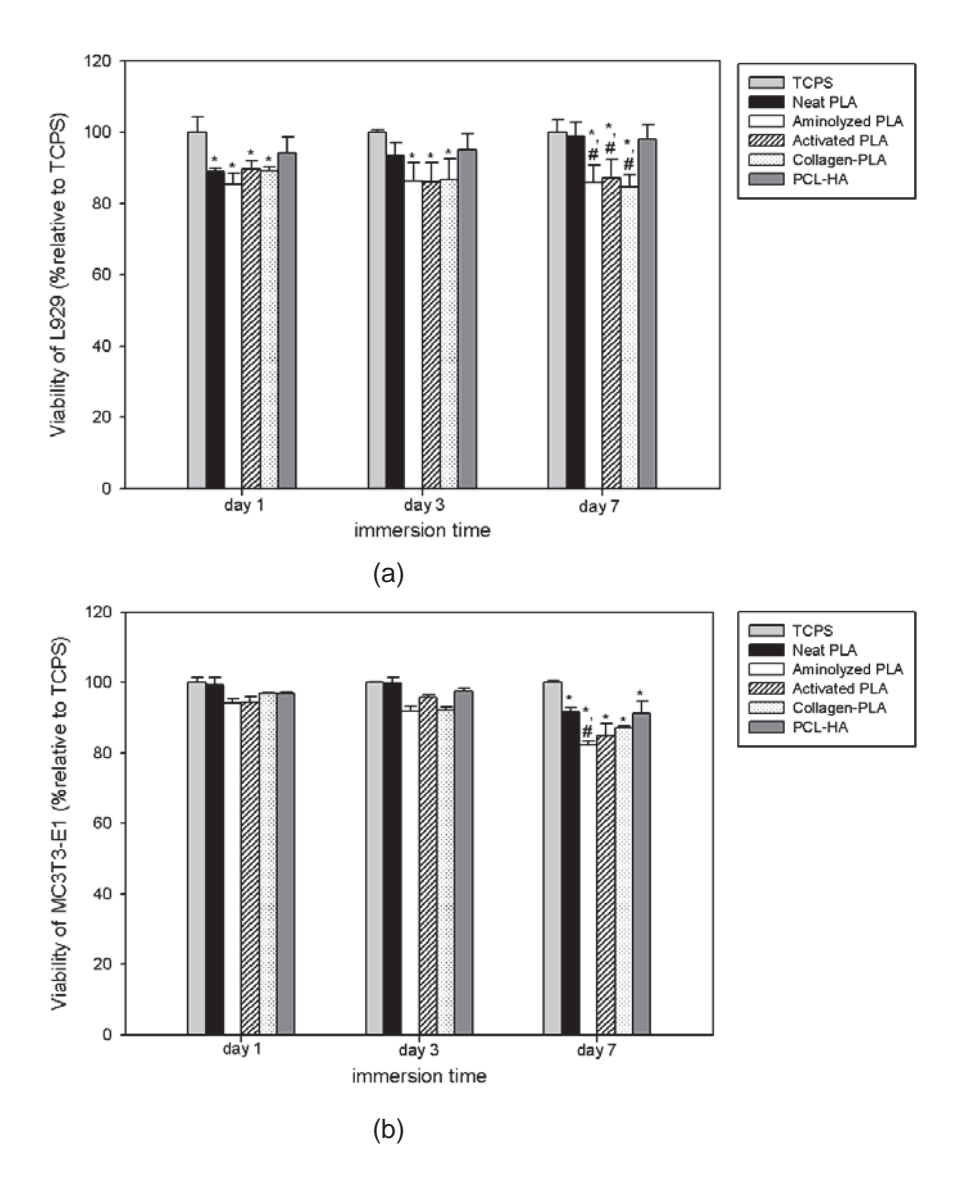


Figure 2. Water dropped on the surface of (a) neat PLA fibrous scaffold, and (b) PLA fibrous scaffold immobilized with 3.0 mg/ml collagen.



**Figure 3.** The survey XPS spectra of (a) neat PLA, (b) PLA aminolyzed in 0.04 g/ml HMD/IPA solution for 15 min at 50 °C, (c) activatedPLA, (d) PLA immobilized with collagen (0.5 mg/ml), and (e) PLA immobilized with collagen (3 mg/ml).



**Figure 4.** Indirect cytotoxic evaluation of neat PLA fibers, modified PLA fibers, and PCL/HA based on viability of (a) mouse fibroblasts (L929) and (b) pre-osteoblast (MC3T3-E1) that had been cultured with the extraction media from each of these materials against the viability of the cells that had been cultured with the respective culture media for 1 day as a function of the incubation time of the extraction and the culture media of 1, 3, or 7 d. Statistical significance:  $^*p$  < 0.05 compared with control and  $^*p$  < 0.05 compared to the neat PLA fibrous scaffolds at any given time point.

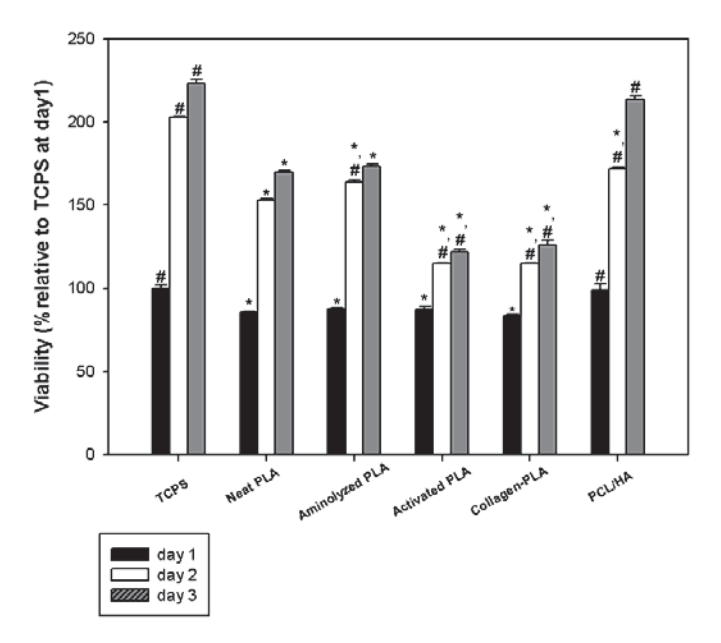


**Figure 5.** Indirect cytotoxic evaluation of neat PLA fibers, modified PLA fibers, and PCL/HA based on viability of pre-osteoblast (MC3T3-E1) that had been cultured with the 7-day extraction media from each of these materials with 2% serum-containing MEM against the viability of the cells that had been cultured with the respective culture media for 1, 2, and 3 day. Statistical significance: \*p < 0.05 compared with control and \*p < 0.05 compared to the neat PLA fibrous scaffolds at any given time point.

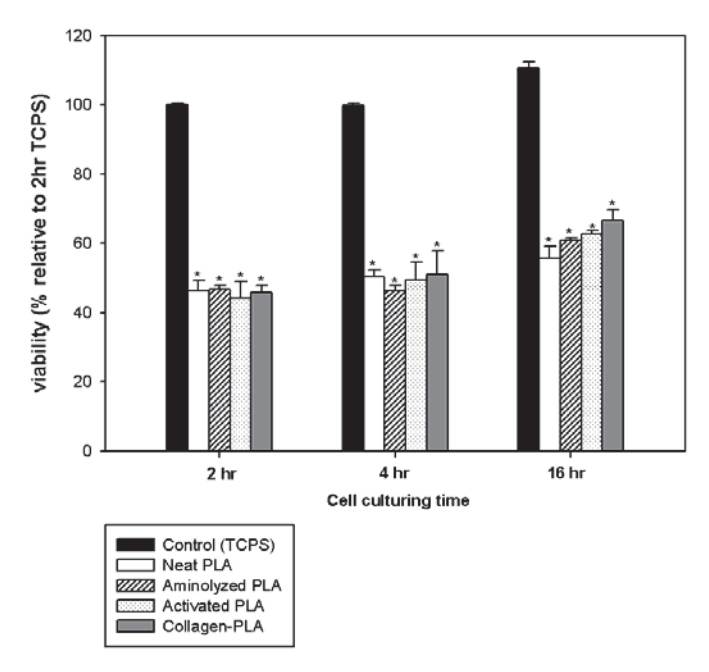


**Figure 6.** Attachment of MC3T3-E1 that had been seeded or cultured on the surfaces of TCPS, the neat and the modified PLA fibrous scaffolds for 2, 4, or 16 h. Statistical significance: p < 0.05 compared and p < 0.05 compared to the neat PLA fibrous scaffolds with control at any given time point.

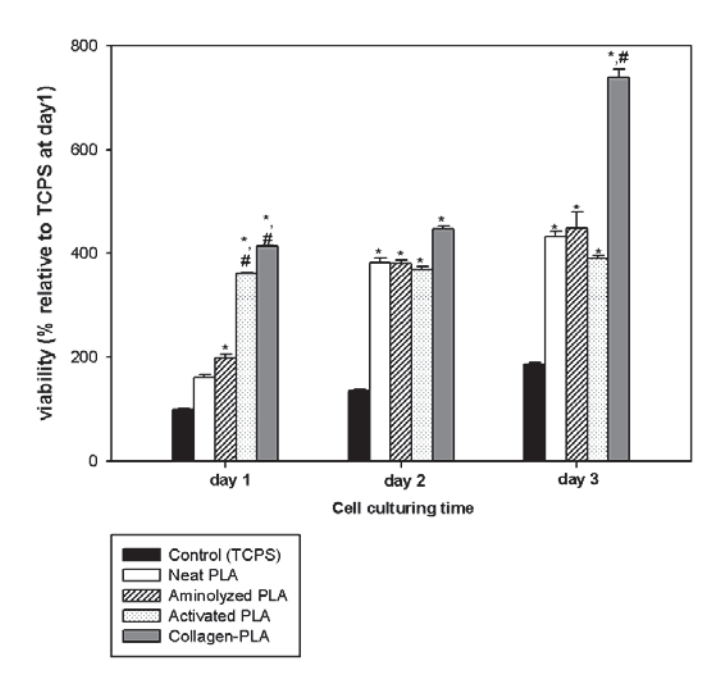


**Figure 7.** Proliferation of MC3T3-E1 that had been seeded or cultured on the surfaces of TCPS, the neat and the modified PLA fibrous scaffolds for 1, 2, or 3d. Statistical significance:  $^*p < 0.05$  compared with control and  $^*p < 0.05$  compared to the neat PLA fibrous scaffolds at any given time point.

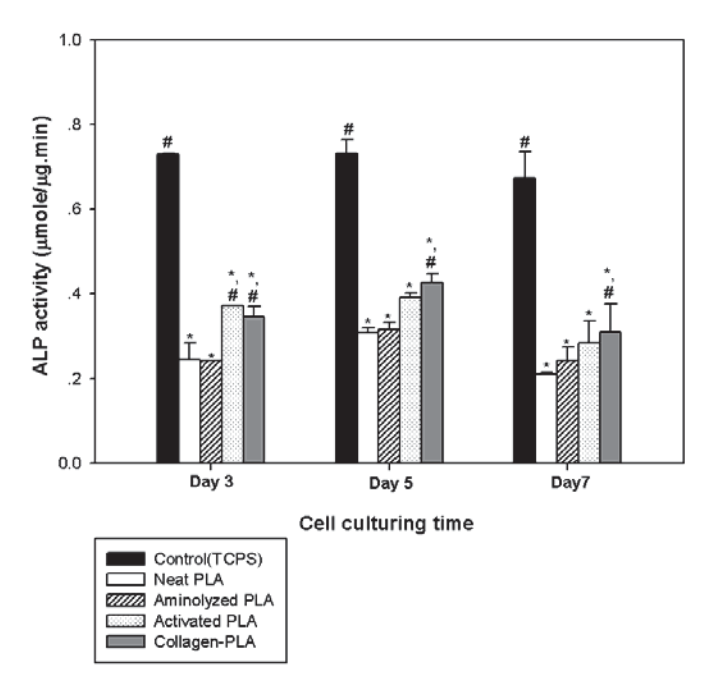


**Figure 8.** Alkaline phosphatase (ALP) activity of MC3T3-E1 that were cultured on the surfaces of TCPS, the neat and the modified PLA fibrous scaffolds for 3, 5, or 7 d.

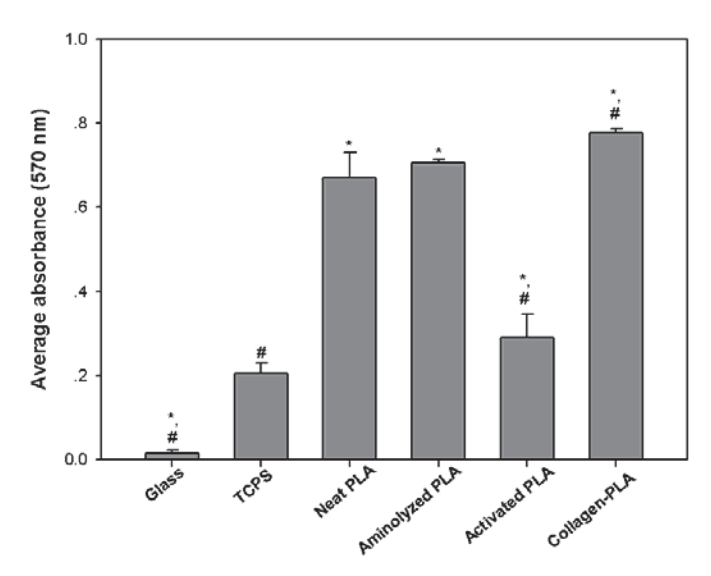


**Figure 9.** Quantification of mineral deposition in MC3T3-E1 by the method of Alizarin Red-S staining. Statistical significance: \*p < 0.05 compared with control and \*p < 0.05 compared to the neat PLA fibrous scaffold at any given time point.

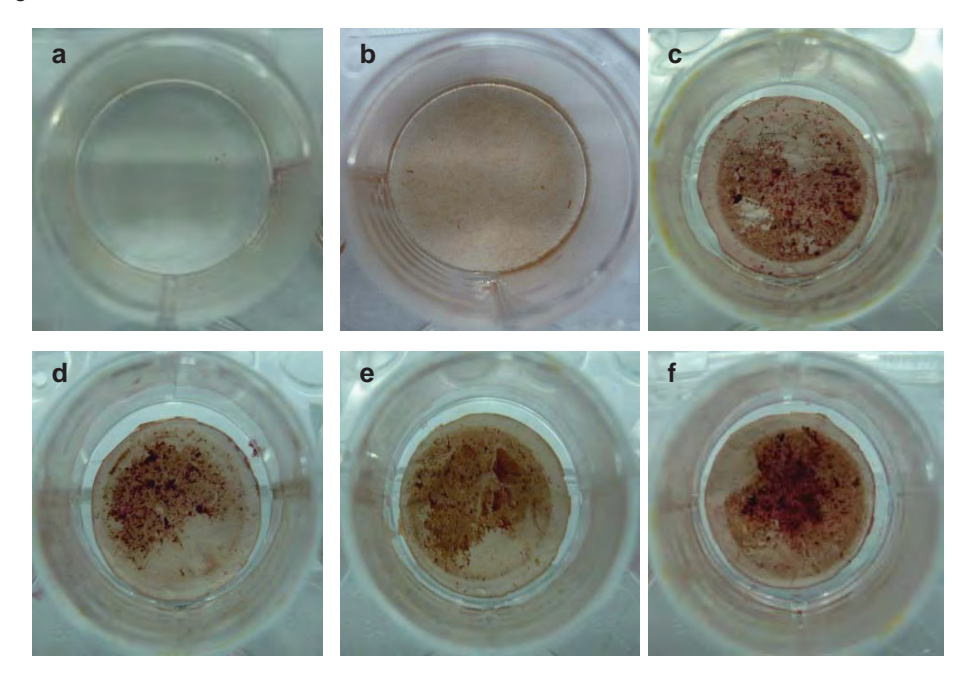


**Figure 10.** Images of Alizarin Red-S staining for the mineralization in MC3T3-E1 for day 16 for (a) glass (b) TCPS (c) neat PLA (d) aminolyzed PLA (e) activated PLA (f) collagen-immobilized PLA fibrous scaffold.

**Table 1.** NH<sub>2</sub> density as a function of 1,6-hexanediamine concentration

Diamine concentration	
(g/ml)	NH <sub>2</sub> conc. (x10 <sup>-7</sup> ) mol/cm <sup>2</sup>
0.02	1.91 ± 0.004
0.04	$2.52 \pm 0.01$
0.06	$3.58 \pm 0.01$
0.08	$3.67 \pm 0.01$
0.10	$5.10 \pm 0.02$

**Table 2.** NH<sub>2</sub> density as a function of aminolyzing time

Aminolyzing time (min)	NH <sub>2</sub> conc. (x10 <sup>-7</sup> ) mol/cm <sup>2</sup>
2	1.51 ± 0.01
4	$1.57 \pm 0.02$
8	$2.52 \pm 0.01$
15	$3.70 \pm 0.02$
20	$2.78 \pm 0.06$
30	$2.60 \pm 0.02$

Table 3. NH<sub>2</sub> density on the surface of the aminolyzed and collagen-immobilized PLA fibrous scaffolds

	NH <sub>2</sub> concentration
Sample	(mol·cm <sup>2</sup> )
Aminolyzed PLA <sup>a</sup>	$3.70 \pm 0.02 \times 10^{-7}$
Collagen Immobilized PLA <sup>b1</sup>	$4.52 \pm 0.08 \times 10^{-9}$
Collagen Immobilized PLA <sup>b2</sup>	$3.21 \pm 0.20 \times 10^{-8}$

<sup>&</sup>lt;sup>a</sup> The PLA e-spun fiber mat was immersed in 0.04 g/ml 1,6-hexanediamine solution at 50 °C for 15 min. <sup>b1,b2</sup> The activated PLA surface was immersed in 0.5 mg/ml or 3.0 mg/ml collagen solution, respectively, for 24 h followed by the rinsing process.

Table 4. Water contact angles of the neat and modified PLA fibrous scaffolds

	Water contact angle/degree
Samples	(Sessile drop)
neat PLA	106.8 ± 0.20
Aminolyzed PLA <sup>a</sup>	$99.5 \pm 0.17$
Activated PLA <sup>b</sup>	$112.5 \pm 0.38$
Collagen Immobilized PLA	
(w/o coupling agent) <sup>c</sup>	92.1 ± 0.19
Collagen Immobilized PLA <sup>d1</sup>	$79.4 \pm 0.30$
Collagen Immobilized PLA <sup>d2</sup>	73.0 ± 1.18

<sup>&</sup>lt;sup>a</sup>The PLA e-spun fiber mat was immersed in 0.04 g/ml 1,6-hexanediamine solution at 50 °C for 15 min.

<sup>&</sup>lt;sup>b</sup>The aminolyzed PLA surface was immersed in 0.1 M DSC solution for 3 h.

<sup>&</sup>lt;sup>c</sup>The aminolyzed PLA surface was immersed in 0.5 mg/ml collagen solutions for 24 h followed by the rinsing process. <sup>d1,d2</sup>The activated PLA surface was immersed in 0.5 mg/ml or 3.0 mg/ml collagen solution, respectively, for 24 h followed by the rinsing process.

Table 5.  $N_{1s}/C_{1s}$  ratios as a function of 1,6-hexanediamine concentration

HMD concentration (g/ml)	N <sub>1s</sub> /C <sub>1s</sub> ratio
0.02	0.0220
0.04	0.0237
0.06	0.0248
0.08	0.0283
0.1	0.0833

The aminolysis reaction took place at  $50^{\circ}\text{c}$  for 8 min.

Table 6.  $N_{1s}/C_{1s}$  ratios as a function of aminolyzing time

Aminolyzing time	
(min)	$N_{1s}/C_{1s}$ ratio
2	0.0133
4	0.0200
8	0.0237
15	0.0290
20	0.0240
30	0.0238

The aminolysis reaction took place at  $50^{\circ}\text{c}$  in 0.04 g/ml HMD/IPA solution.

Table 7.  $N_{1s}/C_{1s}$  ratios of the control and modified PLA fibrous scaffolds

Sample	N <sub>1s</sub> /C <sub>1s</sub> ratio
Neat PLA	0.0068
Aminolyzed PLA <sup>a</sup>	0.0290
Activated PLA <sup>b</sup>	0.0381
Collagen Immobilized PLA <sup>c1</sup>	0.2349
Collagen Immobilized PLA <sup>c1</sup>	0.2401

 $<sup>^{\</sup>mathrm{a}}$ The PLA e-spun fiber mat was immersed in 0.04 g/ml 1,6-hexanediamine solution at 50  $^{\mathrm{o}}$ C for 15 min.

 $<sup>^{\</sup>rm b}\text{The aminolyzed PLA}$  surface was immersed in 0.1 M DSC solution for 3 h.

c1,c2 The activated PLA surface was immersed in 0.5 mg/ml and 3.0 mg/ml collagen solutions, respectively, for 24 h followed by the rinsing process.

**Table 8.** Selected SEM images of cultured specimens, i.e., glass (i.e., control), neat PLA, aminolyzed PLA, activated PLA, and collagen-immobilized PLA fibrous scaffolds at two different time points after MC3T3-E1 were seeded or cultured on their surfaces (magnification = 2000X; scale bar = 10 µm).

	Magnification = 2000X		
Materials	Scale bar = 10 μm		
	Cultured 4 h	Cultured 16 h	
Glass (control)	1510 121020 10000	(h) 140 m2 . 000	
Neat PLA			
Aminolyzed PLA			
Activated PLA		30000	
Collgen-PLA			



Contents lists available at ScienceDirect

# Carbohydrate Polymers





# Use of 2-hydroxypropyl- $\beta$ -cyclodextrin as adjuvant for enhancing encapsulation and release characteristics of asiaticoside within and from cellulose acetate films

Jate Panichpakdee a,b, Pitt Supaphol a,b,\*

- <sup>a</sup> The Petroleum and Petrochemical College, Chulalongkorn University, Phyathai Road, Pathumwan, Bangkok 10330, Thailand
- b The Center for Petroleum, Petrochemicals and Advanced Materials, Chulalongkorn University, Phyathai Road, Pathumwan, Bangkok 10330, Thailand

#### ARTICLE INFO

# Article history: Received 27 August 2010 Received in revised form 13 February 2011 Accepted 14 February 2011 Available online 18 February 2011

Keywords:
Asiaticoside
Centella asiatica
2-Hydroxypropyl-β-cyclodextrin
Host-guest
Cellulose acetate
Drug release

#### ABSTRACT

The inclusion complex between asiaticoside (AC), an active substance from the medicinal plant *Centella asiatica* L., and 2-hydroxypropyl- $\beta$ -cyclodextrin (HP $\beta$ CD) was investigated. The phase solubility profiles of AC in distilled water and 90:10 (v/v) mixture of 80 vol.% acetic acid and N,N-dimethylacetamide (DMAC) both in the absence and the presence of HP $\beta$ CD were classified as AL-type and indicated a 1:1 molar ratio of the AC/HP $\beta$ CD complex. The 1:1 stoichiometric molar ratio of the complex was confirmed by both the 1D and the 2D <sup>1</sup>H-nuclear magnetic resonance spectrometry. Unlike the highly crystalline nature of the native AC, the stoichiometric AC/HP $\beta$ CD complex powder was amorphous in nature. The average diameters of the self-assembling aggregates of the AC/HP $\beta$ CD complex, a priori prepared at various HP $\beta$ CD to AC molar ratios of 0.5, 1, and 2, in the solution state, were about 2.4, 3.3, and 3.8  $\mu$ m, respectively. The solvent-cast CA films containing these complexes showed strong evidence of the aggregates on their surfaces. The maximal cumulative released amounts of AC, a sparingly water-soluble substance, from the CA films containing a mixture of AC/HP $\beta$ CD of varying molar ratios (i.e., 1:0.5, 1:1, and 1:2) in the phosphate buffer saline solution (PBS) containing 10% (v/v) methanol (i.e., PB/M medium) were 2.2, 3.9, and 5.8% (based on the actual weights of the film specimens), respectively, which were clearly an increasing function of the HP $\beta$ CD content in the films.

© 2011 Elsevier Ltd. All rights reserved.

# 1. Introduction

Cellulose acetate (CA) is the acetate ester of cellulose, the primary structural component of cell walls of green plants, and it is one of the most common biopolymers on earth (Anonymous, 2009). CA has been used for a wide variety of applications, including filters (Thostenson, Ren, & Chou, 2001), composite reinforcements (Bergshoef & Vancso, 1999), and topical and/or transdermal delivery of drugs (Wang et al., 2002). In the latter, Taepaiboon, Rungsardthong, and Supaphol (2000) developed electrospun CA fiber mats as carriers for the topical/transdermal delivery of all-trans retinoic acid or vitamin A acid (Retin-A) and  $\alpha$ -tocopherol or vitamin E (Vit-E) from CA solutions in 2:1 (v/v) acetone/dimethylacetamide (DMAc) containing Retin-A or Vit-E in the amount of 0.5 or 5 wt.% (based on the weight of CA), respectively. Electrospun CA fiber mats and the corresponding solvent-cast films as carriers for the topical/transdermal delivery of four different non-steroidal anti-inflammatory drugs (NSAIDs), i.e., naproxen

(NAP), indomethacin (IND), ibuprofen (IBU), and sulindac (SUL), were reported by Tungprapa, Jangchud, and Supaphol (2007), who used CA solutions in 2:1 (v/v) acetone/DMAc as the base solutions into which NAP, IND, IBU, or SUL in the amount of 20 wt.% (based on the weight of the CA) was added.

Asiaticoside (AC; see Fig. 1 for its chemical structure) is one of four major trisaccharide triterpenoid components (i.e., asiatic acid, asiaticoside, madecassic acid and madecassoside) of the extract from the medicinal plant Centella asiatica (L.) Urban which bears a common name in Thai as "Buabok." AC has been regarded as one of the most active compounds associated with the healing of wounds, as evidenced from the observed increase in antioxidant levels at an early stage of recovery of excision-type cutaneous wounds in rats (Shukla, Rasik, & Dhawan, 1999), the observed increase in the proliferation of human dermal fibroblasts and the expression of types I and III pro-collagen mRNA and the protein levels of the cells (Maquart, Bellon, Gillery, Wegrowski, & Borel, 1990; Shim et al., 1996), and the stimulation of extracellular matrix (ECM) accumulation in experimental wounds of rats (Maquart et al., 1999; Suguna, Sivakumar, & Chandrakasan, 1996) in response to the presence of this substance.

Recently, Suwantong, Ruktanonchai, and Supaphol (2008) reported the preparation of electrospun CA fiber mats and the corresponding solvent-cast films containing either *C. asiatica* crude

<sup>\*</sup> Corresponding author at: The Petroleum and Petrochemical College, Chulalongkorn University, Phyathai Road, Pathumwan, Bangkok 10330, Thailand. Tel.: +66 2218 4131; fax: +66 2215 4459.

E-mail address: pitt.s@chula.ac.th (P. Supaphol).

Fig. 1. Chemical structure of asiaticoside (AC).

extract (CACE) or pure AC in the amount of 40 wt.%, based on the weight of the CA powder. The release characteristics of AC from those specimens were tested by the total immersion and the transdermal diffusion through a pig skin methods in either of the acetate or the phosphate buffer solution that contained methanol (i.e., A/B/M or P/B/M medium) at the skin or the physiological temperature of 32 or 37 °C, respectively. However, the release of AC from the CA films containing either CACE or AC was too low (lower than about 2 and 3%, based on the actual weight of the specimens in the A/B/M or P/B/M medium, respectively). This was thought to be a result of the low aqueous solubility of AC (i.e.,  $0.67 \,\mathrm{mg}\,\mathrm{mL}^{-1}$ ) as well as to the dense structure of the CA films and the inherent insolubility of CA in an aqueous medium. To increase the amount of AC that could be released from the CA matrix, the release should be less dependent on the intrinsic solubility of the active compound in the releasing medium (Sangalli et al., 2001) and/or on the microenvironment through which the drug molecules are to diffuse out (i.e., corresponding to the way in which the drug is incorporated within the matrix) should also be modified (Pose-Vilarnovo et al., 2004).

Cyclodextrins (CDs), complexing agents capable of forming host-guest interactions with a variety of compounds, are capable of interacting with many therapeutic agents, e.g., drugs, by encapsulating them, either wholly or partly, into the hydrophobic cavity of their molecules. Such inclusion complexes have been reported to exhibit several advantages, such as improving the solubility, dissolution rate and bioavailability (Freville, Dollo, Le Corre, Chevanne, & Le Verge, 1996; Loftsson & Brewster, 1996; Pose-Vilarnovo et al., 2001), decreasing toxicity (de Araujoa et al., 2008; Irie & Uekama, 1997; Rajewski & Stella, 1996), and increasing the permeation rate of the encapsulating drug molecules (Loftsson, Jarho, Másson, & Sigurjonsdóttir, 2005; Lopez, Collett, & Bentley, 2000). As a result, they are used in many applications, such as in controlled drug delivery: whether dermally, transdermally, or orally (Challa, Ahuja, Ali, & Khar, 2005). The cyclodextrin complexes have also been reported to form self-assembling entities or micelles (Loftsson, Magnúsdósdottir, Másson, & Sigurjónsdóttir, 2002; Mele, Mendichi, & Selva, 1998). Choi, Ruktanonchai, Min, Chun, and Soottitantawat (2010) prepared either self-assembling aggregates of  $\beta$ -CD and fish oil and studied the release characteristics of fish oil from the obtained  $\beta$ -CD-fish oil complexes at different ratios of the substances.

The aim of the present work was to investigate the complexation of AC within 2-hydroxypropyl- $\beta$ -cyclodextrin (HP $\beta$ CD) and the potential for use of the solvent-cast CA films that contained a AC/HP $\beta$ CD mixture of varying molar ratios as carriers for the topical/transdermal delivery of AC. Various properties (i.e., morphology, size of self-assembling aggregates, water retention and weight loss) of both the AC- and the AC/HP $\beta$ CD complex-loaded CA films and the release characteristics of AC from these materials in a phosphate buffer saline solution that contained methanol were investigated.

### 2. Experimental details

#### 2.1. Materials

Cellulose acetate (CA; white powder;  $M_{\rm W} \approx 30,000\,{\rm Da}$ ; acetyl content = 39.7 wt.%; degree of acetyl substitution  $\approx 2.4$ ) and 2-hydroxypropyl- $\beta$ -cyclodextrin (HP $\beta$ CD;  $M_{\rm W} \approx 1,380\,{\rm Da}$ ; average number of substituent per glucopyranose unit  $\approx 0.6$ ) were purchased from Sigma–Aldrich (Switzerland). Asiaticoside (AC; 90% purity) was purchased from Shanghai Angoal Chemical Co., Ltd. (China). N,N-Dimethylacetamide (DMAc, Lab-Scan Asia, Thailand), glacial acetic acid (Carlo Erba, Italy), anhydrous disodium hydrogen orthophosphate, sodium dihydrogen orthophosphate, and sodium chloride (Ajax Chemicals, Australia) were used as-received. All chemicals were of analytical reagent grades and used without further purification.

# 2.2. Stoichiometry of AC/HP $\beta$ CD complex in solution state

## 2.2.1. Phase solubility studies

Phase solubility of AC in HP $\beta$ CD was studied in distilled water. Briefly, excess amounts of AC were put into aqueous HP $\beta$ CD solutions (1 mL). The amount of HP $\beta$ CD in the solutions was varied between 0 and 30 mM. The sample solutions were then stirred at room temperature (25  $\pm$  1 °C) for 24 h. It should be noted that the stirring time of 24 h was enough for the solubilization of AC in HP $\beta$ CD to reach equilibrium. After reaching the equilibrium, unsolubilized AC in the sample solutions was filtered out through a filter membrane (0.45  $\mu$ m in pore diameter). The filtrates were later quantified for the amounts of the solubilized AC by reversed-phase high performance liquid chromatography (HPLC; see later). The association constant ( $K_a$ ) was then calculated from the following equation (Higuchi & Connors, 1965):

$$K_a = \frac{m}{s_0(1-m)},\tag{1}$$

where m is the slope of the plot between the solubility of AC in distilled water as a function of the HP $\beta$ CD concentration and  $s_0$  is the solubility of AC in distilled water in the absence of HP $\beta$ CD.

In addition, the complexation efficiency (CE) and the AC:HP $\beta$ CD molar ratio ([AC]:[CD]) were calculated as follows (Loftsson, Hreindóttir, & Másson, 2007):

$$CE = s_0 K_{1:1} = \frac{[AC]/[CD]}{[CD]} = \frac{m}{1-m},$$
 (2)

$$\frac{[AC]}{[CD]} = \frac{1}{1 + (1/CE)},\tag{3}$$

where  $K_{1:1}$  is the association constant for the AC:HP $\beta$ CD molar ratio of 1:1.

The phase solubility of AC in HP $\beta$ CD was also studied in a 90:10 (v/v) mixture of 80 vol.% acetic acid and DMAc. To ensure the formation of the AC/HP $\beta$ CD complex in the solvent mixture, the preparation procedure was similar to what had been described above, with an exception to the fact that the mixture of acetic acid and DMAc was used instead of the distilled water.

## 2.2.2. <sup>1</sup>H-NMR studies

A Varian <sup>UNITY</sup>INOVA <sup>1</sup>H-nuclear magnetic resonance spectrometer (<sup>1</sup>H-NMR), operating at 400 MHz and 25 °C, was used to determine the stoichiometric ratio of the AC/HP $\beta$ CD complex. Based on the Job's continuous variation method (Job, 1928), the <sup>1</sup>H-NMR spectra were recorded from a mixture of AC (10 mM) and HP $\beta$ CD (10 mM) in 10% (v/v) DMSO- $d_6$ /D<sub>2</sub>O mixture at various volumetric ratios between these two solutions at the final concentrations of AC of 1–10 mM, prior to being stirred for 24 h.

# 2.3. Preparation of AC/HP $\beta$ CD complex in solid state

The AC/HP $\beta$ CD complex was prepared according to the method previously described by Higuchi and Connors (1965), with slight modification. Briefly, a weighed amount of HP $\beta$ CD was first dissolved in distilled water. A weighed amount of AC was then added to the solution and stirred at room temperature (25  $\pm$  1 °C) for 24 h. The stoichiometric AC:HP $\beta$ CD molar ratio, as obtained from the studies in Section 2.2, was utilized throughout the rest of the studies. The solution/suspension was filtered through a nylon filter (average pore size=0.45  $\mu$ m) prior to being frozen at  $-40\pm2$  °C for 24 h. After that, the obtained mass was lyophilized (Labconco FreeZone® 6-Liter Benchtop Freeze Dry System). A physical blend of AC and HP $\beta$ CD at the same molar ratio was also prepared for comparison.

## 2.4. Characterization of solid AC/HPβCD complex

# 2.4.1. X-ray powder diffractometry

X-ray powder diffractograms of the AC/HP $\beta$ CD complex and the corresponding physical mixture were obtained on a Bruker Model D8 Advance, equipped with a Cu K $\alpha$  radiation source, over a scattering (2 $\theta$ ) range of 5 and 60° at room temperature (25 ± 1°C). The scan rate, the operating voltage, and the filament current were set at 0.2° min<sup>-1</sup>, 40 kV, and 30 mA, respectively.

## 2.4.2. Two dimensional <sup>1</sup>H-NMR studies

To obtain the 2D  $^1H$ -NMR spectrum of the AC/HP $\beta$ CD complex, the freeze-dried product was dissolved in D $_2$ O at room temperature (25  $\pm$  1  $^{\circ}$ C) and investigated under the following conditions: acquisition time of 0.205 s, sweep width of 5006.3 Hz, pulse width of 6.3  $\mu$ s, time domain of 2048, Fourier number of 2048 and temperature of 298 K.

# 2.5. Preparation of AC- and AC/HP $\beta$ CD complex-loaded CA films

CA films containing either AC or AC/HP $\beta$ CD complex were prepared by solvent casting technique. AC or a AC/HP $\beta$ CD complex that had been prepared at different mixing molar ratios of HP $\beta$ CD to AC (i.e., 0.5, 1.0, or 2.0) was incorporated at a concentration of 10%, based on the dry weight of CA powder, in a 90:10 (v/v) mixture of 80 vol.% acetic acid and DMAc. The concentration of CA in the final solutions was 4% w/v. The as-prepared solutions were stirred at room temperature (25  $\pm$  1 °C) for 24 h. Prior to the addition of CA powder, each of the sample solutions was characterized for the particle size of the self-assembling aggregates by a Malvern Zetasizer ZS nanosizer [based on the dynamic light scattering (DLS) principle]. CA powder was then added to the sample solution and subsequently stirred at room temperature (25  $\pm$  1 °C)

for 3 h until CA was completely dissolved. The solutions were subsequently poured onto glass Petri dishes and dried under a reduced pressure. The films were dried until of a constant weight and stored in a desiccator in vacuo for at least 24 h, prior to further use. The thicknesses of the as-cast films were  $80\pm10~\mu m$ .

# 2.6. Characterization of AC- and AC/HP $\beta$ CD complex-loaded CA films

Morphologies of AC- and AC/HP $\beta$ CD complex-loaded CA films were studied by a JEOL JSM-6400 scanning electron microscope (SEM). All of the specimens were vacuum-coated with a thin layer of gold using a JEOLJFC-1100E sputtering device. The average diameters of the self-assembling aggregates and the pores that were formed after the films had been immersed in a phosphate buffer saline solution (PBS; see later for its preparation) containing 10% (v/v) methanol (hereafter, P/B/M medium) for 24 h were determined by measuring the diameters of the micro-aggregates and the micro-pores at 100 different points on the SEM images of 7500× magnification with SemAphore 4.0 software. For each sample, the diameters were presented as the average  $\pm$  standard deviation.

Water retention and weight loss behavior of the AC- and the AC/HP $\beta$ CD complex-loaded CA films were investigated after their immersion in the P/B/M medium at 37 °C for 24 h. The water retention and the weight loss behavior were calculated as follows:

Water retention (%) = 
$$\frac{M - M_d}{M_d} \times 100$$
, (4)

and

Weight loss (%) = 
$$\frac{M_i - M_d}{M_d} \times 100$$
, (5)

where M and  $M_d$  are wet and dry weights of the film specimens after immersion in the buffer solution, respectively, and  $M_i$  is the initial, dry weight of the specimens. All measurements were carried out in triplicate.

# 2.7. Release of AC from AC- and AC/HP $\beta$ CD complex-loaded CA films

# 2.7.1. Preparation of releasing medium

To prepare 1 L of the PBS solution, 6.177 g of anhydrous disodium hydrogen orthophosphate and 1.1014 g of sodium dihydrogen orthophosphate were dissolved under mechanical stirring in distilled water at room temperature (25  $\pm$  1  $^{\circ}$ C) until the flakes were completely dissolved. Later, 8.7 g of sodium chloride was added into 20 mL of the solution. The volume was adjusted to the required volume with distilled water. The pH of the final solution was 7.4.

# 2.7.2. Actual AC content

The actual amounts of AC in the AC- and the AC/HP $\beta$ CD complex-loaded CA films were quantified by dissolving the samples (circular disc: about 1.5 cm in diameter) in 4 mL of 2:1 (v/v) acetone/DMAc. After that, 0.5 mL of the solutions were pipetted and diluted into 8 mL of the P/B/M medium. Finally, the AC contents in the diluted sample solutions were determined by HPLC (see later) and then back-calculated from the obtained data against a calibration curve for AC.

### 2.7.3. AC release assay

The release characteristics of AC from the AC- and the AC/HP $\beta$ CD complex-loaded CA films were determined by the total immersion method. Each of the specimens (circular disc of about 1.5 cm in diameter) was immersed in 25 mL of the P/B/M medium at the physiological temperature of 37 °C. At each time point, ranging between 0 and 24 h (1440 min), 1 mL of the medium was withdrawn

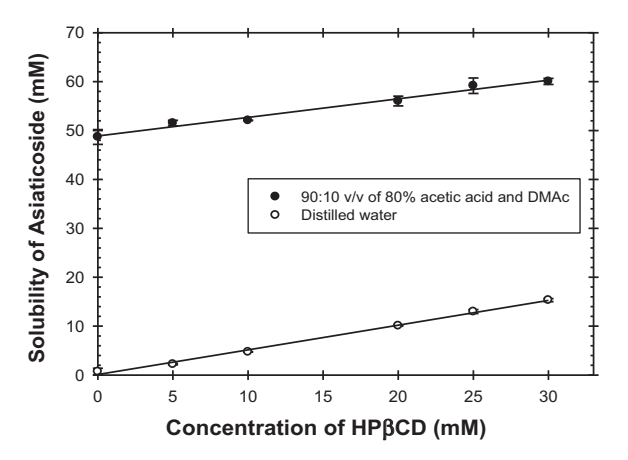


**Fig. 2.** Phase solubility diagrams of AC in the absence or the presence of 2-hydroxypropyl- $\beta$ -cyclodextrin (HP $\beta$ CD) in distilled water and 90:10 (v/v) of 80% acetic acid and DMAc at room temperature.

(i.e., sample solution) and an equal amount of the fresh medium was refilled. The amounts of AC in the sample solutions were quantified by HPLC (see later) and then back-calculated from the obtained data against the calibration curve for AC.

# 2.8. Determination of AC content

The amount of AC in a given sample solution was determined by HPLC (Shimadzu LC-10 AD). The sample solution was filtered through a nylon filter (average pore size = 0.45  $\mu m$ ) and then separated in an Inertsil ODS-3 C18 column (particle size = 5  $\mu m$ ; column dimension = 4.6 mm  $\times$  250 mm) with an Inertsil ODS-3 guard column (particle size = 5  $\mu m$ ; column dimension = 4.0 mm  $\times$  10 mm) at a flow rate of 1 mL min $^{-1}$ . A UV–Visible detector was set at  $(\lambda_{max})$  204 nm. The mobile phase for the AC separation consisted of acetonitrile, methanol, and distilled water at 26:24:50 (v/v/v) and the retention time was 7.7 min. The calibration curve for AC was obtained over a concentration range of 0.005–0.200 mg mL $^{-1}$ .

### 2.9. Statistical analysis

One-way ANOVA was used to analyze the means of different data sets. The significance for all of the tests was accepted at a 0.05 confidence level.

### 3. Results and discussion

# 3.1. Stoichiometry of AC/HP $\beta$ CD complex in solution state

The solubility of AC in the absence or the presence of HP $\beta$ CD was studied in two types of medium (i.e., distilled water or 90:10 (v/v) of 80% acetic acid and DMAc) and the results are graphically shown in Fig. 2. In the absence of HP $\beta$ CD, the solubility of AC in any type of the studied medium (i.e.,  $s_0$ ) was low (i.e., 0.7 mM in distilled water and 48.7 mM in 90:10 (v/v) of 80% acetic acid and DMAc). Marked increase in the amounts of soluble AC in either medium was evident in the presence of HP $\beta$ CD. At the greatest amount of HP $\beta$ CD investigated (i.e., 30 mM), the amounts of soluble AC increased to 15.3 and 60.0 mM in distilled water and 90:10 (v/v) of 80% acetic acid and DMAc, respectively. Obviously, the amounts of soluble AC in both types of medium exhibited linear relationships with the HP $\beta$ CD content in the solutions.

The association constants,  $K_a$ , characterizing the solubility of AC in distilled water and 90:10 (v/v) of 80% acetic acid and DMAc, can be calculated from the slopes of the plots such as those shown in Fig. 2. The slopes of the least-squared lines drawn through both

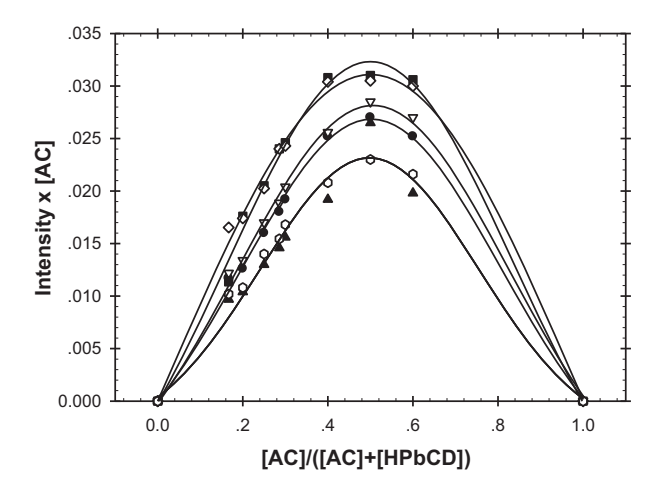


**Fig. 3.** Job's continuous variation plots of the chemical shifts of the protons, i.e., (∇) H-12, (Φ) H-18, (♠) CH<sub>3</sub>-26, (♠) CH<sub>3</sub>-29, (■) Glc-1, and (○) Rha-5, of AC, in the presence of different HPβCD concentrations in the 90:10 (v/v) mixture of D<sub>2</sub>O and DMSO- $d_6$ .

sets of data were less than one, with the values being 0.505 and 0.380, respectively. According to the definition set forth by Higuchi and Connors (1965), these could be categorized as  $A_L$  type and a 1:1 complex between AC and HP $\beta$ CD could be assumed. Based on the values of the slopes obtained, the  $K_a$  values (or the  $K_{1:1}$  values, for this particular case) can be calculated, based in Eq. (1), to be 11,726.5 and 12.5  $M^{-1}$ , respectively. According to Eq. (2), the complexation coefficient values, CE, were determined to be 1.020 and 0.613, respectively, while, according to Eq. (3), the AC:HP $\beta$ CD molar ratios were 1:2 and 1:3, respectively. This means that, despite the stoichiometric 1:1 molar ratio between AC and HP $\beta$ CD in the as-formed complex, only 1 in every 2 or 3 molecules of HP $\beta$ CD underwent the complexation with AC.

One dimensional <sup>1</sup>H-NMR spectroscopy is useful for studying the inclusion complex of HPBCD with various organic compounds. The variation in the chemical shift of the protons of organic compounds ( $\Delta \delta = \delta_c - \delta_0$ , where  $\delta_c$  and  $\delta_0$  are the chemical shifts of a specific chemical species in the complex and the free forms, respectively), due to the screening environment by magnetic nuclei within the HPβCD cavity, was recorded. In particular, changes in the chemical shifts of protons of the guest molecule(s) within the CD cavity can be used to quantify the stoichiometry of the complex, simply by plotting them as a function of the mole fraction of the guest molecule(s) or the CD molecule [i.e., Job's continuous variation plots (Job, 1928)]. The mole fraction at the maximum peak(s) is taken as the stoichiometric ratio of the complex. According to Fig. 3, the chemical shifts of CH<sub>3</sub>-26, CH<sub>3</sub>-29, H-12, H-18, Rha-5, and Glc-1 protons in the AC/HP $\beta$ CD mixtures, in 90:10 (v/v) mixture of  $D_2O$  and DMSO- $d_6$ , exhibited the maximum peaks at  $[AC]/([AC] + [HP\beta CD]) = 0.5$ , corresponding to the AC:HP $\beta$ CD molar ratio of 1:1. In addition, Table 1 shows the chemical shift signals of protons of AC and HP $\beta$ CD, both in the free and the complex states, in D<sub>2</sub>O at equi-molar ratio between AC and HPβCD, along with their differences.

# 3.2. Characterization of AC/HP $\beta$ CD complex in solid state

### 3.2.1. X-ray powder diffractometry

The freeze-dried product from the equi-molar mixture of AC and HP $\beta$ CD was white powder. X-ray powder diffractometry was then used to confirm the formation of the AC/HP $\beta$ CD complex. Fig. 4 shows the X-ray diffractograms of AC, HP $\beta$ CD, the AC/HP $\beta$ CD complex, and the physical mixture of AC and HP $\beta$ CD. Sharp diffraction peaks were evident for the as-received AC, indicating its crys-

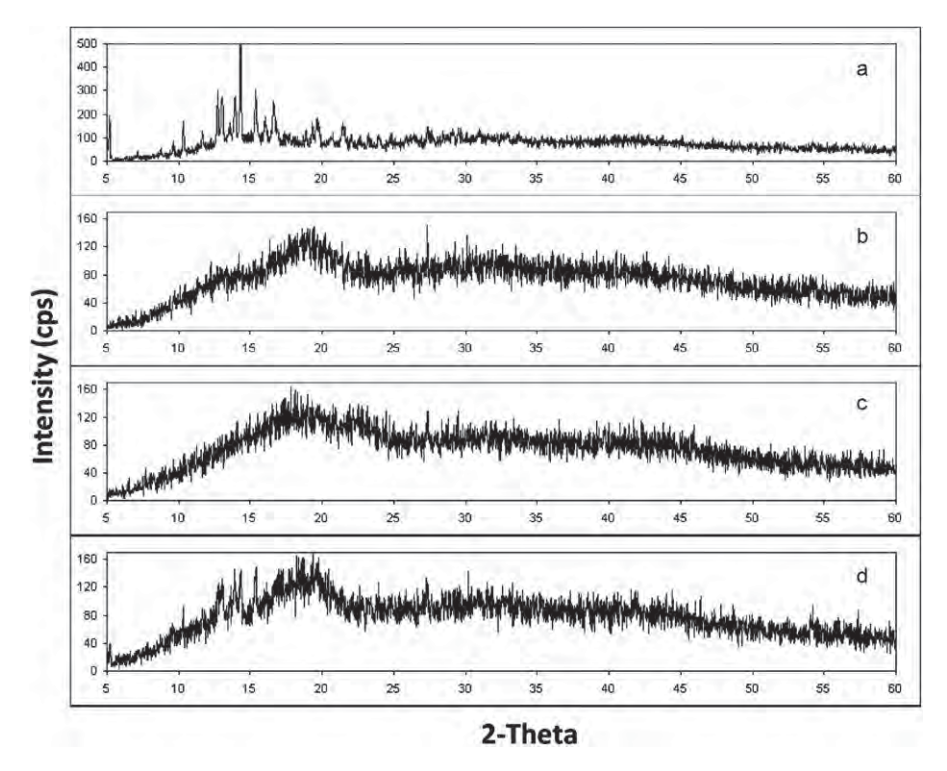


Fig. 4. X-ray diffractograms of (a) AC, (b) HPβCD, (c) AC/HPβCD complex, and (d) physical mixture of AC and HPβCD.

talline nature. On the other hand, only diffused, scattering peaks were observed for the as-received HP $\beta$ CD, with the scattering center being observed at the scattering angle,  $2\theta$ , of about  $18^\circ$ . This indicates the amorphous nature of HP $\beta$ CD. As for the AC/HP $\beta$ CD complex, only the scattering peaks similar to those of HP $\beta$ CD were obtained, indicating the amorphous nature of the material. When AC was physically mixed with HP $\beta$ CD, however, both the sharp diffraction peaks of AC and the diffused, scattering peaks of HP $\beta$ CD were evident. These results confirmed the inclusion of AC within the cavity of HP $\beta$ CD.

# 3.2.2. Two dimensional <sup>1</sup>H-NMR

To investigate the spatial arrangement of AC within the HP $\beta$ CD cavity, Nuclear Overhauser Effect Spectroscopy (NOESY) was applied on the stoichiometric AC/HP $\beta$ CD complex (1:1 molar ratio) that had been dissolved in D $_2$ O and the result is shown in Fig. 5a.

**Table 1** Chemical shift signals of protons (in ppm) of AC and HPβCD in the free  $(\delta_0)$  and the complexed  $(\delta_c)$  states in  $D_2O$  at the equi-molar ratio between AC and HPβCD of the inclusion complex, along with their differences.

Proton	$\delta_0$	$\delta_c$	$\Delta\delta\left(\delta_{c}-\delta_{0}\right)$
AC			
H-12	5.162	5.216	0.054
H-18	2.033	2.087	0.054
$CH_3-24$	0.644	0.667	0.023
CH <sub>3</sub> -26	0.777	0.831	0.054
$CH_3-27$	1.132	1.134	0.002
CH <sub>3</sub> -29	0.844	0.869	0.025
Glc-1	4.385	4.323	-0.062
Rha-CH₃	1.301	1.321	0.002
Rha-5	3.942	3.988	0.046
HPβCD			
H-1	5.090	5.086	-0.004
H-2	3.542	3.546	0.004
H-3	3.817	3.896	0.079
H-4	3.525	3.526	0.001
H-5	3.600	3.620	0.020
H-6	3.682	3.760	0.078

Cross-peaks were observed between the  $CH_3$ -29 and  $CH_3$ -27 protons of AC and the H-3 inner-cavity proton of HP $\beta$ CD (located at the wide side of the cavity) and between the  $CH_3$ -26 and H-6 protons of AC and the H-5 inner-cavity proton of HP $\beta$ CD (located at the narrow side of the cavity). This indicates that the cyclohexene ring moiety of AC is captivated within the cavity of HP $\beta$ CD, as depicted in Fig. 5b, hence confirming the stoichiometric 1:1 molar ratio between AC and HP $\beta$ CD in the solid complex. Notwithstanding, the specific interactions between H-12, H-18, Glc-1, Rha-5, and Rha-Me protons of AC and the H-2, H-4, and H-6 outer-cavity protons of HP $\beta$ CD are believed to be the probable cause for the self-aggregation of adjacent AC/HP $\beta$ CD entities.

# 3.3. Characterization of AC- and AC/HP $\beta$ CD complex-loaded CA films

# 3.3.1. Physical appearance

Prior to the addition of CA powder into the AC/HPBCD solutions, the diametric dimensions of the self-assembling aggregates of the AC/HPβCD complex that had been prepared at different HPβCD to AC molar ratios of 0.5, 1, and 2 were determined by the nanosizer to be 2.38  $\pm$  1.39, 3.34  $\pm$  0.66, and 3.84  $\pm$  0.53  $\mu m$ , respectively (see Supplementary data). Evidently, the size of the aggregates was an increasing function of the HPBCD proportion in the solution. CDs are known to form into self-assembling aggregates, which is facilitated by their ability to form inter-molecular hydrogen bonding (Coleman & Nicolis, 1992; González-Gaitano et al., 2002; Suzuki, Tsutsui, & Ohmori, 1994). In addition, Mele et al. (1998) reported that  $\beta$ -carotene in its complexation with  $\beta$  and  $\gamma$ -CDs in water existed as large aggregates, as revealed by both light scattering and <sup>1</sup>H NMR techniques. Factors that influence the formation of self-assembling aggregates are, for examples, concentration and molecular weight of CDs, pH, and temperature, while high pH, high temperature, and the addition of an electrolyte have been used as means to prevent the aggregation (Bonini et al., 2006; Das, Mallick, Sarkar, & Chattopadhyay, 2008; He, Fu, Shen, & Gao, 2008).

 Table 2

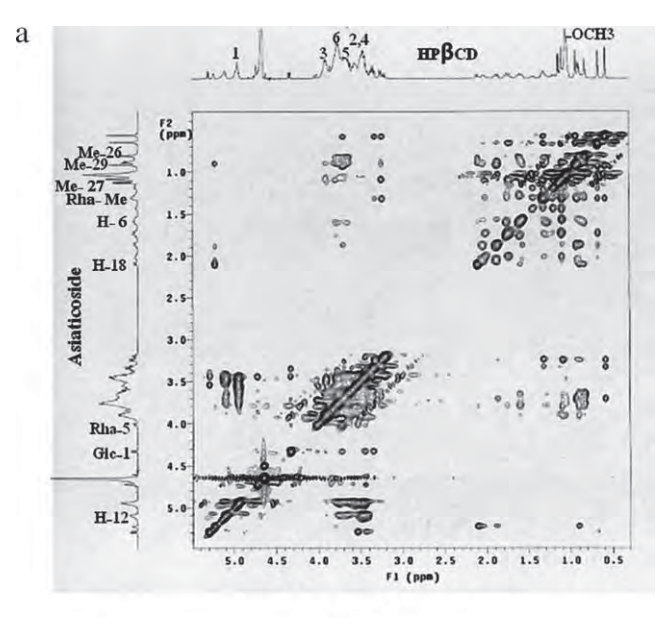
 Representative SEM images of AC- and AC/HPβCD complex-loaded CA films both before and after their immersion in a phosphate buffer saline solution (PBS) containing 10% (v/v) methanol (i.e., P/B/M medium) for 24 h.

Type of CA film sample	Before immersion in P/B/M	After immersion in P/B/M
Containing 10 wt.% AC	15ku k7:520 m41	Make Sal 140 ontones
Containing 10% (w/w) AC/HPβCD at the mixing ratio of 1:0.5	115k U X7. 388	15ku X7. 500 1+m 6888888
Containing 10% (w/w) AC/HPβCD at the mixing ratio of 1:1	น์ ซ.เซ - ซ.ล์อ โคล ออดิตสด	15(U-87)-588 IIAN 888888
Containing 10% (w/w) AC/HPBCD at the mixing ratio of 1:2	Dsku x7.500 1 на овобое	6) U (2) 500 (1) (1) (40 90 U

SEM was used to investigate the morphologies of the obtained AC- and AC/HP $\beta$ CD complex-loaded CA films. Representative images are illustrated in Table 2. Apparently, the surface of the AC-loaded CA film was rough, with no evidence of any specific pattern on it. This should be due to the complete dissolution of AC in the 90:10 (v/v) mixture of 80 vol.% acetic acid and DMAc, prior to the addition of the CA powder, resulting in rather homogeneous distribution of AC throughout the mass of the resulting CA film. On the other hand, specific pattern in the form of spherical aggregates was observed on all of the AC/HP $\beta$ CD complex-loaded CA films. Specifically, an increase in the HP $\beta$ CD to AC molar ratio resulted in a monotonous decrease in the sharpness of the boundary of these aggregates. It is believed that these entities

were the self-assembling aggregates of the AC/HP $\beta$ CD complex that had been formed in the AC/HP $\beta$ CD solutions. The diameters of the aggregates that had been formed at the AC:HP $\beta$ CD molar ratios of 1:0.5 and 1:1 were 0.73  $\pm$  0.13 and 0.84  $\pm$  0.12  $\mu$ m, respectively. However, those of the ones that had been formed at the AC:HP $\beta$ CD molar ratio of 1:2 could not be precisely measured.

Clearly, the dimensions of these self-assembling aggregates of the AC/HP $\beta$ CD complex were much smaller than those determined by the nanosizer. Such discrepancy could be based on a couple of reasons: (i) the dry or the solvated state of the materials during the measurements by the SEM or the nanosizer, respectively, and (ii) the dependence of diametric projection of the spherical aggregates



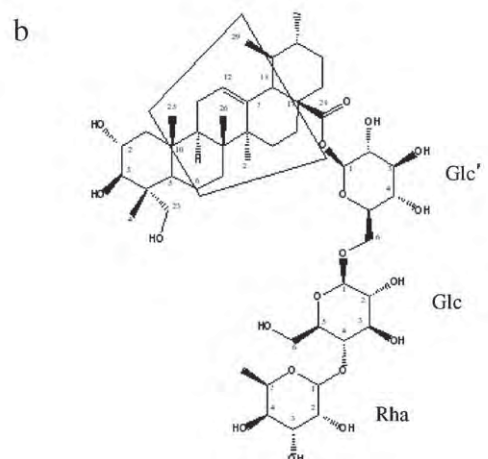
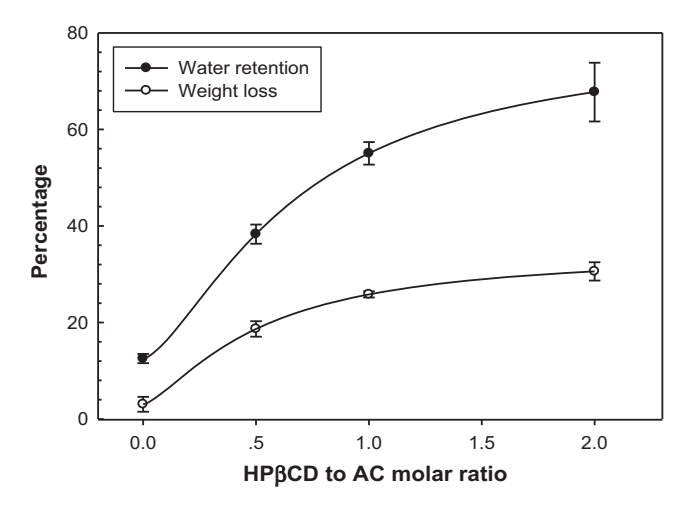


Fig. 5. (a) NOESY diagram of AC/HP $\beta$ CD complex that had been dissolved in D $_2$ O and (b) schematic arrangement of AC within the cavity of HP $\beta$ CD.

of the AC/HP $\beta$ CD complex across the thickness of the AC/HP $\beta$ CD complex-loaded CA films.

# 3.3.2. Water retention and weight loss behavior

The CA films containing either AC or the AC/HPBCD complex were further characterized to investigate water retention and weight loss behavior in the P/B/M medium at 37 °C. After the specified immersion time of 24 h had been reached, the weights of the film specimens were recorded and these were calculated to obtain the property values, as reported in Fig. 6. Among the various CA films investigated, the AC-loaded CA films (shown in the figure as the samples with the HPBCD to AC molar ratio of 0) exhibited the lowest water retention (i.e., at about 12%). Such values for the CA films containing either AC or CACE at 40 wt.%, after immersion in the P/B/M medium at 37 °C for 24 h, were reported to be about 39 and 52%, respectively (Suwantong et al., 2008). Compared with the value obtained in the present work, the greater water retention values as reported in the work of Suwantong et al. (2008) could be due to a couple of reasons: (i) the difference in the solvent type used in the fabrication of the films that could affect the physico-chemical properties of the resulting films (Li, Ren, Fane, Li, & Wong, 2006; Romero, Leite, & Goncalves, 2009; Valente, Polishchuk, Burrows, & Lobo, 2005) and (ii) the difference in the as-loaded amounts of the drug within the films that could affect the porosity of the



**Fig. 6.** Water retention and weight loss behavior of the AC/HP $\beta$ CD complex-loaded CA films at different HP $\beta$ CD to AC molar ratio after immersion in the P/B/M medium at the physiological temperature of 37 °C for 24 h (n = 3).

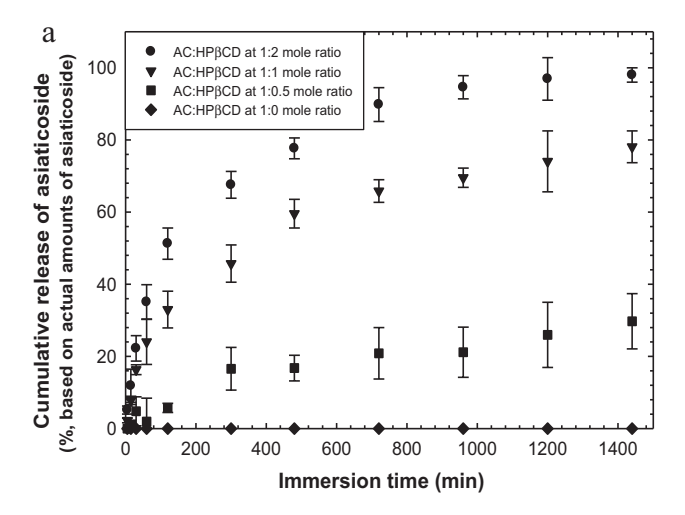
films after the drug molecules had been released into the medium (Suwantong, Opanasopit, Ruktanonchai, & Supaphol, 2007). On the other hand, the water retention of the AC/HP $\beta$ CD complex-loaded CA films was much greater than those of the AC-loaded CA films, with the average value increasing from about 38% at the HP $\beta$ CD to AC molar ratio of 0.5 to about 68% at the HP $\beta$ CD to AC molar ratio of 2.0.

The AC-loaded CA films also exhibited the lowest weight loss after immersion in the medium (at about 3%). Slightly greater values at about 4 or 7% were reported by Suwantong et al. (2008) for the CA films that contained either AC or CACE at 40 wt.%, respectively. The reasons for the discrepancy in the property values as reported in the present work and those in the work of Suwantong et al. (2008) are similar to those given in the previous paragraph. On the contrary, the loss in the weight of the AC/HPBCD complex-loaded CA films was much greater than those of the AC-loaded CA films, with the average value increasing from about 19% at the HPBCD to AC molar ratio of 0.5 to about 30% at the HPBCD to AC molar ratio of 2.0. The loss in the weight of a drug-loaded material in a medium depends on a number of factors, e.g., the solubility of the drug, the solubility of the carrier material, the diffusion of the drug from the carrier material, and so forth. Due to the low aqueous solubility of both AC and CA in water, the presence of methanol in the medium and of HPBCD in the AC/HPBCD complex-loaded CA films were the obvious reasons for the improvement in the aqueous solubility of both the drug and the matrix materials.

# 3.4. Release of AC from AC- and AC/HP $\beta$ CD complex-loaded CA films

The effect of HP $\beta$ CD on the release characteristics of AC from the CA films at different AC:HP $\beta$ CD molar ratios was evaluated by the total immersion method in the P/B/M medium. They were reported as the percentages of the ratios of the cumulative amounts of AC released to the amounts of the drug actually loaded within the films or to the actual weights of the films, as shown in Fig. 7. The actual amounts of AC within the AC- and the AC/HP $\beta$ CD complex-loaded CA films were a priori determined to be 70.7, 80.3, 69.2, and 83.0% on average (based on the as-loaded amounts of AC within the casting solutions), for the CA films that had been prepared at the AC:HP $\beta$ CD molar ratios of 1:0, 1:0.5, 1:1, and 1:2, respectively.

For the AC-loaded CA films (the content of AC initially loaded in the casting solution was 10 wt.%, denoted in Fig. 7 as the samples with the AC:HP $\beta$ CD molar ratio of 1:0), none of the as-loaded



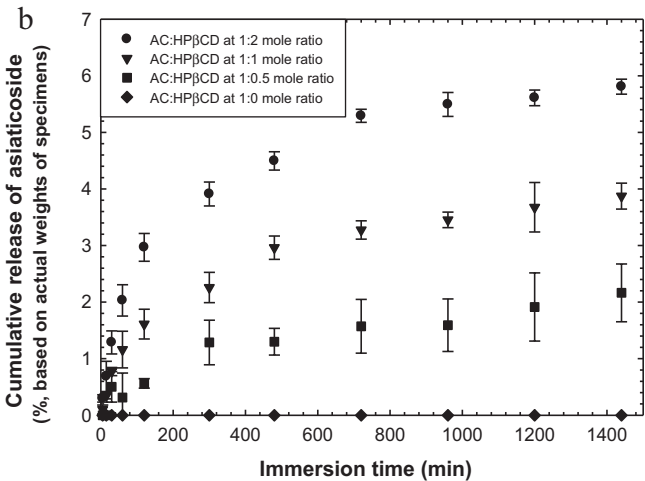


**Fig. 7.** Cumulative amounts of AC released from AC- and AC/HPβCD complex-loaded CA films upon immersion in the P/B/M medium at 37 °C. The results were reported as the percentages of the ratios of the amounts of the as-released AC to (a) the amounts of AC actually loaded within the films or (b) to the actual weights of the films (n = 3).

AC, at any given immersion time point, was able to release into the medium. Suwantong et al. (2008) reported that the maximal amounts of AC released from the CA films that had been prepared from the casting solution containing 40 wt.% of the drug were about 11% on average (based on the AC amounts initially loaded within the films). The discrepancy between the amounts of AC released from the CA films in the present work and those reported in the work of Suwantong et al. (2008) should be influenced by the fact that the amounts of AC initially loaded within the films, as reported in the two studies, were different (i.e., 10 versus 40 wt.%), hence the difference in the driving force for diffusion. The different types of the solvent used in the fabrication of the films [i.e., 90:10 (v/v) mixture of 80 vol.% acetic acid and DMAc as in the present work versus 2:1 (v/v) acetone/DMAc as in the work of Suwantong et al. (2008)], which could render different densities to the obtained films, may also contribute to the discrepancy in the results obtained in the two studies.

In comparison with the AC-loaded CA films, the presence of HP $\beta$ CD in the AC/HP $\beta$ CD complex-loaded CA films was clearly responsible for the significantly greater amounts of AC released into the medium. Furthermore, the cumulative amounts of AC released from the films, at any given immersion time point, increased with an increase in the HP $\beta$ CD content. Specifically, about 25% of the AC actually loaded within the AC/HP $\beta$ CD complex-loaded CA films, *a priori* prepared at the AC:HP $\beta$ CD molar ratios of 1:0.5, 1:1, and 1:2,

was able to release into the medium within about 1200, 60, and 30 min, respectively. The maximal amounts of AC released from these materials, after having been immersed in the medium for 1440 min, were about 30, 78, and 98% of the amounts of AC actually contained within the CA films, respectively. These values corresponded to about 2.2, 3.9, and 5.8% of the released amounts of AC, when calculated based on the actual weights of the film specimens.

As mentioned, as the HPBCD content in the films increased, significantly more amounts of AC could be released into the medium. The complexation of a poorly water-soluble drug with a native cyclodextrin (CD) as well as its derivatives improves tremendously the aqueous solubility and the dissolution rate of the drug within an aqueous medium. This phenomenon is especially important for a highly hydrophilic derivative of CD, such as HPβCD. Pose-Vilarnovo et al. (2001) reported that the aqueous solubility of sulfamethizole (i.e., a sulfonamide antibiotic drug) was improved significantly upon forming into an inclusion complex with  $\beta$ CD or HP $\beta$ CD. The difference as observed in the cumulative amounts of AC released from the AC/HPBCD complex-loaded CA films that had been prepared at various AC:HPβCD molar ratios could be explained based on a couple of reasons. Firstly, the ability of AC to form an inclusion complex with HPBCD disfavored the crystallization of the herb, as evidenced from the X-ray results (see Fig. 4). This allows greater opportunity for the solvent molecules to interact with those of the drug. Secondly, the presence of HPBCD increased the hydrophilicity of the films, as evidenced by the increase in the water retention of the films with an increase in the HP $\beta$ CD content (see Fig. 6). Lastly, due to the highly hydrophilic nature of HPBCD, the dissolution of the unassociated HPBCD as well as the AC/HPBCD inclusion complex into the releasing medium could occur easily, which helped facilitate the solubilization of the drug within the medium. This is evidenced by the observed increases in both the weight loss of the films in and the cumulative amounts of AC released from the films into the medium with an increase in the HPBCD content (see Figs. 6 and 7, respectively).

The latter case was accented by the observation of microholes on the AC/HP $\beta$ CD complex-loaded CA films after having been immersed in the releasing medium (see Table 2). The diametric dimensions of these holes, as measured directly from the SEM images shown in Table 2, were  $0.87 \pm 0.14$ ,  $1.17 \pm 0.28$ , and  $1.20 \pm 0.19$   $\mu$ m for the films that had been prepared at the AC:HP $\beta$ CD molar ratios of 1:0.5, 1:1, and 1:2, respectively. These dimensions were essentially similar to the spherical aggregates that had been observed on the films prior to the immersion (see Table 2 and related texts in Section 3.3.1).

# 3.5. Release kinetics of AC from AC/HP $\beta$ CD complex-loaded CA films

The release kinetics of AC from the AC/HP $\beta$ CD complex-loaded CA films was analyzed by the following equation (Peppas & Khare, 1993; Philip & Peppas, 1987):

$$\frac{M_t}{M_{\infty}} = kt^n$$
, for  $\frac{M_t}{M_{\infty}} < 0.6$ , (6)

where  $M_t$  is the cumulative amount of AC released into the medium at an arbitrary time t,  $M_{\infty}$  is the cumulative amount of AC released into the medium at an infinite time, n is the diffusional exponent used to described the release mechanism, and k is the release rate constant of AC. For the Fickian diffusion, the parameter n is taken as 0.5 and a plot of the fractional cumulative released amounts of AC versus  $t^{0.5}$  should give a straight line with a slope of k (Verreck et al., 2003). The values of k (with the values of  $r^2$ , signifying the quality of the fit, being given in parentheses) for the AC that had been released from the films, a priori prepared at the AC:HP $\beta$ CD molar ratios of 1:0.5, 1:1, and 1:2, were determined to be 0.0010s $^{-0.5}$ 

(0.958),  $0.0026s^{-0.5}$  (0.951), and  $0.0034s^{-0.5}$  (0.899), respectively. Clearly, the rate of AC released from the films increased with an increase in the HP $\beta$ CD content.

### 4. Conclusions

Asiaticoside (AC), from the medicinal plant Centella asiatica L., readily forms a complex with 2-hydroxypropyl-β-cyclodextrin (HP $\beta$ CD) at a 1:1 molar ratio both in distilled water and 90:10 (v/v) mixture of 80 vol.% acetic acid and N,N-dimethylacetamide (DMAc). The average diametric dimension of the self-assembling aggregates of the AC/HP $\beta$ CD complex, in the solvated state, increased from about 2.4 µm at the HPBCD to AC molar ratio of 0.5 to about 3.8 µm at the HP $\beta$ CD to AC molar ratio of 2. In the solid state, the AC/HP $\beta$ CD complex that had been prepared at the stoichiometric molar ratio of 1:1 did not show the crystalline nature of the as-received AC. Two-dimensional NMR revealed that the cyclohexene ring moiety of AC is captivated well within the HPβCD cavity. The solvent-cast cellulose acetate (CA) films that had been prepared in the presence of a mixture of AC/HPβCD of varying molar ratios (i.e., 1:0.5, 1:1, and 1:2) showed evidence of spherical aggregates on their surfaces. The dimensions of these aggregates were lower than those of the selfassembling aggregates of the AC/HPBCD complex in the solvated state. While AC could not be released from the AC-loaded CA films into the phosphate buffer saline solution (PBS) containing 10% (v/v) methanol (i.e., P/B/M medium), its cumulative amounts that had been released from the AC/HPBCD complex-loaded CA films were much greater, with values increasing with an increase in the HPBCD content. At 24h of immersion in the medium at 37 °C, the maximal amounts of AC released from these materials were about 2.2, 3.9, and 5.8% (based on the actual weights of the film specimens), respectively.

# Acknowledgements

The authors acknowledge the partial support received from (1) The Thailand Research Fund (contact grant number: DBG5280015), (2) The Petroleum and Petrochemical College (PPC), Chulalongkorn University, (3) The Development and Promotion of Science and Technology talents project (DPST).

### Appendix A. Supplementary data

Supplementary data associated with this article can be found, in the online version, at doi:10.1016/j.carbpol.2011.02.023.

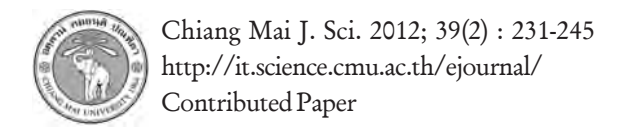
### References

- Anonymous. (2009). Cellulose acetate. http://en.wikipedia.org/wiki/Cellulose acetate
- Bergshoef, M. M., & Vancso, G. J. (1999). Transparent nanocomposites with ultrathin, electrospun nylon-4,6 fiber reinforcement. *Advanced Materials*, 11, 1362–1365.
- Bonini, M., Rossi, S., Karlsson, G., Almgren, M., Lo Nostro, P., & Baglioni, P. (2006). Self-assembly of beta-cyclodextrin in water. Part 1. Cryo-TEM and dynamic and static light scattering. *Langmuir*, 22, 1478–1484.
- Challa, R., Ahuja, A., Ali, J., & Khar, R. K. (2005). Cyclodextrin in drug delivery: An updated review. AAPS PharmScitech, 6. Article 43.
- Choi, M. J., Ruktanonchai, U., Min, S. G., Chun, J. Y., & Soottitantawat, A. (2010). Physical characteristics of fish oil encapsulated by β-cyclodextrin using an aggregation method or polycarpolactone using an emulsion-diffusion method. Food Chemistry, 119, 1694–1703.
- Coleman, A. W., & Nicolis, I. (1992). An explanation of the abnormal solubility of β-cyclodextrin. *Journal of Inclusion Phenomena and Macrocyclic Chemistry*, 13, 139–143.
- Das, P., Mallick, A., Sarkar, D., & Chattopadhyay, N. (2008). Probe-induced self-aggregation of γ-cyclodextrin: Formation of extended nanotubular suprastructure. *Journal of Physical Chemistry C*, 112, 9600–9603.
- de Araujoa, D. R., Tsuneda, S. S., Ceredaa, C. M. S., Carvalho, F. D. G. F., Prete, P. S. C., Fernandes, S. A., et al. (2008). Development and pharmacological evaluation of ropivacaine-2-hydroxypropyl-β-cyclodextrin inclusion complex. *European Journal of Pharmaceutical Science*, 33, 60–71.

- Freville, J. C., Dollo, G., Le Corre, P., Chevanne, F., & Le Verge, R. (1996). Controlled systemic absorption and increased anesthetic effect of bupivacaine following epidural administration of bupivacaine-hydroxypropyl-beta-cyclodextrin complex. Pharmaceutical Research. 13, 1576–1580.
- plex. Pharmaceutical Research, 13, 1576–1580.

  González-Gaitano, G., Rodríguez, P., Isasi, J. R., Fuentes, M., Tardajos, G., & Sanchez, M. (2002). The aggregation of cyclodextrins as studied by photon correlation spectroscopy. Journal of Inclusion Phenomenon, 44, 101–105.
- He, Y., Fu, P., Shen, X., & Gao, H. (2008). Cyclodextrin-based aggregates and characterization by microscopy. *Micron*, 39, 495–516.
- Higuchi, T., & Connors, K. A. (1965). Phase solubility techniques. Advances in Analytical Chemistry and Instrumentation, 4, 117–212.
- Irie, T., & Uekama, K. (1997). Pharmaceutical applications of cyclodextrins. III. Toxicological issues and safety evaluation. *Journal of Pharmaceutical Science*, 86, 147–162.
- Job, P. (1928). Researches sur la formation de complexes mineraux en solution et sur leur stabilité. Annali di Chimica Applicata, 9, 113–203.
- Li, Z., Ren, J., Fane, G. A., Li, D. F., & Wong, F. S. (2006). Influence of solvent on the structure and performance of cellulose acetate membranes. *Journal of Membrane Science*, 279, 601–607.
- Loftsson, T., & Brewster, M. E. (1996). Pharmaceutical applications of cyclodextrins 1. Drug solubilisation and stabilization. *Journal of Pharmaceutical Science*, 85, 1017–1025.
- Loftsson, T., Hreindóttir, D., & Másson, M. (2007). The complexation efficiency. *Journal of Inclusion Phenomena and Macrocyclic Chemistry*, 57, 545–552.
- Loftsson, T., Jarho, P., Másson, M., & Sigurjonsdóttir, J. F. (2005). Cyclodextrins in drug delivery. Expert Opinions in Drug Delivery, 2, 335–351.
- Loftsson, T., Magnúsdósdottir, A., Másson, M., & Sigurjónsdóttir, J. F. (2002). Selfassociation and cyclodextrin solubilization of drugs. *Journal of Pharmaceutical Science*, 91, 2307–2316.
- Lopez, R. F. V., Collett, J. H., & Bentley, M. V. L. B. (2000). Influence of cyclodextrin complexation on the in vitro permeation and skin metabolism of dexamethasone. International Journal of Pharmaceutics, 200, 127–132.
- Maquart, F. X., Bellon, G., Gillery, P., Wegrowski, Y., & Borel, J. P. (1990). Stimulation of collagen synthesis in fibroblast cultures by a triterpene extracted from Centella asiatica. Connective Tissue Research, 24, 107–120.
- Maquart, F. X., Chastang, F., Simeon, A., Birembaut, P., Gillery, P., & Wegrowski, Y. (1999). Triterpenes from Centella asiatica stimulate extracellular matrix accumulation in rat experimental wounds. European Journal of Dermatology, 9, 289–296.
- Mele, A., Mendichi, R., & Selva, A. (1998). Non-covalent associations of cyclomaltooligosaccharides (cyclodextrins) with trans-β-carotene in water: Evidence for the formation of large aggregates by light scattering and NMR spectroscopy. Carbohydrate Research, 310, 261–267.
- Peppas, N. A., & Khare, A. R. (1993). Preparation structure and diffusional behavior of hydrogels in controlled release. *Advances in Drug Delivery Review*, 11, 1–35.
- Philip, L. R., & Peppas, N. A. (1987). A simple equation for description of solute release I. Fickian and non-fickian release from non-swellable devices in the form of slabs, spheres, cylinder or discs. Journal of Controlled Release, 5, 23–36.
- Pose-Vilarnovo, B., Perdomo-Lopez, I., Echezarreta-Lopez, M., Schroth-Pardo, P., Estrada, E., & Torres-Labandeira, J. J. (2001). Improvement of water solubility of sulfamathizole through its complexation with β- and hydroxypropyl-β-cyclodextrin: Characterization of the interaction in solution and in solid state. European Journal of Pharmaceutical Science, 13, 325–331.
- Pose-Vilarnovo, B., Rodriguez-Tenreiro, C., Santos, J. F. R., Vazquez-Doval, J., Concheiro, A., Alvarez-Lorenzo, C., et al. (2004). Modulating drug release with cyclodextrins in hydroxypropyl methlcellulose gels and tablets. *Journal of Controlled Release*, 94, 351–363.
- Rajewski, R. A., & Stella, V. J. (1996). Pharmaceutical applications of cyclodextrins. 2. In vivo drug delivery. *Journal of Pharmaceutical Science*, 85, 1142–1169.
- Romero, R. B., Leite, C. A. P., & Goncalves, M. D. C. (2009). The effect of the solvent on the morphology of cellulose acetate/montmorillonite nanocomposites. *Polymer*, 50, 161–170.
- Sangalli, M. E., Zema, L., Maroni, A., Foppoli, A., Giordano, F., & Gazzaniga, A. (2001). Influence of betacyclodextrin on the release of poorly soluble drugs from inert and hydrophilic heterogeneous polymeric matrices. *Biomaterials*, 22, 2647–2651.
- Shim, P. J., Park, J. H., Chang, M. S., Lim, M. J., Kim, D. H., Jung, Y. H., et al. (1996). Asiaticoside-mimetics as wound healing agent. *Bioorganic & Medicinal Chemistry Letters*, 6, 2937–2940.
- Shukla, A., Rasik, A. M., & Dhawan, B. N. (1999). Asiaticoside-induced elevation of antioxidant levels in healing wounds. *Phytotherapy Research*, 13, 50–54.
- Suguna, L., Sivakumar, P., & Chandrakasan, G. (1996). Effects of centella asiatica extract on dermal wound healing in rats. *Indian Journal of Experimental Biology*, 34, 1208–1211.
- Suwantong, O., Opanasopit, P., Ruktanonchai, U., & Supaphol, P. (2007). Electrospun cellulose acetate fiber mats containing curcumin and release characteristic of the herbal substance. *Polymer*, 48, 7546–7557.
- Suwantong, O., Ruktanonchai, U., & Supaphol, P. (2008). Electrospun cellulose acetate fiber mats containing asiaticoside or centella asiatica crude extract and the release characteristics of asiaticoside. *Polymer*, 49, 4239–4247.
- Suzuki, M., Tsutsui, M., & Ohmori, H. (1994). 2H NMR study of the self-assembly of an azo dye-cyclomaltooctaose (γ-cyclodextrin) complex. Carbohydrate Research, 261, 223–230.
- Taepaiboon, P., Rungsardthong, U., & Supaphol, P. (2007). Vitamin-loaded electrospun cellulose acetate nanofiber mats as transdermal and dermal therapeutic

- agents of vitamin A acid and vitamin E. European Journal of Pharmaceutics and Biopharmaceutics, 67, 387–397.
- Thostenson, E. T., Ren, Z. F., & Chou, T. W. (2001). Advances in the science and technology of carbon nanotubes and their composites: A review. *Composite Science and Technology*, 61, 1899–1912.
  Tungprapa, S., Jangchud, I., & Supaphol, P. (2007). Release characteristics of four
- Tungprapa, S., Jangchud, I., & Supaphol, P. (2007). Release characteristics of four model drugs from drug loaded electrospun cellulose acetate fiber mats. *Polymer*, 48, 5030–5041.
- Valente, A. J. M., Polishchuk, A. Y., Burrows, H. D., & Lobo, V. M. M. (2005). Permeation of water as a tool for characterizing the effect of solvent, film thickness and
- water solubility in cellulose acetate membranes. *European Polymer Journal*, 41, 275–281.
- Verreck, G., Chun, I., Rosenblatt, J., Peeters, J., Dijck, A. V., Mensch, J., et al. (2003). Incorporation of drugs in an amorphous state into electrospun nanofibers composed of a water insoluble nonbiodegradable polymer. *Journal of Controlled Release*, 92, 349–360.
- Wang, F. J., Yang, Y. Y., Zhang, X. Z., Zhu, X., Chung, T. S., & Moochhala, S. (2002). Cellulose acetate membranes for transdermal delivery of scopamine base. *Materials Science and Engineering C*, 20, 93–100.



## Effect of Degree of Acetylation on in Vitro Biocompatibility of Electrospun Cellulose Acetate-Based Fibrous Matrices

Pitt Supaphol\*[a,b], Artphop Neamnark [a,b], Pattama Taepaiboon [a,b], and Prasit Pavasant [c]

- [a] The Petroleum and Petrochemical College, Chulalongkorn University, Bangkok 10330, Thailand.
- [b] The Center for Petroleum, Petrochemicals and Advanced Materials, Chulalongkorn University, Bangkok 10330, Thailand.
- [c] Department of Anatomy, Faculty of Dentistry, Chulalongkorn University, Bangkok 10330, Thailand. \*Author for correspondence; e-mail: pitt.s@chula.ac.th

Received: 20 July 2011 Accepted: 20 December 2011

#### **ABSTRACT**

Ultrafine fibrous matrices of regenerated cellulose (RC) of varying degrees of acetylation were facilely prepared from alkaline hydrolysis of electrospun cellulose acetate (CA; acetyl content  $\approx$  40%) fiber mats. The alkaline treatment was carried out in 0.1 N NaOH solution in 4:1 v/v water/ethanol mixture at 25  $\pm$  1°C for periods of up to 24 h, after the CA fiber mats had been thermally treated at 208 °C for 1 h. After having been treated in the NaOH solution for 10 min, 30 min, and 24 h, the resulting CA-based fibrous matrices exhibited the acetyl contents of about 24, 11, and 4%, respectively. Indirect cytotoxicity evaluation of these CA-based fibrous matrices against human fibroblasts (HFF) and human keratinocytes (HaCaT) indicated that they posed no threat to the cells. The direct culture of the cells on their surfaces suggested that these fibrous matrices only supported the short term culture of both types of cells (i.e., 1 d), while the neat and the 24 h-alkaline treated CA-based fibrous matrices exhibited marginally good support for the proliferation of HaCaT.

Keywords: Electrospinning, Cellulose acetate, Regenerated cellulose, Biocompatibility.

#### 1. INTRODUCTION

Electrospinning has been a subject of intense research, due to its ability to produce ultrafine fibers, with diameters in the range of tens of nanometers to less than ten micrometers, that exhibit high surface area to volume/mass ratios [1,2]. The principle of the process is the use of electrical as opposed to mechanical force as the main driving force

for fiber formation [1-6]. Morphology of the electrospun fibers depends on contributions from solution properties, process settings, and ambient conditions [1-6]. Due to the morphological uniqueness, the proposed uses of the electrospun fibers in the field of biomedical applications are, for examples, as carriers/substrates for enzyme encapsulation/

immobilization [7,8], carriers for drug delivery [9,10], and scaffolds for tissue regeneration [11-13].

Cellulose is one of the most common biopolymers on earth and is the primary structural component of cell walls of green plants [14]. Its usefulness has been known since the ancient time [14]. In the last decade, utilization of cellulose in biomedical applications was well documented [15-20]. Among these, many facets of biocompatibility were studied [15-18]. It has been proposed for uses as substrates/ scaffolds for bone [16,18,19] and cartilage [20] tissue engineering. However, the fabrication of cellulose is hampered by its limited solubility in common solvents and its subservient to thermal degradation prior to melting. As a result, only a few reports on successful electrospinning of cellulose are available in the open literature [21-23]. Alternatively, ultrafine cellulose fibers can be obtained facilely from deacetylation of electrospun fibers of cellulose acetate (CA)a cellulose derivative that is readily soluble in a number of organic solvents [24,25].

In the present contribution, ultrafine RC fiber mats were prepared from alkaline treatment of electrospun CA fiber mats. Various degrees of acetylation of the fiber mats were achieved by varying the treatment conditions. To fathom the possibility of using these CA-based membranes as topical wound dressing materials, biocompatibility of the native electrospun CA fiber mats and the ultrafine RC fiber mats of varying degrees of acetylation was assessed *in vitro* with human foreskin fibroblasts (HFF) and human keratinocytes (HaCaT).

#### 2. EXPERIMENTAL DETAILS

#### 2.1. Materials

Cellulose acetate (CA; white powder;  $M_{\rm w}$  = 30,000 Da; degree of acetyl substitution

≈ 2.4; acetyl content = 39.7%) was purchased from Sigma-Aldrich (USA). Sodium hydroxide (NaOH) was purchased from Ajax Finechem (Australia) and hydrochloric acid (HCl) was from J.T. Baker (USA). Acetone (Carlo Erba, Italy), *N*, *N*-dimethylacetamide [DMAc, Labscan (Asia), Thailand], and ethanol [Labscan (Asia), Thailand] were used as-received.

### 2.2. Preparation of Electrospun CA Fiber Mats

The electrospinning of CA was carried out based on the method described in a published work by some of us and another colleague [26]. Briefly, a weighed amount of CA powder was dissolved in 2:1 v/v acetone/DMAc to obtain a CA solution at a fixed concentration of 17% w/v. Electrospinning of the solution was carried out using a Gamma High Voltage Research ES30P high voltage dc power supply as the power source, a flat-tipped 20-gauge stainless steel needle (OD = 0.91 mm) as the nozzle, and an aluminum foil wrapped around a home-made rotating metal drum (OD = 9 cm) as the fiber collection device. The electric field was 17.5 kV/15 cm, the rotational speed of the rotating drum was  $60 \pm 5$  rpm, and the feed rate of the solutions was 1 mL h-1. For 9 h of continuous electrospinning, the thicknesses of the CA fiber mats were 20-30 μm.

## 2.3. Thermal Treatment and Alkaline Treatment

The CA fiber mats were peeled off from the aluminum foil, sandwiched between two polytetrafluoroethylene (PTFE) sheets, and put in a hot-air oven at 208°C for 1 h [25]. They were then immersed in 0.1 N NaOH solution in 4:1 v/v water/ethanol mixture at room temperature (25  $\pm$  1°C) for varying time intervals, ranging from 10 min

to 24 h. The alkaline-treated CA fiber mats were then rinsed in deionized (DI) water and kept in a desiccator prior to further uses.

#### 2.4. Characterization

#### 2.4.1. Physical characteristics

Morphological appearance of the neat, the heat-treated, and the alkaline-treated CA fiber mats was observed by a JEOL JSM-5200 scanning electron microscope (SEM). They were sputtered with a thin layer of gold using a JEOL JFC-1100E ion sputtering device prior to SEM observation.

## 2.4.2. Chemical functionalities and degree of deacetylation

Chemical functionalities of the neat and the alkaline-treated CA fiber mats were investigated by a Nicolet Nexus 670 Fouriertransform infrared spectroscope (4 cm<sup>-1</sup> resolution with 4 scans over the wavenumber range of 400-4000 cm<sup>-1</sup>). The degree of deacetylation (%DD) of the alkaline-treated CA fiber mats was evaluated by a titration method. Specifically, weighed samples of the CA fiber mats (2.8 cm in diameter) were immersed in 0.1 N of NaOH solution in 4:1 v/v water/ethanol mixture at the ratio of 1:1 w/v. After 10 min to 24 h of immersion, 5 mL of the NaOH solution was pipetted out and then titrated with 0.1 N HCl aqueous solution, with phenolphthalein being used to indicate the basicity-to-acidity crossover. The amount of the hydroxyl ions participated in the deacetylation reaction of CA could then be calculated from the amount of the titrant, which was used to calculate the %DD, i.e.

$$\%DD = \frac{m_i - m_f}{m_i} \times 100$$
, (1)

where  $m_{\rm i}$  and  $m_{\rm f}$  are the moles of the acetyl groups in the CA fiber mats before and after the alkaline treatment.

### 2.4.3. Wide-angle X-ray diffraction studies

The crystalline nature of the neat, the heat-treated, and the alkaline-treated CA fiber mats was examined by a JEOL JDX 3530 wide-angle X-ray diffractometer (30 kV and 40 mA over the 2Theta range of 5 to 50°).

#### 2.4.4. Physico-chemical characteristics

The water retention and the loss in the mass upon submersion in water of the neat and the alkaline-treated CA fiber mats were measured after their submersion in distilled water at 37°C for 24 h. If  $M_1$  denotes the initial mass of each fiber mat sample in its dry state and M and  $M_d$  are its masses after submersion in distilled water in its wet and dry states, respectively, the property values can be calculated as follows:

Water retention (%) = 
$$\frac{M - M_d}{M_d} \times 100$$
, (2)

Mass loss (%) = 
$$\frac{M_i - M_d}{M_i} \times 100$$
. (3)

#### 2.5. Biological Evaluation

The potential for use of the neat and the alkaline-treated CA fiber mats as wound dressing materials was assessed by the indirect cytotoxicity evaluation and the direct cultures of mammalian cells onto their surfaces. Two types of cells were used: 1) human foreskin fibroblasts (HFF) and 2) immortalized non-tumorigenic human keratinocytes (HaCaT). The experiments were done in adaptation from previously-published protocols [12]. Briefly, either type of cells was first cultured in Dulbecco's modified Eagle's medium (DMEM; Sigma-Aldrich, USA), supplemented with fetal bovine serum (FBS; Biochrom, UK), L-glutamine (Invitrogen, USA), penicillin (Gibco®, Invitrogen, USA) and streptomycin (Gibco®, Invitrogen, USA). When the cells reached 80% confluence, they

were trypsinized and counted by a hemacytometer, prior to further uses.

The indirect cytotoxicity of the fibrous materials was assessed based on the method that was adapted from the ISO10993-5 standard test method. Briefly, the specimens (~14 mm in diameter), pre-washed with 70% ethanol for 30 min, were washed with autoclaved phosphate buffer saline (PBS) solution twice and once with the culture medium. Either type of cells was seeded in wells of a 24-well tissue-culture polystyrene plate (TCPS; Corning, USA) at 2×10<sup>4</sup> cells/ well. After 24 h of attachment, the culture medium was replaced with serum-free medium (SFM; DMEM containing penicillin and streptomycin, but without FBS). Each of the specimens was then place into each well and both the cells and the specimen were incubated further for 1, 3, and 5 d. The extraction ratio was fixed at 10 mg mL-1. After each specified time interval was reached, the medium in each well was removed. The viability of the cells was then quantified by 3-(4,5-dimethylthiazol-2-yl)-2,5-diphenyltetrazolium bromide (MTT) assay. The viabilities of the cells that had been cultured with fresh SFM were used as control.

For the direct cell culture studies, the well-washed specimens were placed in wells of 24-well TCPS. A stainless steel metal ring (12 mm in diameter) had been placed on top of each fiber mat specimen and 500 mL of the culture medium had been pipetted into each well, prior to the cell culturing. Subsequently, 2×10<sup>4</sup> cells/well of either type of cells were seeded onto each specimen and allowed to attach and proliferate for 1, 3, and 5 d. After rinsing the specimens with PBS twice to remove unattached cells, the viabilities of the cells were quantified by the MTT assay and the viabilities of the cells that had been cultured on TCPS were used

as control. Lastly, the morphology of the cultured cells was investigated. The cell-cultured specimens were harvested and washed with PBS twice. After the cells had been fixed with 3% glutaraldehyde aqueous solution and washed with 0.2 M PBS aqueous solution, the specimens were dehydrated through a series of graded ethanol solutions and pure ethanol for 2 min and finally dried in air. Finally, they were observed by SEM.

#### 2.6. Statistical Analysis

All the quantitative values were expressed as means  $\pm$  standard deviation values. Statistical comparisons were performed using one-way ANOVA with SPSS 13.0 for Windows software (SPSS, USA). *P* values < 0.05 were considered statistically significant (n = 3).

#### 3. RESULTS AND DISCUSSION

#### 3.1. Morphology

The as-prepared 17% w/v CA solution in 2:1 v/v acetone/DMAc was electrospun under the electric field of 17.5 kV/15 cm for a fixed collection time of about 9 h [26]. A selected SEM image of the obtained fiber mats is shown in Figure 1a. The diameters of these individual fiber segments were determined to be 265  $\pm$  39 nm ( $n \ge 50$ ). Due to the fluffiness of the obtained fibrous matrices, further treatment in an alkaline aqueous solution would become a problem, as the materials could easily lose their physical integrity. Ma et al. [25] suggested that this shortcoming could be solved by thermally-treating the fiber mats at 208°C for 1 h. Figure 1b shows the morphology of the representative heat-treated fiber mat, which is obviously similar to that of the untreated precursor. The thermal treatment not only imparted the ease of handling to the fibrous matrices, but also helped

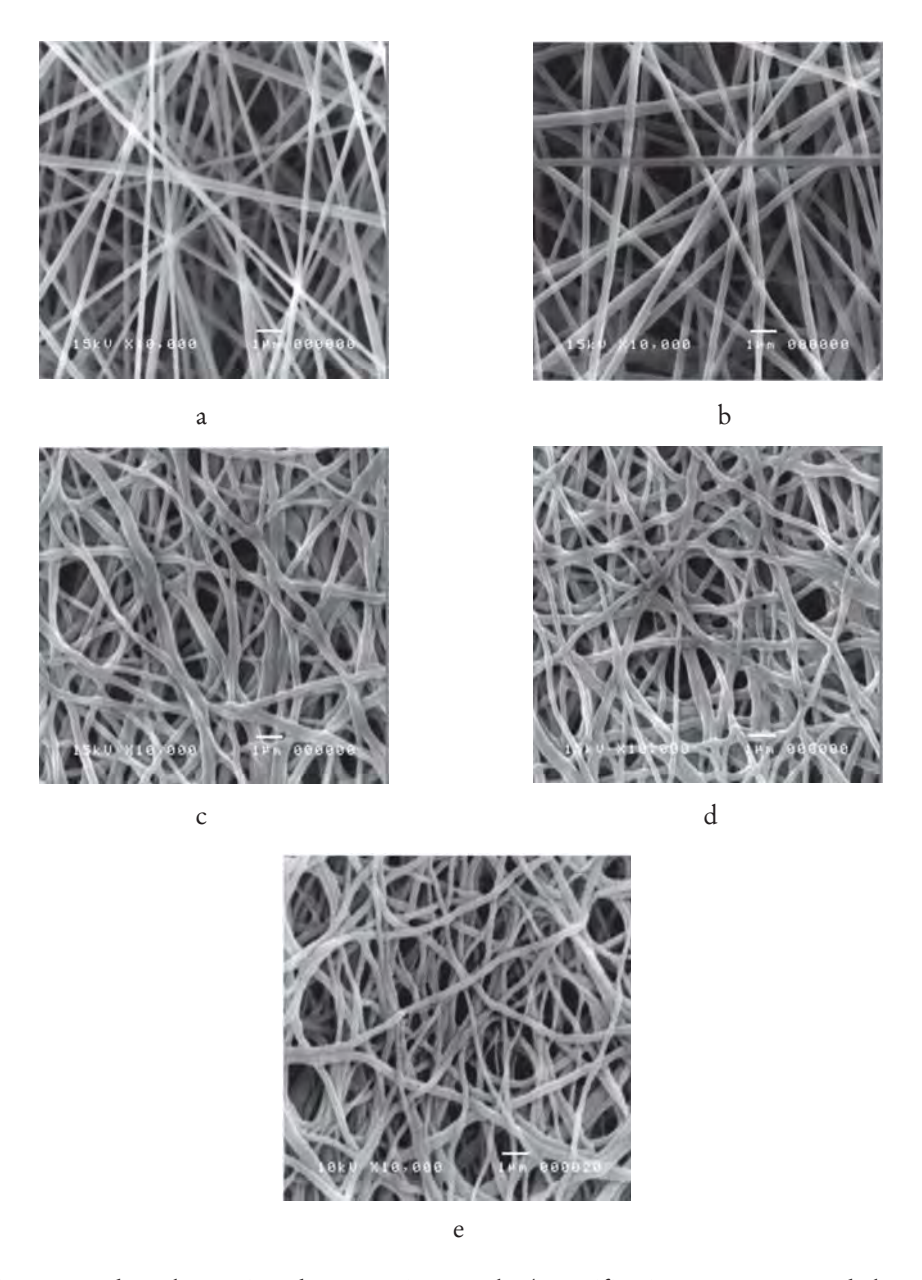


Figure 1. Selected scanning electron micrographs (magnification = 10,000x; scale bar = 1  $\mu m$ ) of electrospun fiber mats from 17% w/v CA solution in 2:1 v/v acetone/DMAc (a) before and (b) after heat treatment at 208°C for 1 h, including those of the thermally-treated fiber mats that had been submerged in 0.1 N NaOH solution in 4:1 v/v water/ethanol mixture at room temperature (25  $\pm$  1°C) for (c) 10 min, (d) 30 min, and (e) 24 h. The electrospun CA fiber mats were fabricated under the electric field of 17.5 kV/15 cm for a fixed collection time of about 9 h.

maintain their physical integrity after having been submerged in 0.1 N NaOH solution in 4:1 v/v water/ethanol mixture at  $25 \pm 1$ °C for periods of up to 24 h. Figure 1c-e shows the morphology of the fiber mats after they had been submerged in the alkaline solution for 10 min, 30 min and 24 h, respectively. Apparently, the fibrous character of the alkaline-treated fiber mats was still intact, with no evidence of the individual fibers being destroyed. On the other hand, Son et al. [24] reported that, after being submerged in a potassium hydroxide (KOH) solution in ethanol for 30 min, obvious destruction of the CA fiber mats was evident.

#### 3.2. Chemical Functionalities and %DD

The deacetylation reaction of the alkaline-treated CA fiber mats was followed qualitatively by FT-IR and quantitatively by titration. Figure 2 illustrates representative FT-IR spectra of a neat CA fiber mat and

some of the CA fiber mats that had been submerged in the alkaline solution for 10 min, 30 min, and 24 h. For the neat CA fiber mat, a strong absorption peak centering at 1750 cm<sup>-1</sup>, corresponding to the carbonyl groups (C=O) of the acetyl esters of CA, was evident. After 10 min of the alkaline treatment, the intensity of this peak decreased appreciably. Further increasing the alkaline treatment time resulted in a monotonous decrease in the intensity of the peak. The peak disappeared completely after submerging the mat in the NaOH solution for 24 h, thereby confirming the successful formation of RC fiber mats. In a similar manner, the presence of the peak centering at 1232 cm<sup>-1</sup>, corresponding to the C-O stretching of the ester/ether groups of CA, decreased in its intensity upon submersion in the alkaline solution and even disappeared completely after 24 h of submersion in the alkaline solution. At 24 h of submersion in the NaOH solution, the presence of the peak

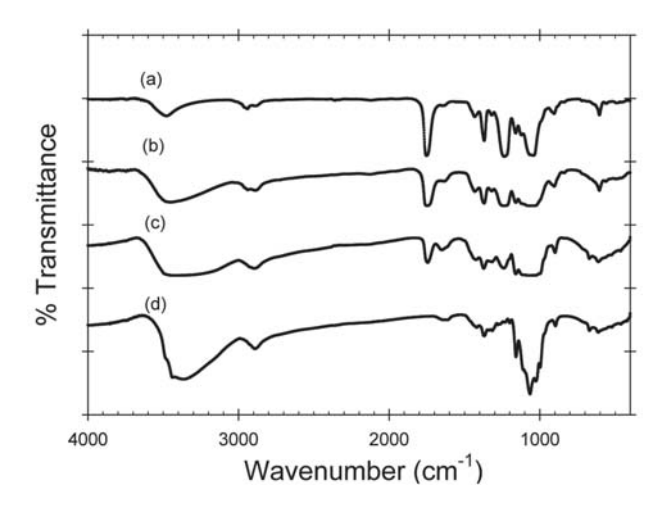


Figure 2. Representative FT-IR spectra of (a) a neat electrospun CA fiber mat and some of the thermally-treated fiber mats that had been submerged in 0.1 N NaOH solution in 4:1 v/v water/ethanol mixture at 25  $\pm$  1°C for a period of (b) 10 min, (c) 30 min, and (d) 24 h.

centering at 1068 cm<sup>-1</sup>, corresponding to the C-O stretching of the alcohol groups of cellulose, was clearly visible. Strikingly, the peak associated with the O-H stretching, centering at 3480 cm<sup>-1</sup>, became more intense and broader for the alkaline-treated CA fiber mats, especially for the ones that had been submerged in the alkaline solution for 24 h.

The %DD values of all of the alkaline-treated CA fiber mats were determined by titration and the results are shown in Figure 3. It should be noted that the degree of acetyl substitution and the acetyl content of the as-received CA were 2.4 and 39.7%. The titration procedure was to quantify, in percentage, the amount of the acetyl groups that had been abstracted by the treatment with the NaOH solution. According to the obtained result, the %DD increased sharply from about 40% after 10 min of submersion in the alkaline solution to about 79% after 60 min of submersion. Further increase in the submersion time interval

only resulted in a slight increase in the %DD to finally reach plateau values of about 88-90% after the CA fiber mats had been submerged in the alkaline solution for 7 to 24 h.

#### 3.3. X-ray Diffraction

Figure 4 shows the X-ray diffraction patterns of the neat, the heat-treated, and some of the alkaline-treated CA fiber mats. For the neat CA fiber mat, two peaks at the 2Theta values of about 10.0 and 17.4° were observed. These peaks correspond respectively to the crystalline domains of CA and cellulose (ca. the acetyl content of the as-received CA was 39.7%). The intensity of these peaks increased appreciably after the thermal treatment, most likely a result of the increase in the mobility of the CA chains during the thermal treatment, hence the increase in the crystallinity of the crystalline domains. Kamide and Saito [27] reported a relationship between the glass transition temperatures  $(T_{o}, {}^{\circ}C)$  and the degrees of

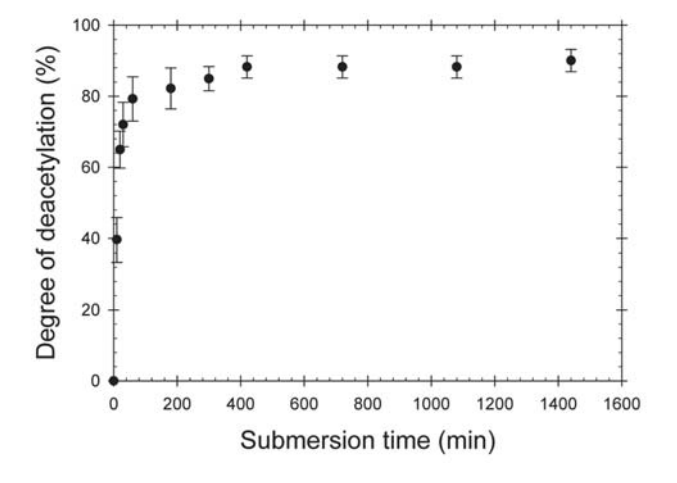


Figure 3. Degrees of deacetylation (%DD) of thermally-treated electrospun CA fiber mats that had been submerged in the NaOH solution as a function of submersion time (n = 5).

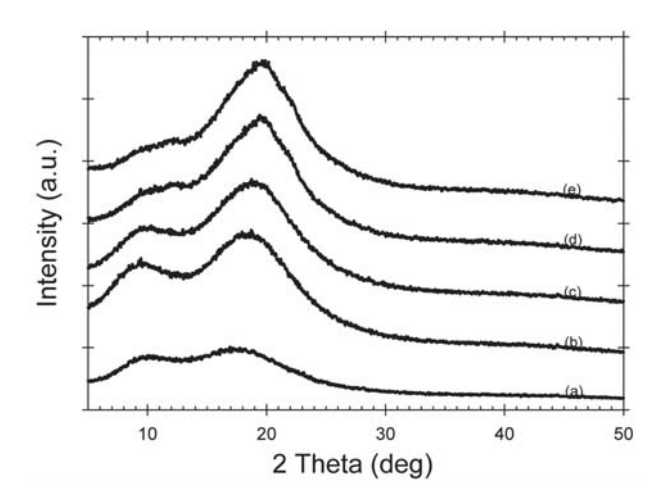


Figure 4. X-ray diffraction patterns of electrospun CA fiber mats (a) before and (b) after thermal treatment at 208°C for 1 h and those of the thermally-treated fiber mats that had been submerged in the NaOH solution for (c) 10 min, (d) 30 min, and (e) 24 h.

acetyl substitution (z,  $\in$  [0,3]) of CA, which was given as  $T_{\rm g} = 249.9 - 20.3z$ . For z = 2.4,  $T_{\rm g}$  of the as-received CA should be about 201°C. At the treatment temperature of 208°C, CA molecules should, therefore, have enough mobility to form more stable crystallites, hence the observed increase in the intensity of the crystalline peaks. The increase in the crystallinity of the thermally-treated CA would increase its stiffness and, at the same time, reduce the subservience to penetration by chemicals, hence an improvement of its physical integrity.

As for the alkaline-treated CA fiber mats, while the intensity of the low-angle peak decreased and shifted towards a higher 2Theta value with an increase in the treatment time interval, that of the high-angle peak increased and also shifted towards a higher 2Theta value. As the intensity of the high-angle peak increased with an increase in the alkaline treatment time, it becomes obvious that the decrease in the acetyl

content along the CA chains was responsible for the observed increase in the crystallinity of the alkaline-treated CA fiber mats as well as the rearrangement of the crystalline packing into that of cellulose. The reappearance of the-OH groups, hence the occurrence of the hydrogen bonding, should be responsible for the observed increase in the crystallinity of the alkaline-treated CA fiber mats.

#### 3.4. Physico-chemical Characteristics

The neat CA fiber mats and the CA fiber mats that had been treated with the alkaline solution for 10 min, 30 min, and 24 h were studied further. Based on Figure 3, the acetyl contents of these fibrous materials were estimated to be about 40, 24, 11, and 4%, respectively. These materials were tested for the water retention and the loss in the mass upon submersion in water for 24 h and the results are summarized in Table 1. The water retention decreased after the CA fiber mats underwent the alkaline treatment and the

**Table 1.** Water retention and the loss in the mass of thermally-treated electrospun CA fiber mats before and after submersion in the NaOH solution for 10 min, 30 min, and 24 h (n = 5).

Sample	Water retention (%)	Mass loss (%)	
Neat	420 ± 19	$0.6 \pm 0.5$	
10 min of alkaline treatment	$335 \pm 13$	$1.0 \pm 0.7$	
30 min of alkaline treatment	$326 \pm 25$	$1.1 \pm 0.7$	
24 h of alkaline treatment	$336 \pm 16$	$1.4 \pm 0.6$	

<sup>\*</sup> These fiber mat samples had been submerged in distilled water at 37°C for 24 h.

variation in the submersion time did not have a strong influence on the property values. It should be noted that the retention of water in an ultrafine fibrous material originates from the absorption of water within the mass of the material and from the retention of water between inter-fibrous pores due to the capillary action. While the latter should increase when the CA fiber mats had been treated with the NaOH solution (i.e., due to the increase in the hydrophillicity), the fact that the water retention values of the alkaline-treated CA fiber mats were lower than that of the neat materials should be a result of the decrease in the absorbed amount of water within the mass of the matrix material. This, in turn, resulted from the fact that the CA fiber mats had to be thermally treated prior to being treated with the NaOH solution. The thermal treatment caused the crystallinity of the matrix material to increase, hence less amount of water to be absorbed. On the other hand, after the alkaline treatment, the loss in the mass of the fiber mats increased very slightly. It is well-known that cellulose undergoes alkaline degradation, the degradation occurs from the reducing ends of the molecule and produces watersoluble D-glucoisosaccharinic acid as a byproduct [28].

#### 3.5. Indirect Cytotoxicity Evaluation

The indirect cytotoxicity of the neat CA

fiber mats and the CA fiber mats that had been treated with the alkaline solution for 10 min, 30 min, and 24 h were evaluated against HFF and HaCaT. Here, it is assumed that the viability of the cultured cells was proportional to the MTT absorbance. Figure 5 shows the viabilities of the cells that had been cultured in SFM both in the absence and in the presence of the fiber mat specimens for 1, 3, or 5 d were reported relatively to that of the cells that had been cultured in the absence of the specimens for 1 d. Evidently, the viabilities of both types of cells that had been cultured on the surface of TCPS, without or with the presence of the fiber mat specimens, increased monotonically with an increase in the cell culturing time. In fact, the viabilities of the cells, at any given cell culturing time point, were statistically the same, without or with the presence of the fiber mat specimens. The results indicate clearly that the proliferative ability of the cultured cells was unaffected, despite the presence of the fiber mat specimens in the culture medium of up to 5 d. In other words, these fibrous materials released no substances in the levels that would be harmful or pose any adverse effect to the growth in the number of the cells.

#### 3.6. Cell Culture Studies

As previously mentioned, the acetyl contents of the neat CA fiber mats and

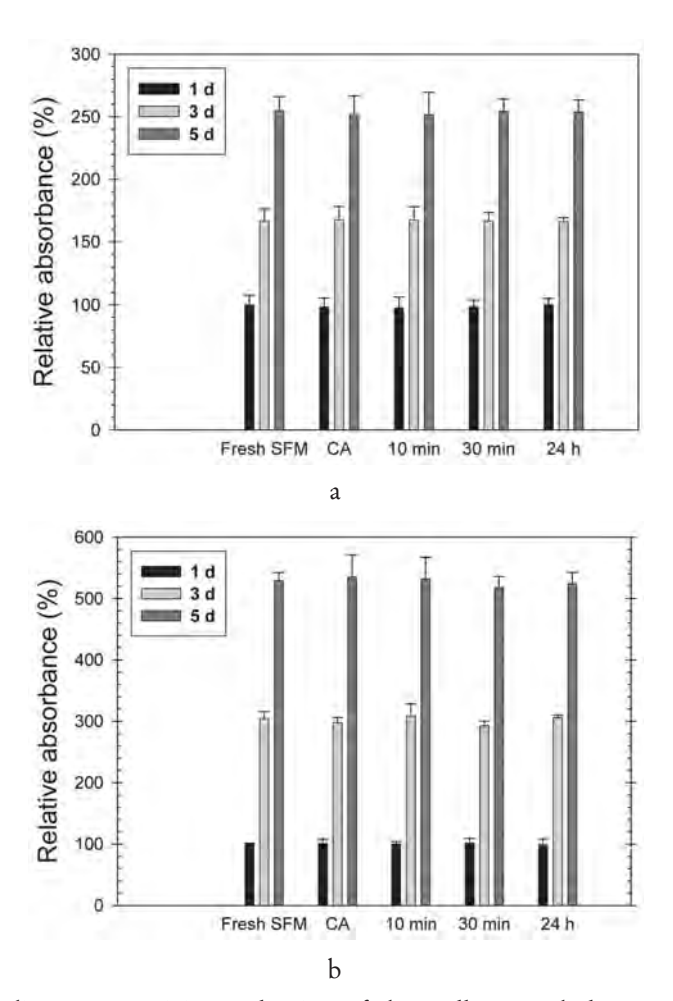


**Figure 5.** Indirect cytotoxicity evaluation of thermally-treated electrospun CA fiber mats before and after submersion in the NaOH solution for 10 min, 30 min, and 24 h, against (a) human foreskin fibroblasts (HFF) and (b) immortalized non-tumorigenic human keratinocytes (HaCaT) (n=3). The fiber mat specimens were placed into the wells, that had been pre-cultured with the cells at  $2\times10^4$  cells/well for 24 h, in serum-free medium (SFM) for a period of 1, 3, or 5 d at the extraction ratio of 10 mg mL<sup>-1</sup>. The viabilities of the cells were reported in terms of the absorbance values relatively to that of the cells that had been cultured in the absence of the specimens for 1 d.

the CA fiber mats that had been treated with the alkaline solution for 10 min, 30 min, and 24 h were about 40, 24, 11, and 4%, respectively. These fibrous materials were tested further for *in vitro* biocompatibility with HFF and HaCaT. The cells were

directly seeded and cultured on these fibrous matrices for 1, 3, and 5 d and those seeded and cultured on bare wells of TCPS were used as positive control. Again, the viability of the seeded and the cultured cells was proportional to the MTT absorbance.

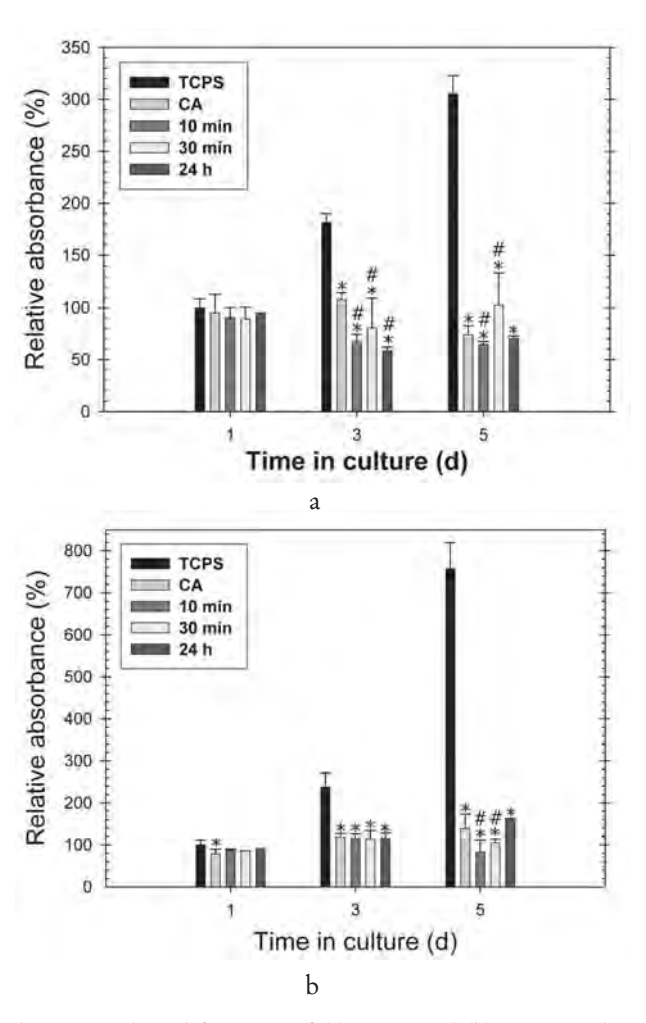


**Figure 6.** Attachment and proliferation of (a) HFF and (b) HaCaT that that had been seeded at  $2\times10^4$  cells/well and cultured on tissue-culture polystyrene plate (TCPS, used as positive control) and thermally-treated electrospun CA fiber mats before and after submersion in the NaOH solution for 10 min, 30 min, and 24 h as a function of culturing time (n = 5). The viabilities of the cells were reported in terms of the absorbance values relatively to that of the cells that had been cultured on TCPS for 1 d. (\*) p < 0.05 compared with TCPS at each specific time point and (#) p < 0.05 compared with CA at each specific time point.

Evidently, both types of cells adhered and proliferated well on the surface of TCPS. On day 1 of cell seeding, the viabilities of both types of cells that had been seeded on all of the fibrous matrices were not significantly different from those on TCPS, except for those of HaCaT that had been seeded on the neat CA fiber mats showing significantly lower values. On days 3 and 5, the viabilities of both types of cells that had

been cultured on all of the fibrous matrices were inferior to those on TCPS.

For HFF, the variation in the acetyl contents of the CA-based fibrous matrices did not pose strong effect on the viabilities of the cells cultured on them on day 1. Such an effect was seen when the cells had been

grown for longer periods of time (i.e., 3 and 5 d). On day 3, only the neat CA fiber mats could support the growth of the cells particularly better than the alkaline-treated counterparts. On day 5, the viabilities of the cells grown on the CA fiber mats that had been treated with the alkaline solution for

**Table 2.** SEM images illustrating morphologies of HFF and HaCaT that had been grown on surfaces of thermally-treated electrospun CA fiber mats before and after submersion in the NaOH solution for 10 min, 30 min, and 24 h for 1 and 3 d.

Type of cells	Cell culturing time (d)	Type of CA-based fibrous matrices			
		CA	10 min	30 min	24 h
HFF*	1		X.W		
	3		• • •		
HaCaT**	1		ibal		
	3	<i>y</i> ,			

Magnification = \*500x and \*\*1500x

30 min increased, while those on the neat CA counterparts decreased, causing the 30 min-alkaline treated CA fiber mats to be the better support for the growth of the cells. For HaCaT, the variation in the acetyl contents of the CA-based fibrous matrices did not affect the viabilities of the cells grown on them on days 1 and 3, despite the slight increase in the viabilities of the cells on day 3, when compared with those on day 1. On day 5, the viabilities of the cells grown on the neat CA fiber mats and the CA fiber mats that had been treated with the alkaline solution for 24 h, which showed equivalent values, increased slightly

from day 3, those of the cells grown on the CA fiber mats that had been treated with the alkaline solution for 10 and 30 min decreased slightly.

The morphologies of both HFF and HaCaT that had been seeded and cultured on the surfaces of the CA-based fibrous matrices are shown in Table 2. On day 1, both types of cells extended their cytoplasm over the surfaces of the fibrous matrices particularly well and even appeared in their normal cell shapes (i.e., spindle-like morphology for HFF and cobblestone morphology for HaCaT). On day 3, HFF on the neat CA fiber mat still appeared

expanded over the surface, but the extent of the cellular expansion was much decreased, when compared with the cells on day 1. HFF on the surfaces of the alkalinetreated CA fiber mats, on the other hand, were completely round. The change of the cell shape from spindle-like into round morphology, as the cell culturing time increased, suggested that the CA-based fibrous matrices are not supportive of the growth of human fibroblasts. This is in line with the observation reported by Sanchavanakit et al. [29] on bacterial cellulose fibrous membranes. Unlike HFF, HaCaT, on day 3 in their culture on the surfaces of all of the fibrous matrices, still retained their cobblestone morphology. However, the cells appeared to be more aggregated, especially those that had been cultured on the surfaces of the CA fiber mat that had been treated with the alkaline solution for 10 and 30 min. Despite the aggregation of the cells, the numbers of HaCaT on the surfaces of the CA fiber mat and the CA fiber mat that had been treated with the alkaline solution for 24 h increased from those on day 1. As reported by Sanchavanakit et al. [29], bacterial cellulose fibrous membranes showed good support for adhesion and proliferation of human keratinocytes.

#### 4. CONCLUSIONS

FT-IR, titration, and X-ray diffraction confirmed partial removal of acetyl groups from the thermally-treated (208°C for 1 h) electrospun CA fiber mats upon submersion in 0.1 N NaOH solution in 4:1 v/v water/ethanol mixture at  $25 \pm 1$ °C. For the CA fiber mats that had been treated with the alkaline solution for 10 min, 30 min, and 24 h, the acetyl contents were about 24, 11, and 4%, respectively (cf. the acetyl content of about 40% for the asreceived CA). The indirect cytotoxicity evaluation of the CA and the RC fibrous matrices against human fibroblasts (HFF)

and human keratinocytes (HaCaT) indicated that these materials did not release any substance in the level that would be toxic or suppress the growth of both types of cells. Further evaluation with the direct culture of the cells on the materials revealed that these materials could only support the short term culture of both types of cells (i.e., 1 d) and only the neat CA fiber mats and the CA fiber mats that had been treated with the NaOH solution for 24 h showed marginally good support for the proliferation of the human keratinocytes. These results suggested the potential for use of the fibrous matrices as temporary dressings of skin wounds and this should be evaluated further in vivo.

#### 5. ACKNOWLEDGMENTS

The authors acknowledge the partial support received from 1) The Thailand Research Fund (TRF, DBG5280015), 2) The Petroleum and Petrochemical College (PPC), Chulalongkorn University, and 3) Center for Petroleum, Petrochemicals, and Advanced Materials (CPPAM), Chulalongkorn University.

#### **REFERENCES**

- [1] Doshi J. and Reneker D.H., Electrospinning process and applications of electrospun fibers, *J. Electrostat.*, 1995; **35**: 151-160.
- [2] Reneker D.H. and Yarin A.L., Electrospinning jets and polymer nanofibers, *Polymer*, 2008; 49: 2387-2425.
- [3] Shim Y.M., Hohman M.M., Brenner M.P. and Rutledge G.C., Experimental characterization of electrospinning: The electrically forced jet and instabilities, *Polymer*, 2001; 42: 9955-9967.

- [4] Ding B., Kim H.Y., Lee H.C., Shao C.L., Lee D.R., Park S.J., Kwag G.B. and Choi K.J., Preparation and characterization of a nanoscale poly(vinyl alcohol) fiber aggregate produced by an electrospinning method, *J. Polym. Sci.*, *B: Polym. Phys.*, 2002; 40: 1261-1268.
- [5] Theron S.A., Zussman E. and Yarin A.L., Experimental investigation of the governing parameters in the electrospinning of polymer solutions, *Polymer*, 2004; **45**: 2017-2030.
- [6] Zhang C., Yuan X., Wu L., Han Y. and Sheng J., Study on morphology of electrospun poly(vinyl alcohol) mats, *Eur. Polym. J.*, 2005; 41: 423-432.
- [7] Ren G., Xu X., Liu Q., Cheng J., Yuan X., Wu L. and Wan Y., Electrospun poly(vinyl alcohol)/ glucose oxidase biocomposite membranes for biosensor applications, *React. Funct. Polym.*, 2006; 66: 1559-1564.
- [8] Ye P., Xu Z.K., Wu J., Innocent C. and Seta P., Nanofibrous poly (acrylonitrile-co-maleic acid) membranes functionalized with gelatin and chitosan for lipase immobilization, *Biomaterials*, 2006; 27: 4169-4176.
- [9] Zeng J., Yang L., Liang Q., Zhang X., Guan H., Xu X., Chen X. and Jing X., Influence of the drug compatibility with polymer solution on the release kinetics of electrospun fiber formulation, J. Control. Release, 2005; 105: 43-51.
- [10] Luong-Van E., Grøndahl L., Chua K.N., Leong K.W., Nurcombe V. and Cool S.M., Controlled release of heparin from poly(e-caprolactone) electrospun fibers, *Biomaterials*, 2006; 27: 2042-2050.
- [11] Chong E.J., Phan T.T., Lim I.J.,

- Zhang Y.Z., Bay B.H., Ramakrishna S. and Lim C.T., Evaluation of electrospun PCL/gelatin nanofibrous scaffold for wound healing and layered dermal reconstitution, *Acta Biomater.*, 2007; 3: 321-330.
- [12] Wutticharoenmongkol Sanchavanakit N., Pavasant P. and Supaphol P., Preparation and characterization of novel bone scaffolds based on electrospun polycaprolactone fibers filled with nanoparticles, Macromol. Biosci., 2006, 6: 70-77; Wutticharoen mongkol P., Sanchavanakit N., Pavasant P. and Supaphol P., Novel bone scaffolds of electrospun polycaprolactone fibers filled with nanoparticles, J. Nanosci. Nanotechnol., 2006, 6: 514-522; Wutticharoenmongkol P., Pavasant P. and Supaphol P., Osteoblastic phenotype expression of MC3T3-E1 cultured on electrospun polycaprolactone fiber mats filled with hydroxyapatite nanoparticles, Biomacromolecules, 2007, 8: 2602-2610.
- [13] Suwantong O., Pavasant P. and Supaphol P., Electrospun zein fibrous membranes using glyoxal as crosslinking agent: Preparation, characterization and potential for use in biomedical applications, *Chiang Mai J. Sci.*, 2011, 38: 56-70.
- [14] Anonymous, Cellulose acetate, 2009; http://en.wikipedia.org/wiki/ Cellulose acetate.
- [15] Miyamoto T., Takahashi S., Ito H., Inagaki H. and Noshiki Y., Tissue biocompatibility of cellulose and its derivatives, *J. Biomed. Mater. Res.*, 1989; 23: 125-133.
- [16] Barbié C., Chauveaux D., Barthe X., Baquey C. and Poustis J., Biological behaviour of cellulosic materials after bone implantation: Preliminary results, *Clin. Mater.*, 1990; **5**: 251-258.

- [17] Mannhalter C., Biocompatibility of artificial surfaces such as cellulose and related materials, *Sens. Actuat.*, *B: Chem.* 1993; 11: 273-279.
- [18] Martson M., Viljanto J., Hurme T. and Saukko P., Biocompatibility of cellulose sponge with bone, *Eur. Surg. Res.*, 1998; **30**: 426-432.
- [19] Barbosa M.A., Granja P.L., Barrias C.C. and Amaral I.F., Polysaccharides as scaffolds for bone regeneration, *ITBM-RBM*, 2005; **26**: 212-217.
- [20] Muller F.A., Muller L., Hofmann I., Greil P., Wenzel M.M. and Staudenmaier R., Cellulose-based scaffold materials for cartilage tissue engineering, *Biomaterials*, 2006; 27: 3955-3963.
- [21] Kulpinski P., Cellulose nanofibers prepared by the N- methylmorpholine-N-oxide method, *J. Appl. Polym. Sci.*, 2005; **98**: 1855-1859.
- [22] Kim C.W., Frey M.W., Marquez M. and Joo Y.L., Preparation of submicron-scale, electrospun cellulose fibers via direct dissolution, *J. Polym. Sci.,B: Polym. Phys.*, 2005; **43**: 1673-1683.
- [23] Kim C.W., Kim D.S., Kang S.Y., Marquez M. and Joo Y.L., Structural studies of electrospun cellulose nanofibers, *Polymer*, 2006; 47: 5097-5107.

- [24] Son W.K., Youk J.H., Lee T.S. and Park W.H., Electrospinning of ultrafine cellulose acetate fibers: Studies of a new solvent system and deacetylation of ultrafine cellulose acetate fiber, *J. Polym. Sci.*, *B: Polym. Phys.*, 2004; 42: 5-11.
- [25] Ma Z., Kotaki M. and Ramakrishna S., Electrospun cellulose nanofiber as affinity membrane, *J. Membr. Sci.*, 2005; **265**: 115-123.
- [26] Taepaiboon P., Rungsardthong U. and Supaphol P., Vitamin-loaded electrospun cellulose acetate nanofiber mats as transdermal and dermal therapeutic agents of vitamin A acid and vitamin E, Eur. J. Pharm. Biopharm., 2007; 67: 387-397.
- [27] Kamide K. and Saito M., Thermal analysis of cellulose acetate solids with total degrees of substitution of 0.49, 1.75, 2.46, and 2.92, *Polym. J.*, 1985; 17: 919-928.
- [28] Mark H.F., Bikales N.M., Overberger C.G. and Menges G., Encyclopedia of Polymer Science and Engineering, New York, John Wiley and Sons, 1985.
- [29] Sanchavanakit N., Sangrungraungroj W., Kaomongkolgit R., Banaprasert T., Pavasant P. and Phisalaphong M., Growth of human keratinocytes and fibroblasts on bacterial cellulose film, *Biotechnol. Prog.*, 2006; 22: 1194-1199.

# PREPARATION CHARACTERIZATION AND STUDY OF CRUDE BONE PROTEIN DELIVERY FORM GELATIN MICROSPHERES AND GELATIN MICROSPHERES INTEGRATED HYALURONAN-GELATIN BLENDED SCAFFOLD FOR BONE TISSUE REGERNATION

Parintorn Hariraksapitak, 1,a Prasit Pavasant, 2 and Pitt Supaphol 1,\*

#### **ABSTRACT**

This study aimed to develop a protein delivery HA-Gelatin blended scaffold for bone tissue regeneration. The designed scaffold was composed of gelatin microspheres as the part of integrated delivery device in which the crude bone protein (CBP) extracted from bone extracellular matrix was encapsulated. Gelatin microspheres were prepared with the thermal gelation in water-in-oil emulsion technique. Two types of gelatin (A and B) at different three pH which were physiologic (5.2 and 4.95 for type A and B respectively), 7.4, and 10.0 were specified as the preparative conditions and investigated for their influences on the microspheres properties. The results showed the effect of interaction between gelatin type and pH on microspheres size, zeta potential, swelling ability, and encapsulation of the CBP, but not on the CBP release characteristic. The significantly highest encapsulation of CBP (> 93%) was achieved in gelatin A, pH 10.0 and gelatin B, pH 4.95 microspheres. Astoundingly, the controlled release of CBP from any gelatin microspheres was not observed, implying that the anticipated ionic interaction between CBP and molecules of gelatin may not occur. However, the microspheres integrated composite scaffolds presented phase of sustained CBP release which suggests the essential influence of scaffold matrix on the release mechanism.

(Key-words: bone scaffolds; bone protein; gelatin microspheres; controlled release)

<sup>&</sup>lt;sup>1</sup> The Petroleum and Petrochemical College, Chulalongkorn University, Bangkok 10330, Thailand

<sup>&</sup>lt;sup>2</sup> Department of Anatomy, Faculty of Dentistry, Chulalongkorn University, Bangkok 10330, Thailand

<sup>.</sup> 

<sup>&</sup>lt;sup>a</sup> On study leave from the Department of Conservative Dentistry, Faculty of Dentistry, Prince of Songkla University, Hatyai, Songkhla 90112, Thailand.

Author to whom correspondence should be addressed (E-mail address: pitt.s@chula.ac.th)

#### 1. INTRODUCTION

Tissue engineering is an approach to regenerate living tissue with an aim at establishing healthy tissue or organ for being a substitute of the damaged or the diseased tissue [1]. Progression in tissue engineering research since 1990 has been encouraging a reappraisal of the surgical approach for the treatment of trauma and degeneration of an individual [2]. Regarding dental practice, sufficient bone support is a major requirement to achieve favorable function and esthetic in the replacement of a losing tooth with a dental implant. Unfortunately, perfect bone structure is not always presented in most patients. Bone resorption easily occurs even in a simple tooth extraction case as the consequence of would heal process [3,4]. Prevention of the alveolar bone resorption caused by a tooth extraction has been of great concern, particularly through the principle of tissue engineering [5-8].

Basically, the fundamental of tissue engineering coalesces cell, supportive material termed "scaffold" and growth-inducing substance to promote three-dimensional tissue growth [9]. Scaffold, which is a three-dimensional construct, serves as a temporary territory for cells ingrowths. Ideal scaffold should perfectly imitate the extracellular matrix and provide the necessary support for cells to proliferate and maintain their differentiated function [10,11]. Scaffolds design was initially focused on their capabilities in supporting cell growth mostly at the physical and mechanical aspects. However, the design has been recently paradigmatically shifted to serve the function of a cellular guidance. This deliberation is in accordance with the concept of cellular guidance which has been extensively discussed and progressively revised as a new knowledge of the cell-material interaction in tissue regeneration [12,13]. Scaffolds have been designed as a route to transport biological factors for cell growth and differentiation and be able to guide and induce cell adhesion, proliferation, differentiation or even recruit the desired cells. The novel tissue engineering scaffold, therefore, can be considered as a special type of drug delivery apparatus [12], or as a drug delivery scaffold.

Drug delivery scaffold can be designed by the integration of a drug encapsulated delivery device into a designated scaffold. Such model has been broadly studied for their efficacy in controlled release and tissue engineering enhancement [14-17]. The drug delivery device itself has been designed in several profiles and configurations. However, most systems base on the encapsulation or entrapment of active substances in biocompatible polymeric devices [18]. Among numerous applicable drug delivery devices, Gelatin microspheres have been frequently studied with several therapeutic agents such as antihypertensive [19], signaling proteins like albumin [20], chondroitin 6-sulfate [21], bFGF [15], IGF and TGF- $\beta$  [16], or even the plasmid DNA [17] can also be encapsulated in gelatin microspheres in which the release profiles was under control. These studies demonstrated satisfactory results of controlled release and tissue regeneration in animal test [21]. Gelatin microsphere apparently is a utility drug delivery device.

Gelatin is commonly used in pharmaceutical and medical application due to its biocompatibility and biodegradability. Structurally, gelatin is a heterogeneous mixture of single or multiple stranded polypeptides (and their oligomers) each of which contains about 300-4000 amino acids [22-24]. Molecules of gelatin are polyelectrolyte, presenting diverse isoelectric point (IEP) which are about 3-5 and 7-9 for the alkaline and acidic treated gelatin, respectively. Gelatin with different IEP

can be selectively used to from complex with the oppositely charged molecule like proteins, to be the polyion complexation which is quite stable and improbable to dissociate simultaneously. Polyion complexes thus are durable than bonding between low molecular weight electrolytes [22].

With an aim to regenerate bone in the dental socket, the crude bone protein (CBP) extracted from bone extracellular matrix is the material of interest. CBP evidently encompasses enormous active proteins and growth factors [25-29] which facilitates new bone formation [26,30]. Extraction of the crude bone protein with the intricate procedures does not obliterate bioactivities of those factors, and these presumptions initiate the plan to exploit CBP extracted from demineralized bone in regenerating bone tissue by applying the concept of the polyion complexation in achieving a degree of molecular interaction between gelatin microspheres and CBP.

This contribution proposes to fabricate a novel scaffold used for alveolar bone regeneration. On the basis of multi-functional scaffold, scaffold is designed and expected to function as not only a delivery device of the crude bone protein but also a supporting structure for the growth of bone cells. Concept of the polyion complexation is applied to achieve a degree of ionic-molecular interaction between the gelatin microspheres and crude bone protein. And it is also applied in fabricating a porous scaffold of which the polyelectolyte HA-gelatin blends are the materials of choice. The encapsulated gelatin microspheres are anticipated to be securely bound in the scaffold and provide controlled release of the crude bone protein in order to facilitate bone tissue regeneration.

#### 2. EXPERIMENTAL SECTION

#### 2.1. Materials

Gelatin from porcine skin (type A, Bloom no.170-180) was purchased form Fluka (Switzerland). Gelatin form bovine skin (type B, Bloom no.175-225) was purchased from Sigma Aldrich (USA). Hyaluronan (MW 1.35x10<sup>6</sup>) was purchased from Coach Industries Inc (Japan). Albumin from bovine serum, tetramethylrhodamine conjugate (MW 66,000 Da) was purchased from Molecular Probes Inc (USA). Rhodamine protein label kit was purchased form Pierce (USA). Saturated Glutaraldehyde aqueous solution (5.6 M) was purchased from Fluka (Switzerland). 1-ethy-3-(3-dimethylaminopropyl)carbodiimide (EDC) was purchased form Fluka (Switzerland). Acetone (AR grade) was purchased from Lab-Scan (Thailand). All other chemical agents were of analytical grade and used without further purification.

#### 2.2. Gelatin microspheres preparation

Gelatin microspheres were prepared by a thermal gelation technique with modification. In detail, 10 ml of 15% w/v gelatin (type A or B) aqueous solution was prepared at 40°C. In addition to the physiologic pH which is 5.2 or 4.95 for the gelatin type A or B respectively, pH of the gelatin solution was adjusted to 7.4 and 10.0 by the addition of 1N HCl or 1M NaOH with an aim to study the effects of pH and type of gelatin on behaviors of the as-prepared microspheres. Then, the solution was added dropwise into 200 ml of Soya oil preheated at 40°C under continuously stirring at 1,000 rpm with a homogenizer to form water-in-oil emulsion. After 10 min, temperature of the emulsion was reduced to be 4°C with an ice bath while stirring was continued for an additional 30 min to allow for

physically thermal gelation of the gelatin. Afterward, 200 ml of pre-cooled (4°C) acetone was added and stirred for the next 60 min in order to dehydrate and flocculate the coaceravate droplets. The microspheres were collected by filtration through a sintered glass filter (1 µm pores size) under vacuum, washed three times with 100 ml of cool (4°C) acetone to remove residual oil, and dried in air at room temperature over 24 h.

To crosslink the gelatin microspheres, 250 mg of the dry microspheres was suspended in 10 ml of acetone-water (2:1, v/v) containing 1% (w/v,~100mM) Glutaraldehyde solution and stirred at 4°C, 500 rpm for 1 h. The crosslinked microspheres were collected through a sintered glass filter and washed with precooled (4°C) acetone. Then, the crosslinked microspheres were suspended in 20 ml of 10 mM aqueous glycine solution containing Tween 80 (0.1 wt%), shaken at 37 °C, 50 rpm for 1 h to block the residual aldehyde groups of the unreacted glutaraldehyde. The crosslinked microspheres were then washed twice with 60 ml of the cool deionized water (4°C), with cool acetone, filtered, and eventually air-dried at room temperature for over 24 h.

#### 2.3. Crude Bone Protein preparation

CBP was extracted from the bovine jaws bone. In particular, bone was initially washed and cleaned thoroughly in tap water and then sectioned into small pieces with a diamond disc driven by a rotor. Pieces of bones were further crushed into powder in liquid Nitrogen. Then, the as-prepared powder was immersed in 0.6 N HCl at 4°C and shaken continuously on an orbital shaker. After three days, the bony solution was centrifuged and the supernatant was collected, dialyzed for 48 h and lyophilized. The dry CBP was kept in desiccators until use.

#### 2.4. Fluorescent labeling of Crude Bone Protein

Crude Bone Protein (CBP) was fluorescent-labeled with the 5-(and carboxytetramethylrhodamine, succinimidyl ester (NHS-Rhodamine). Briefly, 10 mg/ml of CBP solution was prepared with 50mM borate buffer, pH 8.5 and transferred to a reaction tube. Then, 10 mg/ml of NHS-Rhodamine in DMSO was added. The reaction solution was gently mixed well and incubated in the dark at room temperature for 1 hour. To remove the non-reacted NHS-Rhodamine, the reaction solution was filtered through a D-salt dextran desalting column using 10 mM phosphate buffered saline (PBS) with 0.15 M NaCl as a filtrating medium. The effluent solution was collected in 500-µl fraction. All fractions were subsequently detected by measuring the absorbance with spectrophotometer at 280 nm to identify the fraction containing NHS-Rhodamine-labeled CBP (hereafter, CBP-Rhod). The concentration of the CBP-Rhod existing in the selected fraction was further determined using spectrofluorometer (Cary Eclipse™) at 541 and 572 nm for the excitation and emission wavelength respectively, based on a BSA-Rhod (Molecular Probes™) standard curve over the concentration range 1-50 μg/ml (r<sup>2</sup>=0.996). The CBP-Rhod fraction was stored at 4°C and protected from light until ready to use.

#### 2.5. CBP-Rhod loading into gelatin microspheres

Crosslinked gelatin microspheres were loaded with CBP-Rhod by diffusion method. In particular, the aforementioned CBP-Rhod fraction was diluted with 10 mM PBS, 0.15 M NaCl, pH 7.2 to achieve the concentration ~700  $\mu$ g/ml. Gelatin microspheres were immersed in the diluted CBP-Rhod solution to attain the loading dose of 4  $\mu$ g CBP-Rhod per mg dried microspheres. The resulting mixture was vortexed for 1 h and incubated at 4°C for 24 h to let the CBP-Rhod infuse. The impregnated microspheres were frozen at -40°C for 24 h, lyophilized, and kept in the dark at 4°C until use.

#### 2.6. Fabrication of porous composite hyaluronan-gelatin scaffolds

Porous composite hyaluronan (HA)-gelatin scaffolds were fabricated by the solvent casting and freeze-drying technique. Briefly, 2% (w/w) aqueous solution of a HA and gelatin mixture (1:1, w/w) was prepared at 50°C and left to cool down to room temperature. Then, in order to facilitate the blending of HA and gelatin, ionic strength of the mixture was adjusted by adding the equal amount of NaCl to HA (1:1, mole/equ) and being mixed up for 30 min. The resulting mixture became clearer and more translucent. To crosslink the polymers, calculated amount of EDC (1x to HA, mole/equ) was added and reacted under 200 rpm stirring at room temperature for 2 h. Afterward, the neat or the CBP-Rhod labeled microspheres were suspended in HA-gelatin mixture at 1% (w/w) concentration, which equals to 50% (w/w) of the polymer weight. The suspension was continuously stirred until the microspheres were well dispersed in the mixture and the then was cast in polypropylene discs at a constant weight, freezed at -40°C and lyophilized at -50°C. The samples were kept in desiccators until use.

#### 2.7. Characterization

## 2.7.1. Size and morphology of gelatin microspheres and microspheres integrated HA-Gelatin scaffold

Gelatin microspheres were initially inspected under the computer connected Polarizing Optical Microscope (DMRXP, Leica) at 20x magnification. The images were recorded and further used to measure the diameters of the microspheres with the UTHSCSA Image Tool version 3.0 software. One hundred microspheres were measured for each preparative condition and the average values of their sizes were calculated. The data were also used to determine size distribution of the microspheres both before and after crosslinking with 100mM Glutaraldehyde. For the morphological study, gelatin microspheres and the as-prepared scaffolds were mounted on brass stubs, coated with gold using a JEOL JFC-1100 sputtering device, and observed for their microscopic morphology using JEOL JSM-5200 scanning electron microscopy (SEM).

#### 2.7.2. Swelling ability of gelatin microsphere

Swelling ability was determined by the alteration of microspheres' size after water uptake. 20 mg of the dry crosslinked microspheres were incubated in 10 ml of 10 mM PBS with 0.15 M NaCl at 37°C for 24 h. Then, sizes of the swelling microspheres were examined with the same procedure as previously described in 2.7.1. One hundred microspheres of each preparative condition were